AWARD NUMBER: W81XWH-14-1-0403

TITLE: The Roles of the Bone Marrow Microenvironment in Controlling Tumor Dormancy

PRINCIPAL INVESTIGATOR: Yusuke Shiozawa, M.D., Ph.D.

CONTRACTING ORGANIZATION: Wake Forest University Health Sciences
Winstson, NC 27157

REPORT DATE: October 2016

TYPE OF REPORT: Annual

PREPARED FOR: U.S. Army Medical Research and Materiel Command
Fort Detrick, Maryland 21702-5012

REPORT DOCUMENTATION PAGE

Form Approved
OMB No. 0704-0188

1. REPORT DATE	2. REPORT TYPE	3. DATES COVERED
October 2016	Annual	8 Sep 2015 - 7 Sep 2016

4. TITLE AND SUBTITLE
The Roles of the Bone Marrow Microenvironment in Controlling Tumor Dormancy

5a. CONTRACT NUMBER

5b. GRANT NUMBER
W81XWH-14-1-0403

5c. PROGRAM ELEMENT NUMBER

6. AUTHOR(S)

Yusuke Shiozawa, MD, PhD

E-Mail: yshiozaw@wakehealth.edu

5d. PROJECT NUMBER

5e. TASK NUMBER

5f. WORK UNIT NUMBER

7. PERFORMING ORGANIZATION NAME(S) AND ADDRESS(ES)

Wake Forest University Health Sciences
Medical Center Blvd.
Winston-Salem NC 27157

8. PERFORMING ORGANIZATION REPORT NUMBER

9. SPONSORING / MONITORING AGENCY NAME(S) AND ADDRESS(ES)

U.S. Army Medical Research and Materiel Command
Fort Detrick, Maryland 21702-5012

10. SPONSOR/MONITOR'S ACRONYM(S)

11. SPONSOR/MONITOR'S REPORT NUMBER(S)

12. DISTRIBUTION / AVAILABILITY STATEMENT

Approved for Public Release; Distribution Unlimited

13. SUPPLEMENTARY NOTES

14. ABSTRACT

The purpose of this study is to identify the mechanisms whereby the bone marrow microenvironment is involved in regulation of tumor dormancy. Aim1 will identify and explore how disseminated tumor cells (DTCs) stay dormant for long periods of time. We postulate that DTCs drive the bone marrow niche into dormancy through the GAS6 pathway. Aim2 will determine how DTCs escape dormancy, consequently rendering them more susceptible to the chemotherapy.

As a major accomplishment of this study during this period is that the PI, Dr. Yusuke Shiozawa, accepted a position as an Assistant Professor at Wake Forest School of Medicine as of 03/01/15, and as of 07/01/16, a transfer of the award from the University of Michigan to Wake Forest School of Medicine was completed.

We developed an innovative and powerful mouse models that enable us to measure within the same animal: (i) the growth of bone metastatic prostate cancer and (ii) bone remodeling. This newly established mouse model allow us to evaluate the interaction between the bone marrow niche and disseminated prostate cancer cells.

15. SUBJECT TERMS
Prostate Cancer; Bone metastasis; Disseminated tumor cells; Bone marrow microenvironment; Tumor dormancy; GAS6; BMP2

16. SECURITY CLASSIFICATION OF:			17. LIMITATION OF ABSTRACT	18. NUMBER OF PAGES	19a. NAME OF RESPONSIBLE PERSON
a. REPORT	b. ABSTRACT	c. THIS PAGE			USAMRMC
U	U	U	UU	92	19b. TELEPHONE NUMBER *(include area code)*

Table of Contents

Page

1. INTRODUCTION:

Despite improvements in treatments for primary prostate cancer (**PCa**), bone metastasis remains a major cause of death in PCa patients. Several studies have shown that disseminated tumor cells (**DTCs**) shed from a primary tumor may lie dormant in distant tissues for long periods of time, retaining the potential for activation resulting in metastatic growth. Understanding the underlying mechanisms of metastasis is therefore crucial for effective treatment of this disease. Bone marrow has been well established as a regulatory site for hematopoietic function. In the marrow, hematopoietic stem cells (**HSCs**) are believed to localize to a specific microenvironment, the "niche", where they reside in a dormant state. Likewise, growing evidence has suggested that disseminated PCa also resides within the marrow niche. In fact, disseminated PCa uses similar mechanisms as HSCs in order to gain access to the marrow microenvironment, and DTCs target and displace HSCs, establishing metastatic foci within the hematopoietic niche. As a result, these cells parasitize the niche to become dormant, utilizing the mechanisms that keep HSCs in a dormant state. Although bone marrow is known as a fertile microenvironment ("soil") for metastatic tumor cells ("seed"), little is known about how dormancy is established or what leads to re-activation of the dormant cells. Therefore, we hypothesize that **once DTCs become dormant within the bone marrow niche, they stay dormant by stimulating the niche to remain dormant, and eventually escape from dormancy when the niche matures.**

To address our hypothesis the following aims are proposed:
Aim1: Determine the mechanisms whereby DTCs control the dormancy of the niche cells.
Sub hypothesis: DTCs drive the niche into dormancy via GAS6 signaling.
Aim2: Determine if the differentiation of the niche cells triggers the regrowth of DTCs.
Sub hypothesis: Dormant DTCs exit from dormancy when the niche is differentiated via BMP2 signaling.

The proposed studies will provide significant insight into the mechanisms whereby the bone marrow microenvironment is involved in regulation of tumor dormancy. Aim 1 allows us to identify and explore how DTCs stay dormant for long periods of time. We postulate that DTCs drive the bone marrow niche into dormancy through the GAS6 pathway. Aim2 will determine how DTCs escape dormancy, consequently rendering them more susceptible to the chemotherapy. Results from this work will lead to a greater understanding of niche aging effects on metastatic growth, and could result in valuable new treatment approaches.

2. KEYWORDS:

Prostate Cancer; Bone metastasis; Disseminated tumor cells; Bone marrow microenvironment;
Tumor dormancy; GAS6; BMP2

3. ACCOMPLISHMENTS:

What were the major goals and objectives of the project?

The goal of this project is to understand the mechanisms of tumor dormancy and metastatic outgrowth of disseminated prostate cancer within the bone marrow microenvironment.

Task 1: Complete the grant transfer from University of Michigan to Wake Forest School of Medicine.

Months 1-3.

- Upon arrival at Wake Forest School of Medicine, the PI will seek to obtain the necessary approvals (IACUC, IRB, IBC) to complete the grant transfer, and then will initiate the proposed research as soon as possible (**Months 1-3**).

Task 2: Determine the mechanisms whereby DTCs control the dormancy of the niche cells.

Months 4-18.

- To determine the effects of GAS6 on the dormancy of niche cells *in vitro*, co-culture of bone marrow stromal cells (**BMSCs**) (pre-stained with DiD fluorescent dye) with either GAS6-downregulated PCa cells (**PCa^{shGAS6}**) or control PCa (**PCa^{Control}**) will be performed. At the termination of experiments, BMSCs will be harvested, and the retention of DiD dye will be measured with FACS (**Months 4-7**).

  To further characterize the difference, gene and protein expression of proliferation markers and cell cycle status will be analyzed using those isolated BMSCs (**Months 7-9**).

- To determine the effects of GAS6 on the dormancy of niche cells *in vivo*, we will perform a vertebral body implant (vossicle) experiment. We will implant BrdU-incorporated vossicles directly injected with PCa^{shGAS6} or PCa^{Control} into immunocompromized mice, and then will determine the effects of GAS6 on the dormancy of the microenvironment by immunohistochemistry for BrdU (**Months 9-14**).

  Additionally, using immunohistochemistry we will also visualize co-localization of PCa cells with the dormant microenvironment cells using these vossicles (**Months 14-19**).

Task 3: Determine if the differentiation of the niche cells triggers the regrowth of DTCs.

Months 19-36.

- To determine if the differentiation of the niche following exogenous BMP2 treatment stimulates the regrowth of DTCs *in vitro*, co-culture of BMSCs with G1-Red and SG2M-Cyan co-infected PCa cells will be performed. The differentiation of the niche, and the dormancy, proliferation, and cell

cycle status of PCa cells after treatment with recombinant mouse (**rm**) BMP2 will be analyzed (**Months 19-22**).

- To determine if the differentiation of the niche following the exogenous BMP2 treatment stimulates the regrowth of DTCs *in vivo*, we will implant vossicles directly injected with G1-Red and SG2M-Cyan co-infected PCa cells into immunocompromized mice. The differentiation of the niche, and the dormancy, proliferation, and cell cycle status of PCa cells after treatment with rm BMP2 will be analyzed (**Months 22-26**).

- To determine whether BMP2 expressed by DTCs is crucial for metastatic progression *in vitro*, co-culture of BMSCs with BMP2-downregulated PCa (**PCa^{shBMP2}**), upregulated PCa (**PCa^{BMP2OE}**), or control PCa (**PCa^{Control}**) will be performed. Thereafter, the differentiation of the niche, and the dormancy, proliferation, and cell cycle status of PCa cells will be analyzed (**Months 27-30**)

- To determine whether BMP2 expressed by DTCs is crucial for metastatic progression *in vivo*, we will implant vossicles directly injected with PCa^{shBMP2}, PCa^{BMP2OE}, or PCa^{Control}. Thereafter, the differentiation of the niche, and the dormancy, proliferation, and cell cycle status of PCa cells will be analyzed (**Months 31-36**).

What was accomplished under these goals?

The Award transfer.
As of 03/01/15, thanks to receiving this Idea Development Award for Young Investigators, the PI, Dr. Yusuke Shiozawa started an independent faculty job as an Assistant Professor at Wake Forest School of Medicine. Upon his arrival at Wake Forest School of Medicine, the PI obtained the necessary institutional approvals (IACUC, IRB, IBC) and submitted the grant transfer request (06/11/2015) to gain approval from the Department of Defense for a transfer of the award from the University of Michigan to Wake Forest School of Medicine. As of 07/01/16, a transfer of the award from the University of Michigan to Wake Forest School of Medicine was completed.

The development of a mouse model to measure tumor growth and bone remodeling.
To evaluate the interaction between the bone marrow niche and disseminated PCa cells, we must be able to measure (i) the growth of bone metastatic PCa and (ii) bone remodeling within the same animal. To address this concern, we first attempted to establish an innovative and powerful mouse model (**Fig. 1**). For this experiment, PCa cells (DU145) were inoculated intrafemorally into severe combined immunodeficient (**SCID**) mice to establish bone metastases. Thereafter, we measured changes in tumor growth [bioluminescent imaging (**BLI**), immunohistochemistry (**IHC**)] and bone remodeling (microCT, IHC). Using this strategy, we found (i) tumor growth by BLI (**Fig. 1A&B**), (ii) tumor burden in the marrow by histology (**Fig. 1C**), and decreased bone volume density and connective density in tumor-burdened mice on microCT (**Fig. 1D-F**).

The neuropeptide CGRP expressed by sensory neurons around bone influences PCa proliferation through CRLR/JNK pathway.

We recently reported that PCa cells parasitize the mechanisms whereby HSCs home to the marrow to gain access to bone (1). Nerves are a major component of the microenvironment for HSCs (2, 3), and are also involved in the metastatic process of PCa to bone (4). Yet whether the interactions between DTCs and sensory neurons in the bone play a crucial role in controlling later bone metastatic progression remains unclear. Interestingly, our preliminary data demonstrated that bone metastatic PCa increases neuronal hypertrophy of calcitonin-gene related peptide (**CGRP**)-expressing sensory nerves in the periosteum in a time-dependent manner (**Fig. 2A**). It has been demonstrated that levels of CGRP are increased in the serum of patients with advanced PCa compared to low-grade PCa (5, 6), and that CGRP induces osteoblastic differentiation (7). Next, we wondered if CGRP affects PCa progression. We found that CGRP enhances proliferation of PCa cells *in vitro* (**Fig. 2B&C**). PCa patients with metastases express higher levels of CGRP receptor Calcitonin receptor like receptor (**CRLR**) (gene name CALCRL), compared to PCa patients without metastases (**Fig. 2D**). Additionally, CGRP activates JNK in PCa [**Fig. 2E&F**; quantification of pathway array data suggesting that JNK is a potential target (Data not shown)].

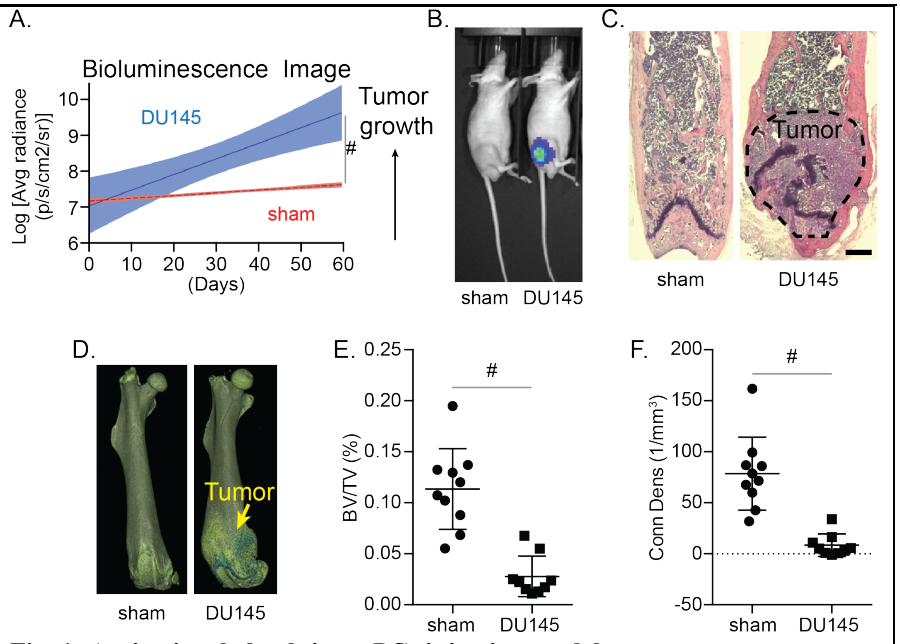

Fig. 1: An *in vivo* skeletal tissue PCs injection models

Luciferase-labeled DU145 cells or sham were placed directly into the femur of the immunodeficient mice. Tumor growth and pain behaviors were followed for 8 weeks. (**A**) BLI was performed over time to measure tumor growth (n = 10 per group). (**B**) Representative image of BLI. Data from **A** is presented as linear mixed effect models. #: time by group interaction, $p < 0.05$ versus sham injected animals. (**C**) Hematoxylin and eosin staining of femur. Magnification, ×20. Bar = 500µm. (**D**) Representative microCT of femur. (**E&F**) Quantifications of (D). (**E**) Bone volume density (BV/TV) and (**F**) Connective density (Conn Dens). Presented as mean ± SD, $^{\#}p < 0.0001$ versus sham injected bones (Student's t-test).

1. Shiozawa Y, Pedersen EA, Havens AM, Jung Y, Mishra A, Joseph J, et al. Human prostate cancer metastases target the hematopoietic stem cell niche to establish footholds in mouse bone marrow. J Clin Invest. 2011;121(4):1298-312.
2. Katayama Y, Battista M, Kao WM, Hidalgo A, Peired AJ, Thomas SA, et al. Signals from the sympathetic nervous system regulate hematopoietic stem cell egress from bone marrow. Cell. 2006;124(2):407-21.
3. Mendez-Ferrer S, Michurina TV, Ferraro F, Mazloom AR, Macarthur BD, Lira SA, et al. Mesenchymal and haematopoietic stem cells form a unique bone marrow niche. Nature. 2010;466(7308):829-34.
4. Magnon C, Hall SJ, Lin J, Xue X, Gerber L, Freedland SJ, et al. Autonomic nerve development contributes to prostate cancer progression. Science. 2013;341(6142):1236361.
5. Suzuki K, Kobayashi Y, Morita T. Serum calcitonin gene-related peptide levels in untreated prostate cancer patients. Int J Urol. 2006;13(6):781-4.

6. Suzuki K, Kobayashi Y, Morita T. Significance of serum calcitonin gene-related peptide levels in prostate cancer patients receiving hormonal therapy. Urol Int. 2009;82(3):291-5.
7. Liang W, Zhuo X, Tang Z, Wei X, Li B. Calcitonin gene-related peptide stimulates proliferation and osteogenic differentiation of osteoporotic rat-derived bone mesenchymal stem cells. Mol Cell Biochem. 2015;402(1-2):101-10.

What opportunities for training and professional development did the project provide?

Thanks to receiving an Idea Development Award for Young Investigators, the PI obtained independent status at Wake Forest School of Medicine with lab space, office space, and start-up costs provided.

Thanks to the Department of Defense, the PI attended IMPaCT Young Investigator Meeting, Baltimore, MD, USA, August 4-5, 2016.

The PI was chosen for the 2016-2018 cohort of the Wake Forest Clinical and Translational Science Institute's Translational Scholar Academy, which supports the scientific and career development of early-stage investigators.

How were the results disseminated to communities of interest?

There is nothing to report at this time.

What do you plan to do during the next reporting period to accomplish the goals and objectives?

Now that we have access to the DoD funds, we will able to address the experiments proposed as Specific Aims. In the next year of the award, we will pursue the effects of the disseminated tumor cells on the dormancy of bone marrow niche (Aim 1), by using the newly established mouse model to enable us to measure both tumor growth and bone remodeling simultaneously. In addition, we will determine whether CGRP induces osteoblastic differentiation, and we will compare the effects on osteoblastic differentiation between BMP2 and CGRP (Aim 2). We will also further elucidate the role of osteoblastic differentiation in the progression of bone metastasis (Aim 2).

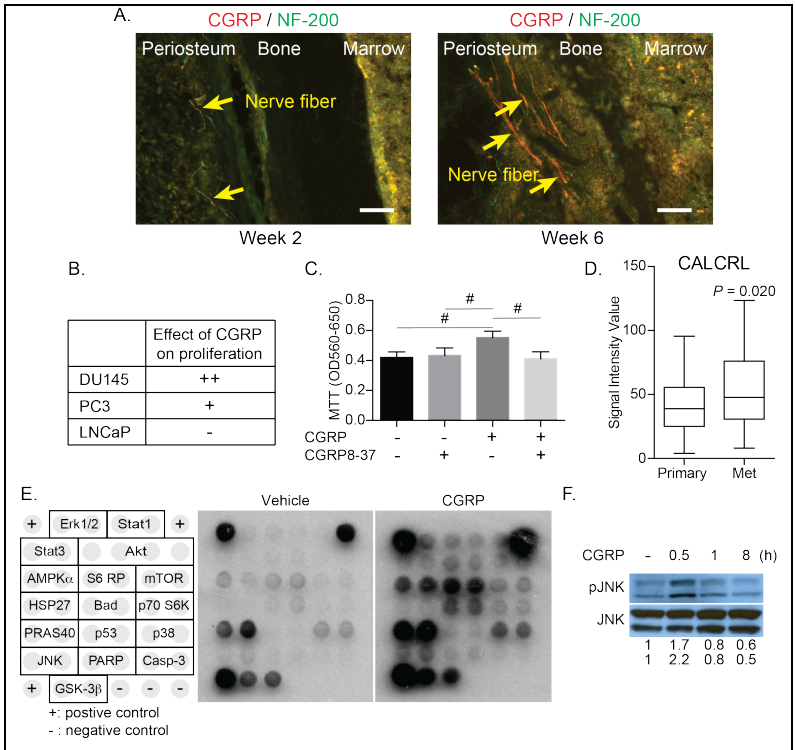

Fig. 2: CGRP influences PCa proliferation through CRLR/JNK

(**A**) DU145 cells were placed directly into the femur of the immunodeficient mice. Co-localization of CGRP and NF-200 (myelinated nerve marker) in the periosteum of tumor inoculated bones was assessed at 2 and 6 weeks. Magnification 20x. Bar = 100µm. (**B**) The effects of CGRP on *in vitro* MTT cell viability assays of PCa cell lines (+ correspond to MTT activity). (**C**) MTT cell viability assays with/without CGRP antagonist (CGRP8-37). Presented as mean ± SD, $^{\#}p < 0.001$ (One-way ANOVA, Tukey's multiple comparisons). (**D**) Box plots of gene expression values for CRLR (gene name CALCRL) in primary PCa (Primary, n=65) and metastatic PCa (Met, n=25) obtained from the GEO database. Presented as mean ± SD, significance versus **primary PCa** (Student's *t*-test). (**E**) Representative images of antibody-based cell pathway array data. Quantification of data suggest that JNK is a potential target (Data not shown). (**F**) CGRP activates pJNK.

4. IMPACT:

What was the impact on the development of the principal discipline(s) of the project?

We developed an innovative and powerful mouse models that enable us to measure within the same animal: (i) the growth of bone metastatic PCa and (ii) bone remodeling.

What was the impact on other disciplines?

There is nothing to report at this time.

What was the impact on technology transfer?

There is nothing to report at this time.

What was the impact on society beyond science and technology?

There is nothing to report at this time.

5. CHANGES/PROBLEMS:

Changes in approach and reasons for change

Nothing to report.

Actual or anticipated problems or delays and actions or plans to resolve them

Nothing to report.

Changes that have a significant impact on expenditures

Nothing to report.

Significant changes in use or care of human subjects, vertebrate animals, biohazards, and/or select agents

Nothing to report.

6. PRODUCTS:

Publications, conference papers, and presentations

Journal Publications

Peer reviewed journal

1. Seib FP, Berry JE, **Shiozawa Y**, Taichman RS, Kaplan DL. Tissue engineering a surrogate niche for metastatic cancer cells. **Biomaterials**. 2015;51:313-9. PMID: 25771021. PMCID: PMC4367489.
   Status of Publication: Published
   Acknowledgement of federal support: Yes

2. Zalucha JL, Jung Y, Joseph J, Wang J, Berry JE, **Shiozawa Y**, Taichman RS. The Role of Osteoclasts in Early Dissemination of Prostate Cancer Tumor Cells. **J Cancer Stem Cell Res**. 2015;3:e1005. PMID: 26097863. PMCID: PMC4469294.
   Status of Publication: Published
   Acknowledgement of federal support: Yes

3. **Shiozawa Y**, Berry JE, Eber MR, Jung Y, Yumoto K, Cackowski FC, Yoon HJ, Parsana P, Mehra R, Wang J, McGee S, Lee E, Nagrath S, Pienta KJ, Taichman RS. The Marrow Niche Controls The Cancer Stem Cell Phenotype Of Disseminated Prostate Cancer. **Oncotarget**. In Press. PMID: 27172799. PMCID: In Progress.
   Status of Publication: Accepted
   Acknowledgement of federal support: Yes

4. Sharma S, Xing F, Liu Y, Wu K, Said N, Pochampally R, **Shiozawa Y**, Lin HK, Balaji KC, Watabe K. Secreted Protein Acidic and Rich in Cysteine (SPARC) Mediates Metastatic Dormancy of Prostate Cancer in the Bone. **J Biol Chem**. 2016;291:19351-63. PMID: 27422817. PMCID: PCM5016675.
   Status of Publication: Published
   Acknowledgement of federal support: No

Invited reviews

1. **Shiozawa Y**[*], Eber MR, Berry JE, Taichman RS[*]. Bone marrow as a metastatic niche for disseminated tumor cells from solid tumors. **BoneKEy Rep**. 2015;4:689. PMID: 26029360. PMCID: PMC4440229. ([*] Co-corresponding authors)
   Status of Publication: Published
   Acknowledgement of federal support: Yes

2. Dai J, Hensel J, Wang N, Kruithof-de Julio M, **Shiozawa Y**. Mouse models for studying prostate cancer bone metastasis. **BoneKEy Rep**. 2016;5:777. PMID: 26916039. PMCID: PMC4757481.
   Status of Publication: Published
   Acknowledgement of federal support: Yes

3. Tsuzuki S, Park SH, Eber MR, Peters CM, **Shiozawa Y**. Skeletal complications in cancer patients with bone metastases. **Int J Urol**. In Press. PMID: 27488133. PMCID: In Progress.
   Status of Publication: Accepted
   Acknowledgement of federal support: Yes

   - **The Figure 1 is chosen as the Cover Figure of Int J Urol Vol. 23 No. 10**

Book

1. Miler SF, Thomas CY, **Shiozawa Y**. (2016) Molecular involvement of the bone marrow microenvironment in bone metastasis. In Ahmad A (Ed.), *Introduction to Cancer Metastasis.* In Press. Philadelphia, Elsevier.
   Status of Publication: Accepted
   Acknowledgement of federal support: Yes

Presentation

1. Tsuzuki S, Eber MR, Miler SF, Park SH, Widner DB, **Shiozawa Y**. The effects of neuropeptides on the prostate cancer progression**.** IMPaCT Young Investigator Meeting, Baltimore, MD, USA, August 4-5, 2016. Poster.

Website(s) or other Internet site(s)

Nothing to report.

Technologies or techniques

Nothing to report.

Inventions, patent applications, and/or licenses

Nothing to report.

Other products

Nothing to report.

7. PARTICIPANTS & OTHER COLLABORATING ORGANIZATIONS

What individuals have worked on the project?

Name: Yusuke Shiozawa
Project Role: PI
Researcher Identifier (e.g. ORCID ID): orcid.org/0000-0001-9814-9230
Nearest person month worked: 2.4
Contribution to Project: Dr. Shiozawa provides oversight of the entire program and development and implementation of all policies, procedures, and processes. In this role, Dr. Shiozawa is responsible for the implementation of the specific aims, and for ensuring that systems are in place to guarantee institutional compliance with US laws, including biosafety and animal research, data and facilities. Dr. Shiozawa supervises other personnel on the project to ensure timely and effective studies.
Funding Support: National Cancer Institution

Has there been a change in the other active support of the PD/PI(s) or senior/key personnel since the last reporting period?

Nothing to report.

What other organizations have been involved as partners?

Nothing to report.

8. SPECIAL REPORTING REQUIREMENTS:

N/A.

9. APPENDICES:

The original copies of manuscript are attached.

Biomaterials 51 (2015) 313–319

Contents lists available at ScienceDirect

Biomaterials

journal homepage: www.elsevier.com/locate/biomaterials

Tissue engineering a surrogate niche for metastatic cancer cells

F. Philipp Seib [a, 1], Janice E. Berry [b], Yusuke Shiozawa [b], Russell S. Taichman [b], David L. Kaplan [c, *]

[a] Strathclyde Institute of Pharmacy and Biomedical Sciences, University of Strathclyde, 161 Cathedral Street, Glasgow G4 0RE, UK
[b] Department of Periodontics and Oral Medicine, University of Michigan School of Dentistry, Ann Arbor, MI 48109, USA
[c] Tufts University, Department of Biomedical Engineering, 4 Colby Street Medford, MA 02155, USA

ARTICLE INFO

Article history:
Received 20 September 2014
Accepted 27 January 2015
Available online 4 March 2015

Keywords:
Bone
Silk
Cancer
Metastasis
Breast cancer

ABSTRACT

In breast and prostate cancer patients, the bone marrow is a preferred site of metastasis. We hypothesized that we could use tissue-engineering strategies to lure metastasizing cancer cells to tissue-engineered bone marrow. First, we generated highly porous 3D silk scaffolds that were biocompatible and amenable to bone morphogenetic protein 2 functionalization. Control and functionalized silk scaffolds were subcutaneously implanted in mice and bone marrow development was followed. Only functionalized scaffolds developed cancellous bone and red bone marrow, which appeared as early as two weeks post-implantation and further developed over the 16-week study period. This tissue-engineered bone marrow microenvironment could be readily manipulated *in situ* to understand the biology of bone metastasis. To test the ability of functionalized scaffolds to serve as a surrogate niche for metastasis, human breast cancer cells were injected into the mammary fat pads of mice. The treatment of animals with scaffolds had no significant effect on primary tumor growth. However, extensive metastasis was observed in functionalized scaffolds, and the highest levels for scaffolds that were *in situ* manipulated with receptor activator of nuclear factor kappa-B ligand (RANKL). We also applied this tissue-engineered bone marrow model in a prostate cancer and experimental metastasis setting. In summary, we were able to use tissue-engineered bone marrow to serve as a target or "trap" for metastasizing cancer cells.

1. Introduction

Metastasis is a highly complex process. In the case of breast and prostate cancers, hematogeneous metastasis is commonly encountered in the red bone marrow [1], and patient survival is poor once disseminated disease is diagnosed [2]; metastasis is responsible for 90% mortality of patients with solid tumors [3]. The lack of suitable *in vivo* tissue models has impeded clinical progress [4]. There are currently two main approaches for studying syngeneic or xenograft breast and prostate cancer bone metastasis in the orthotopic or experimental metastasis setting [5]. In the first, the host's skeleton serves as the site of metastasis and is commonly used to study osteotropism of cancer. In the second, fresh bone chips [6–9] or marrow [10] are used and implanted subcutaneously or in the mammary fat pad. While human fetal bone or marrow has been used in most cases [6,8], materials from discarded femoral heads [9] have also been used.

Tissue-engineering approaches for cancer research [11] have recently emerged as a potential third route for the study of bone metastasis. For example, microfabricated scaffolds seeded with human bone marrow stromal cells have been implanted in a window chamber model to permit intravital microscopy studies [12]. This microfabricated model generated a chimeric microenvironment, but the ability of this model to recapitulate native tissue remains to be established. Bone marrow stromal cells are clearly useful for driving osteogenesis and marrow formation [13]; however, bone morphogenetic proteins (BMPs) also have a robust clinical track record for the *de novo* formation of bone and marrow [14]. In particular, BMP-2 has been associated with bone development and maintenance in the adult skeleton [14,15]. *In vivo* tissue engineering of bone has been successful [16], but no attempts have yet been made to engineer a bone marrow microenvironment (BMM) that can be selectively manipulated. This manipulation of

* Corresponding author. Tel.: +1 617 627 3251; fax: +1 617 627 3231.
E-mail address: David.Kaplan@tufts.edu (D.L. Kaplan).
[1] Previous address: Tufts University, Department of Biomedical Engineering, 4 Colby Street, Medford, MA 02155, USA.

http://dx.doi.org/10.1016/j.biomaterials.2015.01.076
0142-9612/

the BMM would provide opportunities to ask fundamental questions about cancer metastasis to bones, and to explore the possibility that tissue-engineered bone could serve as a surrogate niche or "trap" for cancer metastasis. Several potential avenues are available for manipulating the BMM; chemokines were chosen in the present study.

In 1889, Stephen Paget established that breast cancer has preferred sites for metastasis (tissue tropism) [17], and recent studies have identified chemokines as potential regulators that dictate the actual organ metastasis of breast [18] and prostate [19] cancers (reviewed in Refs. [20,21]). For example, metastatic breast and prostate cancers "home" to bone by following gradients of stromal cell-derived factor 1 (SDF-1); this mechanism emulates the hematopoietic stem trafficking occurring during fetal development and following bone marrow transplantation [20].

Bone colonization by metastatic cancer cells involves the hijacking of a multitude of signaling pathways [22]. For example, osteotropic cancers often induce osteoclast activity through receptor activator of nuclear factor kappa-B ligand (RANKL) signaling. Osteoclast activation in the BMM in turn liberates a myriad of growth factors and chemokines stored in the bone mineral matrix, thereby driving the recruitment of even more cancer cells to the bone [2,22]. Our current understanding of chemokine-mediated metastasis indicated SDF-1 and RANKL as appropriate choices for manipulation of the BMM in the present study.

In summary, this study examined the potential of BMP-2 functionalized scaffolds to support the *in vivo* development of bone and marrow and the subsequent ability of this tissue-engineered BMM to serve as a surrogate niche for metastatic cancer cells attracted by locally released chemokines.

2. Materials and methods

2.1. Preparation of silk scaffolds

Bombyx mori silk solution was prepared as described previously [23]. Briefly, cocoons were cut into 25-mm^2 pieces, boiled for 30 min in an aqueous solution of 20 mM Na_2CO_3, and then rinsed in distilled H_2O to remove sericin proteins. Extracted silk fibroin was subsequently air dried and then dissolved in 9.3 M LiBr solution at 60 °C for 4 h, yielding a 25% w/v solution. This solution was dialyzed against ddH_2O (molecular weight cut off 3500) for 48 h to remove the LiBr salt. The resulting aqueous silk fibroin solution was centrifuged twice at 9.700 g for 20 min to remove the small amount of silk aggregates that formed during processing. A salt-leach method was used where NaCl crystals were embedded within silk fibroin to generate highly porous silk scaffolds. First, the silk fibroin solution was diluted to 6% w/v with ddH_2O. Next, 4 g of NaCl crystals (500–600 μm) were added to 2 ml of this fibroin solution as porogens, and scaffolds were allowed to solidify for 24 h. Scaffolds were washed extensively in ddH_2O to leach out the NaCl to yield highly porous silk scaffolds. The size was optimized by generating scaffolds with a volume of either 125 mm^3 or 27 mm^3 and a constant 5 μg BMP-2 (human BMP-2, Wyeth, Andover, MA, USA) loading. For 125 mm^3 scaffolds, BMP-2 loading was optimized using BMP-2 concentrations between 0.5 and 10 μg. For all samples, the BMP-2 loading was performed by applying 30 μl of a 7% w/v silk solution containing the indicated amount of BMP-2. Scaffolds were air dried under a 0.2-m/s airflow at room temperature overnight. Where indicated, scaffolds were further modified by water annealing at room temperature for 8 h to induce β-sheets [23].

2.2. In vivo scaffold implantation

Animal studies were performed in accordance with the approved institutional protocols B2010–101 and PRO00004354 by the Institutional Animal Care and Use Committee (IACUC) of Tufts University and University of Michigan, respectively. Mice aged 6–10 weeks were purchased from Charles River Laboratories. For scaffold implantation studies, animals were anesthetized using isoflurane, shaved when necessary, and the surgical area was cleaned. As indicated, BMP-2 functionalized or control silk scaffolds were implanted subcutaneously at three different sites, namely the rotator cuff, lower abdomen, and upper thorax. As controls, 10 mg of demineralized human (0.125–0.850 mm particle size; Community Tissue Services, Dayton, OH, USA) or rat bone were added to a size 9 gelatin capsule (Torpac Inc., Fairfield, NJ, USA) and implanted as detailed above. Incisions were closed with a one-layer closure using skin clips. Animals were monitored daily over the course of 10 days, at which time the skin clips were removed. Scaffolds were removed at the indicated time points and processed for analysis as detailed below.

2.3. Cell culture

All cell lines were maintained in a humidified atmosphere of 5% CO_2 at 37 °C, and subconfluent cultures were routinely subcultured every 2–3 days. MDA-MB-231 B16F10, and PC3 cells were cultured in RPMI 1640 + 10% v/v FBS medium. For *in vivo* tumor studies, cells were harvested with trypsin and subsequently prepared as detailed below.

2.4. Tumor models

To examine the potential of tissue-engineered bone to serve as a surrogate niche to cancer metastasis, a syngeneic experimental tumor model employing C57BL/6 mice and B16F10 cancer cells was used [24]. Prior to tumor cell injection, a 125-mm^3 scaffold functionalized with 5 μg BMP-2 was implanted over the rotator cuff in mice and allowed to integrate for more than 4 weeks. On the day of tumor induction, B16F10 cells were washed and harvested with trypsin-EDTA, blocked with complete medium, and pelleted. The pellet was subsequently washed twice with PBS, and cells were resuspended in PBS at a concentration of 10^5 cells/ml and kept on ice. Mice were shaved, cleaned and the landmarks palpitated to facilitate the intracardiac injection of cells into the left ventricle. The spontaneous pulsatile entrance of bright red oxygenated blood into the transparent needle hub indicated proper positioning of the needle. A dose of 10^4 B16F10 cells in 100 μl was administered over 30 s into the left ventricle with a 27-gauge needle. Within 18 days of B16F10 injection, animals were euthanized.

For studies that examined the potential of the scaffolds to serve as a surrogate niche for breast cancer metastasis, a human xenograft model was used. Breast tumors were induced by inoculating MDA-MB-231 derived tumor cells that metastasized following orthotopic injection in mice [25]. Cells were genetically modified to carry the firefly luciferase gene to allow *in vivo* bioluminescence imaging [25]. Analogous to the syngeneic tumor studies, scaffolds were implanted over the rotator cuff in female NOD/SCID mice (NOD.CB17-$Prkd^{scid}$/NcrCrl), 6–10 weeks in age, and allowed to integrate ≥8 weeks. Next, a total of 5×10^5 cells in 20 μl Matrigel (BD Biosciences, Bedford, MA, USA) was injected bilaterally into the 4th or 5th mammary fat pad using a Hamilton syringe equipped with a 22-gauge needle. To manipulate the microenvironment of the tissue-engineered bone, osmotic minipumps (Durect Corporation, Cupertino, CA, USA) were used. Pumps with a nominal pumping rate of 0.11 μl/h over 4 weeks were fitted with an infusion catheter and filled with SDF-1 (100 μg/ml), RANKL (100 μg/ml), or PBS according to the manufacturer's instruction; human SDF-1 alpha (catalogue number 100-20) and mouse RANKL (catalogue number 200-04) were purchased from Shenandoah Biotechnology, Warwick, PA, USA. Twelve days after tumor inoculation, pumps were implanted s.c. and the catheter was implanted into the scaffold. Disease progression was monitored weekly with intraperitoneal injections of D-luciferin (Molecular Probes, Eugene, OR, USA), followed by measuring tumor cell-associated bioluminescence using the Xenogen IVIS 200 imaging system and Living Image Software 4.2 (Caliper Life Sciences, Hopkinton USA). At the study endpoint at 6 weeks post-tumor induction, scaffolds, brain, lung, liver, and bones were examined for metastasis by dissecting them from the carcass. Tibia and femur from hind legs were harvested and dissected free from muscle and tendons to serve as bone samples. Organs were imaged at maximum sensitivity to detect metastatic cancer cells. Tissues were scored for the presence or absence of metastasis. Primary tumors were dissected and weighed.

For prostate cancer studies, one scaffold was implanted on the back of male athymic nude mice (Athymic Nude-*Foxn1*^{nu}), 6–10 weeks in age, and allowed to integrate >6 weeks. PC3 cells were transduced with GFP-luciferase lentivirus to allow for bioluminescence imaging of tumor growth (via luciferase) and localization of cells in tissue sections (via GFP). Next, a total of 1×10^5 cells in 10 μl growth medium was injected into the ossified scaffold with a 30-gauge needle. At the time of cell injection, a single pump with either SDF-1 or PBS was implanted as detailed above.

2.5. Histology and X-ray microtomography

X-ray microtomography was performed on formalin-fixed tissues in 70% v/v ethanol. Measurements were carried out with an HMX ST 225 X-ray tube equipped with a molybdenum target and a 2000 × 2000 pixel detector (Nikon Metrology, Leuven, Belgium). Projections were recorded over 360°, and dataset voxel sizes were typically 10 μm isotropic. The dataset was reconstruction with the CTPro 3D software package (Nikon Metrology) in the absence of noise reduction or binning. Images were rendered using VGStudio MAX version 2.2 (Volume Graphics, Heidelberg, Germany).

Bones and scaffolds were prepared for histology by fixing them for 24 h in buffered formalin and subsequently demineralizing them for 21 days at 4 °C with a 10% w/v EDTA solution at pH 7.4. Next, samples were tissue processed and paraffin embedded as detailed previously [26]. For all histology samples, at least two level sections were cut to ensure representative images. For immunofluorescence images to detect human cells grown in scaffolds, anti-human HLA-ABC antibody (BioLegend) was conjugated using the Zenon Alexa Fluor488 mouse IgG labeling kit (Invitrogen, San Diego, CA). Seven μm thick paraffin sections were blocked with Image-iT FX signal enhancer (Invitrogen) for 30 min before fluorescence-labeled and primary antibodies were applied for 2 h at room temperature in the dark.

Subsequently, the sections were mounted with ProLong Gold anti-fade reagent with DAPI (Invitrogen). Images were taken with Olympus FV-500 confocal microscope (Olympus, Center Valley, PA).

2.6. Statistical analysis

Data were analyzed using GraphPad Instat 5.0b (GraphPad Software, La Jolla, CA, USA). Sample pairs were analyzed with the Student's *t*-test. Multiple samples were evaluated by one-way analysis of variance followed by Dunnett's post hoc tests to evaluate the statistical differences ($p \leq 0.05$) between samples and controls, respectively. An exception was the analysis of explanted scaffolds where a Kruskal–Wallis test was used. All error bars were standard deviation (SD).

3. Results

Here we describe an *in vivo* tissue-engineered bone marrow model that uses bone morphogenetic protein 2 (BMP-2) functionalized three-dimensional (3D) silk protein scaffolds that permit *in situ* bone marrow genesis. The bone marrow can subsequently be modified with an osmotic minipump to locally deliver chemokines or other molecules of interest. We used a water-based silk solution to generate 3D scaffolds that were sponge-like (ca. 50 kPa compressive stress), highly porous (>90%) [27], biocompatible [28], and readily functionalized with defined amounts of BMP-2 with known release kinetics [29]. First, we fixed the amount of BMP-2 loading at 5 μg per scaffold and determined the importance of the post-loading treatment in relation to the implantation site and time for bone marrow genesis (Fig. 1a, Supplementary Fig. 1). Scaffolds that had a low β-sheet (crystalline) content performed best; this was independent of the implantation site. The first signs of bone development occurred at 3 days in C57/B6 mice, and a robust tissue-engineered BMM occurred at 4 weeks, while NOD/SCID mice required 8 weeks. In C57/B6, NOD/SCID, and athymic nude mice, the BMM was maintained for several months (>3); the optimized silk scaffold showed a robust tissue-engineered BMM (Fig. 1b–d). However, control scaffolds showed neither bone nor marrow development in mice (Supplementary Fig. 1e). As a reference or control for our functionalized silk scaffolds, we used human and rat demineralized bone matrix (DBM) [5,30]. While human DBM showed no signs of bone marrow development, rat-derived DBM required at least 8 weeks to develop some bone marrow *in vivo*. Because BMP-2 scaffolds with a low β-sheet content performed best (Fig. 1b–d), we further characterized these scaffolds by changing scaffold size and the degree of BMP-2 functionalization (Fig. 1e–h). In light of orthotopic breast tumor studies, we selected the rotator cuff as an implantation site to physically separate the tissue-engineered BMM from the primary tumor. X-ray microtomography demonstrated that with 0.5–10 μg BMP-2 the amount of bone significantly increased, while there were no differences between the 5 μg and 10 μg BMP-2 scaffolds (Fig. 1e, f). Furthermore, at 5 μg BMP-2 functionalization, the amount of bone formation was independent of scaffold size but increased over 16 weeks (Fig. 1g, h). The 125 mm^3 scaffolds with a 5-μg BMP-2 loading were found to be optimal for this study because the size of the engineered tissue allowed easy access and manipulation with an infusion catheter of the osmotic minipump.

Next, we examined the ability of the tissue-engineered BMM to serve as a surrogate niche for metastasis (Fig. 2a). Using mice with an established BMM, we induced orthotopic breast tumors and subsequently manipulated the BMM by locally delivering receptor activator of nuclear factor kappa-B ligand (RANKL). To rule out the potential systemic impact of this RANKL delivery strategy, we monitored primary tumor growth over 6 weeks, and the extent of metastasis (Fig. 2b–d). There was no significant difference between the control group and mice receiving RANKL in terms of primary tumor growth, tumor weight, and metastasis to distant organs (Fig. 2b–d). However, there was a significant impact on the tissue-engineered BMM as determined by X-ray microtomography (Fig. 2f), but this did not affect the bone volume of the rest of the skeleton (Fig. 2g). The tissue-engineered BMM harbored human breast cancer cells (Fig. 2h, i). Bioluminescence imaging demonstrated that the control scaffold, which did not develop bone marrow, had the lowest signal, whereas substantially higher values were obtained for SDF-1, and significantly higher ones were obtained for the RANKL treatment group (Fig. 2h, i).

Finally, we assessed the ability of our tissue-engineered BMM to serve as a model system to study prostate cancer bone metastasis. While there was tumor engraftment for all animals (5/5), delivery of SDF-1 substantially reduced PC3 growth when compared to controls (Fig. 3c) but with minimal effects on tissue or bone volume (Fig. 3d). Histology confirmed growth of prostate cancer cells in the BMM (Fig. 3e). To complement the human breast and prostate cancer studies, the B16F10 syngeneic experimental metastasis model was used (Fig. 3f). Histology of scaffolds demonstrated that B16F10 cells were able to invade and colonize the tissue-engineered BMM (Fig. 3g–j).

4. Discussion

In 1889, Stephen Paget established that breast cancer has preferred sites for metastasis (tissue tropism) [17], and recent studies have identified chemokines as potential regulators that dictate the actual organ metastasis of breast and prostate cancer [3]. We therefore examined the ability of the tissue-engineered BMM to serve as a surrogate niche for metastasis (Fig. 2a). Using mice with an established BMM, we manipulated the BMM by locally delivering receptor activator of nuclear factor kappa-B ligand (RANKL). RANKL activates osteoclasts, which in turn degrade bone and subsequently release growth factors and chemokines stored in the bone matrix [2,22]; these factors could critically contribute to a pre-metastatic niche. Tumor growth and metastasis was unchanged following local RANKL delivery (Fig. 2b–d); this suggested that RANKL had minimal systemic effects. This was further supported by the observation that RANKL only had a significant impact on the tissue-engineered bone volume (Fig. 2f), but not the bone volume of the rest of the skeleton (Fig. 2g). Most importantly, the tissue-engineered BMM harbored human breast cancer cells (Fig. 2h, i); this colonization could be readily manipulated *in situ*. Bioluminescence imaging demonstrated that the control scaffold, which did not develop bone marrow, had the lowest signal and the highest one was obtained for the RANKL treatment group (Fig. 2h, i). This observation supported our hypothesis that a metastatic niche can be selectively manipulated using tissue engineering. The extent to which this colonization of the BMM recapitulates all steps typically observed in traditional osteotropic cancer models remains to be established. Nonetheless, the idea that metastatic cancer cells exploit a BMM "homing" mechanism analogous to that driving hematopoietic stem trafficking into bone marrow seems quite plausible [20]. We speculate that this luring of metastatic cancer cells into the BMM would then conceivably reduce the overall metastatic burden in systemic host tissues (Fig. 2d).

We next assessed the ability of our tissue-engineered BMM to serve as a model system to study prostate cancer bone metastasis. Previous *in vitro* and *in vivo* studies showed the significance of the CXCR4/7-SDF-1 signaling axis in tissue tropism for prostate cancer metastasis [21], although direct experimental proof has been difficult to obtain because of a lack of methods that permit the selective manipulation of the BMM. By combining local SDF-1 delivery with prostate cancer cell injection into the tissue-engineered BMM (Fig. 3a, b), it was possible to monitor cell response *in situ*.

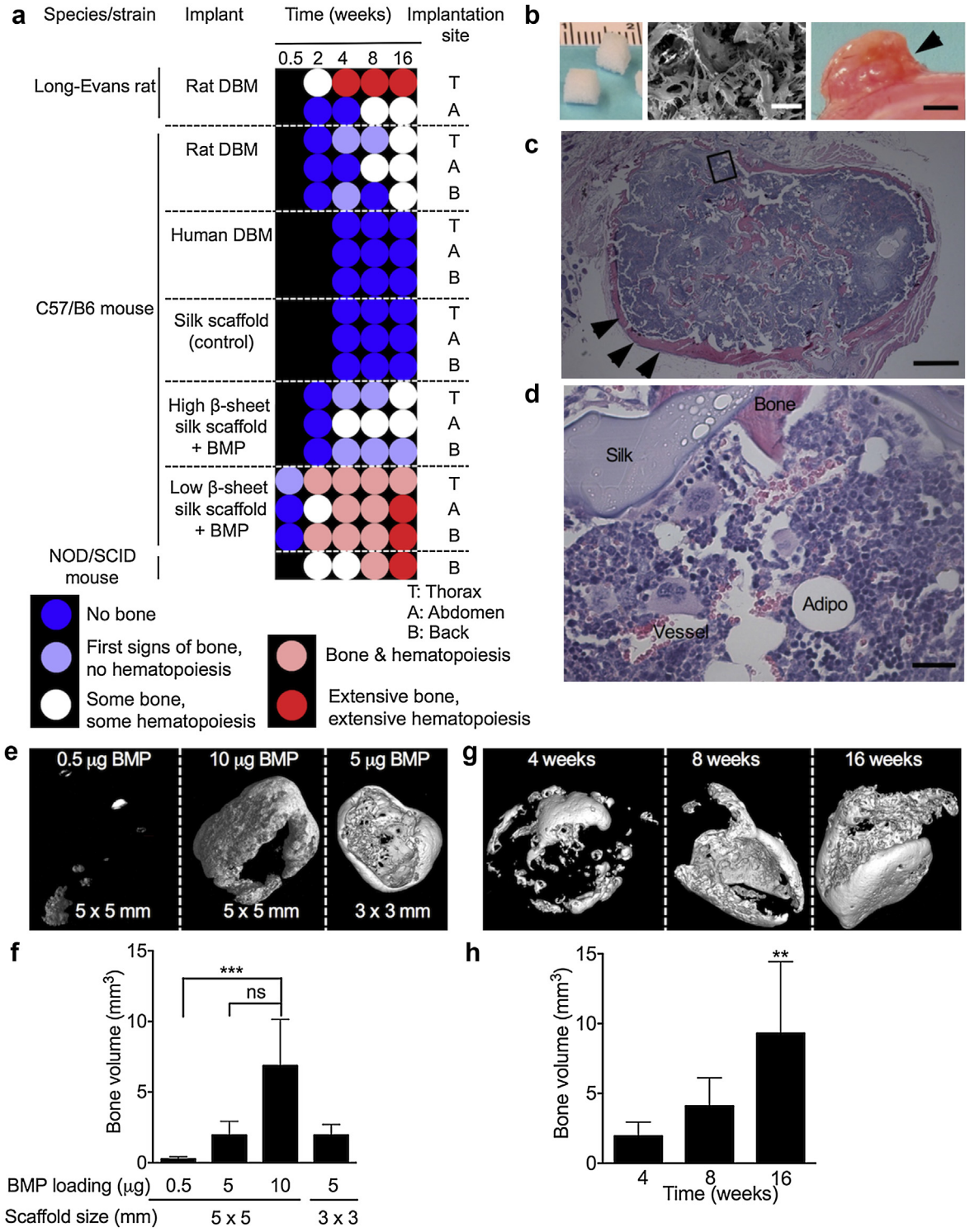

Fig. 1. *In vivo* tissue-engineered bone marrow. (a) Process optimization led to robust tissue-engineered bone and marrow. All silk scaffolds were 125 mm^3 and had a nominal BMP-2 loading of 5 μg, except control scaffold that contained no BMP-2. Rat demineralized bone matrix (DBM) from Long-Evans rats was used as a control [30]. (b) Macroscopic and scanning electron microscopy images (scale bar 200 μm) of scaffolds before and after 16 weeks *in vivo*. (c) Corresponding H&E histology of scaffold with extensive bone (arrows) and hematopoiesis (scale bar 500 μm). Magnified area is shown in (d) with sinusoidal blood vessels, hematopoiesis, mature bone and silk scaffold (scale bar 25 μm). (e) X-ray microtomographic images of 125 mm^3 silk scaffolds with different amounts of BMP-2 after 4 weeks *in vivo* and (f) corresponding quantification. (g) Representative images and (h) bone volume measurements for 125 mm^3 scaffolds loaded with 5 μg BMP-2 over time. (Error bars, s.d.; $^{**}P < 0.01$; $^{***}P < 0.001$; ns, not significant; $n \geq 3$).

While there was tumor engraftment for all animals (5/5), delivery of SDF-1 substantially reduced PC3 growth when compared to controls (Fig. 3c) but with minimal effects on tissue or bone volume (Fig. 3d). This observation was unexpected; one might speculate that SDF-1 delivery induced cancer stem cell quiescence [31] resulting in overall reduced metastatic growth. However, additional studies are needed to better understand the underlying biology in the BMM. We currently also do not know how this engineered BMM supports osteoblastic prostate cancer; this is a limitation of the current study.

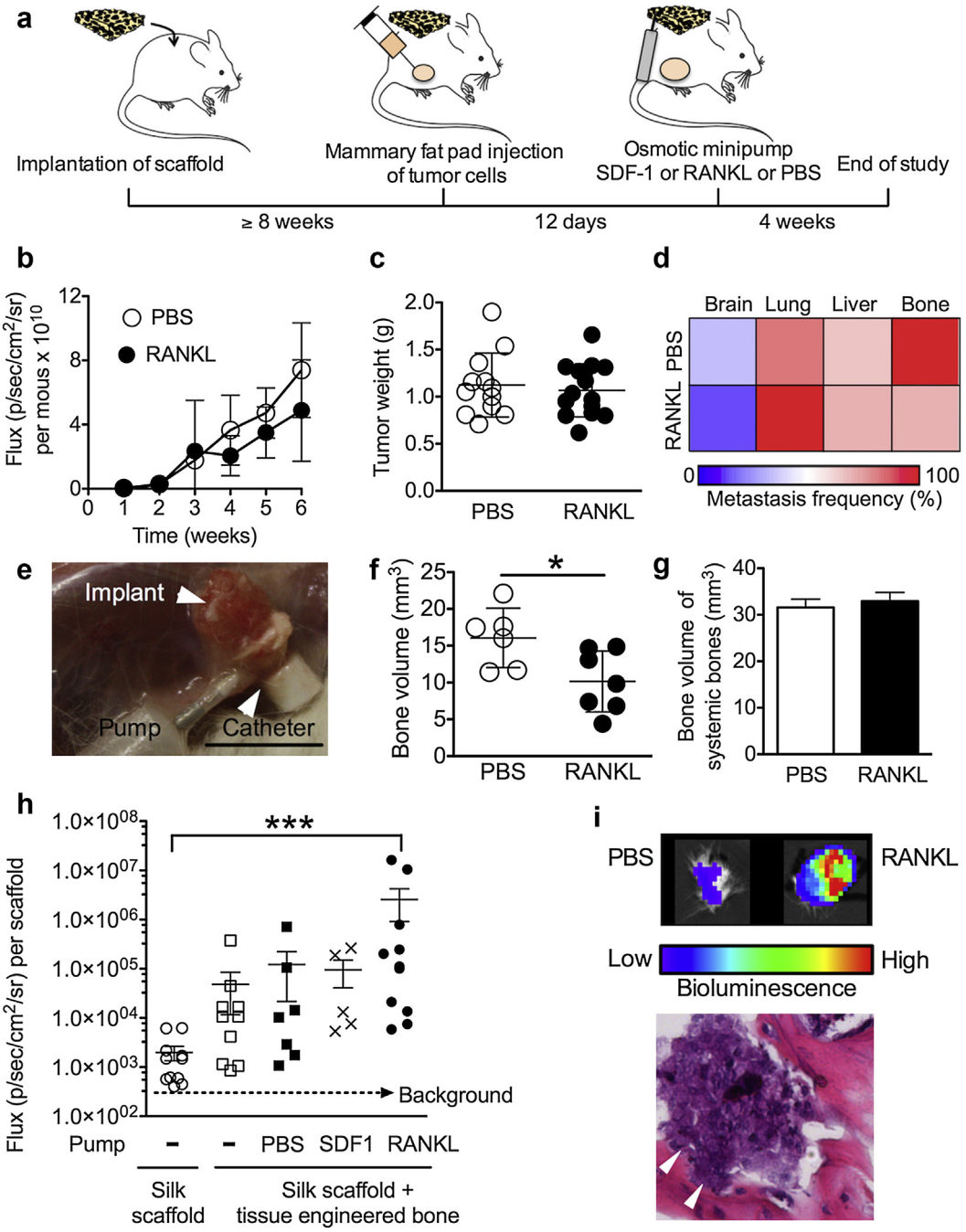

Fig. 2. Engineering a surrogate niche for metastasizing breast cancer cells. (a) Experimental design for the breast cancer study. Delivery of RANKL did not impact (b) primary tumor growth, (c) weight of the primary tumor, and (d) the extent of metastasis. (e) Image of the setup at the end of the study. (f) The RANKL scaffolds contained less bone as determined by X-ray microtomography, (g) but did not affect the bone volume of the systemic bones (femur + tibia + fibula of the front leg). (h) Bioluminescence quantification of explanted scaffolds at the end of the study. (i) Bioluminescence image of scaffolds with corresponding histology of the RANKL scaffold; errors denote areas of bone resorption. (Error bars, s.d.; $^{*}P < 0.05$; $^{***}P < 0.001$; $n \geq 3$).

Current implant-based models for the study of osteotropism of cancers are typically based on fresh bone chips [6,8,9] or marrow [10]; these are implanted subcutaneously or into the mammary fat pads of mice. Human fetal bone or marrow has been used in most cases [6,8], although materials from discarded femoral heads [9] have also been used. These studies are often designed to examine the interaction of human cancer cells with a humanized bone microenvironment; however, a number of limitations arise, as well as logistical and ethical challenges. For example, marrow models are plagued by poor control over the resulting bone microenvironment and by immunological mismatches between the bone marrow-derived immune cells and the human tumor cells (i.e., a potential marrow versus cancer response) (e.g., Ref. [10]). Bone chips have additional limitations and in general show poor vascularization, which often leads to necrosis and subsequent fibrosis [6,8,9]. The sharp edges of bone pieces can also often create wound problems or dehiscence in mice. Bone material from orthopedic surgery, in particular, provides little control over the quality of the bone, coupled with a low capacity to sustain hematopoiesis *in vivo* [9].

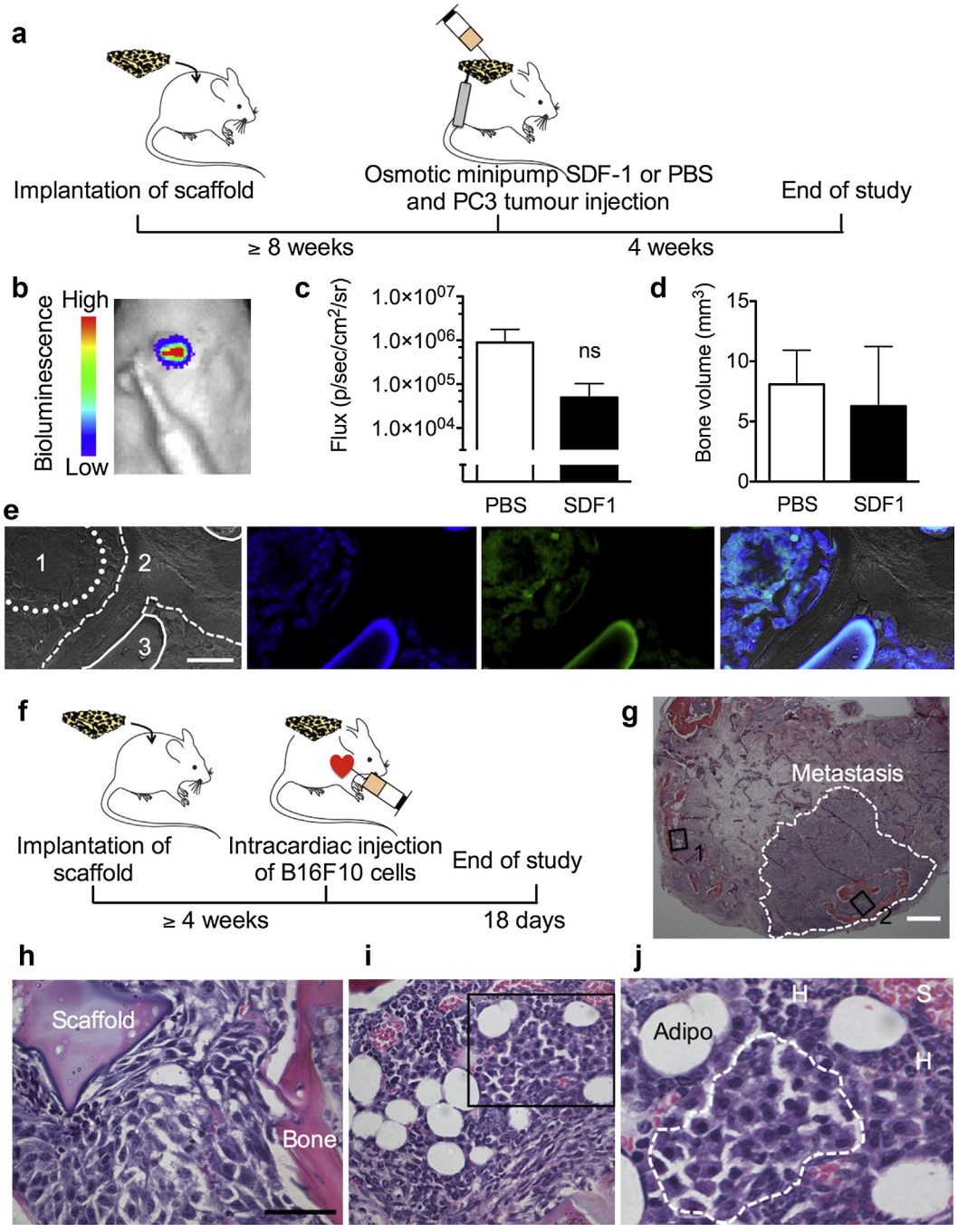

Fig. 3. Engineered bone marrow microenvironment for prostate cancer and experimental metastasis. (a) Experimental design for the prostate cancer study. (b) *In vivo* bioluminescence image of PC3 cells in scaffold with integrated osmotic minipump and (c) respective quantification of bioluminescence at week 2 (Error bars, s.d.; ns, not significant; n = 5). (d) Bone volume measurements of scaffolds at week 4. (e) Phase contrast image of (1) PC3 cells (dotted line), (2) tissue-engineered bone (dashed line), (3) silk scaffold (solid line) and fluorescent images corresponding to nuclei, PC3 cells and stacked images (scale bar 20 μm); all images were from the SDF-1 treatment group. (f) Design for the experimental metastasis study in immune-competent mice. (g) H&E histology of scaffold with macrometastasis (scale bar 400 μm). (h) Magnified view of area 2 and (i) area 1 from panel (g) (scale bar 50 μm). (j) Magnified view of selected area with micrometastasis (dashed line), hematopoiesis (H), sinusoidal vessels (S), and adipocytes (Adipo).

Humanized bone models are emerging as interesting model systems to study osteotropism of cancer [4]; however, they still require a significant amount of refinement. The current study demonstrates that the use of optimized silk scaffolds resulted in robust vascularization and bone and red marrow development in a syngenic setting, while none of the studied scaffolds showed adverse reactions in mice. This observation is in line with previous *in vivo* studies [32]. We selected silk because it is a biocompatible and biodegradable biopolymer with minimal endogenous biological activity [32,33]. Here control scaffolds (i.e., silk scaffolds with no BMP-2 functionalization) showed neither bone nor marrow development in mice (Fig 1a). Furthermore these control scaffolds showed the lowest capacity to capture metastatic cancer cells (e.g., Fig. 2h) indicating that at functional bone marrow is critical to lure cancer cells into a tissue-engineered BMM.

Historically, studies examining the BMM have relied on the epiphyses and diaphysis of long bones that are difficult to access

and cannot be readily subjected to local manipulation *in situ*. More recently, alternatives have been sought, for example, the calvarium for intravital high-resolution microscopy of the bone marrow [34]. However, local *in situ* manipulation of the calvarium has not been attempted and is expected to be technically challenging. Here, we applied a simple yet powerful method to study osteotropism of breast and prostate cancer cells *in situ*. The benefits of employing a tissue-engineered BMM are twofold. First, it provides a simple and robust method to generate a tissue-engineered BMM *in vivo*. Second, it provides flexibility to manipulate the BMM with the use of an osmotic minipump. These features will enable future studies of breast and prostate cancer as well as hematopoietic malignancies and bone marrow in general.

5. Conclusions

Manipulating the metastatic BMM *in vivo* is technically challenging as current models depend heavily on the host's skeleton, with occasional xenogenic or syngeneic models exploiting either fresh bone chips or the osteogenic properties of whole or fractionated marrow. We developed a simple yet powerful method to *in vivo* tissue engineer a BBM that could be readily manipulated *in situ* to understand the biology of bone metastasis. With the methodology described here, we demonstrated that a tissue-engineered BMM can serve as a surrogate niche for bone marrow metastasis. By selectively manipulating the engineered BMM, it was possible to either increase or suppress the number of metastatic cells at this site.

Author contribution

FPS and DLK conceived the study. FPS, JEB, and YS carried out experiments. All authors (FPS, JEB, YS, RST, DLK) designed research, discussed the results, and/or advised on the analysis. FPS wrote the manuscript with support from the other authors.

Acknowledgments

The authors thank Ilona Konrad for technical assistance. Some of the X-ray microtomography was performed at the Center for Nanoscale Systems (CNS), a member of the National Nanotechnology Infrastructure Network (NNIN), which is supported by the National Science Foundation under NSF award no. ECS-0335765. CNS is part of Harvard University. This research was supported by NIH grant P41 EB002520-05 (Tissue Engineering Resource Center) (DLK), The National Cancer Institute CA093900, CA163124, CA166307 (YS, RST), The Department of Defense W81XWH-11-1-0636 and W81XWH-14-1-0403 (YS, RST), the Prostate Cancer Foundation (YS, RST), a Mildred Scheel Postdoctoral fellowship from the German Cancer Aid (FPS), and a Marie Curie FP7 Career Integration Grant 334134 within the 7th European Union Framework Program (FPS).

Appendix ASupplementary data

Supplementary data related to this article can be found online at http://dx.doi.org/10.1016/j.biomaterials.2015.01.076.

References

[1] Weiss L. Comments on hematogenous metastatic patterns in humans as revealed by autopsy. Clin Exp Metastasis 1992;10:191–9.
[2] Coleman RE. Bone cancer in 2011: prevention and treatment of bone metastases. Nat Rev Clin Oncol 2012;9:76–8.
[3] Gupta GP, Massague J. Cancer metastasis: building a framework. Cell 2006;127:679–95.
[4] Holzapfel BM, Thibaudeau L, Hesami P, Taubenberger A, Holzapfel NP, Mayer-Wagner S, et al. Humanised xenograft models of bone metastasis revisited: novel insights into species-specific mechanisms of cancer cell osteotropism. Cancer Metastasis Rev 2013;32:129–45.
[5] Pettway GJ, McCauley LK. Ossicle and vossicle implant model systems. Methods Mol Biol 2008;455:101–10.
[6] Kyoizumi S, Baum CM, Kaneshima H, McCune JM, Yee EJ, Namikawa R. Implantation and maintenance of functional human bone marrow in SCID-hu mice. Blood 1992;79:1704–11.
[7] Nemeth JA, Harb JF, Barroso Jr U, He Z, Grignon DJ, Cher ML. Severe combined immunodeficient-hu model of human prostate cancer metastasis to human bone. Cancer Res 1999;59:1987–93.
[8] Yonou H, Yokose T, Kamijo T, Kanomata N, Hasebe T, Nagai K, et al. Establishment of a novel species- and tissue-specific metastasis model of human prostate cancer in humanized non-obese diabetic/severe combined immunodeficient mice engrafted with human adult lung and bone. Cancer Res 2001;61:2177–82.
[9] Kuperwasser C, Dessain S, Bierbaum BE, Garnet D, Sperandio K, Gauvin GP, et al. A mouse model of human breast cancer metastasis to human bone. Cancer Res 2005;65:6130–8.
[10] Shtivelman E, Namikawa R. Species-specific metastasis of human tumor cells in the severe combined immunodeficiency mouse engrafted with human tissue. Proc Natl Acad Sci U S A 1995;92:4661–5.
[11] Hutmacher DW, Loessner D, Rizzi S, Kaplan DL, Mooney DJ, Clements JA. Can tissue engineering concepts advance tumor biology research? Trends Biotechnol 2010;28:125–33.
[12] Lee J, Li M, Milwid J, Dunham J, Vinegoni C, Gorbatov R, et al. Implantable microenvironments to attract hematopoietic stem/cancer cells. Proc Natl Acad Sci U. S. A 2012;109:19638–43.
[13] Chan CK, Chen CC, Luppen CA, Kim JB, DeBoer AT, Wei K, et al. Endochondral ossification is required for haematopoietic stem-cell niche formation. Nature 2009;457:490–4.
[14] Rosen V. BMP2 signaling in bone development and repair. Cytokine Growth Factor Rev 2009;20:475–80.
[15] Reddi AH. Bone morphogenetic proteins: from basic science to clinical applications. J Bone Jt Surg Am 2001;83-A(Suppl. 1):S1–6.
[16] Bessa PC, Casal M, Reis RL. Bone morphogenetic proteins in tissue engineering: the road from laboratory to clinic, part II (BMP delivery). J Tissue Eng Regen Med 2008;2:81–96.
[17] Paget S. The distribution of secondary growths in cancer of the breast. Lancet 1889;133:571–3.
[18] Muller A, Homey B, Soto H, Ge N, Catron D, Buchanan ME, et al. Involvement of chemokine receptors in breast cancer metastasis. Nature 2001;410:50–6.
[19] Taichman RS, Cooper C, Keller ET, Pienta KJ, Taichman NS, McCauley LK. Use of the stromal cell-derived factor-1/CXCR4 pathway in prostate cancer metastasis to bone. Cancer Res 2002;62:1832–7.
[20] Mishra A, Shiozawa Y, Pienta KJ, Taichman RS. Homing of cancer cells to the bone. Cancer Microenviron 2011;4:221–35.
[21] Shiozawa Y, Pienta KJ, Taichman RS. Hematopoietic stem cell niche is a potential therapeutic target for bone metastatic tumors. Clin Cancer Res 2011;17:5553–8.
[22] Weilbaecher KN, Guise TA, McCauley LK. Cancer to bone: a fatal attraction. Nat Rev Cancer 2011;11:411–25.
[23] Rockwood DN, Preda RC, Yucel T, Wang X, Lovett ML, Kaplan DL. Materials fabrication from Bombyx mori silk fibroin. Nat Protoc 2011;6:1612–31.
[24] Arguello F, Baggs RB, Frantz CN. A murine model of experimental metastasis to bone and bone marrow. Cancer Res 1988;48:6876–81.
[25] Goldstein RH, Reagan MR, Anderson K, Kaplan DL, Rosenblatt M. Human bone marrow-derived MSCs can home to orthotopic breast cancer tumors and promote bone metastasis. Cancer Res 2010;70:10044–50.
[26] Seib FP, Kaplan DL. Doxorubicin-loaded silk films: drug-silk interactions and in vivo performance in human orthotopic breast cancer. Biomaterials 2012;33:8442–50.
[27] Kim UJ, Park J, Kim HJ, Wada M, Kaplan DL. Three-dimensional aqueous-derived biomaterial scaffolds from silk fibroin. Biomaterials 2005;26:2775–85.
[28] Wang Y, Rudym DD, Walsh A, Abrahamsen L, Kim HJ, Kim HS, et al. In vivo degradation of three-dimensional silk fibroin scaffolds. Biomaterials 2008;29:3415–28.
[29] Karageorgiou V, Tomkins M, Fajardo R, Meinel L, Snyder B, Wade K, et al. Porous silk fibroin 3-D scaffolds for delivery of bone morphogenetic protein-2 in vitro and in vivo. J Biomed Mater Res A 2006;78:324–34.
[30] Reddi AH, Huggins CB. Formation of bone marrow in fibroblast-transformation ossicles. Proc Natl Acad Sci U S A 1975;72:2212–6.
[31] Rentala S, Mangamoori LN. Isolation, characterization and mobilization of prostate cancer tissue derived CD133+ MDR1+ cells. J Stem Cells 2010;5:75–81.
[32] Kasoju N, Bora U. Silk fibroin in tissue engineering. Adv Healthc Mater 2012;1:393–412.
[33] Omenetto FG, Kaplan DL. New opportunities for an ancient material. Science 2010;329:528–31.
[34] Lo Celso C, Lin CP, Scadden DT. In vivo imaging of transplanted hematopoietic stem and progenitor cells in mouse calvarium bone marrow. Nat Protoc 2011;6:1–14.

Journal of Cancer Stem Cell Research (2015), 3:e1005
 ISSN 2329-5872
DOI: 10.14343/JCSCR.2015.3e1005
http://cancerstemcellsresearch.com

Research Article Open Access

The role of osteoclasts in early dissemination of prostate cancer tumor cells

J.L. Zalucha[1], Y. Jung[1], J. Joseph[1], J. Wang[1], J.E. Berry[1], Y. Shiozawa[1,2], and R.S. Taichman[1,*]

[1]Department of Periodontics and Oral Medicine, University of Michigan School of Dentistry, Ann Arbor, MI 48109, USA, [2]Department of Cancer Biology and Comprehensive Cancer Center, Wake Forest University School of Medicine, Winston-Salem, NC 27157, USA.

Abstract: Prostate cancer (PCa) is one of the most common neoplasms that metastasize to bone. The aim of this study was to determine if osteoclasts play a role in the seeding of disseminated tumor cells to the bone marrow by mobilizing hematopoietic stem cells (HSCs) out of their marrow niche. Human PC-3^{Luc} cells were introduced into male SCID mice by intracardiac injection after mice were treated with the antiresorptive agent Zoledronic Acid (bisphosphonate (BP)) and/or AMD3100, which mobilizes HSCs out of the marrow. Short term homing of PC-3 was assessed at 24 hours by QPCR for human *Alu* and HSC number was determined by FACS. Mice also received pre and/or post treatments of BP by intraperiteneal injections, in addition to PC-3^{Luc} by intratibial injections. TRAP assays were used to determine the osteoclast (OC) number in both studies. AMD3100 enhanced the release of HSCs from the bone marrow, while BP increased the retention of HSCs. PCa entry into bone was facilitated in AMD3100, BP, and AMD3100+BP treatments. Before PCa injection, the number of TRAP+ OC was increased in mice treated with AMD3100, while treatment with BP resulted in relatively lower TRAP+ OCs. TRAP+ OCs were not detected in the AMD3100 + BP treatment. After PCa injection, however, the number of TRAP+ OCs was dramatically increased, but did not differ significantly amongst the treatment groups. The pre and post BP treatments in the Nude mice decreased the size of PCa lesions in the tibia compared to the control. The results indicate that OC activation is not necessary for PCa metastasis to bone at the earliest stages. These findings are critical in proving that OCs' contribution to metastasis occurs during the growth phase of the tumor rather than at the initiation phase.

Keywords: prostate cancer, disseminated tumor cells, osteoblasts, osteoclasts, cancer stem cells.

INTRODUCTION

Breast and prostate cancer (PCa) represent solid tumors that frequently metastasize to the bone marrow, causing alterations of bone integrity and function, and resulting in a major source of morbidity and mortality. The process of metastasis has been characterized as a multistep cascade, in which tumor cells must first undergo an epithelial to mesenchymal transition to a more motile phenotype, enter vascular or lymphatic structures, and ultimately reverse the transition at the site of metastasis. Previous studies have demonstrated that SDF-1 (stromal cell-derived factor-1 or CXCL12) and its receptor, CXCR4 represent a major mechanism in PCa's metastasis to bone [1, 2]. We have recently shown that the binding of CXCL12 to CXCR4 activates the expression of receptors which facilitate the localization of disseminated tumor cells (DTCs) to the bone marrow microenvironment [3, 4].

More recently, we demonstrated that circulating PCa cells target the 'niche,' in marrow that houses hematopoietic stem cells (**HSC**) [5]. We used a micrometastasis model of PCa metastasis to demonstrate that tumor cells directly compete with HSCs for occupancy of the endosteal HSC niche in during bone marrow transplantation [5]. In fact, based upon observations of their proximity to osteoblasts, it appears very likely that cancer stem cells (**CSC**s) expressing the CD133^{+}/CD44^{+} phenotype preferentially compete for occupancy of the osteoblastic HSC niche [5]. Once in the niche, metastatic cells, like HSCs, may be mobilized back into the peripheral blood using agents that mobilize HSCs [5]. Critically, HSCs co-localize with DTCs to the endosteal bone surfaces, and when the number of HSC niches was altered, DTC numbers in marrow responded accordingly [5, 6]. Importantly, increasing numbers of DTCs in marrow resulted in HSCs mobilizing out of the marrow and into progenitor cell

*Correspondence: Russell S. Taichman, D.M.D., D.M.Sc., Department of Periodontics and Oral Medicine, University of Michigan School of Dentistry, Room 3307, 1011 North University Avenue, Ann Arbor, MI, 48109-1078, USA. Phone: 1-734-764-9952; Fax: 1-734-763-5503; E-mail: rtaich@umich.edu
Received: May 5, 2015; Revised: May 15, 2015;
Accepted: May 15, 2015

pools and the peripheral blood. Together, these findings demonstrate that PCa and HSCs compete for the endosteal HSC niche and use the same mechanisms to access and egress the niche, and provide direct evidence that this HSC niche plays a central role in bone metastases.

The mechanism by which HSCs are mobilized into the peripheral blood in response to cytokines has been an area of active investigation. Recent work has demonstrated that secretion of MMP-9, cathepsin G, and cathepsin K by osteoclasts results in the digestion of CXCL12, leading to the release of HSCs into the blood [1]. Likewise, osteoclastic activity appears to be essential to PCa metastasis. In part, as PCa cells may express the receptor activator of nuclear factor kB ligand, or RANKL, which stimulates osteoclasts and bone resorption osteoclastic activity may be induced facilitating metastasis and growth [1, 2]. Since osteoclasts activate HSC mobilization, the creation of empty niches may make an increase in PCa metastasis more likely [7].

Paralleling the role that they play in HSC biology, osteoclasts are also involved in metastastic growth of solid tumors in bone, including breast and prostate cancer. In fact, the activation of osteoclastic activity by tumor cells releases growth factors and cytokines sequestered in bone matrix, which contributes to the growth of the tumors, a process termed "the vicious cycle." In this model, tumor cell–host interactions result in boney lesions which are predominately osteoclastic (breast cancer) or osteoblastic (PCa) boney lesions.

Based upon the active role that osteoclasts play in regulating HSC retention in the niche and in tumor growth, we speculated that osteoclasts may play a central role in the initial seeding of tumor cells into the HSC niche. Accordingly, we used our ability to track tumor cells with *Q*PCR in the context of osteoclast inhibition with bisphosphonates to question whether osteoclasts participate in the earliest seeding of PCa into the HSC niche - an activity independent of their role in stimulating tumor growth via the "vicious cycle". The clinical implication is that if osteoclasts play a role in the initial seeding of the HSC niche by solid tumors, then the use of agents which modify osteoclastic activities (e.g. bisphosphonates, cathepsin V inhibitors and decoy receptor for osteoblastic RANKL) should be initiated far earlier for individuals with high grade tumor types.

METHODS

Cell culture

PC-3 (CRL-1435) prostate cancer cell line was obtained from the American Type Culture Collection (Rockville, MD). PC-3^{Luc} cells were constructed by stably transducing PC-3 cells with a GFP-luciferase lentivirus, as previously described. Cells were cultured in RPMI 1640 (Invitrogen, Carlsbad, CA), supplemented with 10% fetal bovine serum (**FBS**; Invitrogen) and 1% penicillin-streptomycin (Invitrogen), and maintained at 37°C, 5% CO_2, and 100% humidity.

In vivo metastasis assays

All experimental procedures were approved by the University of Michigan Committee for the Use and Care of Animals (UCUCA). In the first set of animal investigations, male 5–6 week old severe combined immune deficient mice (SCID) were injected with 1×10^6 PCa cells by intracardiac injection (*i.c.*) under isoflurane anesthesia (Figure 1A). In order to mobilize HSCs out of the niche, mice were administered AMD3100 (AMD) (Sigma-Aldrich, St. Louis, MO) or vehicle (0.9% saline) by intraperitoneal injection at 5 mg/kg (100 µl) per day for 5 days preceeding the tumor inoculation. To limit osteoclastic activity, which could participate in PCa seeding to the niche, some of the animals were administered Zoledronic Acid (a bisphosphonate) (Novartis Pharma AG, Basel, Switzerland) [8–10] by intravenous injection (3 µg/kg/day) for 3 and 7 days preceding the *i.c.* injection of tumor cells. Additional groups included no treatment controls and animals treated with both AMD3100 and bisphosphonate.

A second set of studies was designed to evaluate the role of osteoclasts after PCa cells had arrived in the bone marrow. For this study, PC-3^{Luc} cells were inoculated into male nude mice by intratibial (*i.t.*) injection. Recipient mice were randomized into treatment groups which included pretreatment with vehicle or bisphosphonate (3 µg/kg/day) for 5 days preceding *i.t.* injection of tumor cells, or twice per week for 4 weeks following *i.t.* injection; or treatment with bisphosphonate or vehicle preceding and following tumor inoculation. All mice were sacrificed at 4 weeks following *i.t.* tumor inoculation. BioLuminescent Imaging was performed once a week for the four weeks following the *i.t.* injection at the University of Michigan Small Animal Imaging Resource facility using a CCD IVIS system with a 50-mm lens (Xenogen Corp.) and the results were analyzed using LivingImage software (Xenogen). Here the mice were injected with luciferin (40 mg/mL) *i.p.* and ventral images were acquired 15 min postinjection under 1.75% isofluorane/air anesthesia. Total tumor burden of each animal was calculated using regions of interest (ROI) that encompassed the entire animal. For tibia-specific measurements, ROI values were recorded for each individual tibia. The size of tibia-specific lesions was quantified by luminescent signal evident at each week, and the luminescence value of the lesion at week 4 were used in results.

Real time PCR (*Q*PCR)

Tumor cell numbers were assessed using primer/probe sets including those targeting human Alu TaqMan probes (F–5′-CAT GGT GAA ACC CCG TCT CTA-3′, R–5′-GCC TCA GCC TCC CGA GTA G-3′, TaqMan probe–5′-FAM-ATT AGC CGG GCG TGG TGG CG-TAMRA-3′, Applied Biosystems). The data were normalized to

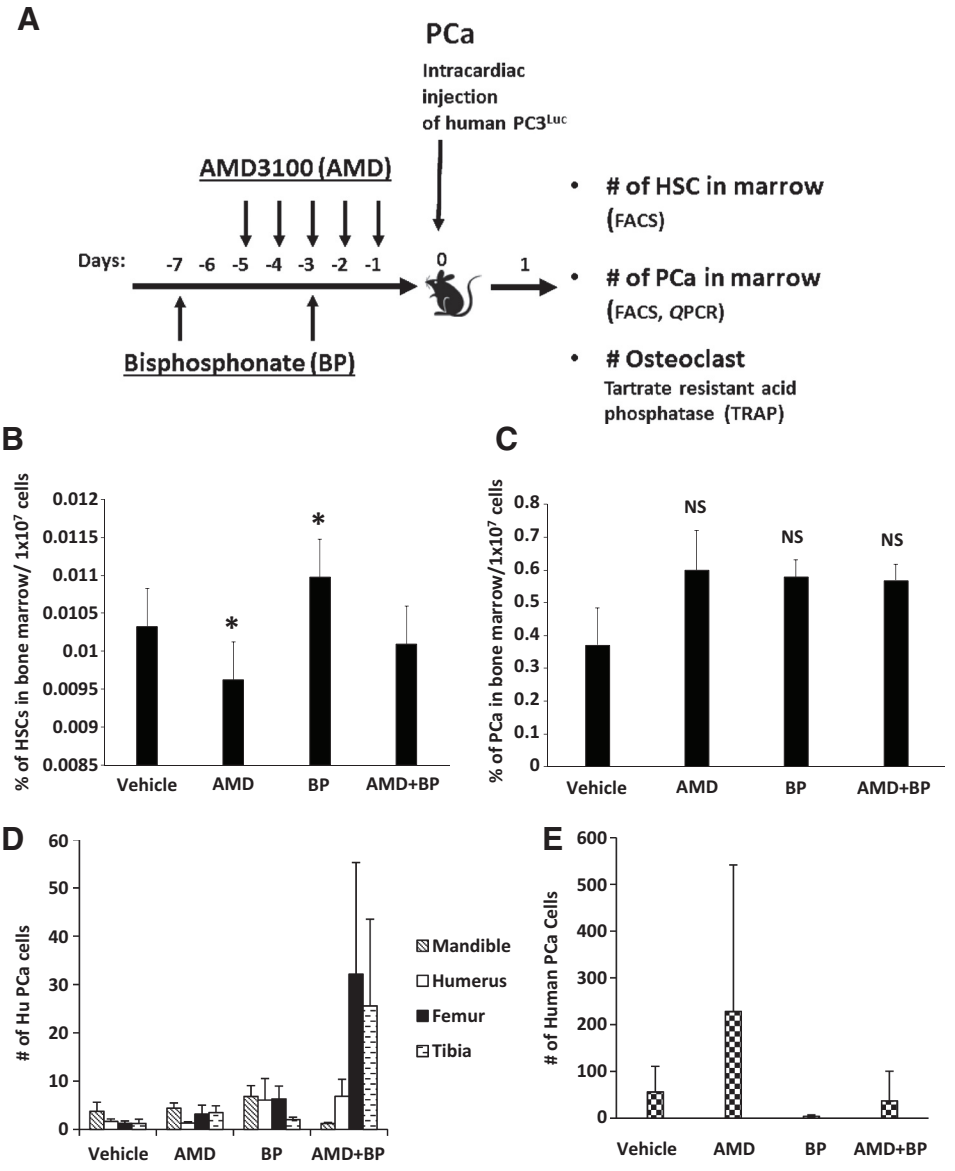

Figure 1. Osteoclasts are not critical for early colonization of DTCs into the bone marrow. (**A**) Experimental outline illustrating the methods and injection strategy for delivery of vehicle, AMD3100 (AMD), and Bisphosphonate (BP) treatments along with inoculation of human PCa into mice. (**B**) HSC numbers in bone marrow were analyzed by FACS. (**C**) The short term homing capabilities of DTCs in marrow were evaluated after 24 hours by quantifying HLA-expressing PCa cells in marrow. Data are presented as the mean ± standard error ($n = 5$). (**D, E**) Short term homing of prostate cancer *in vivo* to bone by real time PCR (*Q*PCR). The short term homing capabilities were evaluated after 24 hours by assessing *Q*PCR for *Alu* and data were normalized to total mouse β-actin. Data are presented as the mean ± standard error ($n = 5$) where significance was determined by using a Kruskal-Wallis test and Dunn's multiple comparisons with the level of significance set at $^*P < 0.05$.

mouse tissue β-Actin (Mm00607939_s1). *Q*PCR was performed using standard techniques. RT products were analyzed by *Q*PCR in TaqMan® Gene Expression Assays, using 15.0 µl of TaqMan® Universal PCR Master Mix (Applied Biosystems), 1.5 µl of TaqMan® Gene Expression Assay (forward and reverse primers at 18 µM and Taqman probe at 5 µM), 1 µl of the RT product, and 12.5 µl of RNAse/DNAse-free water in a total volume of 30 µl. Reactions without template and/or enzyme were used as negative controls. The 2nd step PCR reaction (95°C for 30 seconds, 60°C) ran for 40 cycles after an initial single cycle of 95°C for 15 minutes. The PCR product was detected using an ABI PRISM 7700 instrument (Applied Biosystems). RNA quantity (C_R) was normalized to the housekeeping gene β-Actin control by using the formula $C_R = 2^{(40\text{-Ct of sample})-(40\text{-Ct of control})}$. The threshold cycle (Ct) is the cycle at which a significant increase in fluorescence occurs.

Fluorescence-activated cell sorting (FACS)

The flow cytometric analyses and fluorescence-activated cell sorting (FACS) were performed on a FACS Aria dual-laser flow cytometer (Becton Dickinson, Franklin Lakes, NJ) and data were analyzed with DIVA software (Becton Dickinson). BD cytometer setup and tracking beads kit (BD Biosciences, Franklin Lakes, NJ, Cat no. 642412) are used for the daily instrument standardization and validation procedure. Sorting calibration was performed before each sort by drop-delay using Accudrop beads (BD Biosciences, Cat no. 345249), populations for sorting were gated by forward and side scatter to eliminate the presence of doublets. Sorting of these gated cells was done using a 100-µm nozzle at 20 psi in purity mode. Cells were triturated and filtered through a nylon screen (40 µm; BD Falcon, Bedford, MA) to obtain single-cell suspensions.

For determining HSCs the cells were incubated first with an antibody cocktail of anti-CD150PE (Clone TC15-

12F12.2, BioLengend, San Diego, CA), CD48^{FITC} (Clone BCM-1) and CD41^{FITC} (Clone MWReg30), cKit$^{PE\text{-}Cy7}$ (Clone 2B8) and SCA-1^{APC} Clone E13-161.7) for twenty minutes on ice. Hematopoietic stem cells were sorted on a FACS Vantage dual laser flow-cytometer (Becton Dickinson, San Jose, CA) by gating on cells that are Sca-1^{+}cKit^{+}CD150^{+}CD41^{-}CD48^{-}. For DTCs, the bone marrow was flushed from the femurs of euthanized mice and depleted of hematopoietic-lineage cells using a Lineage Cell Depletion Kit (Miltenyi Biotec, 130-092-211) was used. DTCs were identified in lineage depleted murine marrow using a fluorescein isothiocyanate (FITC)-human leukocyte antigens-A, B, and C loci (HLA-ABC) antibody (Biolegend, San Diego, CA, Cat no. 311404).

TRAP staining

Mouse femurs were fixed in 10% neutral buffered formalin (Sigma HT50) for 24 h at room temperature. Following fixation, the samples were decalcified in 10% EDTA, pH 7.5, for 20 days and embedded in paraffin. Deparaffinized 5 μm sections were rehydrated and stained for TRAP activity ((Kamiya Biolmedical Comp, Seattle WA, KT-008) according to the manufacturer's instructions [2]. TRAP positive, multinucleated cells were quantified in random high power fields under light microscopy at 20X.

Statistical analyses

All experiments were performed at least three times with similar results and representative assays shown. Numerical data is expressed as mean ± standard error. Statistical analysis was performed by ANOVA or Student's *t* test using the GraphPad Instat statistical program (GraphPad Software, San Diego, CA) with significance at $P < 0.05$. For the *Q*PCR assays, a Kruskal-Wallis test and Dunn's multiple comparisons tests were utilized with the level of significance set at $P < 0.05$.

RESULTS

The purpose of these studies was to determine the role that osteoclasts play in the early dissemination of tumor cells to the bone marrow niche. Previously, we demonstrated that DTCs target the HSC niche in marrow as a site for homing, so for these studies we used AMD3100 to mobilized HSCs and progenitor populations out of the niche to provide additional sites for early metastasis of DTCs (Figure 1A). Similarly, the bisphosphonate was employed to limit osteoclastic activity during the initial seeding of DTCs into the marrow. As shown in Figure 1B, HSC numbers identified by FACS in marrow decreased in response to AMD3100. Surprisingly, bisphosphonate treatment resulted in enhanced levels of HSCs present in the bone marrow, presumably by inhibiting the normal osteoclastic role in stem cell mobilization. The combined treatment of both AMD3100 and bisphosphonate did not result in a change of HSC numbers in marrow relative to vehicle.

Mobilization of HSCs out of the niche with AMD3100 increased the number of DTCs identified by FACS staining in the bone marrow niche, albeit not to a significant degree in this short term homing study (Figure 1C). Bisphosphonate treatment also tended to increase the overall number of DTCs present in the marrow, suggesting that osteoclasts may not be critical for the initial colonization of the marrow by DTCs. Consistent with the other groups, the combined treatment of animals with AMD3100 and bisphosphonate facilitated more DTCs in the marrow relative to vehicle alone (Figure 1C); however, these changes were not found to result in significant differences between the treatment and the non-treatment groups, or between treatment groups (Figure 1C).

After sacrificing the animals, the long bones and selected tissues were isolated and tumor cells quantified using *Q*PCR for human *Alu* against a standard curve of human PCa cells mixed with murine marrow, and normalized against total mouse β-actin. As shown in Figure 1D for the mandible, humerus, femur and tibia, there were no significant differences in the number of DTCs present across the treatment groups. In the peripheral blood, while there were no significant differences in the number of PCa identified across the treatment groups, there was a trend for more PCa cells in the blood following AMD3100 treatments, and less following bisphosphonate administration (Figure 1E).

To validate that the treatment with bisphosphonate resulted in osteoclast inhibition, immunohistochemistry for TRAP was performed in long bone samples. Compared to untreated controls, AMD3100 treatment alone resulted in the enhanced expression of TRAP positive multinucleated cells in the long bones of the animals, whereas pretreatment with bisphosphonate reduced the basal levels of TRAP staining in the long bones, however these differences were not statistically significant. Importantly, when PCa was not present, AMD3100 treatment in conjunction with the bisphosphonate reduced the expression of TRAP staining compared to AMD3100 treatment alone. As demonstrated in Figure 2A and quantified in Figure 2B, a significant increase in TRAP staining was evident in the vehicle treated animals even as early as 24 h after injection of PCa. This dramatic increase in TRAP suggests that the presence of PCa cells is rapidly able to activate osteoclastic activity, and this activity remained elevated despite treatment with AMD3100, bisphosphonate, alone or in combination.

To validate that our model was sufficient to determine whether osteoclasts play a role in early tumor dissemination, we further explored the role of osteoclasts in a model where tumor cells are placed directly into the marrow (Figure 3A). Following *i.t.* injection, tumor growth in the vehicle treated animals followed the expected pattern of tumor growth and by 4 weeks the BLI signal intensity prompted us to terminate the study

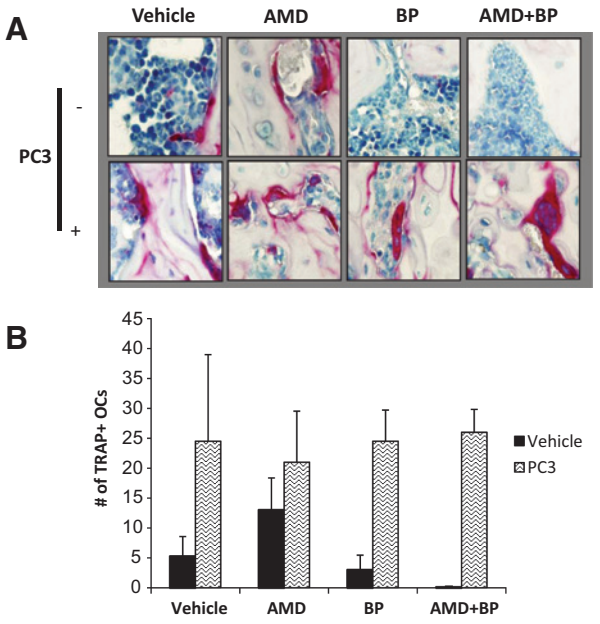

Figure 2. Quantification of osteoclasts during short term PCa homing. After fixation and longitudinal sectioning across an entire femur, TRAP staining was performed. Osteoclasts were defined as TRAP staining positive cells with ≥3 nucli. (**A**) Co-administration of Bisphosphonate and AMD3100 reduces the osteoclast numbers in the absence of prostate cancer but did not exert the same effect in the presence of prostate cancer. The femurs were decalcified and stained for TRAP activity, as shown in Figure 2A. (**B**) Quantification of Figure 2A. Data are presented as the mean ± standard error ($n = 5$).

(Figure 3B). Pretreatment of animals with bisphosphonate prior to inoculation with PCa reduced overall tumor growth in the *i.t.* model; however these differences did not rise to the level of statistical significance. Similarly, treatment of the animals with bisphosphonate after tumor inoculation reduced overall tumor growth during the four-week study, but these differences did not prove to be significant relative to the vehicle treated animals. Osteoclast inhibition prior to and after inoculation of tumor cells directly into the tibia did however significantly blunt tumor growth compared to vehicle treated controls in this model.

DISCUSSION

The use of osteoclast inhibitors is a mainstay of cancer therapy for those individuals with skeletal metastases. Conventional wisdom dictates that inhibition of osteoclast activity in a metastatic environment may help to reduce growth of tumors in bone. Previously, we established an experimental model, which demonstrated that DTCs of PCa are able to compete for occupancy of the HSC niche [5]. Osteoclasts are thought to play a role in HSC mobilization, and are also known to support tumor growth in bone through activation of what has been termed a "vicious cycle", in which bone resorption releases factors which stimulate tumor growth, which in turn stimulates osteoclastic activity. We addressed whether an additional function of osteoclastic activity is involved in regulating the initial seeding of DTCs into the HSC niche.

The results from this study demonstrate that osteoclastic inhibition with bisphosphonate did not influence the number of DTCs identified in the bone marrow of animals with in 24 h of inoculation. Yet when tumors were preestablished in the bones of the animals, osteoclastic inhibition played a role in limiting tumor growth. Within the limits of our studies, we observed that osteoclasts are not necessary for the initial establishment of DTCs from PCa in the marrow (Figure 4). While osteoclasts are apparently not involved in these initial processes, it is likely that multiple cells and molecules regulate the establishment of initial footholds for DTCs in marrow. Many of these are likely to include factors which regulate the adhesion and migration out of the circulation and into the bone marrow parenchyma, including endothelial cells, vascular endothelial adhesion molecules (e.g. VCAM-1), and HSC-regulating factors, including stromal-derived factor-1 (SDF-1 or CXCL12), as well as physical factors including the number and occupancy of HSC niches. Yet, osteoclasts are clearly important for tumor growth within the skeleton, as has been shown clinically with potent osteoclast

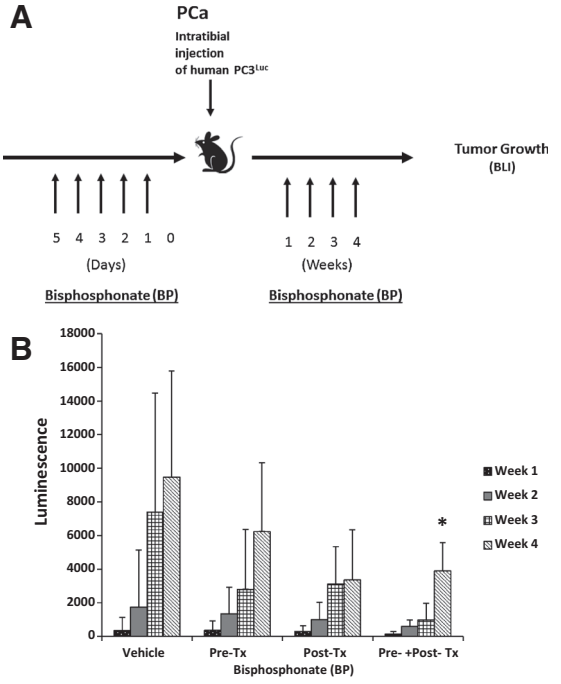

Figure 3. Osteoclastic activity participates in supporting tumor growth after dissemination. (**A**) Experimental outline illustrating the methods and injection strategy for injection of bisphosphonate (BP) treatments prior to (Pre-Tx) and following (Post-Tx) PCa injection. (**B**) Quantification of tumor growth over time by bioluminescent imaging following AMD and BP treatments. The data demonstrate that tumor growth was best inhibited by the combined treatment of bisphosphonate delivered pre and post tumor implantation. The mice were imaged every 4 weeks, with Bio-luminescent Imaging, after intra-tibial injection of $PC3^{Luc}$ cells. Data is presented as the mean ± standard error ($n = 3$).

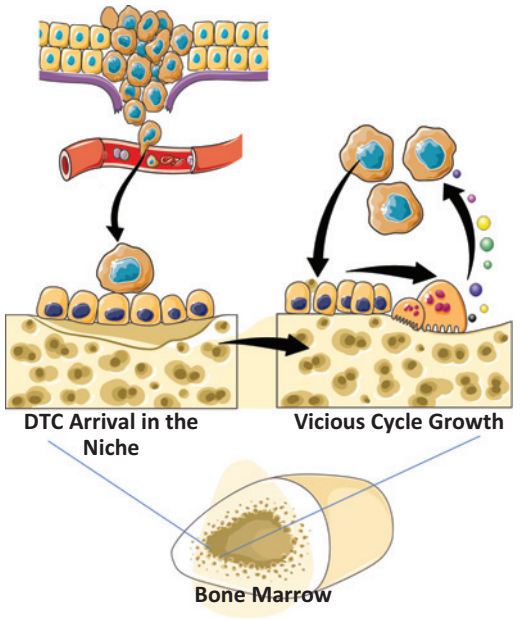

Figure 4. Model For Osteoclastic Support for DTC Dissemination and Metastatic Growth. Osteoclasts play a significant role in regulating HSC number in bone marrow by regulating HSC egress during mobilizing events. Conversely, occupancy of the HSC niche by DTCs during the initial seeding of DTCs is not regulated significantly by osteoclastic activity. Yet once in the niche, osteoclastic activity participates in the support of tumor growth in marrow as described in the Vicious Cycle Theory [13].

inhibitors (bisphosphonates and denosumab), which decrease the risk of skeletal related events (SRE) and thus improve quality of life and survival (Figure 4).

One important caveat, which pertains to our findings and is of particular note, is that osteoclastic TRAP activity was increased in the marrow of the experimental animals as early as 24 h after introduction of PCa into the circulation. This also occurred in animals that were treated with bisphosphonate prior to tumor inoculation. These observations suggest that preexisting osteoclast precursors or mature osteoclasts in our animals were not completely inhibited by our treatments and thus we can not completely rule out that osteoclasts may play in regulating early metastatic seeding. However, our findings that AMD3100 and bisphosphonates do regulate HSC mobilization as predicted, suggests that perhaps the activities of osteoclasts may have many different functions, some of which are not exclusively related to bone turnover. For example, osteoclasts may produce factors which regulate HSC homing independent of tissue resorption. However this notion requires further proof and would prove difficult to dissociate from the known role that HSCs play in bone formation [11].

From a clinical perspective, our findings suggest that osteoclast inhibition therapy for patients with primary disease, aimed at preventing the establishment of DTCs in bone, is not likely to prove beneficial. There are several reasons for this conclusion. First and foremost, by the time of diagnosis of PCa, tumor cells have already disseminated, in the majority of cases [12]. The reason for this is unclear other than to surmise that shedding of tumor cells from a primary tumor must occur relatively early in tumor progression. Thus, if conventional wisdom prevails, in order to have an effect on the prevention of the establishment of DTCs in marrow, it would be necessary to place all men on prophylactic osteoclastic inhibition therapy; for which enforcement would be impossible and benefits might well be minimal. Moreover, most men who are diagnosed with PCa are cured with local/regional or systemic therapeutics, so addition of DTC prophylaxis for most men would not provide any additional therapeutic gain. However for those who do progress to develop skeletal related events (SREs), osteoclastic inhibition used to target dissemination events would probably not be effective since, as our study shows, the establishment of DTCs in marrow appears to be osteoclast-independent.

There are however constraints to our studies. First is the inherent limitation of examining the biology of human PCa in a murine model, which requires the use of immune deficient mice. Moreover, the intracardiac and intratibial injection models bypass the establishment of true circulating tumor cells (CTCs) from a primary tumor in the marrow, and therefore also bypass the mechanisms that may regulate osteoclastic activity prior to the arrival of CTCs/DTCs. This is a real possibility given the rapid induction of TRAP staining in the marrows of animals injected with PCa 24 h prior to sacrifice. Second, the bisphosphonate used in this animal system did not produce absolute elimination of osteoclastic activity. Given the limited numbers of DTCs found in these studies in the marrow of the untreated animals, incomplete blockade is likely to produce bias in our data interpretation.

In summary, our data suggests that osteoclasts are not critical in the earliest stages of metastasis to the bone marrow. Therefore the data suggests that targeting osteoclastic activity prior to DTC seeding is not likely to prove beneficial in a clinical setting. However, once established in bone, osteoclastic activities do play a significant role in driving tumor growth once tumor cells become established in bone. Moreover, our data suggests that osteoclastic induction may be an early response of osteoclastic precursors early in skeletal metastasis, and therefore the induction of these precursors could be indicative of subsequent growth and therefore may serve as an early predictor of the clinical course of disease. Clearly further investigation is warranted.

CONFLICT OF INTEREST

The authors declare no conflict of interest.

ACKNOWLEDGMENTS

J. L. Zalucha was funded by a student fellowship by the American Association for Dental Research (AADR), and the University of Michigan School of Dentistry

Student Research and Pathways Programs. This work is directly supported by the National Cancer Institute (CA093900 to K.J. Pienta and R.S. Taichman, CA163124 to Y. Shiozawa, K.J. Pienta, and R.S. Taichman, U54CA143803 to K.J. Pienta, CA143055 to K.J. Pienta), the Department of Defense (W81XWH-14-1-0403 to Y. Shiozawa, and W81XWH-11-1-0636 to K.J. Pienta, K.J. Pienta, and R.S. Taichman), and the Prostate Cancer Foundation (Y. Shiozawa, K.J. Pienta, and R.S. Taichman). K.J. Pienta receives support as an American Cancer Society Clinical Research Professor.

REFERENCES

[1] Kollet O, Dar A, Lapidot T. The multiple roles of osteoclasts in host defense: bone remodeling and hematopoietic stem cell mobilization. Annu Rev Immunol 2007, 25:51–69.

[2] Kollet O, Dar A, Shivtiel S, Kalinkovich A, Lapid K, Sztainberg Y, Tesio M, Samstein RM, Goichberg P, Spiegel A, et al. Osteoclasts degrade endosteal components and promote mobilization of hematopoietic progenitor cells. Nat Med 2006, 12:657–64.

[3] Wang J, Shiozawa Y, Wang J, Wang Y, Jung Y, Pienta KJ, Mehra R, Loberg R, Taichman RS. The role of CXCR7/RDC1 as a chemokine receptor for CXCL12/SDF-1 in prostate cancer. J Biol Chem 2008, 283:4283–94.

[4] Sun YX, Fang M, Wang J, Cooper CR, Pienta KJ, Taichman RS. Expression and activation of alpha v beta 3 integrins by SDF-1/CXC12 increases the aggressiveness of prostate cancer cells. Prostate 2007, 67:61–73.

[5] Shiozawa Y, Pedersen EA, Havens AM, Jung Y, Mishra A, Joseph J, Kim JK, Patel LR, Ying C, Ziegler AM, et al. Human prostate cancer metastases target the hematopoietic stem cell niche to establish footholds in mouse bone marrow. J Clin Invest 2011, 121:1298–1312.

[6] Visnjic D, Kalajzic Z, Rowe DW, Katavic V, Lorenzo J, Aguila HL. Hematopoiesis is severely altered in mice with an induced osteoblast deficiency. Blood 2004, 103:3258–64.

[7] Shiozawa Y, Havens AM, Pienta KJ, Taichman RS. The bone marrow niche: habitat to hematopoietic and mesenchymal stem cells, and unwitting host to molecular parasites. Leukemia 2008, 22:941–50.

[8] Wang HL, Weber D, McCauley LK. Effect of long-term oral bisphosphonates on implant wound healing: literature review and a case report. J Periodontol 2007, 78:584–94.

[9] Schneider A, Kalikin LM, Mattos AC, Keller ET, Allen MJ, Pienta KJ, McCauley LK. Bone turnover mediates preferential localization of prostate cancer in the skeleton. Endocrinol 2005, 146:1727–36.

[10] Pettway GJ, Meganck JA, Koh AJ, Keller ET, Goldstein SA, McCauley LK. Parathyroid hormone mediates bone growth through the regulation of osteoblast proliferation and differentiation. Bone 2008, 42:806–18.

[11] Jung Y, Song J, Shiozawa Y, Wang J, Wang Z, Williams B, Havens A, Schneider A, Ge C, Franceschi RT, et al. Hematopoietic stem cells regulate mesenchymal stromal cell induction into osteoblasts thereby participating in the formation of the stem cell niche. Stem Cells 2008, 26:2042–51.

[12] Morgan TM, Lange PH, Porter MP, Lin DW, Ellis WJ, Gallaher IS, Vessella RL. Disseminated tumor cells in prostate cancer patients after radical prostatectomy and without evidence of disease predicts biochemical recurrence. Clin Cancer Res 2009, 15:677–83.

[13] Kingsley LA, Fournier PG, Chirgwin JM, Guise TA. Molecular biology of bone metastasis. Mol Cancer Ther 2007, 6:2609–17.

Research Paper

The marrow niche controls the cancer stem cell phenotype of disseminated prostate cancer

Yusuke Shiozawa[1,2], Janice E. Berry[1,*], Matthew R. Eber[1,2], Younghun Jung[1], Kenji Yumoto[1], Frank C. Cackowski[1], Hyeun Joong Yoon[3], Princy Parsana[4,5], Rohit Mehra[6], Jingcheng Wang[1], Samantha McGee[1], Eunsohl Lee[1], Sunitha Nagrath[3], Kenneth J. Pienta[4], Russell S. Taichman[1]

[1]Department of Periodontics and Oral Medicine, University of Michigan School of Dentistry, Ann Arbor, MI 48109, USA

[2]Department of Cancer Biology and Comprehensive Cancer Center, Wake Forest University School of Medicine, Winston-Salem, NC 27157, USA

[3]Department of Chemical Engineering, University of Michigan, Ann Arbor, MI 48109, USA

[4]Department of Urology, The James Buchanan Brady Urological Institute, Johns Hopkins School of Medicine, Baltimore, MD 21287, USA

[5]Department of Computer Science, Johns Hopkins University, Baltimore, MD 21218, USA

[6]Department of Anatomic Pathology, University of Michigan, Ann Arbor, MI 48109, USA

[*]Deceased on February 4, 2016

Correspondence to: Russell S. Taichman, **email:** rtaich@umich.edu

Keywords: *prostate cancer, disseminated tumor cells, bone marrow microenvironment, hematopoietic stem cell niche, cancer stem cells*

Received: *March 04, 2016* ***Accepted:*** *April 19, 2016* ***Published:*** *May 09, 2016*

ABSTRACT

Dissemination of cancer stem cells (CSCs) serves as the basis of metastasis. Recently, we demonstrated that circulating prostate cancer targets the hematopoietic stem cell (HSCs) 'niche' in marrow during dissemination. Once in the niche, disseminated tumor cells (DTCs) may remain dormant for extended periods. As the major function of the HSC niche is to maintain stem cell functions, we hypothesized that the niche regulates CSC activities of DTCs. Here we show that DTCs recovered from marrow were significantly enriched for a CSC phenotype. Critically, the conversion of DTCs to CSCs is regulated by niche-derived GAS6 through the Mer/mTOR; molecules previously shown to regulate dormancy. The data demonstrate that the niche plays a significant role in maintaining tumor-initiating prostate cancer in marrow and suggests a functional relationship between CSCs and dormancy. Understanding how the marrow niche regulates the conversion of DTCs to CSCs is critical for the development of therapeutics specifically targeting skeletal bone metastasis and dormancy.

INTRODUCTION

Every year, patients who thought they were cured of prostate cancer by radiation or surgery present with incurable metastatic disease in their skeleton [1]. Previously, we showed that circulating prostate cancer targets the bone marrow 'niche' that houses hematopoietic stem cells (HSCs) and, critically, that disseminated tumor cells (DTCs) compete with HSCs for occupancy of that niche [2]. Once in the niche, DTCs may remain viable for extended periods [3–7], yet little is understood about how disseminated prostate cancer remains viable and later develop into skeletal metastases. Many believe cancer stem-like cells (CSCs) are culpable.

The hypothesis that tumors depend on a small fraction of cells, or CSCs, for long-term survival was proposed based upon data demonstrating that subsets of human leukemic cells transferred tumor-initiating activities to SCID mice [8]. More recent experimentation suggests that CSCs have the ability to self-renew and to generate multiple 'mature' tumor progeny [9]. Generally, freshly isolated CSCs exhibit low proliferative activity and, as a result, possess chemo- and radio-resistance [10]. From these observations, it has been assumed that CSCs are typically dormant, and their later regrowth is responsible for metastases. As the molecular machinery of the HSC niche is designed to regulate stem cell quiescence

and self-renewal [11], we therefore hypothesized that DTCs may be converted to a CSC phenotype through engagement with the niche, thus establishing a future site of metastasis.

Using murine models of human metastasis, we show that DTCs recovered from marrow are significantly enriched for a CSC phenotype. The conversion to CSCs was observed in DTCs following the injection of only non-CSCs, and occurred primarily in the marrow. The CSCs in marrow were maintained over time, and was not due to effects on proliferation, homing, or cell survival in the circulation. Importantly, growth arrest specific 6 (GAS6), which influences prostate cancer dormancy [12–14], and is secreted by the osteoblastic niche [12], regulates part of the conversion of DTCs into CSCs through its receptor Mer, by activating the mTOR signaling pathway following cell-to-cell contact. These data demonstrate that the HSC niche plays a significant role in the production and maintenance of tumor-initiating CSCs in marrow.

RESULTS

Disseminated prostate cancer are converted to the CSC within the marrow microenvironment

Previously we showed that early in the metastatic process prostate cancer targets and commandeers the marrow microenvironment or "niche" which houses HSCs, using mechanisms similar to those involved in HSC homing [2]. Subsequently, these disseminated prostate cancer parasitizes this microenvironment to become dormant and survive within the marrow [12]. Since the major function of the HSC niche is to maintain stem cell functions, we hypothesized that engagement of DTCs within the niche regulates CSC activities. To test our hypothesis, the expression of CD133 and CD44 was first analyzed on tissue microarrays from prostate cancer patients since prostate cancer expressing both CD133 and CD44 represent a rare population of cells with stem cell-like properties [15]. Intriguingly, the number of CSCs ($CD133^+/CD44^+$) was enhanced with increasing tumor grade (Figure 1A–1B).

To further explore how the niche regulates CSC activities we developed a reproducible assay in which DTCs derived from human tumors grown in SCID mice can be recovered with high fidelity from murine marrow. We found that unlike EpCAM and cytokeratin, antibodies targeting HLA-ABC represent a stable and suitable approach for capturing DTCs. First, we used flow cytometry to evaluate the basal levels of cytokeratin and EpCAM on the surface of human prostate cancer cell lines (PC3, DU145, LNCaP, and C4-2B), with leukemia cell lines (RCH-ACV, 697, Nalm6 and RS4;11) as controls. Prostate cancer cells expressed low or moderate levels of cytokeratin and high levels of EpCAM *in vitro*, while levels of both were low in the leukemia lines (Figure S1A). However, since the cytokeratin and EpCAM levels were variable, we explored using HLA expression as an alternative molecular probe for recovery of human DTCs from murine marrow. We found that the HLA-ABC antigen was highly expressed on all prostate cancer cells tested (Figure S1A). Therefore intracardiac injections of prostate cancer cells into SCID mice were performed to determine if human prostate cancer cells could be isolated from murine marrow using anti-HLA-ABC antibodies (Figure S1B). Depending on the cell line examined, 10.5 ± 2.3 % to 16.7 ± 2.5 % of the lineage depleted marrow cells expressed HLA-ABC 24 hours post injection (Figure S1C). As previously described [16], the expression of cytokeratin and EpCAM varied considerably *in vitro* (Figure S1A) and *in vivo* (Figure S1D), however almost all cytokeratin (Figure S1E) and EpCAM positive prostate cancer cells (Figure S1F) expressed HLA-ABC on their surface. This strategy was validated in two ways: First, prostate cancer cells injected intratibially were visualized after 24 hours *in situ* by immunofluorescent imaging for HLA-ABC (Figure S1G); second, specificity was confirmed by inoculating SCID mice with GFP (green)-labeled PCa cells and recovering the DTCs from the marrow using APC (red)-labeled anti-HLA-ABC antibodies. As predicted, the cells isolated with the anti-HLA-ABC antibodies expressed GFP (Figure S1H–S1I). These data confirmed that HLA-ABC is a suitable marker for capturing human disseminated prostate cancer cells from marrow in animal models.

Using this approach, we compared the relative numbers of CSCs *in vitro* with CSCs *in vivo*. As predicted, the frequency of CSCs *in vitro* was extremely low (Figures 1C and S2A). Interestingly, 24 h after intracardiac injection, the CSC population of DTCs isolated from mouse marrow was more than 20% of total DTCs (Figures 1C and S2B); a significant increase within a short time period. The expansion of the CSCs was observed even following intracardiac injection of a non-CSC ($CD133^-/CD44^-$) (Figures 1D and S3A–S3B). Similar population shifts of non-CSC to CSC were observed *in vitro,* albeit not to the extent observed *in vivo* (Figures 1D and S3A–S3B), suggesting that the enrichment of CSCs is due to the conversion of non-CSCs into CSCs. Significantly, the enrichment of CSCs occurred only when prostate cancer cells spread to the marrow, not the lung or spleen, suggesting organ specificity (Figure 1E).

CSC enrichment in marrow is not due to selection and is not an acute response

To exclude the possibility that the increase in the CSCs is not merely an acute response to the marrow environment, cells were recovered from marrow over time. The conversion to the CSCs *in vivo* was maintained over 4 weeks (Figure 2A–2B), and the expression of stem cell-related genes, KLF4, Bmi-1, and Nanog, increased

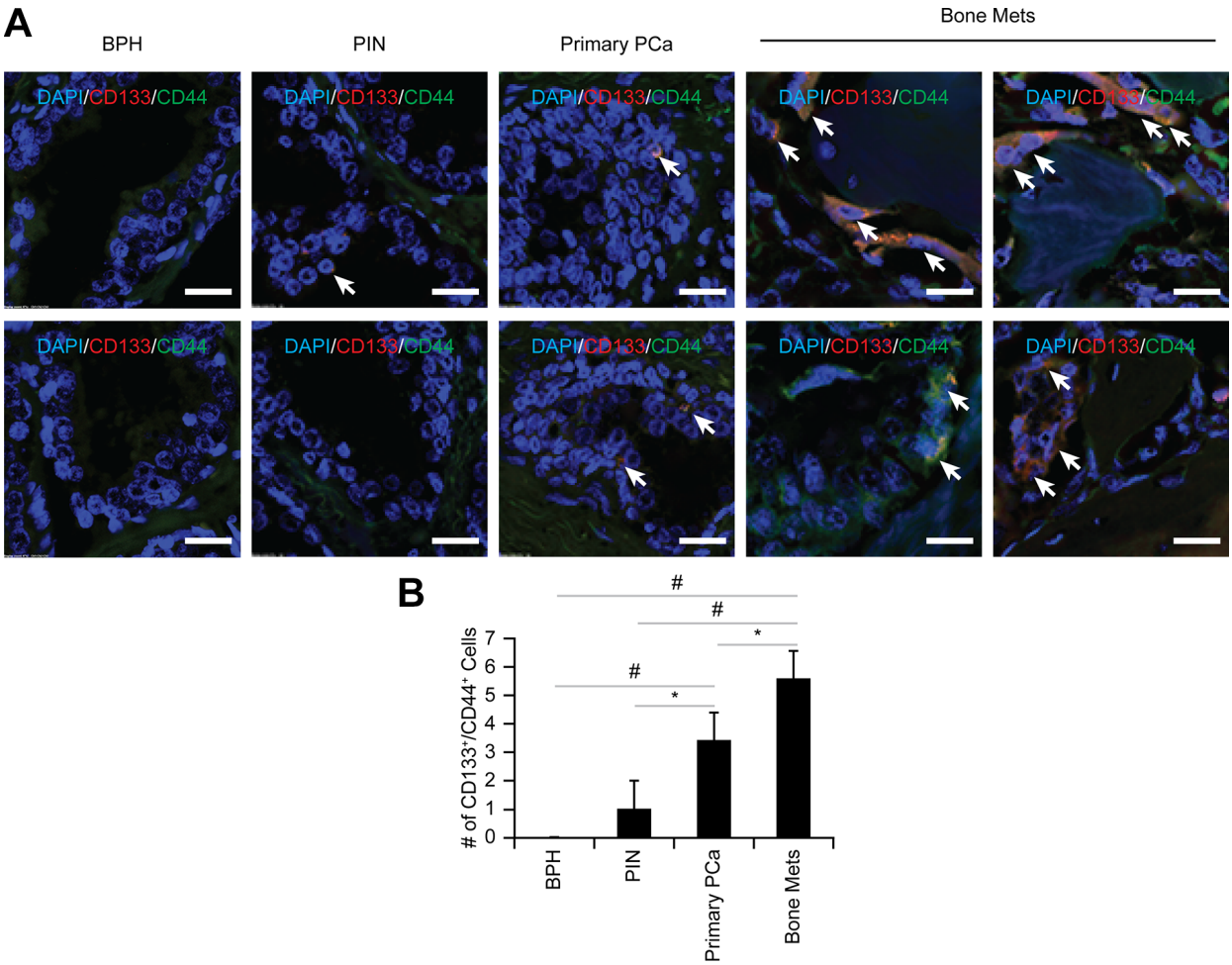

C

% of CSCs	PC3	DU145	LNCaP	C4-2B
In Vitro	0.34 ± 0.06 #	0.17 ± 0.01 #	0.14 ± 0.05 *	0.05 ± 0.02 #
In Vivo DTC	21.70 ± 6.95	33.45 ± 8.41	22.77 ± 13.65	55.50 ± 13.99

D

	% of CSCs	
	PC3	C4-2B
Before non-CSCs Sorting (Basal Levels)	0.7 ± 0.3%	0.3 ± 0.1%
After CSCs Sorting (Purity Check)	0.0 ± 0.0%	0.0 ± 0.0%
Intracardiac Injection of Sorted non-CSCs (24h)	34.3 ± 5.0%	42.6 ± 1.9%
In Vitro Culture of Sorted CSCs (48h)	0.9 ± 0.6%	0.2 ± 0.0%

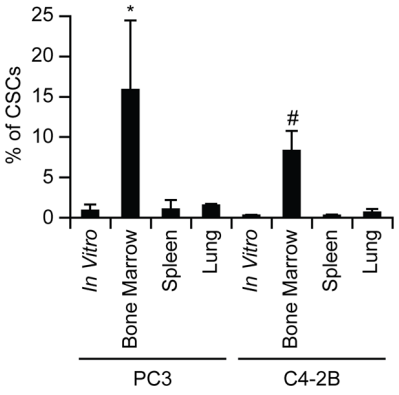

Figure 1: Enrichment of CSCs in disseminated prostate cancer. (**A**) Representative elements of a prostate cancer tissue microarray co-stained with anti-CD133 and anti-CD44 antibodies. Nuclei were identified by DAPI. (60× Zoom2, Bar = 20 μm). (**B**) Quantitative analysis of CSC staining in Figure 1A. *$p < 0.05$ and #$p < 0.01$ (Student's *t*-test). BPH: benign prostatic hyperplasia; PIN: prostatic intraepithelial neoplasia; Primary prostate cancer: primary prostate cancer; and Bone mets: bone metastatic prostate cancer. (**C**) The % of CSC population in *in vitro* cultured prostate cancer and *in vivo* DTCs by flow cytometry. Significance vs. *in vitro* cultured prostate cancer (Student's *t* test). (**D**) Non-CSC prostate cancer cells were sorted and subsequent flow cytometry analyses confirmed no residual contamination of CSC cells. Pure non-CSCs were either inoculated into SCID mice through intracardiac injection ($n = 5$) or cultured *in vitro,* and the CSC population was analyzed. (**E**) CSC expression in prostate cancer recovered from the lung, spleen, or bone marrow following intracardiac injection ($n = 5$). *$p < 0.05$ and #$p < 0.01$ vs. *in vitro* cultured prostate cancer (Student's *t* test).

in the CSCs (Figure 2C–2D). Post intracardiac injection, the presence of DTCs in marrow initially alters cytokine production, but cytokine levels return to basal levels quickly, suggesting these proteins may not play a major role in the CSC conversion (Figure 2E–2F).

We next dissected the mechanisms involved in the conversion to the CSCs. Rapid proliferation was one potential mechanism to account for a larger CSC population. To assess this possibility, prostate cancer cells were stained with BrdU prior to injection. The CSCs recovered from marrow (24 h after injection) retained almost 100% of the BrdU detected before injection, while the population as a whole demonstrated the reductions in BrdU retention (Figure 2G), suggesting that non-CSC populations had undergone replication.

A second possibility worthy of consideration is that of selective CSC homing to marrow. To address this possibility, direct intraskeletal injections of prostate cancer were performed. The increase in CSCs was the same as that seen in intracardiac injections (Figure 2H), suggesting that the homing process does not account for the changes in population frequency. Next, to evaluate the possibility of a specific CSC survival advantage in circulation, a microfluidic device was fabricated (Figure S4A), which exposed cells to sheer stresses comparable to those present in the circulation. To take into account the additional effects of blood cells and serum on survival, prostate cancer cells were incubated with mouse blood. Based upon the results (Figure S4B), selective survival of the CSCs in circulation was an unlikely mechanism to account for the increase in the CSCs.

The CSCs possess stem cell-like properties

We next validated that the CSCs examined in this study exhibit a stem cell-like phenotype. Microarray analyses revealed that *in vivo* DTCs displayed different stem like properties (genes were selected from the GO database using the GO term "stem cell") than cells *in vitro* (expression values) (Figure 3A and Tables S1–S2). However, there were no differences in the gene expression of aldehyde dehydrogenase 1A2 (ALDH1A2) related to ALDH activity (one of the markers for CSCs including prostate cancer [17]) between CSCs and non-CSCs that are used in this study (Figure 3A and Tables S1–S2). Interestingly, 619 genes (including EpCAM) were differentially expressed (Wilcoxon rank sum p-value < 0.05) between CSC and non-CSC obtained from murine marrow (Figures 3B and S5A, and Tables S3), and in particular gene sets associated with stem cell activities were enriched in *in vivo* CSCs including Nuclear Receptors in Lipid Metabolism and Toxicity, Ca++/Calmodulin-dependent Protein Kinase Activation, and Cell Cycle: G2/M Checkpoints (Figure S5B). These global changes in gene expression suggest that the marrow niche plays a significant role in activating CSC programs. These differences were further defined by *Q*RT-PCR. The levels of mRNA expression for KLF 4, Bmi-1, and Nanog were dramatically increased overall in CSCs recovered from marrow verses *in vitro* (Figure 3C–3E). The microarray and PCR data further confirmed that CSCs obtained from murine marrow using HLA-ABC are human disseminated prostate cancer cells. In spite of their rarity, the CSCs isolated from marrow, when placed into culture, formed sphere-like structures (not shown). Additionally, the CSCs increased tumorigenic abilities both *in vitro* (Figure 3F) and *in vivo* (Figure 3G), and resistance to chemotherapy (Figure 3H), as expected for non-proliferating stem-like cells.

Molecular mechanisms used by the osteoblastic niche to convert DTCs to CSCs

To identify the molecular mechanisms that regulate the shift of non-CSCs to CSCs in marrow, we studied co-cultures of prostate cancer and osteoblasts as DTCs compete for the occupancy of the osteoblastic niche [2], although certainly other components of the HSC niche are also involved. Under conditions of direct cell-to-cell contact, a significant shift of non-CSC to CSCs was observed (Figure 4A). Since GAS6 expressed by osteoblasts influences the proliferation of prostate cancer [12], and our microarray data suggests increased expression of Mer (one of the receptors for GAS6) in CSCs (Figure S5A), we asked whether GAS6 influences the conversion of non-CSCs to CSCs. When prostate cancer cells were co-cultured with osteoblasts isolated from GAS6-null mice, the conversion to CSCs was significantly, although not completely, diminished (Figure 4A). Moreover, when prostate cancer cells were injected into wild-type or GAS6-null skeletal tissue, significantly greater CSCs were identified near the endosteal surfaces of GAS6 expressing tissues compared to tissues lacking GAS6 (Figure 4B–4C). Next, we explored the downstream signaling activated by GAS6 that is involved in the expression of the CSC phenotype. Since the mTOR has been demonstrated to play a pivotal role in maintaining both a CSC phenotype and an HSC phenotype in the niche [18, 19], we explored the possibility that GAS6 activation of mTOR may represent a critical switch regulating the CSC phenotype. We found that GAS6 triggered mTOR signaling in prostate cancer, with increases seen in both mTORC1 and mTORC2 (Figures 4D and S6A–S6B), and these were diminished by the mTORC1 inhibitor rapamycin and the dual mTORC1/2 inhibitor pp242 (Figures 4E, S6C–S6D, and S7A–S7B).

To identify which of the GAS6 receptors (Tyro3, Axl, and Mer) is responsible for mTOR activation, targeted deletion of each of the three receptors was performed (Figure S8A–S8B). When Mer was reduced in prostate cancer via shRNA (Figures 5A, S9, and S10), or a Mer inhibitor was employed (Figures 5B and S11),

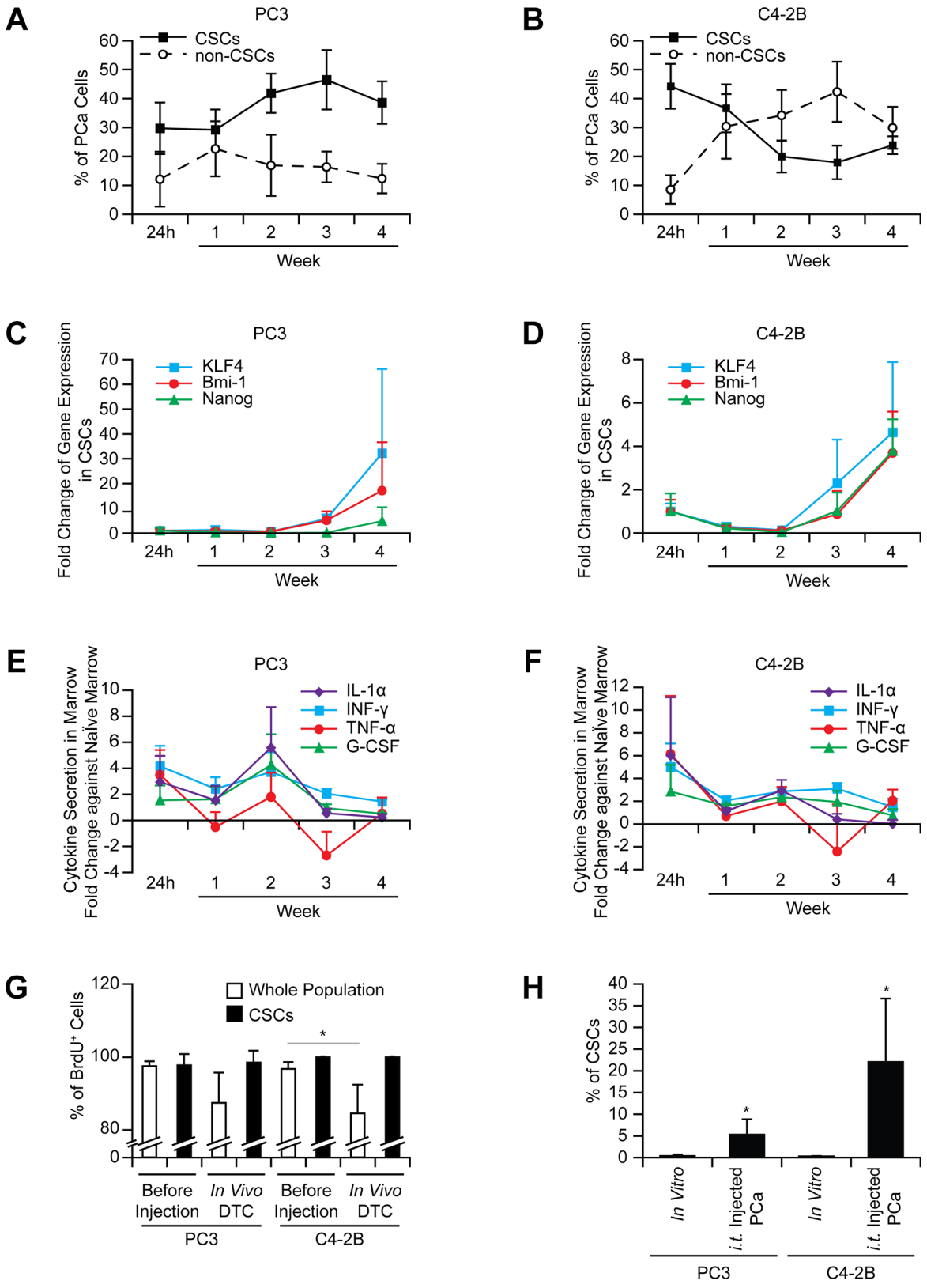

Figure 2: The increase in the CSCs in marrow is not an acute phase response and not due to selection. The CSCs in prostate cancer recovered from bone marrow ((**A**) PC3 and (**B**) C4-2B), mRNA expression in prostate cancer cells ((**C**) PC3 and (**D**) C4-2B), and secretion of inflammatory cytokines in marrow ((**E**) PC3 and (**F**) C4-2B) analyzed over time ($n = 5$ per week). (**G**) Intracardiac injection of BrdU stained prostate cancer was performed ($n = 5$). After 24 h injection, BrdU levels in DTCs were examined in the CSC vs. whole populations. *$p < 0.05$ (Student's t-test). (**H**) Prostate cancer was inoculated intratibially, and evaluated for CSCs after 24 h ($n = 5$). *$p < 0.05$ vs. *in vitro* cultured prostate cancer (Student's t-test).

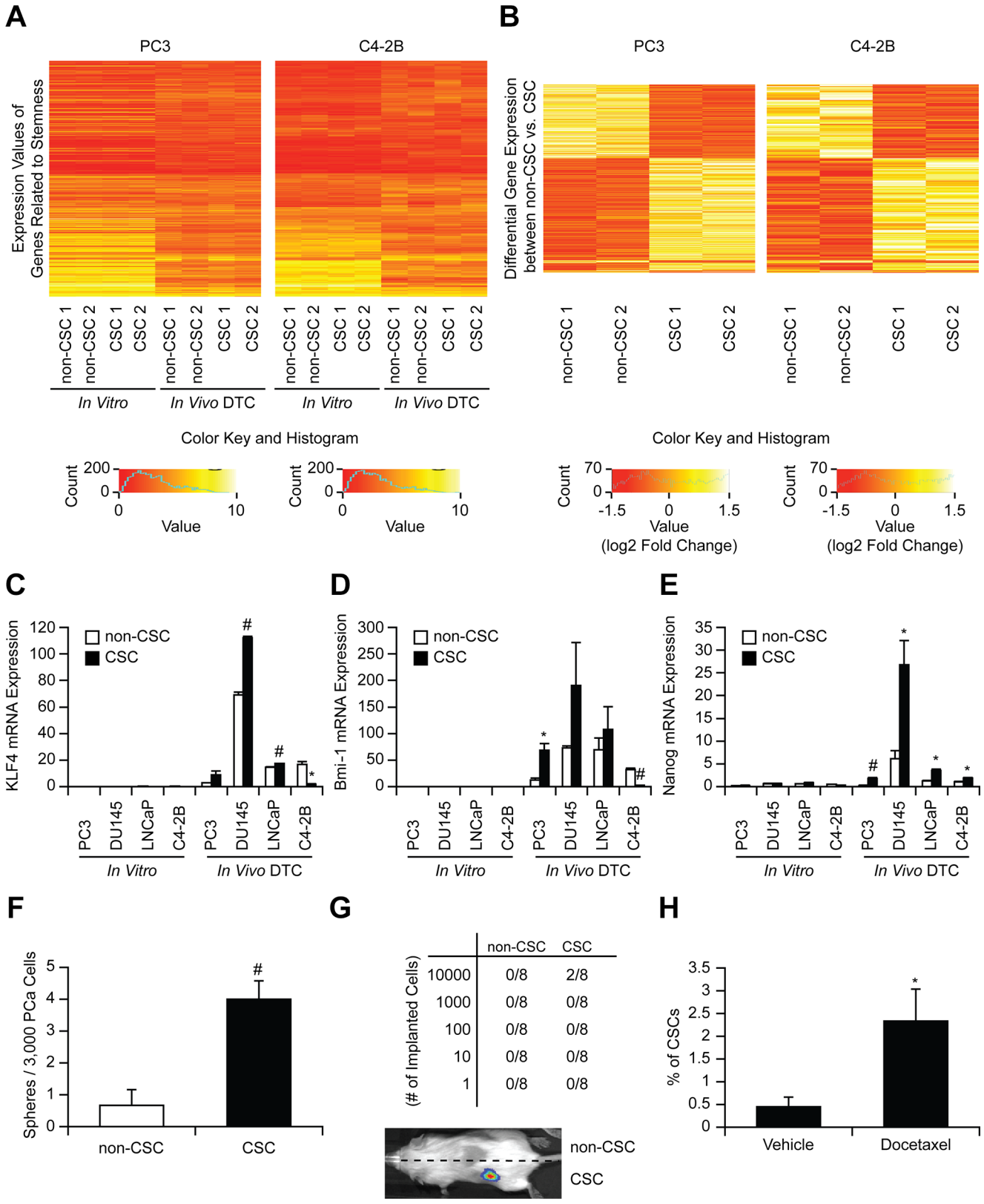

Figure 3: Stem-like properties of CSCs. (**A**) Heatmap of stem cell related genes comparing CSC and non-CSC (*in vitro* and *in vivo*). (**B**) Heatmap of 619 differentially expressed genes in CSCs and non-CSCs (Wilcoxon Rank Sum $p < 0.05$, cells were obtained from 5 animals / experiments). mRNA expression of (**C**) KLF4, (**D**) Bmi-1, and (**E**) Nanog in CSC and non-CSC (*in vitro* and *in vivo*). $^{*}p < 0.05$ and $^{\#}p < 0.01$ vs. non-CSC (Kruskal-Wallis test). (**F**) *In vitro* sphere formation assays, (**G**) *In vivo* serial dilution stem cell assays (numbers correspond to tumors/implant), and (**H**) Chemo-resistance assays after docetaxel treatment (% of CSCs with/without docetaxel treatment). $^{*}p < 0.05$ and $^{\#}p < 0.01$ vs. vehicle treatment (Student's *t*-test).

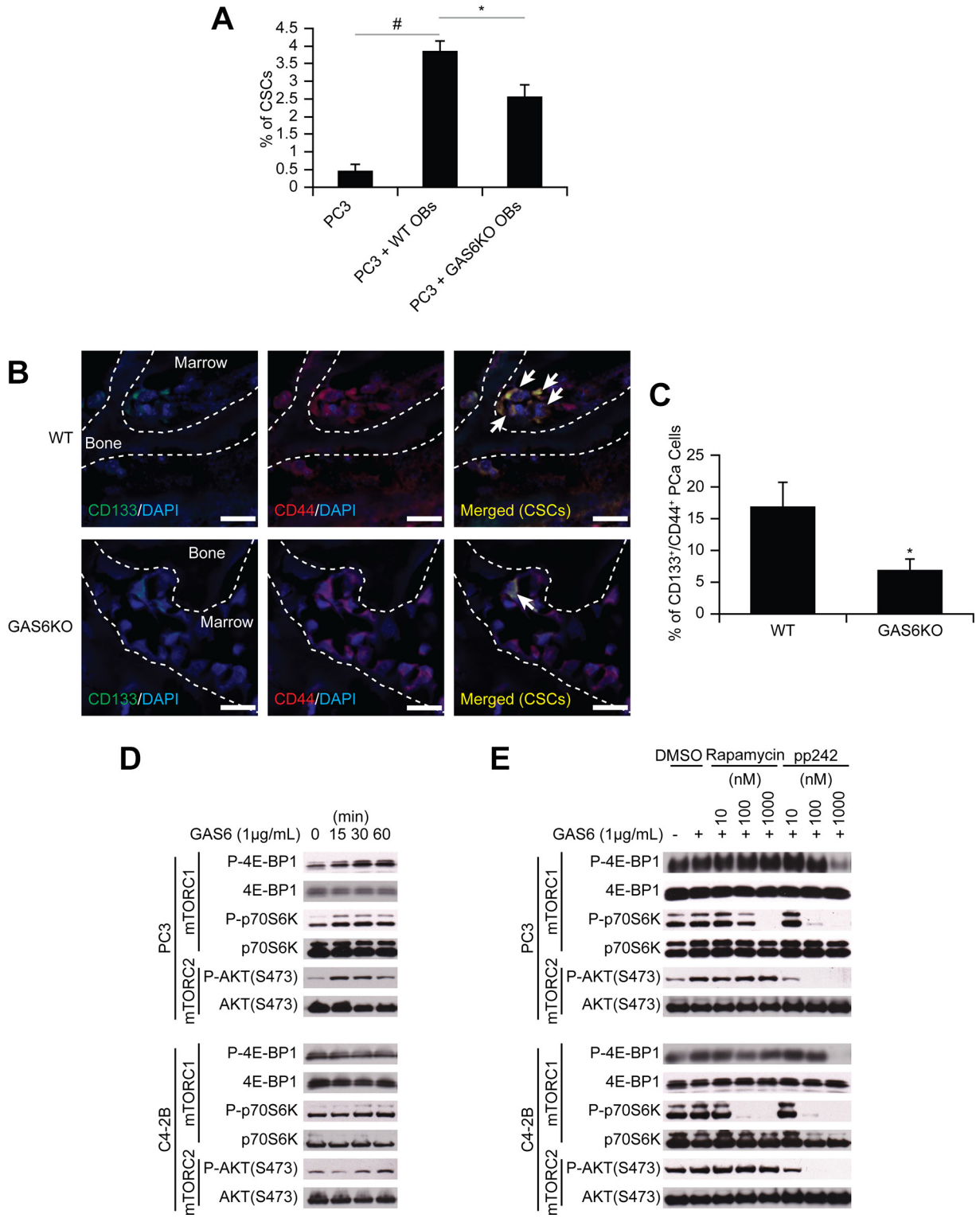

Figure 4: GAS6 expressed by the osteoblastic niche controls the conversion of DTCs to CSCs through mTOR signaling. (**A**) The % of CSCs by flow cytometry in PC3 cells co-cultured with osteoblasts from *GAS6*$^{+/+}$ (WT) and *GAS6*$^{-/-}$ (GAS6KO) mice (Student's *t*-test). (**B**) PC3 cells (1×10^4 cells per 10 μL) were placed directly into vertebral bodies (vossicles) derived from WT and GAS6KO mice and transplanted into immunodeficient mice ($n = 6$). At 1 month, the vossicles were dissected, and the expression of CSCs by prostate cancer was evaluated by immunohistochemistry. (60× Zoom 2.5, Bar = 20 μm). Arrows denote CSCs. (**C**) Quantitative analysis of CSC staining in Figure 4B. The $CD133^+CD44^+$ cells within six randomly selected representative images per group were counted, and then normalized with total numbers of cells. $*p < 0.05$ vs. CSCs in WT vossicle (Student's *t*-test). (**D**) Activation of mTOR signaling with GAS6 treatment in prostate cancer. (**E**) Activation of mTOR signaling with GAS6 treatment in prostate cancer in the presence/absence of mTOR inhibitors (Rapamycin, 13346, Cayman Chemical; and pp242, 13643, Cayman Chemical).

mTORC2 signaling activated by GAS6 was decreased, which was not observed with reduced Tyro3 and Axl expression. Activation of mTORC1 in shMer cells was also reduced compared to shTyro3 and shAxl cells (Figure 5A). These results suggest that the increase in the CSCs is mediated through the GAS6/Mer axis. To test the roles of PTEN in this system, DU145 was used, since DU145 expresses PTEN, while PC3 and C4-2B are PTEN deficient [15, 20]. As in PC3 and C4-2B, Mer inhibitor blocked mTORC2 activation in DU145 (Figures S12A and S13A). However, when shMer DU145 cells were treated with GAS6, mTORC2 signaling was unaffected (Figures S12B and S13B), which we attributed to the high residual levels of MER, when compared to PC3 and C4-2B (Figure S14). These data suggest that PTEN status is likely involved in mTOR activation through GAS6/Mer, but PTEN is unable to prevent the conversion to CSCs in DU145 (Figure 1C). Moreover, the Mer inhibitor prevents sphere-forming ability of prostate cancer (Figures 6A–6B and S15), while it did not affect cell viability (Figure 6C). Additionally, the conversion to CSC by direct contact with osteoblasts was inhibited both *in vitro* (Figure 6D, shControl vs. shMer) and *in vivo* (Figure 6E, Vehicle vs. Mer inhibitor), when the Mer in prostate cancer was inhibited. Similarly, fewer CSCs were recovered from the marrow of animals inoculated with shControl vs. shMer, although the difference did not reach statistical significance (Figure S16). Importantly, the increase in CSCs was also inhibited both *in vitro* (Figure 6F) and *in vivo* (Figure 6G), when the mTOR signaling pathway in prostate cancer was blocked. However, the conversion to CSCs was not seen when Wnt or CXCR4 pathways were blocked, which are also believed to regulate stemness (Figure 6G).

DISCUSSION

Local or distant tumor recurrence, in spite of early therapeutic interventions, suggests that dissemination of tumor cells occurs very early in cancer development. In prostate cancer, epithelial-like cells can be isolated from bone marrow in 72% of prostate cancer patients when diagnosed, and even in 8.8% of healthy controls [7]. However, whether those cells are normal epithelial cells or DTCs derived from an unknown primary prostate cancer remains unclear. In addition, DTCs are believed to become occult in bone marrow, as prostate-specific antigen (PSA), which correlates with tumor volume, persists at undetectable levels years after radical prostatectomy [21], and yet metastatic tumors can occur long after initial treatment. The development of new therapeutic regimens to augment existing chemotherapies, surgery and radiation are essential if we hope to establish long-term treatments for prostate cancer. However, our lack of understanding of the biology of DTCs remains a major stumbling block in the process.

In this study, we first explored that disseminated prostate cancer recovered from marrow were highly enriched for CSCs. We elected $CD133^{+}/CD44^{+}$ as a CSC surface marker combination, since this is widely used to isolate prostate CSCs [2, 15, 22–24]. However, there is no difference in the ALDH1A2 gene expression between

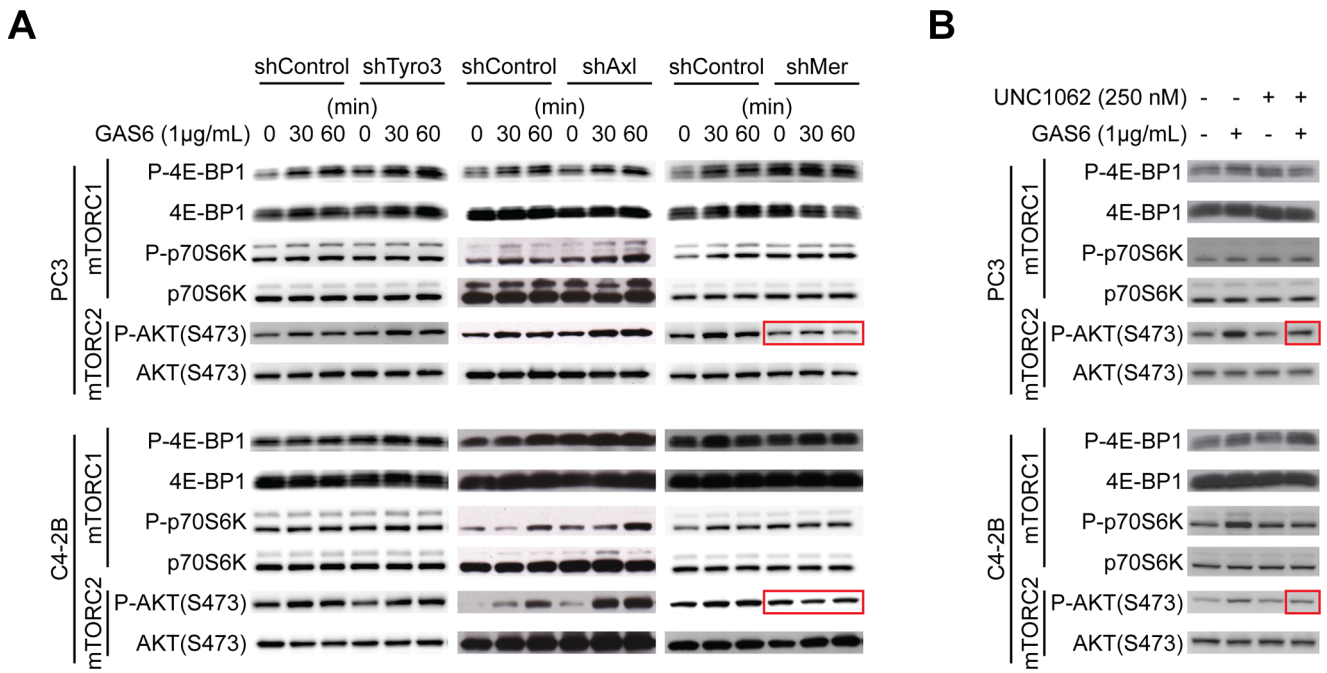

Figure 5: GAS6 activates mTOR signaling through Mer. (**A**) Activation of mTOR signaling with GAS6 treatment in prostate cancer with TAM (Tyro3, Axl, Mer) receptors knocked down. (**B**) Activation of mTOR signaling with GAS6 treatment in prostate cancer in the presence/absence of Mer inhibitor (UNC1062).

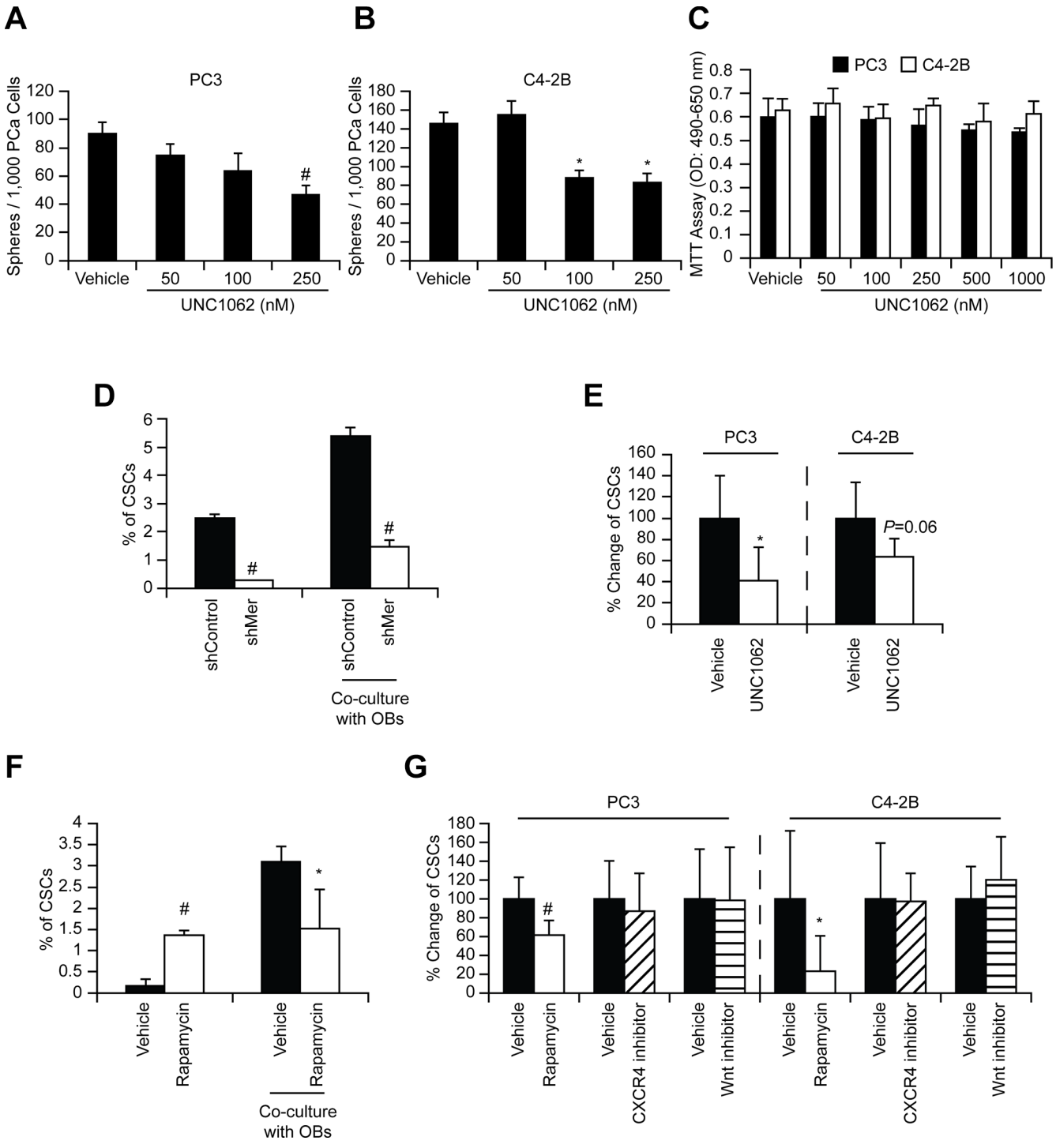

Figure 6: GAS6 activates mTOR signaling involved in the conversion of DTCs to CSCs through Mer. *In vitro* sphere formation assays ((**A**) PC3 and (**B**) C4-2B)) and (**C**) MTT cell viability assays with/without Mer inhibitor (UNC1062). Significance vs. vehicle treatment (Student's *t*-test). (**D**) PC3 cells (shControl and shMer) were co-cultured with osteoblasts and 48 h later the CSCs in prostate cancer were measured by flow cytometry. Significance vs. shControl (Student's *t*-test). (**E**) Prostate cancer cells, pre-incubated (24 h) with UNC1062 (250 nM), were inoculated intracardially and 24 h later the CSCs in disseminated prostate cancer obtained from the bone marrow of mice inoculated with prostate cancer cells were measured by flow cytometry ($n = 5$). The % of CSCs population in the marrow was normalized to the vehicle control group that equals 100 %, and presened as % change. Significance vs. vehicle treated prostate cancer (Student's *t*-test). (**F**) PC3 cells, pre-incubated (1 h) with Rapamycin (10 nM), were co-cultured with osteoblasts and 48 h later the CSCs in prostate cancer were measured by flow cytometry. (**G**) Prostate cancer cells, pre-incubated (1 h) with Rapamycin (13346, Cayman Chemical, 10 nM), CXCR4 inhibitor (AMD3100, A-5602, Sigma-Aldrich, 10 nM), or Wnt inhibitor (IWR-1-endo, 13659, Cayman Chemical, 10 μM), were inoculated intracardially and 24 h later the CSCs in disseminated prostate cancer were measured by flow cytometry ($n = 5$). Significance vs. vehicle treated prostate cancer (Student's *t*-test). $^{*}p < 0.05$ and $^{\#}p < 0.01$.

CSCs and non-CSCs (Figure 3A and Tables S1–S2), suggesting that there may be other population of CSCs do not express the selected CSC surface marker combination. Further studies are clearly needed as no consensus has yet been reached regarding specific markers for prostate CSC.

Next, when uniformly non-CSCs were inoculated into the mice, a conversion to CSCs was observed in prostate cancer cells recovered from marrow. Importantly, this conversion was seen only in the prostate cancer cells localized to the marrow, but not lung or spleen. Further, this enrichment of CSC population was not due to the effects of cell proliferation, survival within the circulation, or homing. Additionally, the CSCs exhibit expression of the self-renewal genes KLF4, Bmi-1, and Nanog, and have the ability to form sphere-like structures *in vitro*, and tumor *in vivo* although not robust. Under conditions of direct cell-to-cell contact between prostate cancer cells and osteoblasts, a significant shift of non-CSCs to CSCs was observed. With further analysis, we found that within the marrow the osteoblastic niche controls conversion of disseminated prostate cancer cells to CSCs through the GAS6/Mer/mTOR pathway (Figure 7). Collectively, our findings suggest that the bone marrow niche plays an important role in the accumulation of self-renewing prostate cancer cells in the marrow, which further indicates that DTCs may be capable of serving as metastatic seeds for bone tumors, and that this model and strategy may be useful in further exploration of the nature and phenotype of DTCs. Understanding how the niche regulates the conversion of DTCs to CSCs will be instrumental for the development of therapeutics specifically targeting early dissemination of prostate cancer to the bone, and for understanding how metastatic growth is regulated.

We previously identified that the osteoblastic niche regulates the proliferation of prostate cancer via the GAS6 pathway [12, 14, 25]. The growth of prostate cancer in the marrow depends on the levels of GAS6 that bones express [25]. That is, human prostate cancer xenografts

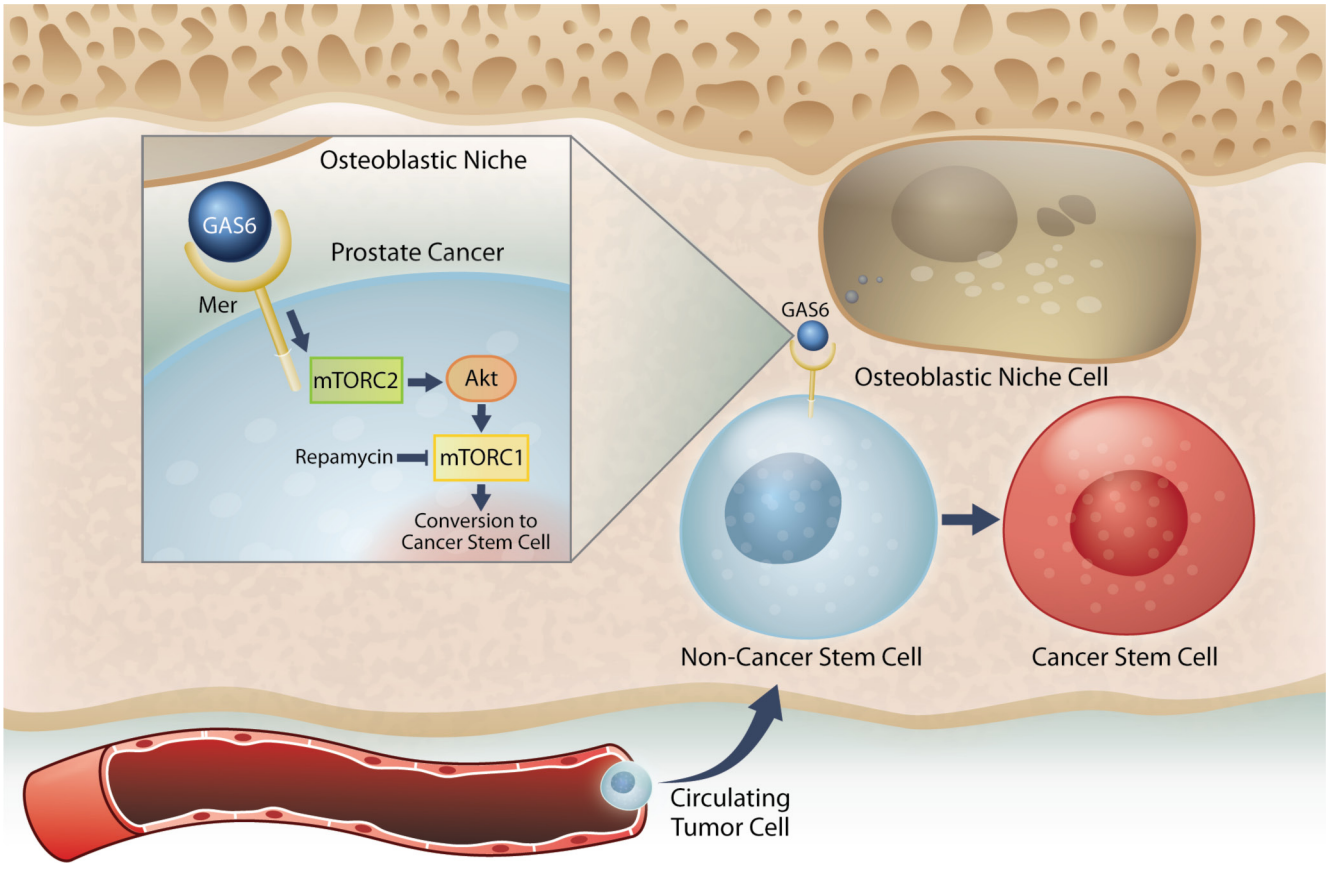

Figure 7: Model system for the induction of a CSC phenotype in marrow by the HSC niche. Prostate cancer cells preferably spread to the bone and survive within the marrow microenvironment for a long period of time. However, the mechanisms underlying the survival of these disseminated tumor cells (DTCs) remain unclear. Our previous work revealed that prostate cancer DTCs target the osteoblastic hematopoietic stem cell (HSC) niche, and that these DTCs parasitize the niche to survive there. The major function of the niche is maintaining the stem cell phenotype. This study demonstrated that the conversion of cancer cells to stem-like cancer cells (CSC) occurs when DTCs directly contact the osteoblastic niche. GAS6 expressed by the osteoblastic niche activates mTOR signaling in the prostate cancer DTCs through the Mer receptor, contributing to the conversion to CSCs. Furthermore, our data suggests that these activations uniquely progress first through mTORC2 and then mTORC1, which can be blocked by rapamycin. Therefore, targeting mTOR signaling in DTCs could be a promising therapy for bone metastatic disease.

grow rapidly in the osseous environment expressing less GAS6, compared to high GAS6-expressing bones [25]. Prostate cancer growth also depends on the expression levels of GAS6 receptors on prostate cancer cells [14]. Dormant prostate cancer expresses higher Axl (Axl > Tyro3), but cells expressing Tyro3 (Tyro3 > Axl) grow rapidly [14]. Consistently, when prostate cancer reaches the bone, Axl expression in prostate cancer and GAS6 expression in osteoblasts both increase simultaneously [12]. These findings suggest that GAS6 is important for the proliferation of disseminated prostate cancer. However, in the present study we discovered a new, important role for GAS6 in the progression of prostate cancer in the marrow: GAS6 expressed by osteoblasts converts disseminated prostate cancer to a stem-like phenotype through its receptor, Mer. This discrepancy is very similar to the effects of TGF-ß and BMP signaling on bone metastasis. Whether these factors influence CSC phenotype and tumor dormancy in bone metastatic diseases is highly dependent on cell type and/or extracellular microenvironment [26–31]. Likewise, we speculated that the effects of GAS6 on the progression of DTCs are dependent on the expression levels of its receptor. Since the interactions between ligands and receptors are complex, further study is needed to determine the exact role of each GAS6 receptor in the fate of disseminated prostate cancer.

Metastasis remains a life-threatening complication of solid tumors. Once the tumor cells spread to distant organs such as bone, survival rates of cancer patients decline drastically. Despite the controversies over the CSC hypothesis [32, 33], consensus has been reached that the most effective therapies will also need to target chemo-resistant CSCs. Our data suggests that the niche plays a central role in activating in the conversion of disseminated prostate cancer to CSCs. Thus, it appears that targeting only CSCs could be of limited therapeutic value, since stem cell programs can become activated in DTCs. Similar to our findings, other recent reports have demonstrated that conversions between somatic cells and stem cells [15, 34], somatic cells and CSCs [35], and non-CSCs and CSCs [36] are possible.

Considering that CSCs likely represent a heterogeneous population with a wide spectrum of epithelial and mesenchymal characteristics (e.g. EMT CSCs and MET CSCs) [37], these findings further suggest an addendum to the "seed and soil" hypothesis first proposed by Stephan Paget in 1889 [38]. In this theory, the "seed" (tumor cells) favorably metastasize to the "soil" (their specific microenvironment). However, our data infers that the "soil" (the niche) is also a major driver of the creation/maintenance of the "seed" (CSCs). While further studies in different cancer types are clearly needed, the identification of alternative mechanisms whereby CSCs are generated expands our knowledge and understanding as to how tumors are propagated, and sets the stage for future therapeutic developments to target prostate cancer bone metastases.

MATERIALS AND METHODS

Tissue microarray and immunostaining

Human prostate adenocarcinoma tissue microarray (TMA) was obtained from The Tissue Core of the University of Michigan Comprehensive Cancer Center. Tumors were examined to identify areas of benign prostatic hyperplasia, prostatic intraepithelial neoplasia, primary prostate cancer, and bone metastatic prostate cancer. TMA slides were de-waxed with xylenes and re-hydrated with 100%, 90%, 70%, and 50% ethanol. The slides were then permeabilized with PBST (1/500 Triton X-100 in PBS), blocked with Image-iT FX signal enhancer (136933, Life Technology, Carlsbad, CA) for 30 min, and incubated for 2 h at room temperature with anti CD44 (ab51037, Abcam, Cambridge, MA, pre-stained with Zenon Alexa Fluor 488, Z-25302, Invitrogen, San Diego, CA) and anti CD133 (130-090-422, Miltenyi Biotec, San Diego, CA, pre-stained with Zenon Alexa Fluor 555, Z-25005) antibodies. After washing with PBS, these slides were mounted with ProLong Gold antifade reagent with DAPI (P-36931, Life Technology). Images were taken with Olympus FV-500 confocal microscope (Olympus, Center Valley, PA). The $CD133^{+}CD44^{+}$ area was measured in randomly selected 5–16 different fields of the each group (BPH, PIN, Primary prostate cancer, or Bone Mets).

Cell culture

Human prostate cancer cell lines (PC3, CRL-1435; DU145, HTB-81; LNCaP, CRL-1740) were obtained from the American Type Culture Collection (Rockville, MD). The metastatic subclone of LNCaP, C4-2B, was a subline derived from bone metastasis of LNCaP bearing-mouse. Luciferase-expressing prostate cancer cells were established by lentiviral transduction. Murine osteoblast cells were established as previously reported [2]. All prostate cancer cell lines were routinely grown in RPMI 1640 (11875–093, Life Technologies), and murine osteoblast cells were grown in α-MEM (12571–063, Life Technologies). Cultures were supplemented with 10% (v/v) fetal bovine serum (900–108, GEMINI Bio-Products, Sacramento, CA), 1% (v/v) penicillin-streptomycin (15140–122, Life Technologies) and maintained at 37°C, 5% CO_2, and 100% humidity. These cells were certified by DDC Medical.

Flow cytometry

Cells were stained with FITC- or APC-anti-HLA-ABC antibody (clone W6/32: 311404 (FITC), 311410 (APC), BioLegend, San Diego, CA), PE-cytokeratin antibody (347204, Becton Dickinson, Franklin Lakes, NJ), PE-EpCAM antibody (130-091-253, Miltenyi Biotec),

PE-anti-CD133 antibody (130-080-801, Miltenyi Biotec), APC-anti-CD44 antibody (559942, BD Biosciences, San Diego, CA), or isotype-matched IgG control for 20 min at 4°C. Flow cytometric analyses were performed in a FACSAria II High-Speed Cell Sorter (Becton Dickinson).

In vivo isolation of disseminated prostate cancer

Prostate cancer cells (1×10^6 cells) were injected into male CB.17. SCID mice (4–6 weeks of age: Charles River, Wilmington, MA) by intracardiac or intratibial injection. Bone marrow cells were flushed from femurs and tibias 24 h later. Single cell preparations were incubated first with a Lineage Cell Depletion Kit magnetic labeling system with biotinylated anti-Lineage (CD5, CD45R (B220), CD11b, Gr-1 (Ly-6G/C), and Ter-119) antibody cocktail (130-092-613, Miltenyi Biotec) and anti-Biotin MicroBeads (130-090-485, Miltenyi Biotec), and then enriched for murine Lineage negative population using an AutoMACS machine (Miltenyi Biotec). The enriched cells were incubated with a FITC- anti-HLA-ABC antibody, PE-anti-CD133 antibody, and APC-anti-CD44 antibody for another 20 min at 4°C. Thereafter, the $CD133^+/CD44^+$ and $CD133^-/CD44^-$ fractions were sorted with a FACSAria II Cell Sorter by gating on HLA-ABC positive cells. All experimental procedures were approved by the University of Michigan Committee for the Use and Care of Animals.

Cytokine arrays

Bone marrow extracellular fluid was obtained by flushing femur and tibia of tumor-bearing mice with 500 µL ice-cold phosphate-buffered saline containing protease inhibitor cocktail (P8340, Sigma-Aldrich, St. Louis, MO), and the supernatant was harvested by centrifugation at 400 *g* for 5 min. Cytokine levels in the marrow fluids were analyzed by antibody sandwich enzyme-linked immunosorbent assay (Human Inflammatory Cytokines Multi-Analyte ELISArray Kit, MEH004A, QIAGEN, Valencia, CA), according to the manufacturer's protocol. The marrow fluids obtained from non-tumor bearing mice were used as controls. Cytokine levels were normalized to total protein.

In vivo cell proliferation assays

Prostate cancer cells were stained with BrdU Labeling Reagent (00-0103, Life Technologies) according to the manufacturer's protocol. These BrdU-stained prostate cancer cells were then injected into male SCID mice by intracardiac injection. Bone marrow cells were flushed from the femurs and tibias 24 h later, and resulting cells were incubated with a FITC-anti-HLA-ABC antibody and anti-BrdU antibody (ab8039, Abcam), followed by PE-Cy7-secondary antibody (406614, BioLegend). Retention of BrdU in prostate cancer cells was analyzed by gating on HLA-ABC positive cells with a FACSAria II Cell Sorter.

Microarray analyses

The $CD133^+/CD44^+$ fraction and $CD133^-/CD44^-$ fraction were sorted with a FACSAria II Cell Sorter from *in vitro* cultured prostate cancer cells and *in vivo* disseminated prostate cancer cells obtained from bone marrow of SCID mice innoculated with prostate cancer cells (24 h) by intracadiac injection. The extractions and purifications of RNA from the resulting cells were performed using RNeasy Plus Micro RNA kit, which allowed RNA isolation and DNAse treatment from small cell numbers. RNA samples were submitted to the University of Michigan Sequencing core for quality evaluation followed by microarray analysis using an Affymetrix platform (Affymetrix, Santa Clara, CA). Data normalization and analysis was done using R and Bioconductor. The affymetrix CEL files were pre-processed and quantile normalized using Robust Multiarray Average (RMA). The probesets were annotated and mapped to gene symbols using 'hugene21sttranscriptcluster.db' on Bioconductor. In the case of multiple probes mapping to one gene symbol, the probe with the maximum mean was selected (WCGNA, R package). The Wilcoxon Rank Sum test was used to determine the differentially expressed genes between CSCs and non-CSCs. Hierarchical clustering of the samples was done using Euclidean distance and average linkage. To identify gene sets enriched in CSCs, GSEA at Broad (Broad Institute, MIT; http://www.broad.mit.edu/gsea/index.jsp) and Biocarta genesets were used. The signal to noise ratio was used as the gene list ordering mode.

RNA extraction and real-time RT-PCR

Total RNA was isolated using RNeasy Mini Kit (74106, QIAGEN). First-strand cDNA was synthesized in a 20 µL reaction volume using 0.4 µg of total RNA. RT products were analyzed by real-time RT-PCR in TaqMan® Gene Expression Assays (KLF4, Hs00358836_m1; Bmi1, Hs00995536_m1; Nanog, Hs04399610_g1; Tyro3, Hs00170723_m1; Axl, Hs01064444_m1; Mer, Hs01031973_m1; β-actin, Hs01060665_g1, Applied Biosystems, Foster City, CA). The 2nd step PCR reactions were run for 40 cycles (95°C for 15 sec and 60°C 1 min) after an initial single cycle of 50°C for 2 min and 95°C for 10 min. The PCR product was detected as an increase in fluorescence using an ABI PRISM 7700 instrument (Applied Biosystems). RNA quantity (C_R) was normalized to the housekeeping gene β-Actin control, using the formula $C_R = 2^{(40\text{-Ct of sample})-(40\text{-Ct of control})}$. The threshold cycle (Ct) is the cycle at which a significant increase in fluorescence occurs.

In vitro prostatosphere formation assays

Prostatosphere formation assays were performed using a slight modification of previously described techniques [39, 40]. Cells were plated in DMEM F-12 (11320-033, Life Technologies) containing 10 ng/mL bFGF (233-FB/CF, R&D Systems, Minneapolis, MN), 20 ng/mL EGF (236-EG, R&D Systems), 5 mg/mL insulin (3435, R&D Systems), and 0.4% (v/v) bovine serum albumin (BSA) (5217, R&D Systems) supplemented with 1% (v/v) knockout serum replacement (10828-028, Life Technologies) at 500-3,000 cells per well in 6-well ultra low attachment plates. In some case, the cultures were treated with the Mer inhibitor UNC1062 (AOB4488, AOBIOUS, Gloucester, MA). Prostatosphere formation (cell clusters of 10 cells or greater) was observed at 7–10 days under a light microscopy.

In vivo serial dilution tumor-propagating assays

The $CD133^+/CD44^+$ fraction and $CD133^-/CD44^-$ fraction were sorted from *in vitro* cultured luciferase expressing prostate cancer cells with a FACSAria II High-Speed Cell Sorter. The resulting cells were suspended in serum-free RPMI/cytokine reduced collagen gel mixture (1:1 volume) and then implanted subcutaneously into SCID mice (1 to 1×10^4 viable cells). Tumor growth was tracked by bioluminescence imaging, performed as previously described [37], through the University of Michigan Small Animal Imaging Resource facility.

In vitro chemoresistance assays

Prostate cancer cells were treated with/without docetaxel (1 μg/mL, 01885, Sigma-Aldrich) and the cultures were incubated at 37°C for 48 h. Thereafter, the $CD133^+/CD44^+$ fraction in resulting cells was analyzed with a FACSAria II Cell Sorter.

In vitro co-culture

Prostate cancer cells were cultured on murine calvarial osteoblasts obtained from wild type or *GAS6*-deficient ($GAS6^{-/-}$) mice for 48 h, and then the $CD133^+/CD44^+$ fraction was analyzed using a FACSAria II Cell Sorter by gating on HLA-ABC positive cells. The laboratory of Dr. Peter Carmeliet (University of Leuven, Leuven, Belgium) generated the $GAS6^{-/-}$animals and graciously provided our laboratory with a pair of the homozygous $GAS6^{-/-}$ mice for breeding.

Vossicle transplant

Lumbar vertebrae were isolated from 4- to 7-day-old $GAS6^{+/+}$ or $GAS6^{-/-}$ mice. The vertebrae were sectioned into single vertebral bodies (a.k.a. vossicles). SCID mice were used as transplant recipients. Two vossicles per mouse were implanted into subcutaneous space as previously described [2]. Before implantation, PC3 cells were introduced into both vossicles (10,000 cells/10 μL of PBS). Mice were sacrificed at 3 weeks, and the vossicles prepared for immunohistochemistry.

Immunohistochemistry

To detect human cells grown in mice, anti-human HLA-ABC antibody (311402, BioLegend) was conjugated using the Zenon Alexa Fluor 555 mouse IgG_{2a} labeling kit (Z-25105). To detect human CD133 antigen, purified mouse IgG1 antibody (Miltenyi Biotec) was conjugated using the Zenon Alexa Fluor 488 mouse IgG1 labeling kit (Z-25002). For detection of human CD44 antigen, the antibody (Abcam) was conjugated using the Zenon Alexa Fluor 555 Rabbit IgG labeling kit (Z-25305). 7 μm thick paraffin sections were generated, and antigen retrieval performed with a pepsin solution at 37°C for 15 min, followed by washing with PBT (PBS plus 0.2% Triton X-100) for 5 min at room temperature. Each section was blocked with Image-iT FX signal enhancer (Invitrogen) for 30 min before fluorescence-labeled primary antibodies were applied for 2 h at room temperature in the dark. Subsequently, the sections were washed twice by submersion in PBS for 10 min, subjected to post-stain fixation with 10% formalin (Sigma-Aldrich), and mounted with ProLong Gold anti-fade reagent with DAPI. Images were taken with Olympus FV-500 confocal microscope.

Western blots

Prostate cancer cells were prepared in lysis buffer (CelLytic MT Mammalian Tissue Lysis Reagent, C3228, Sigma-Aldrich), and protein concentration was quantified using a DC Protein Assay Kit II (5000112, Bio-RAD, Hercules, CA). Cell extracts (30 μg of protein per lane) were loaded and separated on SDS-PAGE (4–20% Bis-Glycine gradient gels, EC6025BOX, Invitrogen) and transferred to a PVDF membrane. Membranes were incubated with 5% milk for 1 h and incubated with anti-Tyro3 (585S) -Axl (4977), -Mer (4319), -GAPDH (2118), -P-4E-BP1 (2855), -4E-PB1 (9644), -P-p70S6K (9234), -p70S6K (2708), -P-AKT(S473) (9271), or -AKT(S473) (9272) antibody (all primary antibodies were obtained from Cell Signaling Technology, Danvers, MA) overnight at 4°C. Primary antibody was used with 5% dry milk. Blots were incubated with peroxidase-coupled secondary antibodies (W4011, Promega, Madison, WI) for 1 h at a ratio of 1:3000. Protein expression was detected with SuperSignal West Pico Chemiluminescent Substrate (34080, Thermo Scientific, Rockford, IL). The densitometric analysis of the Western blot were performed with ImageJ software (version 1.50i; National Institutes of Health, Bethesda, MD).

TAM receptors knockdown

Stable knockdowns of TAM receptors (Tyro3, Axl, Mer) in prostate cancer cells were generated by lentiviral infection. Lentiviruses were constructed at the Vector Core in University of Michigan (Ann Arbor, MI) using GIPZ Lentiviral shRNAmir vectors containing either TAM receptors (Tyro3, Axl, Mer) shRNA or nonsilencing (scrambled) shRNA (Open Biosystems, Lafayette, CO).

Statistical analyses

Numerical data are expressed as mean ± standard deviation. Statistical analysis was performed by unpaired two-tailed Student's *t* test using the GraphPad Instat statistical program (GraphPad Software, San Diego, CA) with significance at $P < 0.05$. For the real-time RT-PCR assays, a Kruskal-Wallis test and Dunn's multiple comparisons tests were utilized with the level of significance set at $P < 0.05$.

Abbreviations

Cancer stem cells (CSCs); hematopoietic stem cell (HSCs); disseminated tumor cells (DTCs); prostate-specific antigen (PSA); tissue microarray (TMA); bovine serum albumin (BSA).

ACKNOWLEDGMENTS

We are grateful to the following lab members for their contributions towards parts of this project: Drs. Anjali Mishra and Jeena Joseph. We also thank Dr. Peter Carmeliet for providing the GAS6$^{-/-}$ mice. The work is dedicated to the memory of Janice E. Berry.

CONFLICTS OF INTEREST

The authors declare that there are no conflicts of interest.

GRANT SUPPORT

This work is directly supported by the National Cancer Institute (CA093900 to K.J. Pienta and R.S. Taichman, CA163124 to Y. Shiozawa, K.J. Pienta, and R.S. Taichman, U54CA143803 to K.J. Pienta, CA143055 to K.J. Pienta), the Department of Defense (W81XWH-14-1-0403 to Y. Shiozawa, and W81XWH-11-1-0636 to K.J. Pienta and R.S. Taichman), and the Prostate Cancer Foundation (Y. Shiozawa, K.J. Pienta, and R.S. Taichman). K.J. Pienta receives support as an American Cancer Society Clinical Research Professor, and R.S. Taichman is supported as the Major M. Ash Professor.

REFERENCES

1. Semenas J, Allegrucci C, Boorjian SA, Mongan NP, Persson JL. Overcoming drug resistance and treating advanced prostate cancer. Current drug targets. 2012; 13:1308–23.
2. Shiozawa Y, Pedersen EA, Havens AM, Jung Y, Mishra A, Joseph J, Kim JK, Patel LR, Ying C, Ziegler AM, Pienta MJ, Song J, Wang J, et al. Human prostate cancer metastases target the hematopoietic stem cell niche to establish footholds in mouse bone marrow. J Clin Invest. 2011; 121:1298–312.
3. Riethdorf S, Pantel K. Disseminated tumor cells in bone marrow and circulating tumor cells in blood of breast cancer patients: current state of detection and characterization. Pathobiology. 2008; 75:140–8.
4. Hensel JA, Flaig TW, Theodorescu D. Clinical opportunities and challenges in targeting tumour dormancy. Nature reviews Clinical oncology. 2013; 10:41–51.
5. Ranganathan AC, Adam AP, Aguirre-Ghiso JA. Opposing roles of mitogenic and stress signaling pathways in the induction of cancer dormancy. Cell Cycle. 2006;5:1799–807.
6. Pantel K, Alix-Panabieres C, Riethdorf S. Cancer micro-metastases. Nature reviews Clinical oncology. 2009; 6:339–51.
7. Morgan TM, Lange PH, Porter MP, Lin DW, Ellis WJ, Gallaher IS, Vessella RL. Disseminated tumor cells in prostate cancer patients after radical prostatectomy and without evidence of disease predicts biochemical recurrence. Clin Cancer Res. 2009; 15:677–83.
8. Lapidot T, Sirard C, Vormoor J, Murdoch B, Hoang T, Caceres-Cortes J, Minden M, Paterson B, Caligiuri MA, Dick JE. A cell initiating human acute myeloid leukaemia after transplantation into SCID mice. Nature. 1994; 367:645–8.
9. Al-Hajj M, Wicha MS, Benito-Hernandez A, Morrison SJ, Clarke MF. Prospective identification of tumorigenic breast cancer cells. Proc Natl Acad Sci U S A. 2003;100:3983–8.
10. Visvader JE, Lindeman GJ. Cancer stem cells in solid tumours: accumulating evidence and unresolved questions. Nat Rev Cancer. 2008; 8:755–68.
11. Shiozawa Y, Taichman RS. Getting blood from bone: an emerging understanding of the role that osteoblasts play in regulating hematopoietic stem cells within their niche. Experimental hematology. 2012; 40:685–94.
12. Shiozawa Y, Pedersen EA, Patel LR, Ziegler AM, Havens AM, Jung Y, Wang J, Zalucha S, Loberg RD, Pienta KJ, Taichman RS. GAS6/AXL axis regulates prostate cancer invasion, proliferation, and survival in the bone marrow niche. Neoplasia. 2010; 12:116–27.
13. Mishra A, Wang J, Shiozawa Y, McGee S, Kim J, Jung Y, Joseph J, Berry JE, Havens A, Pienta KJ, Taichman RS. Hypoxia stabilizes GAS6/Axl signaling in metastatic prostate cancer. Molecular cancer research. 2012; 10:703–12.
14. Taichman RS, Patel LR, Bedenis R, Wang J, Weidner S, Schumann T, Yumoto K, Berry JE, Shiozawa Y, Pienta KJ.

GAS6 receptor status is associated with dormancy and bone metastatic tumor formation. PloS one. 2013; 8:e61873.

15. Dubrovska A, Kim S, Salamone RJ, Walker JR, Maira SM, Garcia-Echeverria C, Schultz PG, Reddy VA. The role of PTEN/Akt/PI3K signaling in the maintenance and viability of prostate cancer stem-like cell populations. Proc Natl Acad Sci U S A. 2009; 106:268–73.
16. Deng G, Herrler M, Burgess D, Manna E, Krag D, Burke JF. Enrichment with anti-cytokeratin alone or combined with anti-EpCAM antibodies significantly increases the sensitivity for circulating tumor cell detection in metastatic breast cancer patients. Breast Cancer Res. 2008; 10:R69.
17. Burger PE, Gupta R, Xiong X, Ontiveros CS, Salm SN, Moscatelli D, Wilson EL. High aldehyde dehydrogenase activity: a novel functional marker of murine prostate stem/progenitor cells. Stem Cells. 2009; 27:2220–8.
18. Huang J, Nguyen-McCarty M, Hexner EO, Danet-Desnoyers G, Klein PS. Maintenance of hematopoietic stem cells through regulation of Wnt and mTOR pathways. Nature medicine. 2012; 18:1778–85.
19. Kim JK, Jung Y, Wang J, Joseph J, Mishra A, Hill EE, Krebsbach PH, Pienta KJ, Shiozawa Y, Taichman RS. TBK1 regulates prostate cancer dormancy through mTOR inhibition. Neoplasia. 2013; 15:1064–74.
20. Chetram MA, Odero-Marah V, Hinton CV. Loss of PTEN permits CXCR4-mediated tumorigenesis through ERK1/2 in prostate cancer cells. Molecular cancer research : MCR. 2011; 9:90–102.
21. Pound CR, Partin AW, Eisenberger MA, Chan DW, Pearson JD, Walsh PC. Natural history of progression after PSA elevation following radical prostatectomy. JAMA. 1999; 281:1591–7.
22. Oktem G, Bilir A, Uslu R, Inan SV, Demiray SB, Atmaca H, Ayla S, Sercan O, Uysal A. Expression profiling of stem cell signaling alters with spheroid formation in CD133/CD44 prostate cancer stem cells. Oncol Lett. 2014; 7:2103–9.
23. Wang L, Huang X, Zheng X, Wang X, Li S, Zhang L, Yang Z, Xia Z. Enrichment of prostate cancer stem-like cells from human prostate cancer cell lines by culture in serum-free medium and chemoradiotherapy. International journal of biological sciences. 2013; 9:472–9.
24. Steinmetz NF, Maurer J, Sheng H, Bensussan A, Maricic I, Kumar V, Braciak TA. Two Domains of Vimentin Are Expressed on the Surface of Lymph Node, Bone and Brain Metastatic Prostate Cancer Lines along with the Putative Stem Cell Marker Proteins CD44 and CD133. Cancers (Basel). 2011; 3:2870–85.
25. Jung Y, Shiozawa Y, Wang J, McGregor N, Dai J, Park SI, Berry JE, Havens AM, Joseph J, Kim JK, Patel L, Carmeliet P, Daignault S, et al. Prevalence of prostate cancer metastases after intravenous inoculation provides clues into the molecular basis of dormancy in the bone marrow microenvironment. Neoplasia. 2012; 14:429–39.
26. Bragado P, Estrada Y, Parikh F, Krause S, Capobianco C, Farina HG, Schewe DM, Aguirre-Ghiso JA. TGF-beta2 dictates disseminated tumour cell fate in target organs through TGF-beta-RIII and p38alpha/beta signalling. Nat Cell Biol. 2013; 15:1351–61.
27. Ghajar CM, Peinado H, Mori H, Matei IR, Evason KJ, Brazier H, Almeida D, Koller A, Hajjar KA, Stainier DY, Chen EI, Lyden D, Bissell MJ. The perivascular niche regulates breast tumour dormancy. Nat Cell Biol. 2013; 15:807–17.
28. Gao H, Chakraborty G, Lee-Lim AP, Mo Q, Decker M, Vonica A, Shen R, Brogi E, Brivanlou AH, Giancotti FG. The BMP inhibitor Coco reactivates breast cancer cells at lung metastatic sites. Cell. 2012; 150:764–79.
29. Zhang H, Wu H, Zheng J, Yu P, Xu L, Jiang P, Gao J, Wang H, Zhang Y. Transforming growth factor beta1 signal is crucial for dedifferentiation of cancer cells to cancer stem cells in osteosarcoma. Stem Cells. 2013; 31:433–46.
30. Kobayashi A, Okuda H, Xing F, Pandey PR, Watabe M, Hirota S, Pai SK, Liu W, Fukuda K, Chambers C, Wilber A, Watabe K. Bone morphogenetic protein 7 in dormancy and metastasis of prostate cancer stem-like cells in bone. The Journal of experimental medicine. 2011; 208:2641–55.
31. Buijs JT, Henriquez NV, van Overveld PG, van der Horst G, ten Dijke P, van der Pluijm G. TGF-beta and BMP7 interactions in tumour progression and bone metastasis. Clin Exp Metastasis. 2007; 24:609–17.
32. Quintana E, Shackleton M, Foster HR, Fullen DR, Sabel MS, Johnson TM, Morrison SJ. Phenotypic heterogeneity among tumorigenic melanoma cells from patients that is reversible and not hierarchically organized. Cancer cell. 2010; 18:510–23.
33. Meacham CE, Morrison SJ. Tumour heterogeneity and cancer cell plasticity. Nature. 2013; 501:328–37.
34. Takahashi K, Yamanaka S. Induction of pluripotent stem cells from mouse embryonic and adult fibroblast cultures by defined factors. Cell. 2006; 126:663–76.
35. Chaffer CL, Brueckmann I, Scheel C, Kaestli AJ, Wiggins PA, Rodrigues LO, Brooks M, Reinhardt F, Su Y, Polyak K, Arendt LM, Kuperwasser C, Bierie B, et al. Normal and neoplastic nonstem cells can spontaneously convert to a stem-like state. Proc Natl Acad Sci U S A. 2011; 108:7950–5.
36. Chaffer CL, Marjanovic ND, Lee T, Bell G, Kleer CG, Reinhardt F, D'Alessio AC, Young RA, Weinberg RA. Poised chromatin at the ZEB1 promoter enables breast cancer cell plasticity and enhances tumorigenicity. Cell. 2013; 154:61–74.
37. Liu S, Cong Y, Wang D, Sun Y, Deng L, Liu Y, Martin-Trevino R, Shang L, McDermott SP, Landis MD, Hong S, Adams A, D'Angelo R, et al. Breast Cancer Stem Cells Transition between Epithelial and Mesenchymal States Reflective of their Normal Counterparts. Stem cell reports. 2014; 2:78–91.

38. Paget S. The distribution of secondary growths in cancer of the breast. Lancet. 1889; 1:571–3.

39. Yu C, Yao Z, Dai J, Zhang H, Escara-Wilke J, Zhang X, Keller ET. ALDH activity indicates increased tumorigenic cells, but not cancer stem cells, in prostate cancer cell lines. *In vivo*. 2011; 25:69–76.

40. Duhagon MA, Hurt EM, Sotelo-Silveira JR, Zhang X, Farrar WL. Genomic profiling of tumor initiating prostatospheres. BMC genomics. 2010; 11:324.

THE JOURNAL OF BIOLOGICAL CHEMISTRY VOL. 291, NO. 37, pp. 19351–19363, September 9, 2016

Secreted Protein Acidic and Rich in Cysteine (SPARC) Mediates Metastatic Dormancy of Prostate Cancer in Bone*[S]

Received for publication, May 9, 2016, and in revised form, July 15, 2016 Published, JBC Papers in Press, July 15, 2016, DOI 10.1074/jbc.M116.737379

Sambad Sharma[‡], Fei Xing[‡], Yin Liu[‡], Kerui Wu[‡], Neveen Said[§], Radhika Pochampally[¶], Yusuke Shiozawa[‡], Hui-Kuan Lin[‡], K. C. Balaji[‖], and Kounosuke Watabe[‡1]

From the Departments of [‡]Cancer Biology, [§]Pathology, and [‖]Urology, Wake Forest University School of Medicine, Winston-Salem, North Carolina 27157 and the [¶]Department of Biochemistry and Cancer Institute, University of Mississippi Medical Center, Jackson, Mississippi 39216

Prostate cancer is known to frequently recur in bone; however, how dormant cells switch its phenotype leading to recurrent tumor remains poorly understood. We have isolated two syngeneic cell lines (indolent and aggressive) through *in vivo* selection by implanting PC3mm stem-like cells into tibial bones. We found that indolent cells retained the dormant phenotype, whereas aggressive cells grew rapidly in bone *in vivo*, and the growth rates of both cells in culture were similar, suggesting a role of the tumor microenvironment in the regulation of dormancy and recurrence. Indolent cells were found to secrete a high level of secreted protein acidic and rich in cysteine (SPARC), which significantly stimulated the expression of BMP7 in bone marrow stromal cells. The secreted BMP7 then kept cancer cells in a dormant state by inducing senescence, reducing "stemness," and activating dormancy-associated p38 MAPK signaling and p21 expression in cancer cells. Importantly, we found that SPARC was epigenetically silenced in aggressive cells by promoter methylation, but 5-azacytidine treatment reactivated the expression. Furthermore, high SPARC promoter methylation negatively correlated with disease-free survival of prostate cancer patients. We also found that the COX2 inhibitor NS398 down-regulated DNMTs and increased expression of SPARC, which led to tumor growth suppression in bone *in vivo*. These findings suggest that SPARC plays a key role in maintaining the dormancy of prostate cancer cells in the bone microenvironment.

Prostate carcinoma at an early stage is generally treated with surgical resection or radiotherapy with or without combination of androgen deprivation therapy (1–3). However, patients often develop fatal recurrent disease months or years after treatment of the primary tumor. The culprits for the recurrent disease are the small number of residual cells that are disseminated from the primary tumor prior to treatment (4). Even patients with asymptomatic disease or no evidence of primary disease progression are known to often harbor cancer cells at distant organs such as bone, and they can be isolated from the bone marrow aspirate (5). These cells include quiescent cancer stem cells (CSCs)[2] and may reacquire clonogenic growth in a favorable environment and cause recurrent disease, which is evident in 20–50% of patients who were treated for localized primary disease (6).

Metastatic dormancy at a distant site is known to be determined by intrinsic molecular characteristics of the cell as well as extrinsic cues from the microenvironment. Dormancy of micrometastasis and cellular dormancy have been described as the adapted modes of dormant survival in a distant environment (7–10). The ratio of p38 to Erk activation is considered to be one of the molecular indications that dictate the fate of cancer cells. A high ratio of activated p38 to Erk signals for inhibition of cell proliferation or cellular dormancy, whereas a low ratio reverts the phenotype to the proliferative state (8, 11, 12). Recently, it was also demonstrated that dormant cells are reprogrammed by epigenetic regulation that leads to a quiescence state (13). In addition, interaction between tumor cells and the stroma, angiogenesis, and immune surveillance of cancer cells are also known to regulate dormancy and recurrence (8, 14).

The lack of an established model for dormancy has been a major hurdle for research advancement in this field. Although several *in vitro* models have been described previously, *in vivo* working models for dormant and recurrent growth have yet to be developed. Recent attempts have characterized syngeneic head and neck squamous cell carcinoma cells (T-Hep and D-Hep) or a pair of breast cancer cell lines (D2.OR and D2A1 cells) that recapitulates dormant growth *in vivo* (13, 15–17). However, there is still no appropriate *in vivo* model that mimics dormancy and recurrence for prostate cancer, especially one that replicates the phenomenon of bone recurrence in patients. In an approach to identify dormant prostate cancer cells in bone, we isolated a pair of cell lines from the bones of mice that showed either aggressive growth or indolent disease when their CSCs were injected in the tibiae. Gene profiling of the paired cell lines revealed the role of secreted protein acidic and rich in cysteine (SPARC), also known as Osteonectin, in dormancy of tumor cells in bone. Our results suggest that SPARC maintains

* This work was supported by National Institutes of Health Grants R01CA173499 and R01CA185650 (to K. W). The authors declare that they have no conflicts of interest with the contents of this article. The content is solely the responsibility of the authors and does not necessarily represent the official views of the National Institutes of Health.

[S] This article contains supplemental Figs. S1–S5 and Table S1.

[1] To whom correspondence should be addressed: Dept. of Cancer Biology, Wake Forest University School of Medicine, Winston-Salem, NC 27157. Tel.: 336-716-0231; Fax: 336-716-0255; E-mail: kwatabe@wakehealth.edu.

[2] The abbreviations used are: CSC, cancer stem cell; SPARC, secreted protein acidic and rich in cysteine; BMP, bone morphogenetic protein; BMSC, bone marrow stromal cell(s); CM, conditioned medium/media; BMPR, bone morphogenetic protein receptor; TCGA, The Cancer Genome Atlas; DNMTs, DNA methyltransferases; hBMSC, human bone marrow stromal cells; rSPARC, recombinant SPARC.

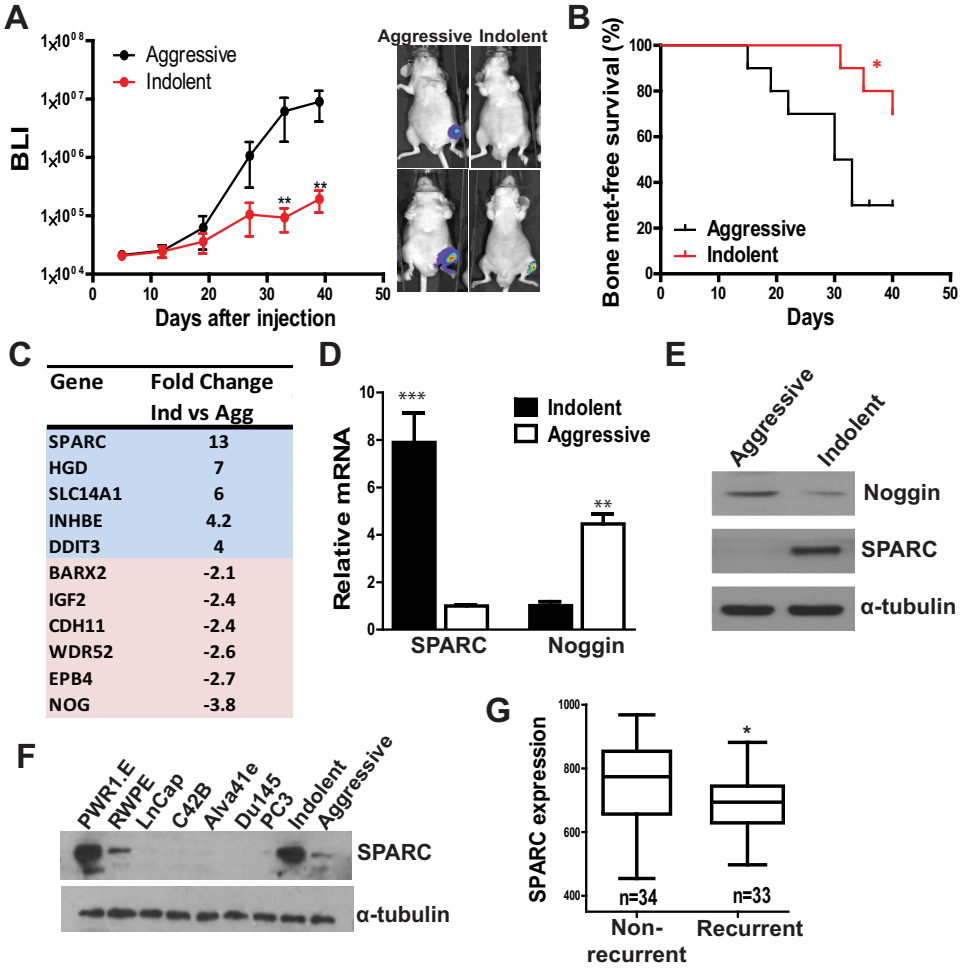

FIGURE 1. **Establishing model cell lines for dormancy recurrence.** *A*, indolent and aggressive cells were injected into the tibial bone of mice ($n = 8$), followed by examination of tumor growth by bioluminescence for 6 weeks. *Right panel*, representative pictures of aggressive and indolent cell growth in the tibiae of mice on day 40. **, $p < 0.01$ *versus* indolent. *BLI*, bioluminescence imaging. *B*, indolent and aggressive cells were injected via the intracardiac route, followed by examination of bone metastasis-free survival of the mice by bioluminescence ($n = 10$/group). *, $p = 0.0277$ by log-rank test. *C*, indolent (*Ind*) and aggressive (*Agg*) cells were subjected to comprehensive gene expression analysis by using Affymetrix microarray 2.0. The five most significantly up-regulated and six down-regulated genes are shown. *D* and *E*, SPARC and Noggin expression in indolent and aggressive cells was examined by quantitative RT-PCR (*D*) and Western blotting (*E*). *F*, SPARC expression was examined in normal and various prostate cancer cell lines by Western blotting. *G*, analysis of a Gene Expression Omnibus dataset for SPARC expression in patients with or without recurrent disease (GSE25136). 15% outliers were removed from the analysis. *, $p < 0.05$; **, $p < 0.01$; ***, $p < 0.0001$.

the dormant state of cancer cells by stimulating the secretion of bone morphogenetic protein 7 (BMP7), a TGF-β family member protein, from the bone stroma. SPARC was also found to be epigenetically controlled, and a COX2 inhibitor effectively suppressed tumor growth in bone by up-regulating SPARC, suggesting this microenvironmental cue as a potential therapeutic target for recurrent disease.

Results

Isolation of Paired Prostate Cell Lines as a Model for Dormancy and Recurrent Growth in Bone—To establish a model for dormancy and recurrent growth of prostate cancer, we first prepared CSCs from the PC3mm cell line using the defined cell surface markers $CD24^{low}/CD44^{high}/CD133^{high}$, as reported previously (18). CSCs were then implanted into mouse tibial bones with a dose by which ~50% of tibiae developed overt tumors after 1 month. The cells were then isolated from the bone with or without overt tumor growth, followed by colony expansion of each cell in culture (supplemental Fig. S1*A*). The cells derived from bone with overt growth or no growth were designated as "aggressive" and "indolent" cells, respectively. When the cells were reinjected into the tibial bone of mice, indolent cells grew significantly slower with a long lag time compared with aggressive cells (Fig. 1*A*). Furthermore, indolent cells also showed a decreased ability to colonize in bone when injected intracardially (Fig. 1*B*). However, in contrast to their striking difference in *in vivo* growth in bone, aggressive and indolent cells showed no difference in *in vitro* cell proliferation, invasion, migration, CSC population, and self-renewal abilities (supplemental Fig. 1, *B–F*), suggesting a role of the bone microenvironment in differential *in vivo* growth. We then performed Affymetrix microarray profiling to analyze differentially expressed genes between indolent and aggressive cells. As shown in Fig. 1*C*, SPARC and Noggin were most significantly overexpressed in indolent cells and aggressive cells, respectively. Both SPARC and Noggin are secretory proteins that are known to be present in the bone (19–22), which provides clues that the bone environment may play a pivotal role in the differ-

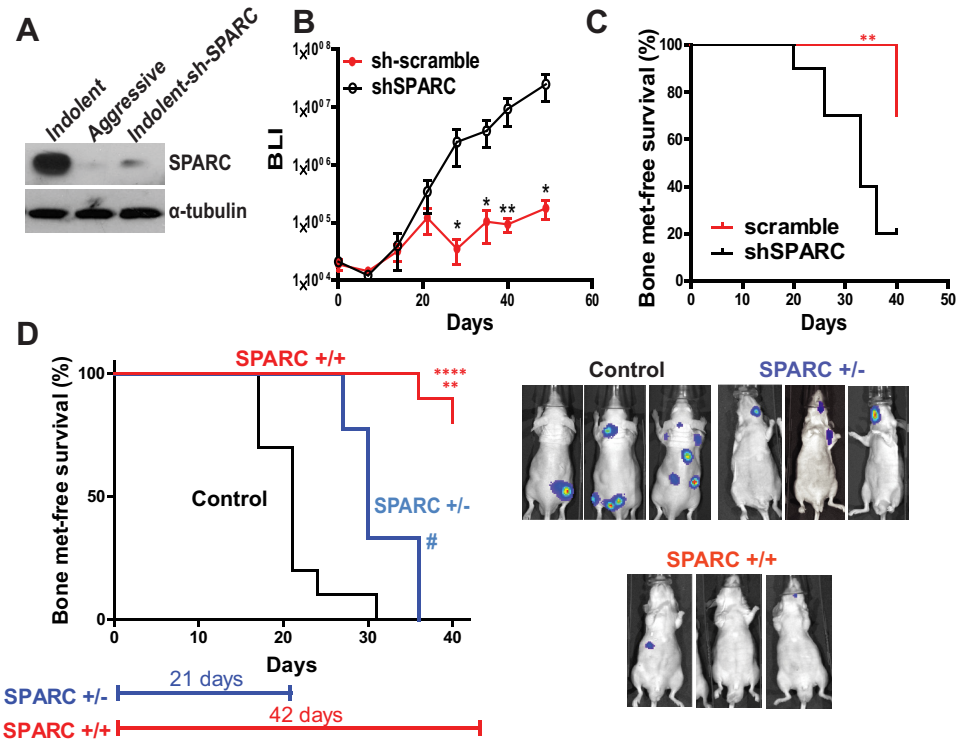

FIGURE 2. **SPARC plays a critical role in dormancy and recurrence.** *A*, SPARC knockdown by shRNA in indolent cells was verified by Western blotting. *B*, tumor growth was observed after intratibial injection of indolent-sh-SPARC or sh-Scramble cells by bioluminescence ($n = 10$/group). *, $p < 0.05$ *versus* scramble; **, $p < 0.01$ *versus* scramble. *BLI*, bioluminescence imaging. *C*, indolent-sh-SPARC or sh-Scramble cells were implanted into nude mice intracardially ($n = 10$/group), and bone metastasis-free survival was examined by bioluminescence. Indolent-Scramble *versus* indolent-sh-SPARC: **, $p = 0.0032$. *D*, aggressive cells were implanted into nude mice via intracardiac injection ($n = 10$/group), and bone metastasis-free survival was examined in the following three groups of animals: rSPARC (200 μg/kg) was administered by tail vein injection twice a week until day 42 (*red line*, +/+); rSPARC was administered until day 21, followed by withdrawal of rSPARC injection (*blue line*, ±); and a control group (*black line*) without administration of rSPARC. *Right panel*, representative images of mice from each group. Control *versus* SPARC+/+: ****, $p < 0.0001$; control *versus* SPARC ±: #, $p = 0.0117$; SPARC ± *versus* SPARC+/+: **, $p = 0.0099$ by log-rank test.

ential growth of indolent and aggressive cells *in vivo*. We further verified that the expression of Noggin was increased whereas the SPARC level was decreased in aggressive cells (Fig. 1, *D* and *E*). In addition, we found that SPARC expression in indolent cells was significantly higher compared with a series of prostate cancer cell lines and similar to that of normal immortalized prostate cells (Fig. 1*F*). Interestingly, when we analyzed a Gene Expression Omnibus database for expression of SPARC in a retrospective cohort of patients, we found that SPARC expression was significantly up-regulated in patients with no recurrence status for at least 5 years after radical prostatectomy (Fig. 1*G*) (23). These results strongly suggest that SPARC and Noggin play critical roles in the dormancy of prostate cancer.

SPARC Induces Dormancy in Vivo—SPARC is a matrix-associated protein, and it has been reported to be involved in cell cycle regulation, whereas Noggin is an inhibitor of BMPs (24–26). To further clarify the role of SPARC, the gene was silenced by introducing shRNA with a lentiviral expression system to indolent cells (Fig. 2*A*). Silencing SPARC in indolent cells or treating aggressive cells with recombinant SPARC did not confer any *in vitro* proliferative advantage to these cells (data not shown). We then transplanted indolent cells with or without expression of shRNA into tibial bone in nude mice. As shown in Figs. 2*B*, we found that knockdown of SPARC significantly stimulated the growth of tumor in bone, whereas scrambled shRNA did not affect the growth (Fig. 2*B*). Similarly, when tumor cells were transplanted via the intracardiac route, indolent cells that were silenced for SPARC expression showed a significant decrease in bone metastasis-free survival (Fig. 2*C*). To further examine the effect of SPARC on dormancy, we performed a recurrence assay *in vivo* by injecting aggressive cells into the nude mice via the intracardiac route, followed by administration of recombinant SPARC through intravenous injection every 3 days (Fig. 2*D*). We found that SPARC significantly delayed the incidence of bone metastasis. Importantly, withdrawal of SPARC injection after 3 weeks nullified the suppressive effect and significantly accelerated the onset of bone metastasis. These results suggest that SPARC leads to dormant survival of aggressive cells in bone and that the withdrawal of SPARC confers recurrent growth ability to cancer cells residing in bone (Fig. 2*D*).

SPARC Enhances Paracrine Dormancy Signaling from the Bone Stroma—The striking growth difference of indolent cells between *in vitro* and *in vivo* settings and the effect of recombinant SPARC *in vivo* strongly suggest that the secreted SPARC from indolent cells affects bone environmental cells to induce growth-suppressive effects on tumor cells. To test this hypothesis, we first cultured indolent and aggressive cells in a transwell plate with various cell types known to reside in bone. We found a significant reduction in the growth of indolent compared with aggressive cells when co-cultured with either BMSC or the HS5 bone stromal cell line, suggesting that secreted factor(s) from indolent cells induce an inhibitory response from bone stromal cells (Figs. 3, *A* and *B*, and supplemental Fig. S2*A*). Treatment of

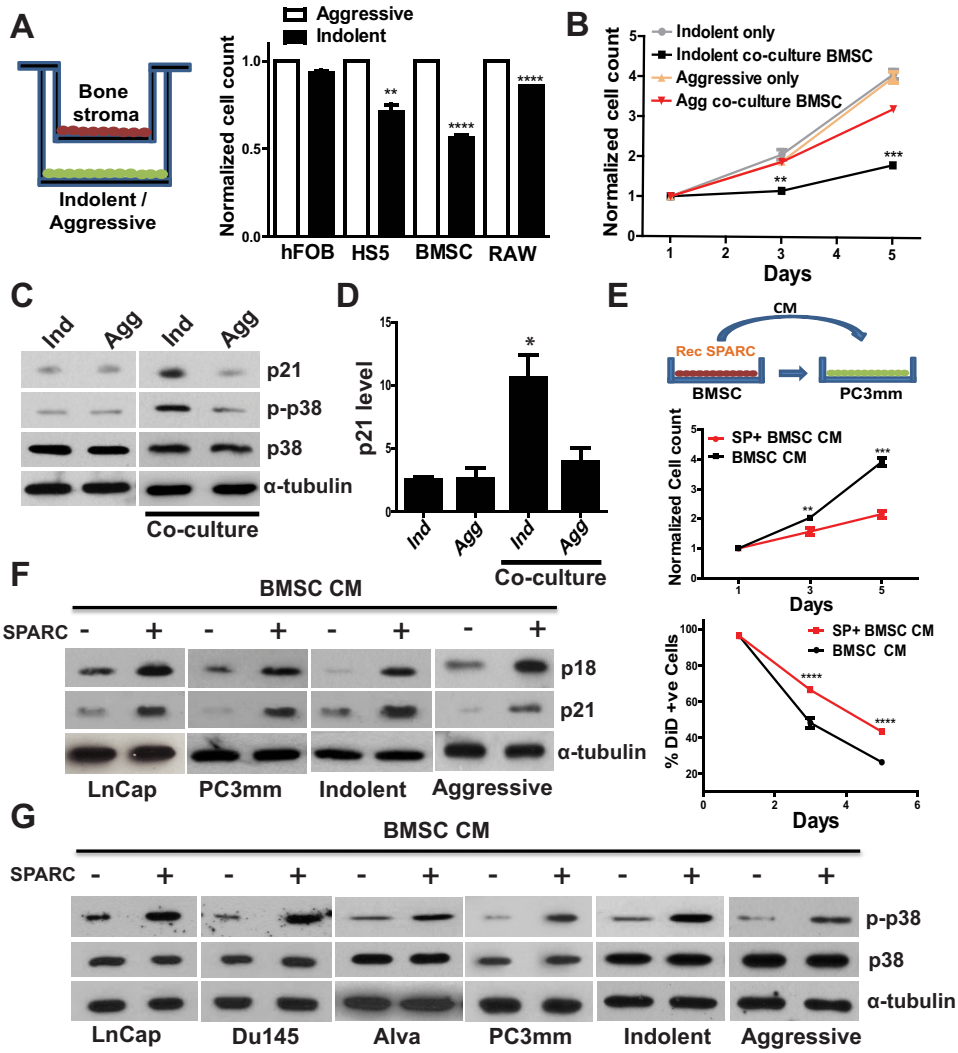

FIGURE 3. **SPARC-induced secretory factor from bone stroma activates p38 MAPK pathway.** *A*, indolent or aggressive cells were co-cultured with various bone stromal cells in a transwell, as shown in the *left panel*, followed by a cell proliferation assay of cancer cells in the lower chamber on day 5. *B*, indolent or aggressive cells were co-cultured with BMSC in a transwell plate, followed by quantifying cell proliferation of cancer cells. *C*, expression of p21, total p-38, and phosphorylated-p-38 was examined in indolent (*Ind*) and aggressive (*Agg*) cells with or without co-culture with BMSC for 3 days. *D*, p21 expression was examined by quantitative RT-PCR for *C*. *E*, *top panel*, BMSC were treated with or without rSPARC (200 ng/ml) for 24 h, and then the medium was replaced with fresh medium (DMEM) and incubated for 24 h to generate CM. *BMSC CM* and *SP+ BMSC CM* represent rSPARC-untreated or -treated BMSC CM, respectively. *Center* and *bottom panels*, PC3mm cells were seeded in a 96-well plate and treated with CM from SPARC-treated or -untreated BMSC as mentioned above, followed by examination of cell proliferation by (3-(4,5-dimethylthiazol-2 yl)-5-(3-carboxy phenyl)-2-(4-sulfophenyl)-2H-tetrazolium assay (*center panel*) and DiD membrane labeling assay (*bottom panel*) on days 1, 3, and 5. *F*, CM generated from BMSC as shown in *E*, *top panel*, were used to treat prostate cancer cells (LnCaP, PC3mm, indolent, and aggressive) for 24 h, and p21 and p18 expression was examined by Western blotting. *G*, CM generated as shown in *E*, *top panel*, were used to treat a series of prostate cancer cells lines (as indicated) for 24 h, and phosphorylated as well as total p38 levels were examined by Western blotting. *, $p < 0.05$; **, $p < 0.01$; ***, $p < 0.0001$.

tumor cells with conditioned medium (CM) generated from BMSC or HS5 cells alone showed no differential proliferative effect (supplemental Fig. S2, *B* and *C*), suggesting a need of stroma-cancer cell interaction to exert the tumor-suppressive effect of stromal cells. Furthermore, we found that the transwell co-culture of indolent cells activated the dormancy-associated p38 pathway and also induced the p21 cell cycle inhibitor (Fig. 3, *C* and *D*). To examine whether the inhibitory response is indeed induced by SPARC, we first generated CM by treating BMSC with or without recombinant SPARC (as outlined in Fig. 3*E*, *top panel*) and treated cancer cells with the CM to examine cell proliferation by (3-(4,5-dimethylthiazol-2 yl)-5-(3-carboxy phenyl)-2-(4-sulfophenyl)-2H-tetrazolium, or label retention assay (Fig. 3*E*, *center* and *bottom panels*). We found that the CM generated from SPARC-treated BMSC significantly lowered cell proliferation of PC3mm cells. Furthermore, CM of SPARC-treated BMSC activated p38-MAPK signaling and up-regulated expression of its downstream cell cycle inhibitors p21 and p18 in a panel of prostate cancer cells (Fig. 3, *F* and *G*). We also observed a significant decrease in cell proliferation and increase in p21 expression when CM were generated from BMSC or HS5 cells that were pretreated with aggressive or indolent cell-derived CM (supplemental Fig. S2, *D* and *E*). In addition, we also verified that SPARC secreted by indolent cells was significantly higher than that secreted by bone-residing cells (supplemental Fig. S2 *F*). These results strongly suggest that indolent cells secrete SPARC, which then stimulates BMSC to release factor(s) that, in turn, activate dormancy signaling in cancer cells in bone.

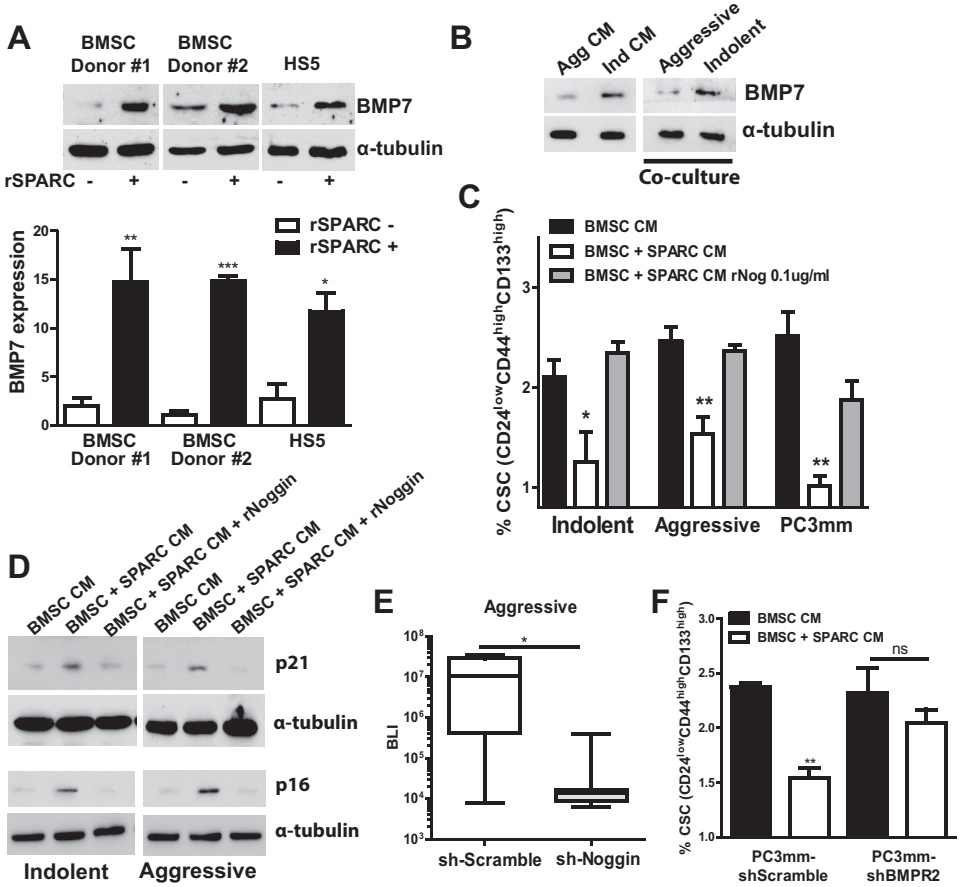

FIGURE 4. **SPARC up-regulates BMP7 from BMSC.** *A*, BMSC from two different donors (BMSC#1 and BMSC#2) and the HS5 cell line were treated with rSPARC (200 ng/ml) for 24 h, and BMP7 expression was examined by Western blotting and quantitative RT-PCR. *B*, BMSC#1 was treated with CM generated from indolent (*Ind*) or aggressive (*Agg*) cells for 24 h, followed by examination of BMP7 expression by Western blotting (*left panel*). BMP7 expression was also examined in BMSC co-cultured in a transwell with indolent or aggressive cells for 24 h (*right panel*). *C*, indolent, aggressive, and PC3mm cells were treated with the indicated CM for 48 h, followed by examination of the CSC population ($CD24^{low}/CD44^{high}/CD133^{high}$) by FACS. *D*, aggressive and indolent cells were treated with the indicated CM for 48 h, followed by examination of p21 (*top panel*) and p16 levels (*bottom panel*) by Western blotting. *E*, aggressive-sh-Noggin or -Scramble cells were implanted into the tibial bone of mice ($n = 6$/group), and the tumor growth was observed on day 28. *, $p < 0.05$ *versus* scramble. *F*, PC3mm-shScramble or PC3mm-shBMPR2 cells were treated with CM (as indicated) for 48 h, followed by examining the CSC marker-positive cells by FACS. *, $p < 0.05$; **, $p < 0.01$; ***, $p < 0.0001$; *ns*, not significant.

SPARC Up-regulates BMP7 Expression and Secretion from Bone Stroma—We reported previously that stromal expression of BMP7 induced dormancy by reducing "stemness" and inducing reversible senescence of prostate cancer cells in bone (18). Therefore, we wondered whether it was possible that SPARC up-regulates BMP7 expression in bone stromal cells. When we treated human primary BMSC that were isolated from two different donors or the bone stromal cell line HS5 with recombinant SPARC, we found that BMP7 was indeed significantly up-regulated (Fig. 4*A*). Furthermore, BMP7 was also up-regulated in BMSC that were treated with CM derived from indolent cells compared with CM from aggressive cells or from indolent-sh-SPARC cells (Fig. 4*B* and supplemental Fig. S3*A*). BMP7 was also found to be augmented in BMSC when co-cultured with indolent cells in transwell culture, and knockdown of SPARC in indolent cells significantly reduced BMP7 expression from BSMC in transwell culture (Fig. 4*B* and supplemental Fig. S3*A*). To further verify whether SPARC-induced BMP7 increases the dormancy phenotype of cancer cells, we generated CM by treating BMSC with recombinant SPARC and incubated cancer cells with the CM for 48 h. We found that the CM from SPARC-treated BMSC significantly decreased the stem cell population and sphere-forming ability and also increased senescence in cancer cells (Fig. 4*C* and supplemental Fig. S3, *B* and *C*). Furthermore, SPARC-treated BMSC CM increased p16 and p21 expression in cancer cells (Fig. 4*D*). Importantly, when recombinant Noggin, a competitive inhibitor of BMPs, was added to the SPARC-treated BMSC CM, the inhibitory effect of SPARC-treated BMSC CM was rescued (Fig. 4, *C* and *D*), further verifying that the dormancy phenotype is indeed mediated by BMP7. In addition, silencing Noggin expression in aggressive cells significantly inhibited its ability to grow in bone *in vivo* (Fig. 4*E* and supplemental Fig. S3*D*), suggesting that the absence of Noggin enhanced stromal BMP7-mediated growth suppression of tumor cells. The activation of bone morphogenetic protein receptors (BMPRs) by BMP7 is known to trigger the downstream signaling cascade (27). We have previously shown that BMPR2 is one of the major receptors associated with dormancy of prostate cancer cells and that BMP7 selectively binds this receptor (18). Therefore, to examine whether the decrease in cancer stemness is mediated through BMPR2, we knocked down BMPR2 in PC3mm

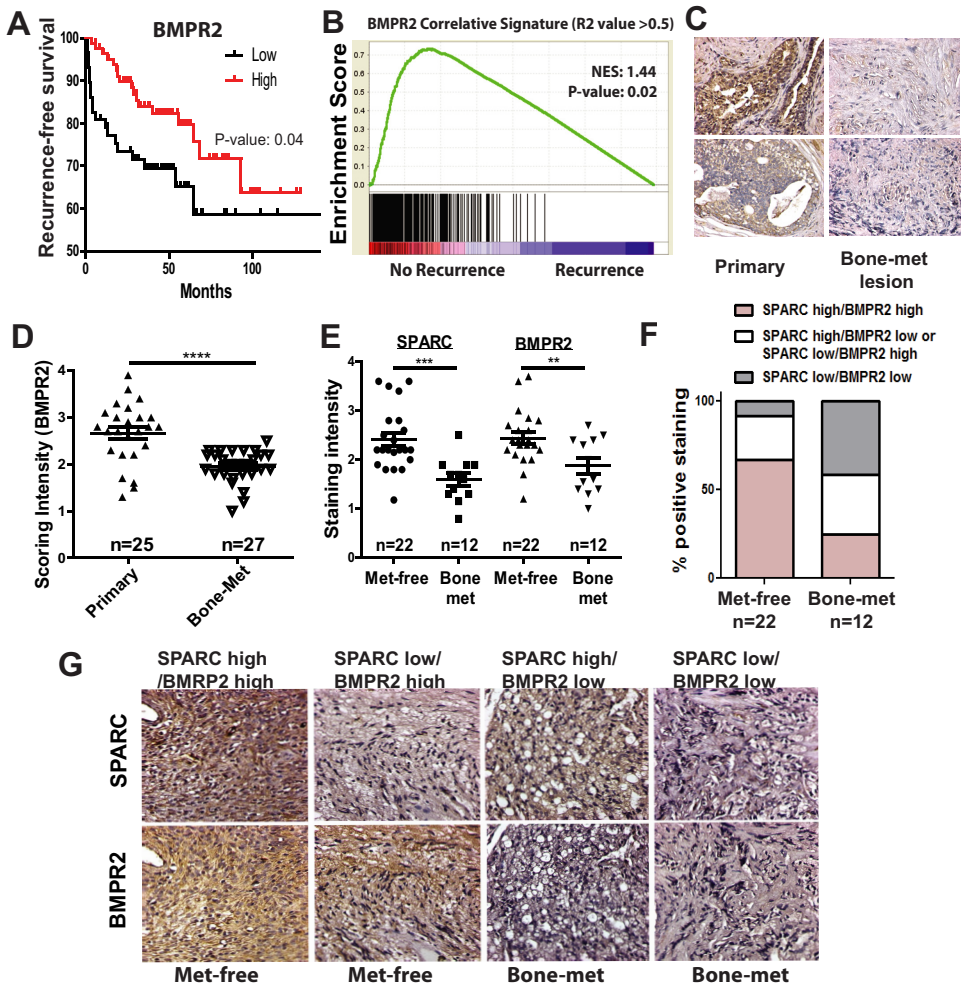

FIGURE 5. **SPARC and BMPR2 expression is negatively correlated with bone metastasis.** *A*, patients were stratified based on BMPR2 gene expression, and recurrence-free survival was examined using the GSE21034 database ($n = 140$). *B*, BMPR2 correlative signature ($n = 378$, $R^2 > 0.5$) was established using TCGA database for prostate cancer, and enrichment of the signature was examined in patients with or without recurrent disease (GSE21034). *NES*; normalized enrichment score. *C*, representative images of BMPR2 staining in primary tumor tissue and bone metastatic lesion. *D*, quantitation of BMPR2 staining in primary tumor tissue and bone metastatic lesion. *E*, SPARC and BMPR2 expression was examined in a primary tumor of patients with or without bone metastasis by immunohistochemistry, and the staining intensity was quantified. Consecutive sections of formalin-fixed, paraffin-embedded samples were used to stain SPARC and BMPR2 for each patient. *Met*, metastasis. *F*, the stained samples were divided into three groups (positive for either SPARC or BMPR2 (−/+ and ±, respectively), positive for both SPARC and BMPR2, and negative for both BMPR2 and SPARC expression based on their staining intensity), and the number of samples in each group was plotted as the percentage of total stained samples from either metastasis-free (localized disease) or bone metastatic primary tumor. *G*, representative images for SPARC and BMPR2 staining. *, $p < 0.05$; **, $p < 0.01$; ***, $p < 0.0001$.

cells that were then treated with CM generated from BMSC with or without SPARC treatment. As shown in Fig. 4*F*, the treatment of PC3mm cells with the CM significantly reduced the CSC population, whereas knockdown of BMPR2 blocked this suppressive effect of CM, indicating that the decrease in stemness is signaled through BMPR2. These results strongly suggest that stromal education by tumor-secreted SPARC up-regulates BMP7, which binds the BMPR2 receptor on the cancer cell to promote the dormancy phenotype.

Prognostic Significance of BMPR2 and SPARC Expression—To examine the clinical significance of BMPR2 in dormancy, we analyzed a Gene Expression Omnibus dataset and found that high BMPR2 expression predicts longer recurrence-free survival in prostate cancer patients (Fig. 5*A*) (28). However, BMPR2 expression did not correlate with presurgical prostate specific antigen, age, stage, or grade of the disease (supplemental Fig. S4, *A–F*, and Table S1). We also established a correlative gene signature from prostate cancer patients who had high BMPR2 expression in their primary tumor using The Cancer Genome Atlas (TCGA) database and found that this signature is highly enriched in patients who did not experience recurrent disease (Fig. 5*B*). In addition, we performed immunohistochemical staining of patient samples with bone metastasis and found that BMPR2 was significantly down-regulated in bone metastatic lesions compared with the primary tumor in these patients (Fig. 5, *C* and *D*), suggesting that decreased expression of BMPR2 is a key factor for metastatic growth in bone. We also observed that primary tumors of patients with bone metastasis expressed significantly lower levels of SPARC and BMPR2 compared with patients with localized disease (Fig. 5, *E–G*). Tumors from metastasis-free patients were significantly more positive for both SPARC and BMPR2 expression, whereas low SPARC, low BMPR2, or low SPARC and BMPR2 levels defined patients with bone metastatic disease. These results strongly support the notion that both SPARC and BMPR2 are crucial

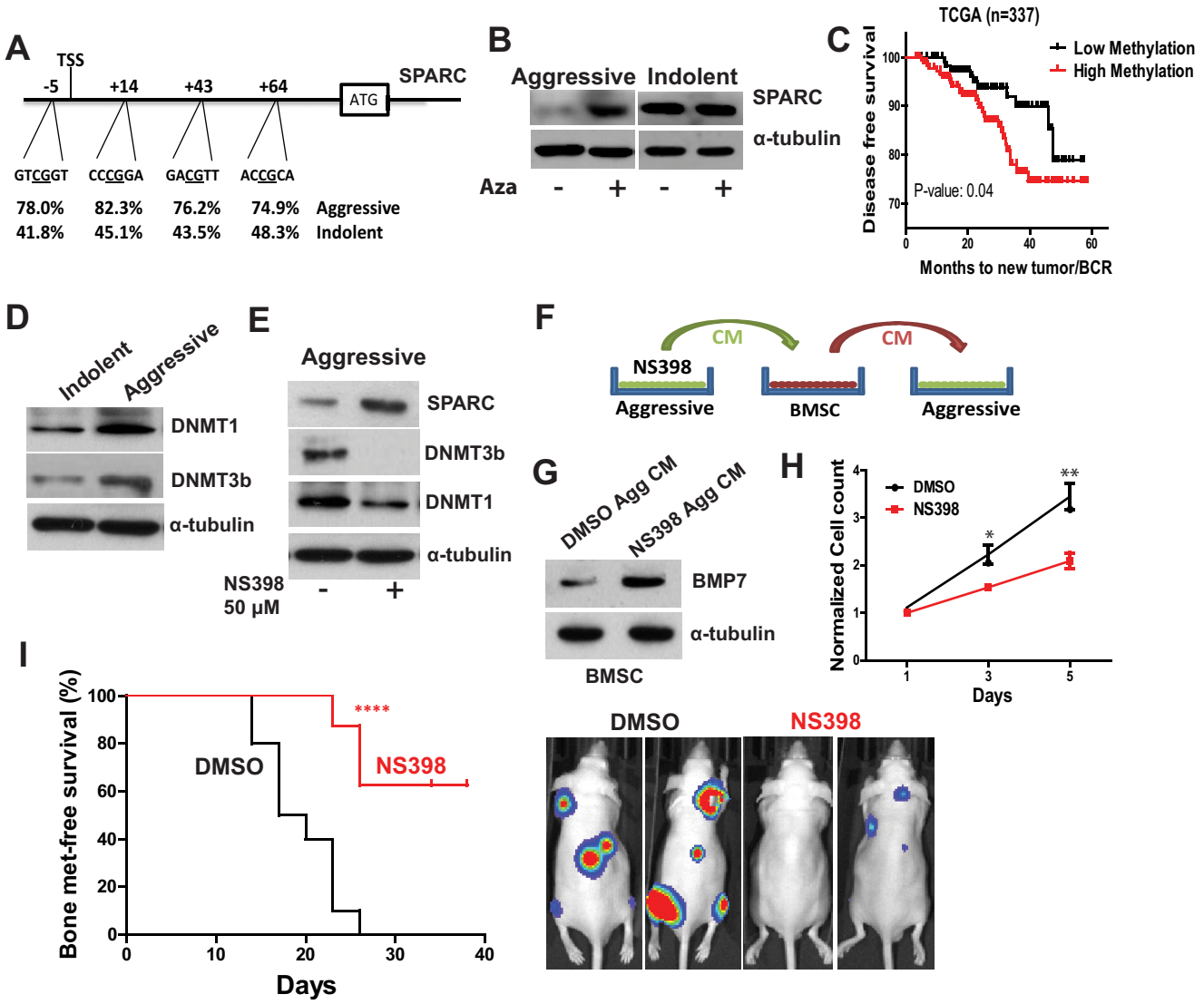

FIGURE 6. **SPARC is regulated by promoter methylation.** *A*, methylation of the SPARC promoter around the transcription start site (*TSS*) was examined for indolent and aggressive cells. *B*, aggressive and indolent cells were treated with 5-azacytidine (*Aza*, 50 nM), and SPARC expression was examined by Western blotting. *C*, prostate cancer patients in TCGA database were stratified based on the level of average SPARC promoter methylation, and new incidence or disease-free survival was examined for 5 years ($n = 337$). *BCR*; biochemical recurrence. *D*, DNMT1 and DNMT3b expression was examined in indolent and aggressive cells by Western blotting. *E*, aggressive cells were treated with NS398 (50 μM) for 24 h, and the expression of SPARC, DNMT1, and DNMT3b was examined by Western blotting. *F*, schematic of the collection of conditioned medium from aggressive cells treated with or without NS398, followed by treatment of BMSC. *G*, the expression of BMP7 was examined in BMSC after treatment with the indicated CM by Western blotting. *Agg*, aggressive. *H*, a cell proliferation assay was performed after treating aggressive cells with the CM outlined in *F*, and cell growth was examined on days 1, 3, and 5. A normalized cell count relative to day 1 is shown. *, $p < 0.05$; **, $p < 0.01$. *I*, aggressive cells were injected via the intracardiac route, and bone metastasis-free survival was examined in DMSO- or NS398-treated groups ($n = 10$/group). ****, $p < 0.0001$.

in dormancy and that the SPARC-BMP7-BMPR2 axis enhances dormant survival of cancer cells in bone.

The SPARC Gene Is Epigenetically Regulated in Aggressive Cells—The striking difference in the expression of SPARC between indolent and aggressive cells prompted us to test whether SPARC is epigenetically regulated during dormancy and recurrence. We therefore examined the methylation status of the SPARC promoter in indolent and aggressive cells. As shown in Fig. 6*A*, we found that several CpG islands in the promoter region of SPARC are significantly more methylated in aggressive cells compared with indolent cells. In addition, treatment with the demethylating agent 5-azacytidine reversed SPARC expression in aggressive cells but not in indolent cells (Fig. 6*B* and supplemental Fig. S5*A*). Furthermore, analysis of TCGA database for SPARC promoter methylation revealed that the SPARC promoter is highly methylated in prostate tumors compared with normal tissues (supplemental Fig. S5*B*). To examine the clinical relevance of SPARC promoter methylation, we stratified patients in TCGA database according to their SPARC methylation levels and found that low SPARC promoter methylation was significantly associated with increased disease-free survival in prostate cancer patients (Fig. 6*C*). In addition, we found that DNMT1 and DNMT3b, two dominant *de novo* DNA methylases that have also been known previously to regulate gene expression in tumor cells, were highly expressed in aggressive cells (Fig. 6*D*). Furthermore, the results of a clinical data analysis indicate that patients expressing high levels of DNMT1 and DNMT3b showed decreased

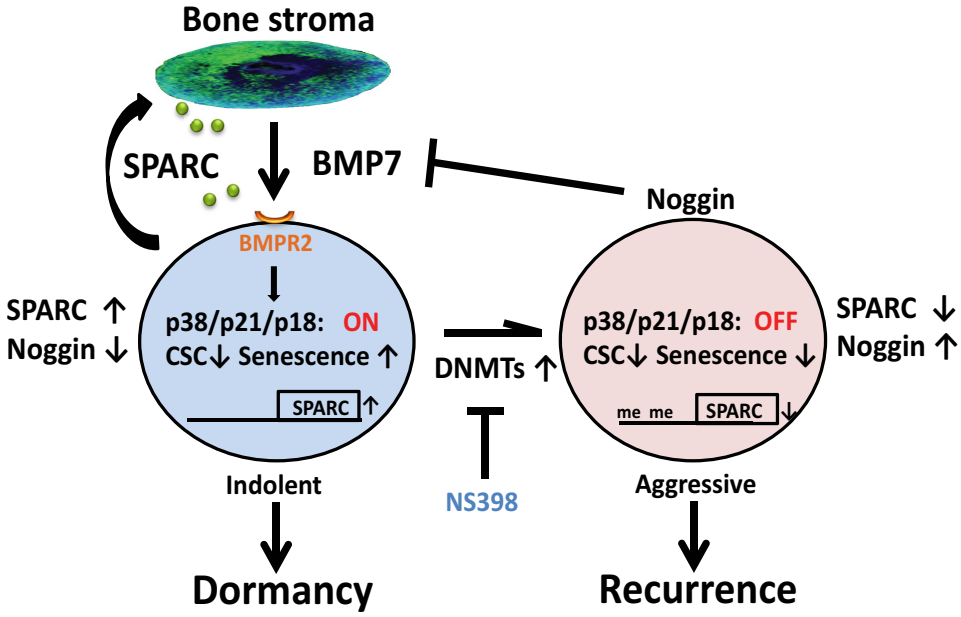

FIGURE 7. **Schematic illustrating how SPARC in the bone microenvironment induces dormancy.**

recurrence-free survival (supplemental Fig. S5, *C* and *D*). Interestingly, SPARC was shown previously to be down-regulated by the COX2 inhibitor NS398 via down-regulation of DNMT1 and DNMT3b in lung cancer cells (29). We found that NS398 treatment also reduced the expression of both DNMT1 and DNMT3b and increased SPARC expression in aggressive cells in a COX2-independent manner (Fig. 6*E* and supplemental Fig. S5, *E* and *F*).

To clarify the functional significance of this epigenetic control in dormancy, we first treated aggressive cells with NS398, followed by collecting CM, as illustrated in Fig. 6*F*. When BMSC were treated with this CM, BMP7 was significantly up-regulated (Fig. 6*G*). Furthermore, CM generated by treating BMSC with CM derived from NS398-treated aggressive cell was able to significantly lower the cell proliferation ability of aggressive cells (Fig. 6*H*). In addition, CM generated from azacytidine-treated aggressive cells was also able to up-regulate BMP7 in BMSC and decreased the cell proliferation ability of cancer cells (supplemental Fig. S5, *G* and *H*). These results suggest that reversal of SPARC methylation offers a window of therapeutic opportunity for recurrent disease by enhancing inhibitory signaling from the bone stroma. We transplanted aggressive cells intracardially and treated the animals with NS398. As shown in Fig. 6*I*, treatment with NS398 significantly suppressed tumor incidence in the bones of these animals. These results suggest that reversal of SPARC promoter methylation induces dormant survival of cancer cells in bone by educating stromal cells for an inhibitory response via BMP7 secretion.

Discussion

Prostate tumor cells are known to often disseminate at the very early stage of tumorigenesis, and ~90% of metastatic disease is related to bone, suggesting that tumor cells reside in bone for a prolonged period of time before growing as overt metastases (30). The well established tumor-supportive niche provided by the bone environment makes it one of the sanctuary sites for dormant survival of disseminated tumor cells, as evidenced by the isolation of dormant disseminated tumor cells from the bone marrow of a patient with a history of prostate cancer (5). In our study, by injecting CSC in the tibial bone of mice, we isolated a pair of cell lines (aggressive and indolent cells) that mimic the phenomenon of metastatic dormancy in bone. To our knowledge, this is the first established pair of cell lines that mimics the phenotype of dormant and aggressive growth in bone *in vivo*. Importantly, the recurrence assay shown in Fig. 2*D* verified the reversibility of dormant tumor cells, and therefore our model can provide a valuable tool to study dormancy and recurrence. The indolent cells activated the p38 MAPK pathway and its downstream cell cycle inhibitors only when co-cultured with bone stromal cells, which illustrates the importance of cancer-stroma cross-talk and p38 activation in the maintenance of the dormant niche in bone. Our results also showed that this cross-talk was mediated via SPARC secreted by indolent cells and that SPARC stimulated the paracrine inhibitory response through the BMP7-BMPR2 axis. Importantly, SPARC was epigenetically silenced by promoter methylation in aggressive cells, and treatment with NS398 reversed SPARC methylation and enhanced dormant survival in bone by down-regulating DNA methylase enzymes. Therefore, this potential therapeutic strategy may keep cancer cells in perpetual dormancy. Fig. 7 illustrates how SPARC induces dormancy in the bone microenvironment.

SPARC is an extracellular matrix-associated protein known for its oncogenic and tumor-suppressive roles (31). SPARC has been documented for its role in the formation of extracellular matrix and mineralization of bone (19, 20, 32, 33). SPARC plays a significant role in tissue remodeling, maintaining cell matrix integrity and interaction and collagen fiber assembly (34). Stroma- as well as tumor-secreted SPARC is known to affect tumor growth in cell type- and context-dependent manners by regu-

lating cell proliferation, adhesion, migration, invasion, and angiogenesis (25, 35–38). In prostate cancer, apparent conflicting results regarding SPARC expression in both clinical and experimental studies suggest that the role of SPARC is even more complex. The studies that involved unbiased screening by gene expression analysis have shown SPARC expression to be correlated with high-grade, androgen-resistant, and metastatic disease. In addition, SPARC was shown previously to attract prostate cancer cells into bone by promoting a migratory and invasive phenotype (39–42). Indeed, a moderate level of expression of SPARC was observed in bone metastases of prostate cancer patients by immunohistochemistry (43). On the contrary, several lines of evidence indicate tumor-suppressive roles of SPARC in prostate cancer (44–47). Wong *et al.* (47) found a significantly diminished SPARC level in patients with metastatic disease. Similarly, Kwabi-Addo *et al.* (48) have shown that SPARC is silenced by promoter methylation in African-American patients who often develop aggressive prostate cancer with 2-fold higher mortality rate than Caucasian American patients (48). The apparent disagreement between these studies may be due to multiple factors, including expression profiling of the primary tumor, batch variability, and lack of clinical data for the site of metastasis. Moreover, the controversy of the pathological role of SPARC in prostate cancer was further affirmed in two separate studies that utilized the SPARC knockout and transgenic adenocarcinoma of the mouse prostate (TRAMP) mouse models. Although Said *et al.* (25) found an inhibitory role of SPARC in tumor and metastatic growth, another study did not identify any role of SPARC in tumor progression and metastasis (49). The discrepancy in the pathological outcome evident in these studies might be due to the differences in genetic background of the mice used in the study. Similarly, controversy over the role of SPARC was also evident in carcinoma of breast and skin, where both oncogenic and tumor-suppressive roles were observed in multiple *in vitro*, *in vivo*, and clinical studies (50). On the other hand, the tumor- and metastasis-suppressive role of SPARC has been well documented for gastrointestinal, ovarian, pancreatic, and colon cancers, whereas the oncogenic role was verified in glioma (38, 51–55). Therefore, the role of SPARC in tumor progression appears to be complex and specific to the tissue type and stages of the disease. Our data suggest the new paradigm that SPARC is highly expressed by dormant cancer cells residing in bone, which demonstrates that the role of SPARC is contextually and spatiotemporally regulated. We found that bone stromal cells specifically responded to tumor-induced SPARC by secretion of tumor-inhibitory BMP7, which, in turn, activated the p38 MAPK pathway via BMPR2 in cancer cells. Moreover, BMP7 also decreased stem cell population and enhanced reversible senescence of cancer cells. On the other hand, disruption of BMP7-BMPR2 signaling axis by Noggin, a potent competitive inhibitor of BMPs, rescued the inhibitory effect of BMP7 in the bone microenvironment. Therefore, the precise role of SPARC is greatly dependent on the tumor-niche proteome profile and crosstalk with the microenvironment. It is conceivable that education of tumor stroma by SPARC and explicit stromal response at various stages of tumor progression greatly dictates the functional fate of SPARC.

Multiple types of cancer cells are known to interact and communicate with cells in the bone marrow microenvironment through secretion of cytoactive molecules. McCabe *et al.* (56) observed that SPARC suppressed osteoclast differentiation, a key step during bone tumor growth, wherein SPARC knockout mice showed increased osteolysis after intraosseous implantation of RM1 murine prostate cancer cells. Similarly, when cancer cells were grown in the bone matrices generated *in vitro* using SPARC knockout osteoblasts, the bone growth of PC3 cells was greatly enhanced (57). Furthermore, the bone metastasis-suppressive function of SPARC was reported previously for breast cancer by utilizing an *in vivo* systemic inoculation model (51). Based on our results of SPARC-mediated cross-talk with BMSC, it is plausible that inhibition of cancer growth in these models involves inhibitory paracrine factor(s), such as BMP7, from the stroma. Interestingly, a previous study has shown that tumor-stroma interaction in the bone elevates SPARC expression in the bone microenvironment, followed by proteolytic cleavage by the stromal collagenase cathepsin K, although the specific role of SPARC fragments in bone metastasis was not examined (58). It is noteworthy that opposing biological roles of SPARC fragments have been identified previously (50). Therefore, the differences in the protease profile of the microenvironment may potentially dictate the functional fate of the cleaved fragments, which warrants further studies to identify the functions of individual peptides during the pathological stages of bone metastasis.

Bone stromal cells were reported previously to induce dormancy of cancer cells either through exosome-mediated secretion of inhibitory microRNAs or through secretion of stromal proteins such as TGFβ2 and BMP7(18, 59). BMP7 is known to affect invasion and migration by inhibiting epithelial-to-mesenchymal transition of cancer cells (60, 61). We showed previously that BMP7 released by the bone stroma decreased stemness and promoted reversible senescence of cancer cells via signaling through BMPR2. Intriguingly, we found in this study that SPARC elevates BMP7 expression from BMSC, which led to senescence of indolent cells. In addition, the CM from SPARC-treated BMSC also promoted the senescence phenotype and reduced the stem cell population in cancer cells. Therefore, indolent cells maintain a dormant state in the bone microenvironment through activation of inhibitory signaling mediated by the BMP7-BMPR2 axis. Notably, aggressive cells expressed a high level of Noggin, and therefore it is highly probable that the elevated Noggin expression in cancer cell or the bone microenvironment disrupts BMP7-BMPR2 signaling, rescues cancer cells from the dormant state, and triggers the onset of recurrent disease.

Our finding shows that BMPR2 expression plays a key role in dormant survival of cancer cells in bone. The major molecular phenotype of dormancy, reduction in stemness, was not evident when BMPR2 expression was knocked down in PC3mm cells. In addition, the BMPR2 level in the tumor of a patient negatively correlated with the status of recurrent disease, and the BMPR2-correlative signature was highly enriched in patients who did not experience recurrent disease. In support of our finding, BMPR2 expression was reported previously to be lost in aggressive disease of bladder and colon cancers (62, 63).

Importantly, our immunohistochemical analysis also revealed decreased expression of BMPR2 in bone metastatic primary tumors as well as bone lesions compared with the primary tumor without metastasis. Therefore, it is conceivable that decreased BMPR2 expression or downstream signaling activation may lead to a conducive environment in bone for recurrent tumor growth. These results further underline the potential utility of BMPR2 and its downstream proteins as biomarkers for patient prognosis.

The differential methylation status of the SPARC promoter in indolent and aggressive cells suggests that environmental stress reprograms tumor cells for dormant survival via epigenetic modification. Indeed, our results revealed that reversal of SPARC promoter methylation in Aggressive cells either by 5-azacytidine or NS398 treatment enhanced SPARC expression and induced the inhibitory signal from stromal cells. Methylation of promoters of prominent tumor-suppressive genes has been known to enhance aggressive growth at distant sites (64). Sosa *et al.* (13, 14) have shown that NR2F1, an orphan nuclear receptor of RA signaling, rendered the dormancy phenotype *in vivo* by activating global repressive chromatin marks in cancer cells. Interestingly, NR2F1 binds and regulate the SPARC promoter in head and neck squamous cell carcinoma, suggesting a possibility that selection of an indolent clone is dependent on an epigenetic master regulator that changes the expression of prominent gene promoters (13). The increased expression of *de novo* methylase genes DNMT1 and DNMT3b in aggressive cells further supports the notion that epigenetic silencing of the SPARC promoter by methylation may be a potential key for recurrent growth in bone (Fig. 7). In support of this notion, patients with low promoter methylation status of SPARC showed prolonged disease-free survival. Furthermore, NS398 induced SPARC via down-regulation of DNMT1 and DNMT3b, which is in agreement with a previous study showing a DNMT-dependent increase of SPARC in A549 lung carcinoma cells by NS398 (29). In addition, NS398 has been studied previously for its effect on limiting cell proliferation, angiogenesis, invasion, and metastasis of multiple cancer types (65–67). It should be noted that NS398 was also shown previously to significantly inhibit bone metastasis of breast cancer cells by suppressing TGF-β dependent activation of COX-2. It is conceivable to induce SPARC by NS398 to maintain the dormant state of cancer cells in bone (68). To this end, we transplanted aggressive cells and found that treatment with NS398 significantly inhibited metastatic growth in bone. This finding shows a potential use of NS398 to maintain cancer cells in the dormant state and offers therapeutic windows to treat bone recurrent disease.

Experimental Procedures

Cell Culture—Indolent and aggressive cell lines were isolated from tibial bone of nude mice after injection of PC3mm cancer stem like cells as described in supplemental Fig. S1*A*. The PC3mm cell line was provided by I. J. Fidler (University of Texas MD Anderson Cancer Center, Houston, TX). DU145 was obtained from the American Type Culture Collection. ALVA41[e] was provided by W. Rosner (Columbia University, New York, NY). LNCaP cells were obtained from the University of Texas MD Anderson Cancer Center. hBMSCs (donors 7075 and 7083) were obtained from the Texas A&M Institute for Regenerative Medicine. hBMSCs were maintained in minimum essential medium with 20% fetal bovine serum, 100 μg/ml streptomycin, and 100 units/ml penicillin. Other cells were grown in RPMI 1640 medium with 10% fetal bovine serum, 100 μg/ml streptomycin, and 100 units/ml penicillin and incubated at 37 °C in a 5% CO_2 atmosphere. The PC3mm cell line was transduced with a lentiviral vector carrying the firefly luciferase gene for bioluminescence tracking. Recombinant human SPARC and BMP7 were purchased from ProSpec. For transwell co-culture, 10^4 cancer cells were seeded on a 24-well plate, and a culture insert with 0.4-μm pore size (Corning) was placed on top of each well, followed by seeding the upper chamber with 10^5 BMSCs.

Preparation of Conditioned Medium—For generating BMSC + SP CM, hBMSC were treated with 0.2 μg/ml recombinant SPARC and incubated for 24 h, and the medium was replaced with serum-free RPMI medium. After 24 h of incubation with serum-free RPMI medium, the CM was collected and added to cancer cells at a ratio of 50:50 with 10% RPMI. For supplemental Fig. S4*D*, aggressive cells were treated with 0.5 μM 5-azacytidine or vehicle (1:1, acetic acid:water) for 4 days, followed by replacing the medium with serum-free RPMI medium. The cells were then incubated for 24 h, and CM was collected. This CM was further added to hBMSC and incubated for 24 h, followed by changing of the medium to serum-free RPMI. After 24 h, CM was collected and added to aggressive cells.

Isolation of CSCs—CSCs were isolated by magnetic bead sorting using a magnetic-assisted cell sorting (MACS) separator (Miltenyi Biotec) as described previously (18). PC3mm cells were incubated with the following specific antibodies: anti-CD24-biotin (STEMCELL Technologies), anti-CD44-APC (BioLegend), and anti-CD133-biotin (Miltenyi Biotec). $CD24^{low}/CD44^{high}/CD133^{high}$ cells were then enriched by using a magnetic-assisted cell sorting magnet and MS columns (Miltenyi Biotec). All magnetic-assisted cell sorting procedures were performed according to the instructions of the manufacturer.

FACS—Prostate cancer cells were treated with CM for 48 h. CM was replaced after 24 h. Cells were then collected after 48 h, washed twice in PBS, incubated with CD24-FITC, CD44-APC and CD133-PE for 20 min, and analyzed for CSC positive population ($CD24^{low}/CD44^{high}/CD133^{high}$) in a BD Accuri instrument.

Western Blotting—The cells were lysed and analyzed by immunoblotting using antibodies specific for the following proteins: p21, p18, α-tubulin, and GAPDH (Cell Signaling Technology); SPARC (R&D Systems); DNMT3b, Noggin, and BMP7 (Abcam); and DNMT1 (Genetex).

Sphere-forming Assay—Cancer cells were plated (200 cells/well) in 96-well ultra-low attachment plates (Corning) with DMEM/F12 supplemented with 2% B27 (Invitrogen), 20 ng/ml EGF (Sigma-Aldrich), and 4 μg/ml insulin (Sigma-Aldrich). They were then incubated with CM generated with or without treatment of BMSC with recombinant SPARC. The number of prostaspheres was counted, and data are represented as the mean ± S.E.

Proliferation Assay—Cells were seeded into 96-well plates (500 cells/well) in regular growth medium. The cells were then cultured overnight, followed by treating them with conditioned medium. Cell viability was measured by (3-(4,5-dimethylthiazol-2 yl)-5-(3-carboxy phenyl)-2-(4-sulfophenyl)-2H-tetrazolium assay according to the recommendations of the manufacturer (Promega).

Animal Experiments—All animal experiments were done in accordance with a protocol approved by the Wake Forest Institutional Animal Care and Use Committee. Athymic nude mice (Harlan) 4–5 and 7–8 weeks of age were used for the xenograft experiment. For isolating indolent and aggressive cells, 4000 PC3mm CSCs labeled with luciferase were injected into the tibial bone of nude mice. After 6 weeks, tibial bones with aggressive or indolent tumor growth were flushed with PBS, followed by selection of the cells with puromycin. For verification of differential growth, 10^4 indolent or aggressive cells were injected into the tibial bone. For bone metastasis-free survival experiments, 10^5 CSCs isolated from indolent or aggressive cells were injected into the left cardiac ventricles of mice. For the recurrence assay, 200 μg/kg SPARC or vehicle alone was subsequently injected every 2 days into the tail vein. For NS398 treatment, 10^6 aggressive cells were injected into the left cardiac ventricle, and mice were treated with either DMSO or NS398 (20 mg/kg) every 2 days until day 40. The progression of cell growth and development of metastases was monitored by bioluminescence imaging.

Wound Healing Assay—Cells were grown until confluence, and cells were scratched by a 1-ml pipette tip. The migration of cells was monitored under the microscope after 9, 12, 24, and 48 h. The percentage of wound healing was counted in three different fields for each cell line.

Invasion Assay—Cell culture inserts with a microporous membrane were coated with Matrigel (BD Biosciences), followed by seeding 10^5 cancer cells. RPMI medium containing 20% fetal bovine serum was added to the bottom chamber. The cells were then incubated for 24 h at 37 °C. The upper chamber was removed, and the cells in the bottom chambers were stained with tetrazolium dye and counted under a microscope.

Bisulphite Sequencing—Genomic DNA was isolated using a cell and soft tissue DNA isolation kit (Zymo Research). The methylation of the CpG island was examined by bisulphite sequencing (Epigendx).

Quantitative RT-PCR Analysis—Total RNA was isolated from the cells and reverse-transcribed. The cDNA was then amplified with a pair of forward and reverse primers to validate the results of the microarray. The thermal cycling conditions consisted of an initial denaturation step at 95 °C for 1 min, followed by 35 cycles of PCR using the following profile: 94 °C for 30s, 58 °C for 30 s, and 72 °C for 30 s.

Statistical Analysis—Results are reported as mean ± S.E. For *in vitro* experiments, Student's *t* test or one-way analysis of variance was applied. For *in vivo* experiments, group comparisons were performed using nonparametric Mann-Whitney test or unpaired Student's *t* test. Kaplan-Meier curve comparison was performed with a log-lank test.

Senescence-associated β-gal Staining—Cells were treated with or without SPARC-treated BMSC CM as indicated in the figure legends, and a senescence-associated β-gal assay was performed using the senescence-associated β-gal staining kit (Cell Signaling Technology) according to the instructions of the manufacturer.

Gene Set Enrichment Analysis—The Gene MatriX file (.gmx) was generated by combining the top 378 genes that were significantly correlated ($R^2 > 0.5$) to BMPR2 in TCGA database with 502 prostate cancer patients. The Gene Cluster Text file (.gct) was generated from Taylor's cohort (GSE21034) by separating prostate cancer patients based on their status of recurrence. Patients who did not experience recurrence for at least 5 years were placed in the "no recurrence" group ($n = 32$), whereas patients who experienced recurrence before 5 years were placed in the "recurrence" group ($n = 34$). Similarly, the Categorical class file (.cls) was also generated based on the recurrence status of each patient. The number of permutations was set to 1000, and we used GPL10264 as the chip platform.

Immunohistochemistry—Primary prostate cancer tissue microarrays were obtained from US Biomax, Inc. (PRT195 and PR242b). The tissue microarray generated from bone metastatic lesions was obtained from Tirstar Inc. (79562475). Formaldehyde-fixed and paraffin-embedded human prostate tissue specimens were obtained from the surgical pathology archives of the Akita Red Cross Hospital (Akita, Japan) and Iwate Medical School (Iwate, Japan). The sections were baked at 60 °C for 1 h, deparaffinized in xylene, and rehydrated and fixed in 10% neutral buffered formalin. Immunohistochemical staining of histological sections was performed according to a protocol published previously (18) using the EnVision Plus system (Dako) and antibodies specific to BMPR2 (Abcam) and SPARC (R&D Systems).

Cell Labeling with DiD Dye—Cells were stained with DiD dye (Molecular Probes, Eugene, OR; catalog no. V22887) according to the instructions of the manufacturer. Briefly, cells (1×10^6 cells/ml) were incubated with DiD dye (0.5 μM) in serum-free medium at 37 °C for 40 min, washed with serum-free medium three times, resuspended in PBS, and analyzed for staining by FACS (BD Biosciences, Accuri).

Author Contributions—S. S. conducted most of the experiments, analyzed the results, and wrote most of the manuscript. F. X. conducted intracardiac injections. Y. L. conducted the bioinformatics analysis. K. Wu conducted tail vein injections. Y. S. conducted intratibial injections. R. P. prepared conditioned medium from BMSC. N. S., H. K. L., and K. C. B. contributed to immunohistochemistry staining and Western blotting. K. Watabe conceived the idea for the project and contributed to editing the manuscript.

Acknowledgment—We thank Dr. Aya Kobayashi for help with the initial work of isolation and characterization of the clones. The Flow Cytometry Shared Resources, Cell and Viral Vector Core Lab are supported by the Comprehensive Cancer Center of Wake Forest University NCI, National Institutes of Health Grant (P30CA012197).

References

1. Horwich, A., Parker, C., de Reijke, T., Kataja, V., and ESMO Guidelines Working Group (2013) Prostate cancer: ESMO clinical practice guidelines for diagnosis, treatment and follow-up. *Ann. Oncol.* **24,** vi106–vi114
2. Mohler, J. L., Kantoff, P. W., Armstrong, A. J., Bahnson, R. R., Cohen, M.,

D'Amico, A. V., Eastham, J. A., Enke, C. A., Farrington, T. A., Higano, C. S., Horwitz, E. M., Kawachi, M. H., Kuettel, M., Lee, R. J., Macvicar, G. R., *et al.* (2013) Prostate cancer, version 1.2014. *Journal of the National Comprehensive Cancer Network* **11,** 1471–1479

3. Zietman, A. L., Bae, K., Slater, J. D., Shipley, W. U., Efstathiou, J. A., Coen, J. J., Bush, D. A., Lunt, M., Spiegel, D. Y., Skowronski, R., Jabola, B. R., and Rossi, C. J. (2010) Randomized trial comparing conventional-dose with high-dose conformal radiation therapy in early-stage adenocarcinoma of the prostate: long-term results from Proton Radiation Oncology Group/American College Of Radiology 95–09. *J. Clin. Oncol.* **28,** 1106–1111
4. Morgan, T. M., Lange, P. H., Porter, M. P., Lin, D. W., Ellis, W. J., Gallaher, I. S., and Vessella, R. L. (2009) Disseminated tumor cells in prostate cancer patients after radical prostatectomy and without evidence of disease predicts biochemical recurrence. *Clin. Cancer Res.* **15,** 677–683
5. Chéry, L., Lam, H. M., Coleman, I., Lakely, B., Coleman, R., Larson, S., Aguirre-Ghiso, J. A., Xia, J., Gulati, R., Nelson, P. S., Montgomery, B., Lange, P., Snyder, L. A., Vessella, R. L., and Morrissey, C. (2014) Characterization of single disseminated prostate cancer cells reveals tumor cell heterogeneity and identifies dormancy associated pathways. *Oncotarget* **5,** 9939–9951
6. Weckermann, D., Müller, P., Wawroschek, F., Harzmann, R., Riethmüller, G., and Schlimok, G. (2001) Disseminated cytokeratin positive tumor cells in the bone marrow of patients with prostate cancer: detection and prognostic value. *J. Urol.* **166,** 699–703
7. Almog, N. (2010) Molecular mechanisms underlying tumor dormancy. *Cancer Lett.* **294,** 139–146
8. Aguirre-Ghiso, J. A. (2007) Models, mechanisms and clinical evidence for cancer dormancy. *Nat. Rev. Cancer* **7,** 834–846
9. Lu, X., Mu, E., Wei, Y., Riethdorf, S., Yang, Q., Yuan, M., Yan, J., Hua, Y., Tiede, B. J., Lu, X., Haffty, B. G., Pantel, K., Massagué, J., and Kang, Y. (2011) VCAM-1 promotes osteolytic expansion of indolent bone micrometastasis of breast cancer by engaging alpha4beta1-positive osteoclast progenitors. *Cancer Cell* **20,** 701–714
10. McAllister, S. S., Gifford, A. M., Greiner, A. L., Kelleher, S. P., Saelzler, M. P., Ince, T. A., Reinhardt, F., Harris, L. N., Hylander, B. L., Repasky, E. A., and Weinberg, R. A. (2008) Systemic endocrine instigation of indolent tumor growth requires osteopontin. *Cell* **133,** 994–1005
11. Aguirre-Ghiso, J. A., Estrada, Y., Liu, D., and Ossowski, L. (2003) ERK(MAPK) activity as a determinant of tumor growth and dormancy; regulation by p38(SAPK). *Cancer Res.* **63,** 1684–1695
12. Aguirre-Ghiso, J. A., Liu, D., Mignatti, A., Kovalski, K., and Ossowski, L. (2001) Urokinase receptor and fibronectin regulate the ERK(MAPK) to p38(MAPK) activity ratios that determine carcinoma cell proliferation or dormancy *in vivo*. *Mol. Biol. Cell* **12,** 863–879
13. Sosa, M. S., Parikh, F., Maia, A. G., Estrada, Y., Bosch, A., Bragado, P., Ekpin, E., George, A., Zheng, Y., Lam, H. M., Morrissey, C., Chung, C. Y., Farias, E. F., Bernstein, E., and Aguirre-Ghiso, J. A. (2015) NR2F1 controls tumour cell dormancy via SOX9- and RARβ-driven quiescence programmes. *Nat. Commun.* **6,** 6170
14. Sosa, M. S., Bragado, P., and Aguirre-Ghiso, J. A. (2014) Mechanisms of disseminated cancer cell dormancy: an awakening field. *Nat. Rev. Cancer* **14,** 611–622
15. Ossowski, L., Russo, H., Gartner, M., and Wilson, E. L. (1987) Growth of a human carcinoma (HEp3) in nude mice: rapid and efficient metastasis. *J. Cell. Physiol.* **133,** 288–296
16. Morris, V. L., Tuck, A. B., Wilson, S. M., Percy, D., and Chambers, A. F. (1993) Tumor progression and metastasis in murine D2 hyperplastic alveolar nodule mammary tumor cell lines. *Clin. Exp. Metastasis* **11,** 103–112
17. Barkan, D., Kleinman, H., Simmons, J. L., Asmussen, H., Kamaraju, A. K., Hoenorhoff, M. J., Liu, Z. Y., Costes, S. V., Cho, E. H., Lockett, S., Khanna, C., Chambers, A. F., and Green, J. E. (2008) Inhibition of metastatic outgrowth from single dormant tumor cells by targeting the cytoskeleton. *Cancer Res.* **68,** 6241–6250
18. Kobayashi, A., Okuda, H., Xing, F., Pandey, P. R., Watabe, M., Hirota, S., Pai, S. K., Liu, W., Fukuda, K., Chambers, C., Wilber, A., and Watabe, K. (2011) Bone morphogenetic protein 7 in dormancy and metastasis of prostate cancer stem-like cells in bone. *J. Exp. Med.* **208,** 2641–2655
19. Termine, J. D., Kleinman, H. K., Whitson, S. W., Conn, K. M., McGarvey, M. L., and Martin, G. R. (1981) Osteonectin, a bone-specific protein linking mineral to collagen. *Cell* **26,** 99–105
20. Delany, A. M., Amling, M., Priemel, M., Howe, C., Baron, R., and Canalis, E. (2000) Osteopenia and decreased bone formation in osteonectin-deficient mice. *J. Clin. Invest.* **105,** 915–923
21. Chen, C., Uludag, H., Wang, Z., and Jiang, H. (2012) Noggin suppression decreases BMP-2-induced osteogenesis of human bone marrow-derived mesenchymal stem cells *in vitro*. *J. Cell. Biochem.* **113,** 3672–3680
22. Secondini, C., Wetterwald, A., Schwaninger, R., Thalmann, G. N., and Cecchini, M. G. (2011) The role of the BMP signaling antagonist noggin in the development of prostate cancer osteolytic bone metastasis. *PLoS ONE* **6,** e16078
23. Stephenson, A. J., Smith, A., Kattan, M. W., Satagopan, J., Reuter, V. E., Scardino, P. T., and Gerald, W. L. (2005) Integration of gene expression profiling and clinical variables to predict prostate carcinoma recurrence after radical prostatectomy. *Cancer* **104,** 290–298
24. Marcelino, J., Sciortino, C. M., Romero, M. F., Ulatowski, L. M., Ballock, R. T., Economides, A. N., Eimon, P. M., Harland, R. M., and Warman, M. L. (2001) Human disease-causing NOG missense mutations: effects on noggin secretion, dimer formation, and bone morphogenetic protein binding. *Proc. Natl. Acad. Sci. U.S.A.* **98,** 11353–11358
25. Said, N., Frierson, H. F., Jr, Chernauskas, D., Conaway, M., Motamed, K., and Theodorescu, D. (2009) The role of SPARC in the TRAMP model of prostate carcinogenesis and progression. *Oncogene* **28,** 3487–3498
26. Zhang, J., Wang, P., Zhu, J., Wang, W., Yin, J., Zhang, C., Chen, Z., Sun, L., Wan, Y., Wang, X., Chen, G., and Liu, Y. (2014) SPARC expression is negatively correlated with clinicopathological factors of gastric cancer and inhibits malignancy of gastric cancer cells. *Oncol. Rep.* **31,** 2312–2320
27. Leyton, P. A., Beppu, H., Pappas, A., Martyn, T. M., Derwall, M., Baron, D. M., Galdos, R., Bloch, D. B., and Bloch, K. D. (2013) Deletion of the sequence encoding the tail domain of the bone morphogenetic protein type 2 receptor reveals a bone morphogenetic protein 7-specific gain of function. *PLoS ONE* **8,** e76947
28. Taylor, B. S., Schultz, N., Hieronymus, H., Gopalan, A., Xiao, Y., Carver, B. S., Arora, V. K., Kaushik, P., Cerami, E., Reva, B., Antipin, Y., Mitsiades, N., Landers, T., Dolgalev, I., Major, J. E., *et al.* (2010) Integrative genomic profiling of human prostate cancer. *Cancer Cell* **18,** 11–22
29. Pan, M. R., Chang, H. C., Chuang, L. Y., and Hung, W. C. (2008) The nonsteroidal anti-inflammatory drug NS398 reactivates SPARC expression via promoter demethylation to attenuate invasiveness of lung cancer cells. *Exp. Biol. Med.* **233,** 456–462
30. Bubendorf, L., Schöpfer, A., Wagner, U., Sauter, G., Moch, H., Willi, N., Gasser, T. C., and Mihatsch, M. J. (2000) Metastatic patterns of prostate cancer: an autopsy study of 1,589 patients. *Hum. Pathol.* **31,** 578–583
31. Nagaraju, G. P., Dontula, R., El-Rayes, B. F., and Lakka, S. S. (2014) Molecular mechanisms underlying the divergent roles of SPARC in human carcinogenesis. *Carcinogenesis* **35,** 967–973
32. Framson, P. E., and Sage, E. H. (2004) SPARC and tumor growth: where the seed meets the soil? *J. Cell. Biochem.* **92,** 679–690
33. Brekken, R. A., and Sage, E. H. (2001) SPARC, a matricellular protein: at the crossroads of cell-matrix communication. *Matrix Biol.* **19,** 816–827
34. Podhajcer, O. L., Benedetti, L., Girotti, M. R., Prada, F., Salvatierra, E., and Llera, A. S. (2008) The role of the matricellular protein SPARC in the dynamic interaction between the tumor and the host. *Cancer Metastasis Rev.* **27,** 523–537
35. Said, N., Frierson, H. F., Sanchez-Carbayo, M., Brekken, R. A., and Theodorescu, D. (2013) Loss of SPARC in bladder cancer enhances carcinogenesis and progression. *J. Clin. Invest.* **123,** 751–766
36. Said, N., and Motamed, K. (2005) Absence of host-secreted protein acidic and rich in cysteine (SPARC) augments peritoneal ovarian carcinomatosis. *Am. J. Pathol.* **167,** 1739–1752
37. Said, N. A., Elmarakby, A. A., Imig, J. D., Fulton, D. J., and Motamed, K. (2008) SPARC ameliorates ovarian cancer-associated inflammation. *Neoplasia* **10,** 1092–1104
38. Chlenski, A., Liu, S., Guerrero, L. J., Yang, Q., Tian, Y., Salwen, H. R., Zage, P., and Cohn, S. L. (2006) SPARC expression is associated with impaired tumor growth, inhibited angiogenesis and changes in the extracellular matrix. *Int. J. Cancer* **118,** 310–316

39. Chen, N., Ye, X. C., Chu, K., Navone, N. M., Sage, E. H., Yu-Lee, L. Y., Logothetis, C. J., and Lin, S. H. (2007) A secreted isoform of ErbB3 promotes osteonectin expression in bone and enhances the invasiveness of prostate cancer cells. *Cancer Res.* **67,** 6544–6548
40. De, S., Chen, J., Narizhneva, N. V., Heston, W., Brainard, J., Sage, E. H., and Byzova, T. V. (2003) Molecular pathway for cancer metastasis to bone. *J. Biol. Chem.* **278,** 39044–39050
41. Jacob, K., Webber, M., Benayahu, D., and Kleinman, H. K. (1999) Osteonectin promotes prostate cancer cell migration and invasion: a possible mechanism for metastasis to bone. *Cancer Res.* **59,** 4453–4457
42. Derosa, C. A., Furusato, B., Shaheduzzaman, S., Srikantan, V., Wang, Z., Chen, Y., Siefert, M., Ravindranath, L., Young, D., Nau, M., Dobi, A., Werner, T., McLeod, D. G., Vahey, M. T., Sesterhenn, I. A., *et al.* (2012) Elevated osteonectin/SPARC expression in primary prostate cancer predicts metastatic progression. *Prostate Cancer Prostatic Dis.* **15,** 150–156
43. Thomas, R., True, L. D., Bassuk, J. A., Lange, P. H., and Vessella, R. L. (2000) Differential expression of osteonectin/SPARC during human prostate cancer progression. *Clin. Cancer Res.* **6,** 1140–1149
44. Dhanasekaran, S. M., Barrette, T. R., Ghosh, D., Shah, R., Varambally, S., Kurachi, K., Pienta, K. J., Rubin, M. A., and Chinnaiyan, A. M. (2001) Delineation of prognostic biomarkers in prostate cancer. *Nature* **412,** 822–826
45. Lapointe, J., Li, C., Higgins, J. P., van de Rijn, M., Bair, E., Montgomery, K., Ferrari, M., Egevad, L., Rayford, W., Bergerheim, U., Ekman, P., DeMarzo, A. M., Tibshirani, R., Botstein, D., Brown, P. O., *et al.* (2004) Gene expression profiling identifies clinically relevant subtypes of prostate cancer. *Proc. Natl. Acad. Sci. U.S.A.* **101,** 811–816
46. Welsh, J. B., Sapinoso, L. M., Su, A. I., Kern, S. G., Wang-Rodriguez, J., Moskaluk, C. A., Frierson, H. F., Jr, and Hampton, G. M. (2001) Analysis of gene expression identifies candidate markers and pharmacological targets in prostate cancer. *Cancer Res.* **61,** 5974–5978
47. Wong, S. Y., Haack, H., Kissil, J. L., Barry, M., Bronson, R. T., Shen, S. S., Whittaker, C. A., Crowley, D., and Hynes, R. O. (2007) Protein 4.1B suppresses prostate cancer progression and metastasis. *Proc. Natl. Acad. Sci. U.S.A.* **104,** 12784–12789
48. Kwabi-Addo, B., Wang, S., Chung, W., Jelinek, J., Patierno, S. R., Wang, B. D., Andrawis, R., Lee, N. H., Apprey, V., Issa, J. P., and Ittmann, M. (2010) Identification of differentially methylated genes in normal prostate tissues from African American and Caucasian men. *Clin. Cancer Res.* **16,** 3539–3547
49. Wong, S. Y., Crowley, D., Bronson, R. T., and Hynes, R. O. (2008) Analyses of the role of endogenous SPARC in mouse models of prostate and breast cancer. *Clin. Exp. Metastasis* **25,** 109–118
50. Tai, I. T., and Tang, M. J. (2008) SPARC in cancer biology: its role in cancer progression and potential for therapy. *Drug Resist. Updates* **11,** 231–246
51. Koblinski, J. E., Kaplan-Singer, B. R., VanOsdol, S. J., Wu, M., Engbring, J. A., Wang, S., Goldsmith, C. M., Piper, J. T., Vostal, J. G., Harms, J. F., Welch, D. R., and Kleinman, H. K. (2005) Endogenous osteonectin/SPARC/BM-40 expression inhibits MDA-MB-231 breast cancer cell metastasis. *Cancer Res.* **65,** 7370–7377
52. Nagai, M. A., Gerhard, R., Fregnani, J. H., Nonogaki, S., Rierger, R. B., Netto, M. M., and Soares, F. A. (2011) Prognostic value of NDRG1 and SPARC protein expression in breast cancer patients. *Breast Cancer Res. Treat.* **126,** 1–14
53. Tai, I. T., Dai, M., Owen, D. A., and Chen, L. B. (2005) Genome-wide expression analysis of therapy-resistant tumors reveals SPARC as a novel target for cancer therapy. *J. Clin. Invest.* **115,** 1492–1502
54. Yiu, G. K., Chan, W. Y., Ng, S. W., Chan, P. S., Cheung, K. K., Berkowitz, R. S., and Mok, S. C. (2001) SPARC (secreted protein acidic and rich in cysteine) induces apoptosis in ovarian cancer cells. *Am. J. Pathol.* **159,** 609–622
55. Golembieski, W. A., Thomas, S. L., Schultz, C. R., Yunker, C. K., McClung, H. M., Lemke, N., Cazacu, S., Barker, T., Sage, E. H., Brodie, C., and Rempel, S. A. (2008) HSP27 mediates SPARC-induced changes in glioma morphology, migration, and invasion. *Glia* **56,** 1061–1075
56. McCabe, N. P., Kerr, B. A., Madajka, M., Vasanji, A., and Byzova, T. V. (2011) Augmented osteolysis in SPARC-deficient mice with bone-residing prostate cancer. *Neoplasia* **13,** 31–39
57. Kapinas, K., Lowther, K. M., Kessler, C. B., Tilbury, K., Lieberman, J. R., Tirnauer, J. S., Campagnola, P., and Delany, A. M. (2012) Bone matrix osteonectin limits prostate cancer cell growth and survival. *Matrix Biol.* **31,** 299–307
58. Podgorski, I., Linebaugh, B. E., Koblinski, J. E., Rudy, D. L., Herroon, M. K., Olive, M. B., and Sloane, B. F. (2009) Bone marrow-derived cathepsin K cleaves SPARC in bone metastasis. *Am. J. Pathol.* **175,** 1255–1269
59. Bragado, P., Estrada, Y., Parikh, F., Krause, S., Capobianco, C., Farina, H. G., Schewe, D. M., and Aguirre-Ghiso, J. A. (2013) TGF-β2 dictates disseminated tumour cell fate in target organs through TGF-β-RIII and p38α/β signalling. *Nat. Cell Biol.* **15,** 1351–1361
60. Ye, L., Lewis-Russell, J. M., Kynaston, H., and Jiang, W. G. (2007) Endogenous bone morphogenetic protein-7 controls the motility of prostate cancer cells through regulation of bone morphogenetic protein antagonists. *J. Urol.* **178,** 1086–1091
61. Zeisberg, M., Hanai, J., Sugimoto, H., Mammoto, T., Charytan, D., Strutz, F., and Kalluri, R. (2003) BMP-7 counteracts TGF-β1-induced epithelial-to-mesenchymal transition and reverses chronic renal injury. *Nat. Med.* **9,** 964–968
62. Kim, I. Y., Lee, D. H., Lee, D. K., Kim, W. J., Kim, M. M., Morton, R. A., Lerner, S. P., and Kim, S. J. (2004) Restoration of bone morphogenetic protein receptor type II expression leads to a decreased rate of tumor growth in bladder transitional cell carcinoma cell line TSU-Pr1. *Cancer Res.* **64,** 7355–7360
63. Kodach, L. L., Wiercinska, E., de Miranda, N. F., Bleuming, S. A., Musler, A. R., Peppelenbosch, M. P., Dekker, E., van den Brink, G. R., van Noesel, C. J., Morreau, H., Hommes, D. W., Ten Dijke, P., Offerhaus, G. J., and Hardwick, J. C. (2008) The bone morphogenetic protein pathway is inactivated in the majority of sporadic colorectal cancers. *Gastroenterology* **134,** 1332–1341
64. Schulz, W. A., Elo, J. P., Florl, A. R., Pennanen, S., Santourlidis, S., Engers, R., Buchardt, M., Seifert, H. H., and Visakorpi, T. (2002) Genomewide DNA hypomethylation is associated with alterations on chromosome 8 in prostate carcinoma. *Genes Chromosomes Cancer* **35,** 58–65
65. Nishikawa, M., Stapleton, P. P., Freeman, T. A., Gaughan, J. P., Matsuda, T., and Daly, J. M. (2004) NS-398 inhibits tumor growth and liver metastasis of colon cancer through induction of apoptosis and suppression of the plasminogen activation system in a mouse model. *J. Am. Coll. Surg.* **199,** 428–435
66. Ferrario, A., Fisher, A. M., Rucker, N., and Gomer, C. J. (2005) Celecoxib and NS-398 enhance photodynamic therapy by increasing *in vitro* apoptosis and decreasing *in vivo* inflammatory and angiogenic factors. *Cancer Res.* **65,** 9473–9478
67. Jones, M. K., Wang, H., Peskar, B. M., Levin, E., Itani, R. M., Sarfeh, I. J., and Tarnawski, A. S. (1999) Inhibition of angiogenesis by nonsteroidal anti-inflammatory drugs: insight into mechanisms and implications for cancer growth and ulcer healing. *Nat. Med.* **5,** 1418–1423
68. Hiraga, T., Myoui, A., Choi, M. E., Yoshikawa, H., and Yoneda, T. (2006) Stimulation of cyclooxygenase-2 expression by bone-derived transforming growth factor-β enhances bone metastases in breast cancer. *Cancer Res.* **66,** 2067–2073

Secreted Protein Acidic and Rich in Cysteine (SPARC) Mediates Metastatic Dormancy of Prostate Cancer in the Bone

Sambad Sharma[1], Fei Xing[1], Yin Liu[1], Kerui Wu[1], Neveen Said[2], Radhika Pochampally[3], Yusuke Shiozawa[1], Hui-Kuan Lin[1], K.C. Balaji[4], and Kounosuke Watabe[*1]

SUPPLEMENTAL FIGURE LEGENDS:

SUPPLEMENTARY FIGURE 1:

(*A*) Schematic outline for isolation of Indolent and Aggressive cells from mice. Stem-like cell population ($CD24^{low}/CD44^{high}/CD133^{high}$) was isolated from PC3mm cells followed by injecting 4000 cells into the tibial bone of the nude mice. About 50 percent of the mice showed tumor incidence (overt growth) whereas rest of the mice did not show tumor incidence as examined by bioluminescence at Day 40. The tibial bones from all the mice were flushed out and cancer cells were isolated by adding puromycin into the culture media and growing for 2 weeks. (*B-E*) Indolent and Aggressive cells were evaluated for their proliferative ability (*B*), sphere formation ability (*C*), $CD24^{low}/CD44^{high}/CD133^{high}$ Cancer Stem-like population (*D*), invasive ability (*E*) and migration ability (*F*).

SUPPLEMENTARY FIGURE 2:

(*A*) Indolent or Aggressive cells were co-cultured with HS5 bone stromal cell line in the transwell plate. Cancer cells were seeded on the lower chamber and HS5 cell was seeded in upper chamber and cell proliferation of cancer cells were examined at days 1, 3 and 5 by MTS assay. (*B,C*) Indolent and Aggressive cells were treated with Conditioned Medium (CM) prepared from bone marrow stroma cells (BMSC) (*B*) and HS5 cell line (*C*) followed by examining cell proliferation at days 1, 3 and 5 by MTS assay. (*D*) Schematic diagram for isolation of CMs that were used to treat Indolent cells. BMSC or HS5 cells were treated with either Indolent or Aggressive cell CM. After 24 hours of incubation, the media was replaced by serum-free FBS DMEM for BMSC and serum-free FBS RPMI for HS5. Cells were then incubated for 24 hours and CMs were isolated. (*E*) CM generated after treating BMSC/HS5 with Indolent or Aggressive CMs (as shown in *D*) were treated to Indolent cells followed by examining cell proliferation by MTS assay at day 5 (lower panels) and p21 expression after 48 hours of treatment (picture inserts). (*F*) SPARC expression was examined in CMs isolated from

human osteoblast cell line hFOB, BMSC, Indolent and Aggressive cell line. Cell lysate GAPDH expression was used as a loading control. *, P-value<0.05 and ** P-value<0.01.

SUPPLEMENTARY FIGURE 3:

(*A*) BMSC was treated with CMs generated from Indolent cells with or without expression of SPARC gene for 24 hrs followed by examination of BMP7 expression by western blot (left panel). BMP7 expression was also examined in BMSC co-cultured in a transwell with Indolent cells either silenced for SPARC expression using shRNA or control cells for 24 hrs (Right panel). (*B*) Conditioned mediums (CM) were generated from BMSC with or without rSPARC (200 ng/ml) treatment, SP+BMSC CM or BMSC CM respectively. Cancer cells (PC3mm, Indolent and Aggressive) were seeded in the low binding 96-well cell culture plate and treated with BMSC CM or SP+ BMSC CM in a 50:50 ratio with sphere media. The numbers of sphere formed at day 6 were counted. Representative images of spheres are shown in right panels. (*C*) PC3mm, Indolent and Aggressive cells were treated seeded in 12-well plate followed by treatment with BMSC CM or SP+ BMSC CM for 48 hours. SA-β-galactosidase staining was performed to stain senescent cells, and staining positive cells were quantified. Representative images of senescent cells are shown in right panels. (*D*) Noggin expression was examined in Aggressive cells with or without shRNA mediated knockdown of Noggin by RT-PCR (left) and western blot (right).*, P-value<0.05 and ** P-value<0.01.

SUPPLEMENTARY FIGURE 4:

(*A*) BMPR2 expression was analyzed in patients with different gleason grade in GSE21034 dataset. (*B, C*) Correlation analysis between BMPR2 expression and pre-surgical PSA (*B*) or age (*C*) of the patient was performed using GSE21034 dataset. (*D-F*) BMPR2 expression was examined between different stages (*D*), and different sub stages (*E* and *F*) in cancer patients using GSE21034.

SUPPLEMENTARY FIGURE 5:

(*A*) Indolent and Aggressive cells were treated with 5-Azacytidine (50nM) for five days followed by examination of SPARC expression by qRT-PCR. (*B*) Methylation of SPARC promoter in normal (n=50) and cancer samples (n=502) from prostate cancer patients was examined by

analyzing TCGA database. (*C* and *D*) Recurrence-free survival of DNMT1 and DNMT3b was examined using GSE27103 (*C*) and TCGA database (*D*). (*E*) Aggressive cells were treated with either DMSO or NS398 (50 μM) for 24 hours and SPARC expression was examined by qRT-PCR. (*F*) Lower panel: Schematic diagram for generation of CMs that were used to treat Aggressive cells. Aggressive cells were treated with or without 5-Azacytidine (50 nM) for five days and media was replaced with serum-free RPMI for collection of CM. This CM was used to treat BMSC for 24 hours, and the media was collected and treated to Aggressive cells. Upper panel: Western blot was performed to examine BMP7 expression in BMSC after treatment with Aza-/+ Aggressive CM for 24 hours. (*G*) The CMs from F were used to treat Aggressive cells followed by examining cell proliferation at days 1, 3 and 5 by MTS assay. *, P-value<0.05, **, P-value<0.01 and ****, P-value<0.00001.

Supplementary table 1:

(a) Clinical details of the patients with low BMPR2 expression

Sample ID	DxAge	PreTx PSA	Path Stag	Path GG1	Path GG2	Path GGS	BCR_FreeTime	ECE	SVI	LNI
PCA0008	64.24	10.40	T3A	3	3	6	149.19	ESTABLISHED	Negative	Normal_N0
PCA0017	55.92	7.65	T3A	3	4	7	104.38	FOCAL	Negative	Normal_N0
PCA0024	56.58	18.41	T2C	3	4	7	3.94	NONE	Negative	Normal_N0
PCA0030	60.28	12.80	T2B	3	4	7	115.09	INV_CAPSULE	Negative	Normal_N0
PCA0031	54.53	6.30	T3A	4	3	7	35.35	ESTABLISHED	Negative	Normal_N0
PCA0033	61.38	14.47	T2B	3	3	6	69.09	NONE	Negative	Normal_N0
PCA0040	46.84	4.60	T2B	3	4	7	89.50	INV_CAPSULE	Negative	Normal_N0
PCA0054	54.98	39.90	T3C	3	5	8	2.10	ESTABLISHED	Positive	Abnormal_N1
PCA0057	67.46	5.43	T2B	3	4	7	82.86	INV_CAPSULE	Negative	Normal_N0
PCA0074	58.69	5.11	T2B	3	4	7	84.31	INV_CAPSULE	Negative	Normal_N0
PCA0075	54.45	4.62	T2B	3	4	7	49.35	NONE	Negative	Normal_N0
PCA0077	48.32	2.77	T2B	3	3	6	61.70	INV_CAPSULE	Negative	Normal_N0
PCA0084	70.81	3.69	T2B	3	3	6	39.66	INV_CAPSULE	Negative	Not Done_NX
PCA0089	57.31	7.00	T2C	3	3	6	70.18	INV_CAPSULE	Negative	Normal_N0
PCA0094	44.43	8.60	T2B	3	4	7	66.10	NONE	Negative	Normal_N0
PCA0097	62.54	5.30	T2B	3	3	6	1.87	NONE	Negative	Normal_N0
PCA0110	58.85	5.70	T2C	3	3	6	58.91	NONE	Negative	Not Done_NX
PCA0111	60.49	6.69	T2C	3	4	7	49.84	INV_CAPSULE	Negative	Normal_N0
PCA0112	58.77	33.71	T3A	4	4	8	13.21	ESTABLISHED	Negative	Normal_N0
PCA0113	56.91	4.20	T2C	3	4	7	60.45	INV_CAPSULE	Negative	Normal_N0
PCA0114	66.58	9.00	T3A	4	3	7	38.77	ESTABLISHED	Negative	Normal_N0
PCA0117	58.37	22.36	T3B	3	4	7	18.83	ESTABLISHED	Positive	Normal_N0
PCA0119	63.34	2.80	T2B	4	3	7	46.49	INV_CAPSULE	Negative	Normal_N0
PCA0122	51.28	4.20	T2B	3	3	6	52.47	INV_CAPSULE	Negative	Not Done_NX
PCA0128	64.02	1.48	T2C	4	3	7	53.82	NONE	Negative	Normal_N0
PCA0129	62.39	11.70	T2C	3	4	7	56.87	INV_CAPSULE	Negative	Normal_N0
PCA0130	64.53	2.21	T2C	4	4	8	27.86	INV_CAPSULE	Negative	Normal_N0
PCA0135	56.85	6.10	T2B	3	4	7	51.65	INV_CAPSULE	Negative	Not Done_NX
PCA0136	53.52	4.66	T3A	4	3	7	5.72	ESTABLISHED	Negative	Not Done_NX
PCA0141	60.57	5.44	T2A	3	4	7	41.76	NONE	Negative	Normal_N0
PCA0144	56.15	5.60	T2C	3	3	6	37.59	NONE	Negative	Normal_N0
PCA0149	52.52	20.40	T3B	3	4	7	59.17	ESTABLISHED	Positive	Normal_N0
PCA0150	58.72	11.84	T3A	4	3	7	51.35	ESTABLISHED	Negative	Normal_N0
PCA0151	58.37	4.50	T2B	3	3	6	47.34	INV_CAPSULE	Negative	Not Done_NX
PCA0155	57.54	11.10	T2B	4	3	7	47.61	NONE	Negative	Normal_N0
PCA0157	47.38	3.50	T3A	3	3	6	39.85	FOCAL	Negative	Not Done_NX
PCA0158	56.90	3.20	T2C	3	3	6	31.61	INV_CAPSULE	Negative	Not Done_NX
PCA0159	45.98	5.36	T3B	4	4	8	1.41	ESTABLISHED	Positive	Abnormal_N1
PCA0160	62.42	4.00	T2A	3	3	6	12.98	NONE	Negative	Not Done_NX
PCA0162	55.88	7.11	T2B	3	4	7	11.83	INV_CAPSULE	Negative	Normal_N0
PCA0163	67.70	2.65	T3A	3	4	7	45.37	ESTABLISHED	Negative	Not Done_NX
PCA0164	58.15	7.67	T2B	3	3	6	54.54	NONE	Negative	Not Done_NX
PCA0165	64.81	6.34	T2B	3	3	6	30.52	INV_CAPSULE	Negative	Not Done_NX
PCA0167	55.26	2.98	T2B	3	4	7	26.84	NONE	Negative	Not Done_NX
PCA0171	60.87	8.20	T3A	NA	NA	NA	8.84	ESTABLISHED	Negative	Normal_N0
PCA0174	54.32	4.60	T2B	4	3	7	43.30	NONE	Negative	Normal_N0
PCA0175	51.00	5.60	T2B	3	3	6	36.01	NONE	Negative	Normal_N0
PCA0176	53.55	8.66	T3B	4	5	9	2.56	ESTABLISHED	Positive	Normal_N0
PCA0179	64.89	46.36	T3B	4	5	9	2.92	ESTABLISHED	Positive	Abnormal_N1
PCA0180	67.17	13.34	T3A	4	5	9	1.38	ESTABLISHED	Negative	Abnormal_N1
PCA0181	69.01	27.00	T3A	4	5	9	30.03	ESTABLISHED	Negative	Normal_N0
PCA0187	66.00	506.00	T2B	4	3	7	18.00	NONE	Negative	Normal_N0
PCA0200	53.33	9.70	T3B	4	5	9	2.89	ESTABLISHED	Positive	Abnormal_N1
PCA0201	66.73	13.32	T3B	4	4	8	4.11	ESTABLISHED	Positive	Abnormal_N1
PCA0206	57.55	15.99	T4	4	4	8	1.61	ESTABLISHED	Positive	Abnormal_N1
PCA0207	67.17	13.34	T3A	4	5	9	1.38	ESTABLISHED	Negative	Abnormal_N1
PCA0208	64.09	6.20	T3B	NA	NA	NA	11.79	INV_CAPSULE	Positive	Normal_N0
PCA0213	54.84	9.40	T3C	4	5	9	64.66	ESTABLISHED	Positive	Abnormal_N1

(b) Clinical details of the patients with high BMPR2 expression

Sample ID	DxAge	PreTx PSA	Path Stage	Path GG1	Path GG2	Path GGS	BCR_Free Time	ECE	SVI	LNI
PCA0001	72.77	43.90	T3C	4	3	7	18.50	ESTABLISHED	Positive	Normal_N0
PCA0002	58.09	43.20	T2A	5	3	8	58.02	INV_CAPSULE	Negative	Normal_N0
PCA0003	67.94	11.30	T3A	3	4	7	93.14	ESTABLISHED	Negative	Abnormal_N1
PCA0005	64.70	5.90	T2C	3	4	7	126.10	NONE	Negative	Normal_N0
PCA0007	56.77	3.80	T2C	3	4	7	98.60	NONE	Negative	Normal_N0
PCA0009	56.58	12.90	T2C	3	4	7	64.76	NONE	Negative	Normal_N0
PCA0010	49.87	5.20	T4	3	3	6	35.06	NONE	Negative	Normal_N0
PCA0011	52.12	6.70	T2C	3	3	6	82.17	NONE	Negative	Normal_N0
PCA0012	66.18	3.26	T2C	3	3	6	128.43	NONE	Negative	Normal_N0
PCA0013	54.21	9.35	T3A	3	4	7	10.38	NONE	Negative	Normal_N0
PCA0014	60.35	2.91	T2C	3	4	7	76.45	INV_CAPSULE	Negative	Not Done_NX
PCA0015	58.71	2.90	T3A	3	4	7	22.70	ESTABLISHED	Negative	Not Done_NX
PCA0018	55.23	9.23	T3A	4	3	7	18.96	ESTABLISHED	Negative	Not Done_NX
PCA0020	59.89	3.80	T3A	3	4	7	56.94	ESTABLISHED	Negative	Normal_N0
PCA0021	57.99	9.64	T3A	3	4	7	61.50	ESTABLISHED	Negative	Normal_N0
PCA0022	57.67	5.80	T2C	3	3	6	39.95	INV_CAPSULE	Negative	Normal_N0
PCA0025	61.16	3.70	T2C	3	4	7	68.04	NONE	Negative	Normal_N0
PCA0026	57.11	9.49	T2A	3	4	7	78.16	NONE	Negative	Normal_N0
PCA0027	50.75	6.69	T2B	3	3	6	116.83	INV_CAPSULE	Negative	Normal_N0
PCA0028	61.47	3.82	T3B	5	3	8	27.60	ESTABLISHED	Positive	Normal_N0
PCA0029	53.81	6.82	T2B	3	4	7	26.68	INV_CAPSULE	Negative	Normal_N0
PCA0032	56.37	16.71	T3A	4	5	9	3.71	ESTABLISHED	Negative	Normal_N0
PCA0034	57.00	5.40	T2B	3	3	6	92.98	NONE	Negative	Normal_N0
PCA0035	62.75	13.10	T3A	3	3	6	77.80	ESTABLISHED	Negative	Normal_N0
PCA0036	53.58	6.92	T2A	4	3	7	85.32	INV_CAPSULE	Negative	Normal_N0
PCA0037	42.79	5.00	T2A	3	4	7	104.05	NONE	Negative	Normal_N0
PCA0038	64.26	5.50	T2B	4	3	7	100.21	INV_CAPSULE	Negative	Normal_N0
PCA0050	59.69	6.70	T2B	3	4	7	83.85	NONE	Negative	Normal_N0
PCA0052	56.67	12.00	T3A	3	4	7	102.54	ESTABLISHED	Negative	Normal_N0
PCA0056	83.00	NA	T2A	3	3	6	25.00	NONE	Negative	Normal_N0
PCA0058	67.72	7.66	T2C	3	3	6	30.19	NONE	Negative	Normal_N0
PCA0062	52.46	1.15	T2B	3	3	6	42.94	NONE	Negative	Normal_N0
PCA0063	61.19	15.00	T2B	4	4	8	74.12	ESTABLISHED	Positive	Normal_N0
PCA0064	45.09	5.52	T2B	3	3	6	24.28	INV_CAPSULE	Negative	Normal_N0
PCA0065	70.19	5.04	T2B	3	4	7	77.37	INV_CAPSULE	Negative	Normal_N0
PCA0066	51.62	13.60	T3B	3	4	7	77.11	ESTABLISHED	Positive	Normal_N0
PCA0068	60.88	7.62	T2B	4	3	7	45.54	INV_CAPSULE	Negative	Normal_N0
PCA0073	51.76	4.26	T3A	4	3	7	13.04	FOCAL	Negative	Normal_N0
PCA0080	48.19	10.02	T2B	4	3	7	55.39	INV_CAPSULE	Negative	Normal_N0
PCA0081	49.99	5.80	T4	3	4	7	9.86	ESTABLISHED	Negative	Normal_N0
PCA0082	60.68	4.13	T2B	3	3	6	58.97	INV_CAPSULE	Negative	Normal_N0
PCA0083	68.04	14.00	T3A	4	3	7	31.80	ESTABLISHED	Negative	Abnormal_N1
PCA0086	37.30	6.63	T2A	3	4	7	60.85	INV_CAPSULE	Negative	Not Done_NX
PCA0087	50.99	4.90	T3A	3	4	7	56.84	FOCAL	Negative	Normal_N0
PCA0090	58.98	7.40	T3B	3	4	7	48.43	ESTABLISHED	Positive	Normal_N0
PCA0092	67.45	5.00	T4	4	4	8	16.82	ESTABLISHED	Negative	Normal_N0
PCA0093	46.13	4.97	T2B	3	4	7	46.42	INV_CAPSULE	Negative	Normal_N0
PCA0095	56.22	4.50	T4	3	3	6	51.58	NONE	Negative	Normal_N0
PCA0096	71.20	8.32	T3B	4	5	9	42.38	ESTABLISHED	Positive	Normal_N0
PCA0099	68.50	12.47	T3A	4	3	7	5.78	ESTABLISHED	Negative	Normal_N0
PCA0100	60.31	6.95	T2B	3	4	7	38.21	INV_CAPSULE	Negative	Normal_N0
PCA0101	59.52	5.00	T2B	3	3	6	62.36	NONE	Negative	Normal_N0
PCA0103	59.43	4.50	T2B	3	4	7	28.65	INV_CAPSULE	Negative	Normal_N0
PCA0104	69.89	1.60	T2B	3	4	7	43.47	FOCAL	Negative	Not Done_NX
PCA0105	54.51	3.80	T2B	4	3	7	23.00	INV_CAPSULE	Negative	Normal_N0
PCA0107	46.49	1.80	T2C	3	3	6	56.15	INV_CAPSULE	Negative	Normal_N0
PCA0108	49.50	4.90	T3A	3	3	6	59.14	ESTABLISHED	Negative	Normal_N0
PCA0109	58.91	5.38	T2B	3	3	6	13.86	NONE	Negative	Normal_N0
PCA0115	60.26	5.97	T2C	3	4	7	26.22	INV_CAPSULE	Negative	Normal_N0
PCA0118	51.40	5.08	T2B	3	4	7	43.83	NONE	Negative	Normal_N0
PCA0120	53.47	4.07	T2A	3	3	6	62.65	NONE	Negative	Normal_N0
PCA0123	67.84	6.60	T2C	3	3	6	60.06	INV_CAPSULE	Negative	Not Done_NX
PCA0124	50.50	10.80	T2C	3	4	7	55.20	INV_CAPSULE	Negative	Normal_N0
PCA0125	54.35	4.11	T3A	3	4	7	61.37	FOCAL	Negative	Normal_N0
PCA0126	61.61	3.33	T2C	3	4	7	51.85	INV_CAPSULE	Negative	Normal_N0
PCA0127	51.97	5.93	T2C	4	3	7	43.53	INV_CAPSULE	Negative	Normal_N0
PCA0132	55.92	5.29	T2C	3	3	6	48.56	INV_CAPSULE	Negative	Not Done_NX
PCA0133	58.36	6.98	T2B	3	4	7	28.06	NONE	Negative	Normal_N0
PCA0134	65.71	26.02	T2B	4	3	7	8.18	INV_CAPSULE	Negative	Normal_N0
PCA0145	56.29	6.60	T2C	3	4	7	48.43	INV_CAPSULE	Negative	Normal_N0
PCA0146	48.39	3.10	T2C	3	3	6	50.89	INV_CAPSULE	Negative	Not Done_NX
PCA0147	52.48	5.40	T2C	3	3	6	45.73	NONE	Negative	Normal_N0
PCA0156	51.43	13.30	T4	3	4	7	10.81	FOCAL	Negative	Normal_N0
PCA0161	64.00	6.90	T2B	3	4	7	19.02	NONE	Negative	Not Done_NX
PCA0168	56.75	4.27	T2B	3	4	7	49.02	NONE	Negative	Normal_N0
PCA0169	52.85	6.70	T2B	3	3	6	42.94	NONE	Negative	Not Done_NX
PCA0170	61.79	8.97	T3A	4	3	7	52.17	ESTABLISHED	Negative	Normal_N0
PCA0172	52.00	22.82	T4	4	5	9	30.56	ESTABLISHED	Positive	Normal_N0
PCA0173	66.16	5.24	T3B	3	3	6	32.69	NONE	Positive	Normal_N0
PCA0178	61.83	4.65	T2B	3	3	6	37.68	NONE	Negative	Normal_N0
PCA0210	59.00	2.86	T3C	4	3	7	20.04	ESTABLISHED	Positive	Abnormal_N1
PCA0215	48.00	NA	T3A	4	4	8	5.95	INV_CAPSULE	Negative	Normal_N0

Abbreviations:
PreTx PSA: Pre-surgical PSA; Path Stage: Pathological Stage; Path GG1: Pathological gleason grade 1; Path GG2: Pathological gleason grade 2: Path GGS: Pathological gleason grade score; BCR-free time: Biochemical recurrence-free survival time (in months); ECE: Extracapsular extension; SVI: Seminal vesicle involvement; LNI: Lymph node involvement.

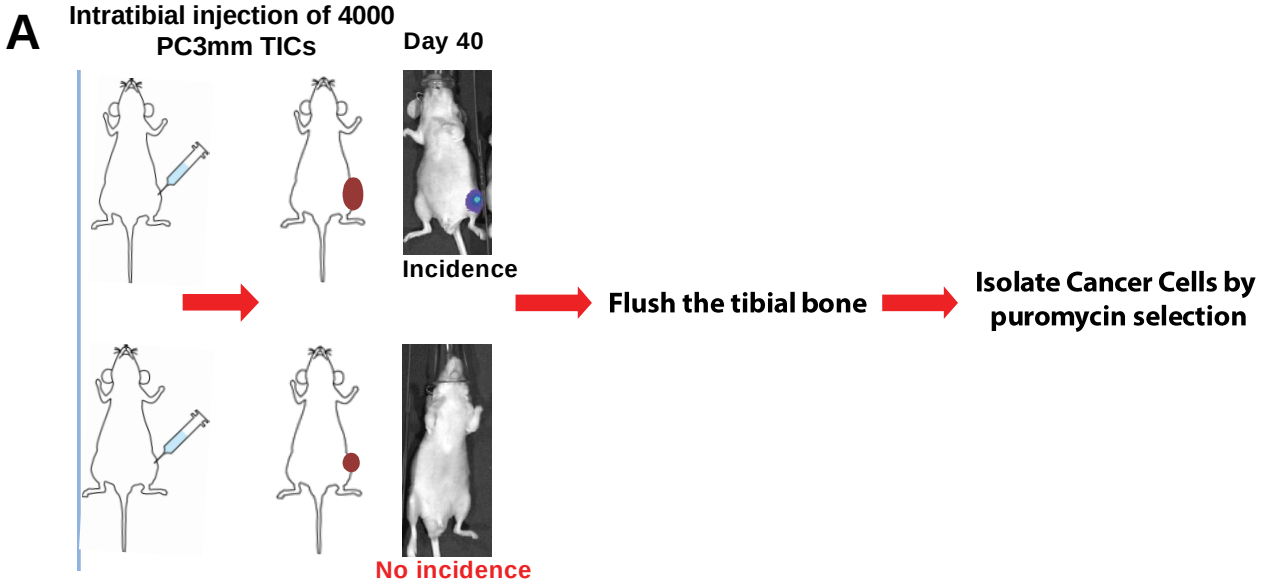

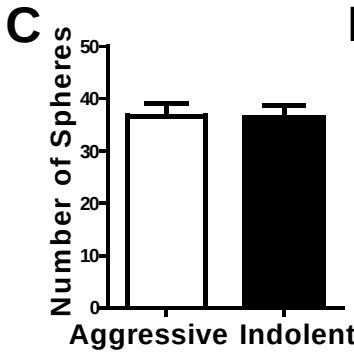

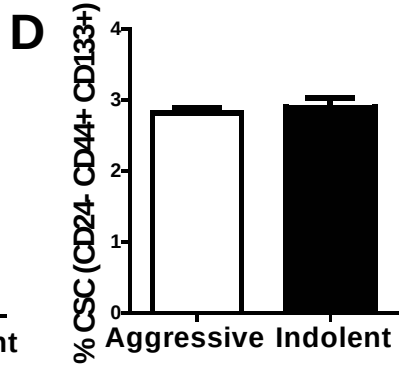

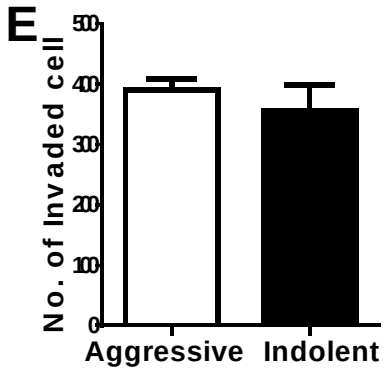

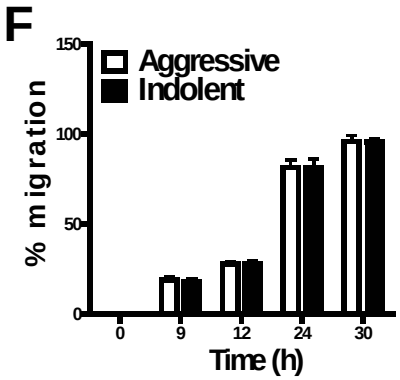

Supplementary Figure S1

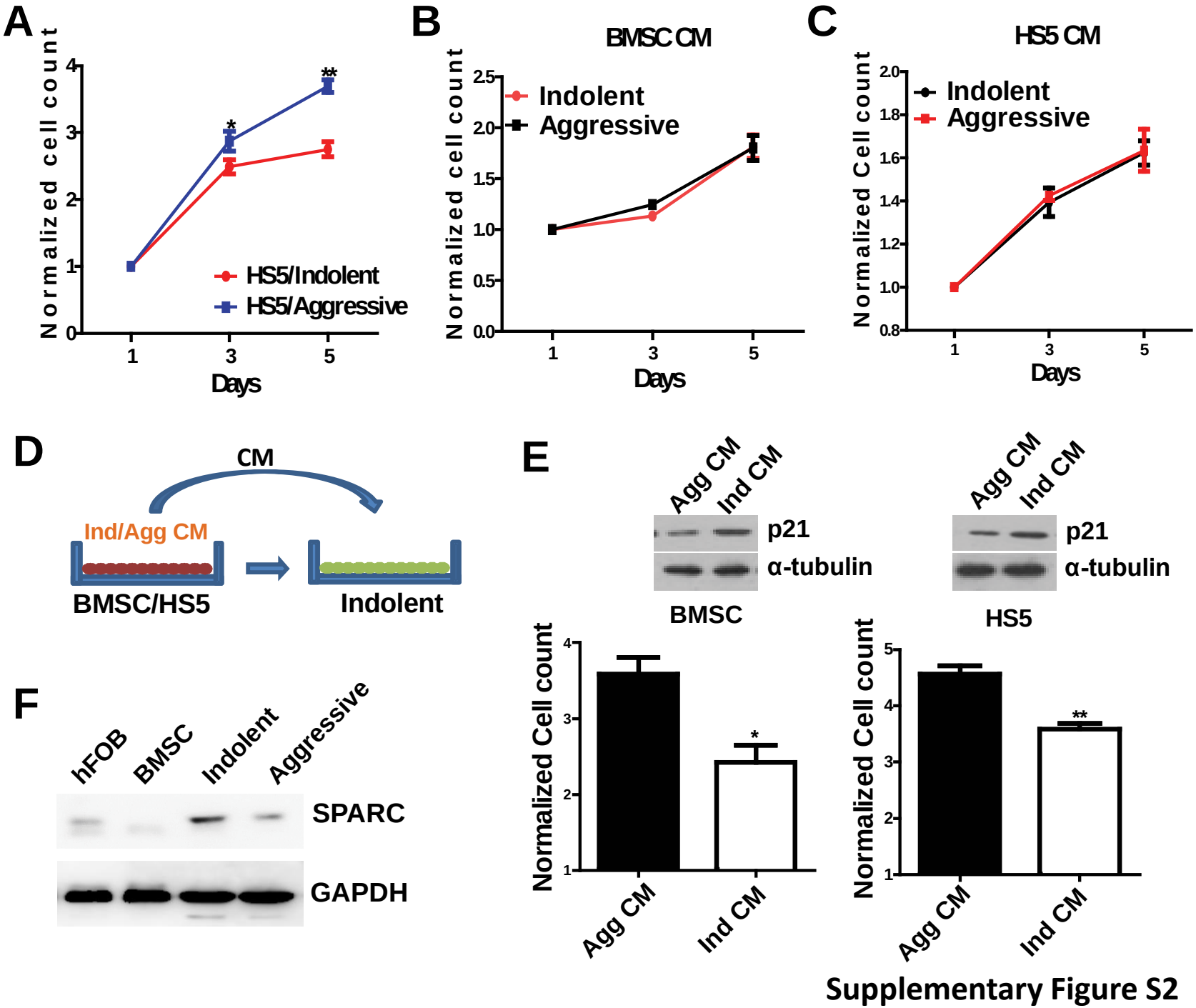

Supplementary Figure S2

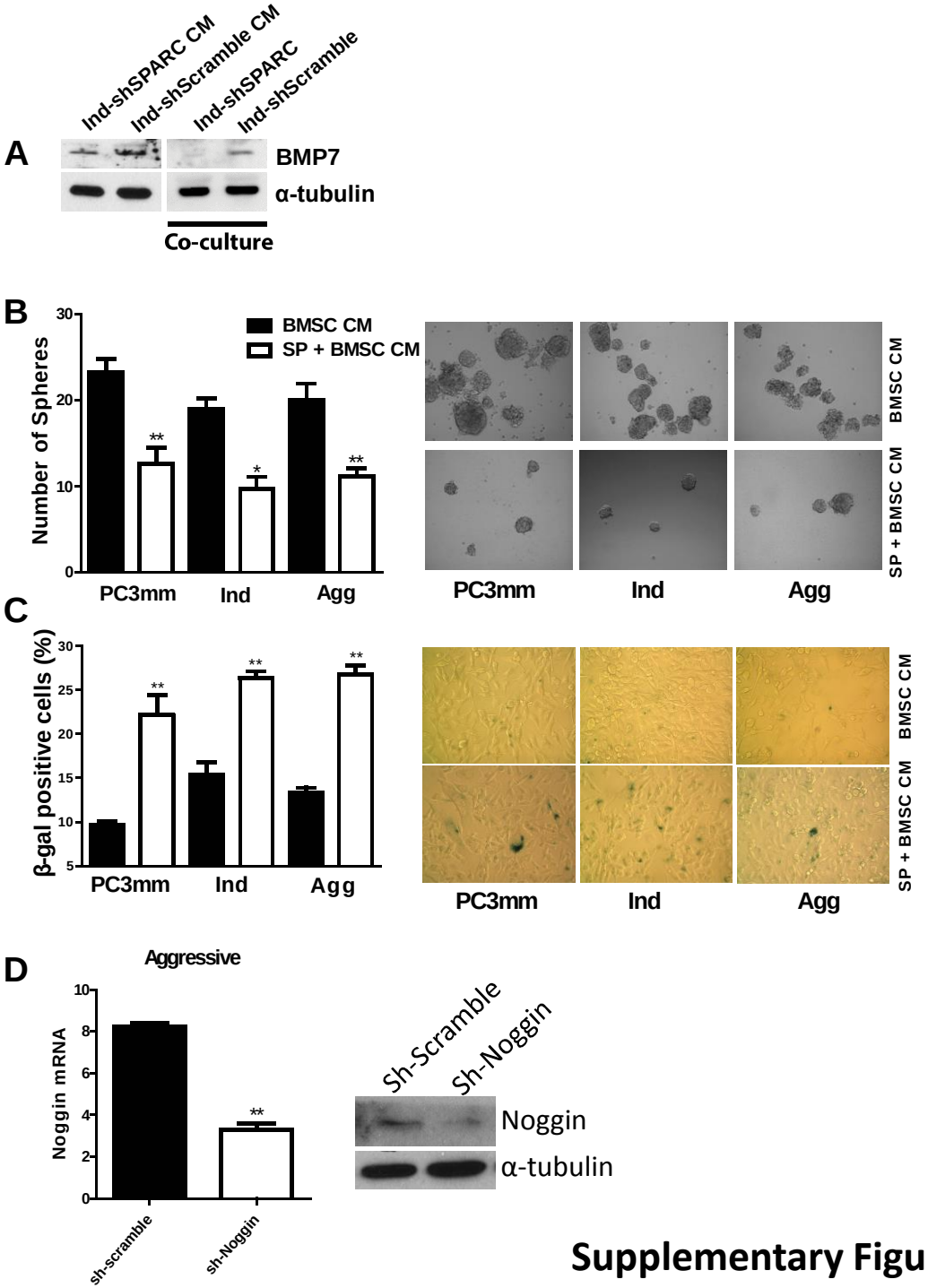

Supplementary Figure S3

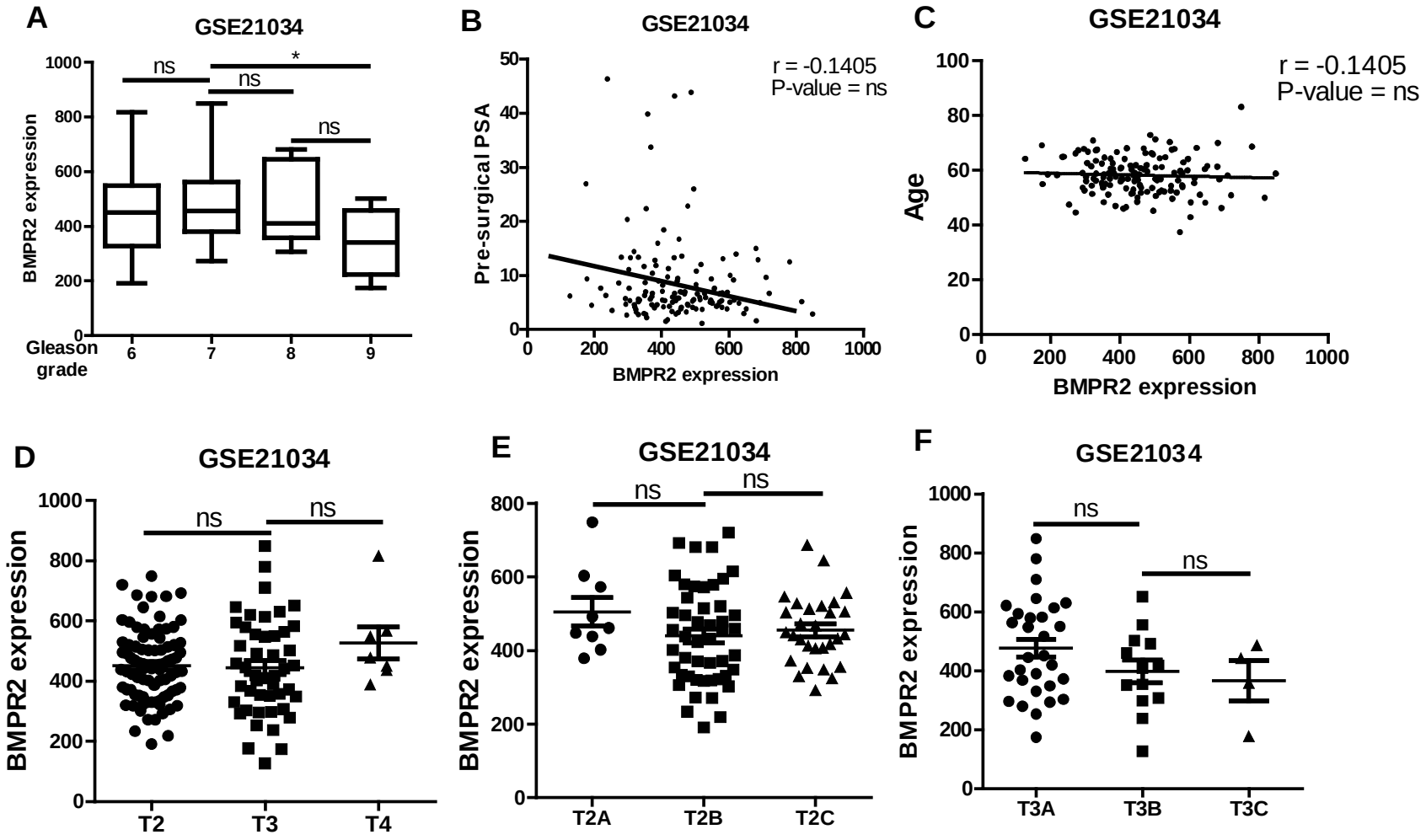

Supplementary Figure S4

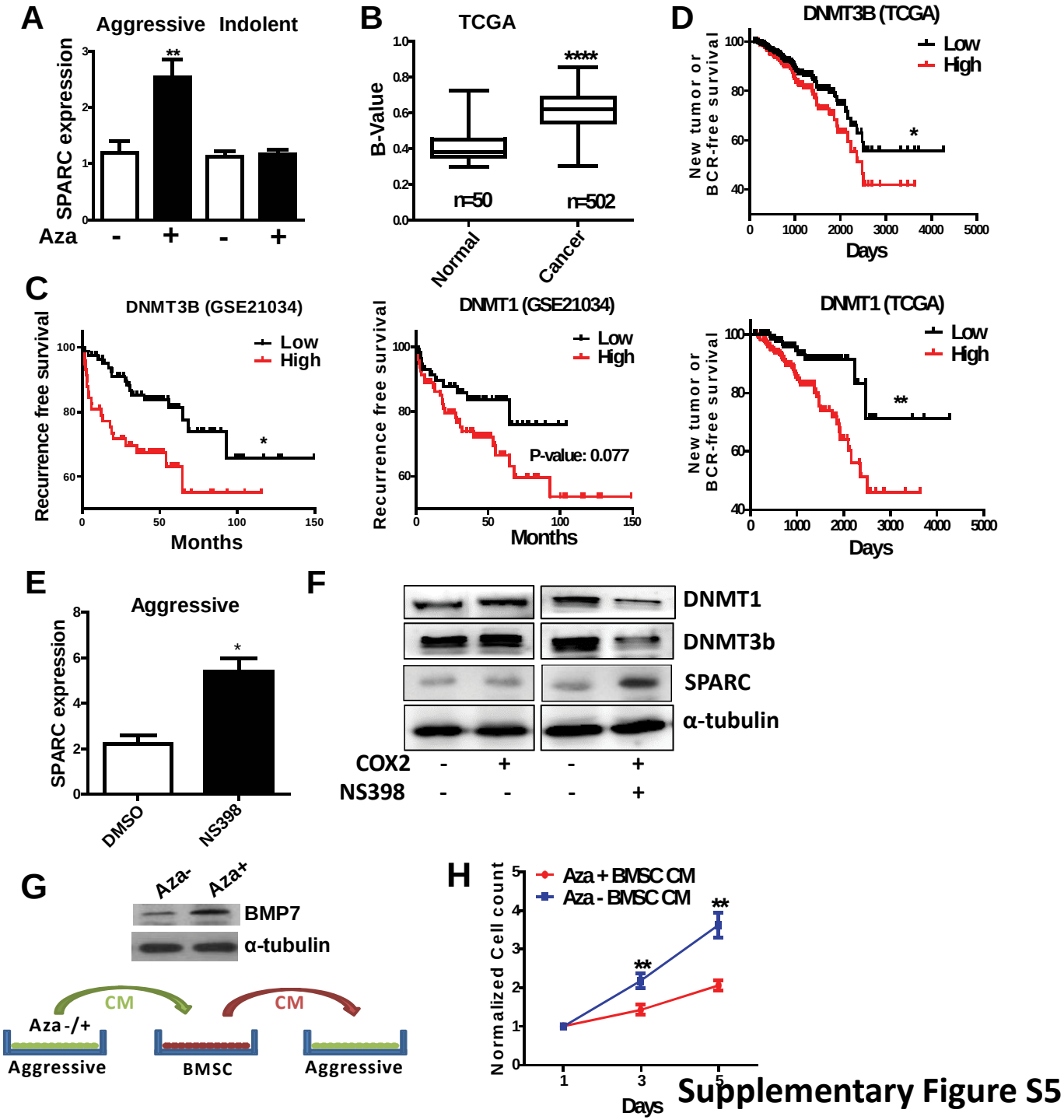

Supplementary Figure S5

Secreted Protein Acidic and Rich in Cysteine (SPARC) Mediates Metastatic Dormancy of Prostate Cancer in Bone

Sambad Sharma, Fei Xing, Yin Liu, Kerui Wu, Neveen Said, Radhika Pochampally, Yusuke Shiozawa, Hui-Kuan Lin, K. C. Balaji and Kounosuke Watabe

J. Biol. Chem. 2016, 291:19351-19363.
doi: 10.1074/jbc.M116.737379 originally published online July 15, 2016

Citation: BoneKEy Reports **4**, Article number: 689 (2015) | doi:10.1038/bonekey.2015.57

www.nature.com/bonekey

REVIEW

Bone marrow as a metastatic niche for disseminated tumor cells from solid tumors

Yusuke Shiozawa[1,2], Matthew R Eber[2], Janice E Berry[2] and Russell S Taichman[2]

[1]Department of Cancer Biology and Comprehensive Cancer Center, Wake Forest University School of Medicine, Winston-Salem, NC, USA. [2]Department of Periodontics and Oral Medicine, University of Michigan School of Dentistry, Ann Arbor, MI, USA.

Bone marrow is a heterogeneous organ containing diverse cell types, and it is a preferred metastatic site for several solid tumors such as breast and prostate cancer. Recently, it has been shown that bone metastatic cancer cells interact with the bone marrow microenvironment to survive and grow, and thus this microenvironment is referred to as the 'metastatic niche'. Once cancer cells spread to distant organs such as bone, the prognosis for the patient is generally poor. There is an urgent need to establish a greater understanding of the mechanisms whereby the bone marrow niche influences bone metastasis. Here we discuss insights into the contribution of the bone marrow 'metastatic niche' to progression of bone metastatic disease, with a particular focus on cells of hematopoietic and mesenchymal origin.

BoneKEy Reports **4**, Article number: 689 (2015) | doi:10.1038/bonekey.2015.57

Introduction

Primary tumors, with proper treatment, do not typically result in patient death. However, once tumors are established in other organs, the mortality of cancer patients increases markedly. Once detached from the primary tumor, a single tumor cell or a cluster of tumor cells can circulate throughout the body, and later take up residence in a distant site. Interestingly, each type of tumor has a distinct pattern of dissemination. It has been speculated that anatomical and mechanical structures in the human body result in organ preference of tumor metastasis.[1] This hypothesis, however, fails to explain all aspects of the metastatic behavior of disseminated tumor cells (DTCs).

Over a century ago, Stephen Paget famously stated in his 'seed and soil' theory that tumor cells seek a specific accommodating location to survive outside of the primary lesion.[2] That is, a hospitable microenvironment in the potential metastatic site selectively affects the dissemination route of DTCs. Consistent with this notion, recent studies have revealed that the communication between DTCs and the distant microenvironment, or 'metastatic niche', is crucial for the progression of DTCs.[3–5] A better understanding of the tumor-supportive aspects of this interaction is clearly needed for the development of more effective metastatic disease treatments.

Bone, or bone marrow, is a major target organ for metastasis, evidently providing a fertile 'soil' for DTCs. Prostate and breast cancers are particularly well known to metastasize to the bone. Bone marrow contains various cell types, including cells of hematopoietic origin and cells involved in bone formation and remodeling. One major function of the marrow is to regulate hematopoiesis. In the marrow, osteoblasts,[6–8] endothelial cells,[9,10] nerve cells,[11,12] adipocytes,[13] CXCL12-abundant reticular (CAR) cells[14] and mesenchymal stem cells[15,16] collectively serve as a specific 'niche' for hematopoietic stem cells (HSCs), maintaining the functions of HSCs including homing, self-renewal, quiescence and differentiation.[17–19]

It is now known that malignant cells that disseminate to and develop in the bone marrow do so by hijacking the bone marrow niche.[20] In fact, prostate and breast cancer both home to the marrow using mechanisms similar to HSC homing.[21,22] Not only are the DTCs supported by their chosen niche, but they can also instigate niche changes that preferentially cater to malignant cells. Indeed, myeloproliferative neoplasms remodel the normal osteoblastic HSC niche into a malignant niche that impairs normal hematopoiesis.[23] Thus, studying the cross talk between malignancy and the bone marrow microenvironment has rightfully become an area of great interest. However, detailed mechanisms underlying these interactions remain largely unknown. In this review, we will explore what is currently known about DTC-mediated bone marrow niche conversion and also suggest future directions for 'metastatic niche' research.

The Metastatic Niche in the Marrow

Bone marrow is a very heterogeneous organ, containing cells of hematopoietic origin (HSCs, osteoclasts, macrophages,

Correspondence: Dr Y Shiozawa, Department of Cancer Biology, Wake Forest University School of Medicine, Medical Center Blvd, Winston-Salem, NC 27157, USA. E-mail: yshiozaw@wakehealth.edu
or Dr RS Taichman, Department of Periodontics and Oral Medicine, University of Michigan School of Dentistry, Room 3307, 1011 North University Avenue, Ann Arbor, MI 48109-1078, USA. E-mail: rtaich@umich.edu

Received 5 December 2014; accepted 20 March 2015; published online 20 May 2015

lymphocyte and so on), mesenchymal origin (mesenchymal stem cells (MSCs), osteoblasts, adipocytes and so on), endothelial cells and nerve cells. Osteoblasts, adipocytes, endothelial cells and nerve cells are well studied as the specific microenvironment, or niche, for HSCs. Osteoblasts and osteoclasts are also involved in bone remodeling directly or indirectly by interacting with HSCs. The cells in the marrow interact to support their unique functions and maintain bone structure. Recent studies have revealed that DTCs from primary tumors commandeer this supportive microenvironment, suggesting that DTCs may adapt to and alter a pre-existing niche (the 'HSC niche') to survive and grow as full-blown metastases (the 'metastatic niche').

Mesenchymal stem Cells

It has long been demonstrated that prostate and breast cancers have the potential to assume many properties indicative of osteoblast lineage cells.[24–26] This capacity for osteomimicry is thought to be a key feature of its bone metastatic potential. More recently, the differentiation potential of prostate cancer cells to assume an adipocyte lineage phenotype was revealed.[27] Human prostate cancer cell lines PC3 and DU145 reversibly differentiate into an adipocyte-like phenotype *in vitro* under adipogenic induction conditions, leading to growth arrest and apoptosis.[27] Similarly, human prostate cancer bone metastatic tissue microarray (TMA) samples exhibit a brown fat-specific marker, UCP1, suggesting that prostate cancer cells may also differentiate into an adipocyte phenotype *in vivo*.[27] As the differentiation potential of prostate cancer is likened to that of MSCs,[27] it is also possible that disseminated prostate cancer acquires an MSC-like phenotype to colonize the bone marrow.

In the bone marrow, MSCs may also be involved in establishing tumor dormancy. When the bone metastatic clone of human breast cancer cell line MDA-BM-231-BM2 is cocultured with human MSC line R14, the proliferation and migration of MDA-BM-231-BM2 cells are reduced, evidently by R14-derived exosomes.[28] The mechanism behind this transition is the high expression of microRNA mir-23b in the exosomes, which causes suppression of the *MARCKS* gene and subsequently its encoded protein, myristoylated alanine-rich C kinase substrate. As expected, exosome-treated or miR-23b-overexpressing MDA-BM-231-BM2 cells both exhibit dormancy in mice.[28]

It has been demonstrated that bone marrow-derived MSCs are capable of transforming into cancer-associated fibroblasts (CAFs) within the primary tumor,[29,30] whereupon CAFs promote lung metastases of human breast cancer cell line MDA-MB-231 through the Chemokine (C-C motif) ligand 5 (CCL5)/ C-C chemokine receptor type 5 (CCR5) axis,[29] and bone metastases of murine prostate cancer cell line RM-1 through the chemokine (C–X–C motif) ligand 16 (CXCL16)/ C-X-C chemokine receptor type 6 (CXCR6) axis.[30] In fact, MSC-derived CAFs may select for Src hyperactive, bone metastatic and triple negative breast cancer.[31] Specifically, CAF expression of CXCL12 and insulin-like growth factor-1 (IGF-1) was shown to strongly activate Src (PI3K-Akt pathway) in the triple negative human breast cancer cell lines MDA-MB-231 and CN34, which resulted in bone metastatic phenotype enrichment.[31] The bone metastases of Src hyperactive MDA-MB-231 and CN34 cells were prevented, however, when tumor-bearing mice were treated with AMD3100 and BMS754807, which are inhibitors of the receptors for CXCL12 and IGF-1 (CXCR4 and IGF1R), respectively.[31] These findings suggest that MSC-derived CAFs may have a crucial role in the initiation step of bone metastasis.

Adipocytes

Metabolic dysfunctions associated with obesity and aging are often recognized as risk factors for cancer progression. The marrows of these patients contain large numbers of adipocytes. Adipocytes are known to be involved in tumor progression and metastasis,[32,33] which may be partly owing to their negative effects on hematopoiesis;[13] however, little is known regarding the specific roles that these cells have in the metastatic process. A recent study demonstrated that marrow adipocytes support bone metastasis of prostate cancer,[34] as more PC3 cells, a prostate cancer cell line, grew in the bone marrow of animals receiving a high-fat diet than in that of animals on a regular diet.[34] Conditioned medium (CM) from adipocyte lineage cultures were obtained from differentiated mouse bone marrow stromal cells and found to increase gene expression of fatty acid binding protein 4 (FABP4), interleukin (IL)-1β and heme oxygenase (decycling) 1 (HMOX-1) in PC3 cells *in vitro*; however, this could be stopped by PPAR γ inhibitors.[34] In addition, this CM enhanced the proliferation and invasion of PC3 cells *in vitro*, whereas inhibitors of FABP4 and IL-1β prevented invasion.[34] Interestingly, in an *in vivo* study, the increase of *FABP4*, *IL-1β* and *HMOX-1* genes was observed in tumors within the marrow, but not in tumors grown subcutaneously.[34] Consistent with this, high levels of FABP4 expression are observed in human bone metastatic tumors near adipocytes.[34] Of added interest, aside from metabolic dysfunction, daily dietary intake may also alter the effects of adipocytes on metastatic niche development. Arachidonic acid, a polyunsaturated omega-6 fatty acid, stimulates adipogenesis of human primary bone marrow stromal cells.[35] When PC3 cells are cocultured with adipocytes, the uptake of arachidonic acid by PC3 cells is increased.[35] Simultaneously, arachidonic acid induces the migration of PC3 cells toward adipocytes, suggesting that high levels of arachidonic acid intake may facilitate prostate cancer bone metastasis.[35]

Osteoblasts

Although the unique cell types of the HSC niche in the marrow remain controversial,[18,19] osteoblasts have been well studied as the 'niche' for HSCs,[6–8,17] and our recent studies using animal xenograft models have revealed that bone metastatic prostate cancer cells target this same niche during dissemination.[36] When prostate cancer cell lines (PC3 and C4-2B) reach the bone marrow, they prevent the engraftment of transplanted HSCs, suggesting that disseminated prostate cancer cells compete with HSCs for occupancy of the HSC niche.[36] This observation is confirmed when the niche sizes are manipulated: more dissemination is observed in animals that have more niches, and vice versa.[36] In addition, more tumor cells disseminate into the niche when this niche is vacated by stem cell mobilizing drugs (for example, granulocyte-colony stimulating factor (G-CSF) or CXCR4 inhibitor AMD3100).[36] As a result of this competition for the niche, disseminated prostate cancer cells displace HSCs from the marrow and induce the differentiation of HSCs into hematopoietic progenitor cells (HPCs).[36] Correspondingly, more HPCs are found in peripheral blood obtained from prostate cancer patients with bone

metastases compared with healthy controls or patients with local prostate cancer.[36]

Once DTCs establish residency in the niche, they frequently become dormant, probably in part through cell-to-cell contact with the niche. For example, when osteoblasts are cocultured with prostate cancer cell line, PC3 cells, the secretion of growth arrest-specific 6 (GAS6) by the osteoblasts is significantly enhanced.[37] Interestingly, GAS6 inhibits the proliferation of PC3 cells, while preventing apoptosis.[37] In addition, when PC3 cells are inoculated into murine skeletal tissues, the expression of Axl, one of three receptors (Axl, Tyro3, Mer) for GAS6, is markedly increased.[37] Along with this notion, in mice inoculated with prostate cancer cells, tumor growth is mainly observed in bones expressing low levels of GAS6 (forelimb), whereas tumors rarely grow in bones expressing abundant GAS6 (hindlimb).[38] Moreover, PC3 and DU145 cells, which are proliferating in the bones, express relatively low levels of Axl, compared with when they are in a dormant state.[39] These findings suggest that the osteoblastic niche controls dormancy of disseminated prostate cancer through a GAS6/Axl axis.

Hematopoietic Stem Cells

In the marrow, HSCs reside in their niche to maintain their phenotype; however, HSCs are not only influenced by the niche, but they are also active in the actual development of the niche.[40] Similarly, DTCs are involved in the development of a malignant niche, indirectly using HSCs. When HPCs, but not HSCs, obtained from the bone marrow of mice inoculated with osteoblastic prostate cancer cell line C4-2B cells are cocultured with murine bone marrow stromal cells, the osteoblastic differentiation of the bone marrow stromal cells is stimulated.[41] These HPCs express high levels of bone morphogenetic proteins (BMP)-2 and -6, and the osteoblastogenesis induced by C4-2B-bearing HPCs is inhibited by pan BMP inhibitor Noggin.[41] In contrast, HSCs isolated from the marrow of mice inoculated with osteolytic prostate cancer cell line PC3 express high levels of IL-6, and they differentiate into osteoclasts under the induction of macrophage colony-stimulating factor (M-CSF) and receptor activator of nuclear factor kappa-B ligand (RANKL).[41] This osteoclastogenesis is prevented by anti-IL-6 antibody treatment.[41] These findings suggest that targeting HSCs or HPCs may be a potential therapy for bone metastatic disease.

Osteoclasts

Bone resorption, one of the key features of bone metastasis, is mediated by DTCs inducing the formation and activation of osteoclasts.[42] Therefore, targeting osteoclastogenesis with bisphosphonates[43] or the RANKL inhibitor denosumab[44] is a treatment strategy used in bone metastatic disease. Human breast cancer coexpresses high levels of metalloproteinase (MMP)-13 and its activator MT1-MMP in bone metastatic lesions.[45] The bone metastatic breast cancer cell line MDA-MB-231 expresses higher levels of MMP-13 than the less aggressive cell line MCF-7, and the MMP-13 expression in MDA-MB-231 cells is enhanced by IL-8 and parathyroid hormone-related protein (PTHrP) treatments.[45] CM obtained from IL-8- or PTHrP-treated MDA-MB-231 cells increases tartrate-resistant acid phosphatase (TRAP)-positive osteoclastic differentiation and the bone resorptive ability of human preosteoclasts. Yet this osteoclastogenesis is inhibited by the pan-MMP inhibitor GM6001, and partially by the MMP-13-specific inhibitor CL-82197 or MMP-13 knockdown in cancer cells using shRNA.[45] MMP-13-induced osteoclastogenesis may be explained in part by the activation of pro-MMP-9 and cleavage of an osteoclastogenesis suppressor galectin-3.[45] When shMMP-13 MDA-MB-231 cells are implanted into the bones of mice, bone resorption and osteoclastogenesis are reduced when compared with control, although there are no significant differences in tumor size.[45] When murine breast cancer cell line Cl66 cells are implanted into the subcutaneous spaces of mice near the calvarial bone, MMP-13, MMP-9, transforming growth factor (TGF)-β and phosphorylated Smad2 are expressed greater in the area where tumor interfaces with bone (TB interface), compared with areas of tumor alone.[46] It is in this TB interface where larger numbers of osteoclasts and bone resorption areas are found.[46] In addition, osteoclast number, osteolytic lesion frequency and MMP-13 expression at the TB interface are all significantly reduced when mice are treated with MMP-13 antisense oligonucleotides.[46] Furthermore, MMP-13 antisense oligonucleotide treatments also impair the expression of MMP-9, TGF-β and phosphorylated Smad2 in the TB interface.[46] Increased expression of placental growth factor (PIGF) is observed when MDA-MB-231 cells reach the marrow, and PIGF induces migration of MDA-MB-231 cells via the ERK pathway.[47] Anti-murine PIGF antibody 5D11D4 treatments prevent metastasis to bone and bone resorption in mice inoculated with either MDA-MB-231 cells or murine melanoma cell line B16/F10 cells.[47] 5D11D4 treatment inhibits osteoclastogenesis by reducing RANKL expression in murine bone marrow cells without affecting angiogenesis.[47] Heptapeptide hormone angiotensin-(1–7) (Ang-(1–7)) decreases the secretion of vascular endothelial growth factor (VEGF) and PIGF from PC3 and DU145 prostate cancer cells, and it prevents cancer cell proliferation and migration, inhibiting bone metastasis and osteoclastogenesis.[48]

Although some recent studies caution against the paradigm of a purely hypoxic niche,[10,19] bone marrow has long been thought to be a hypoxic environment. When treated with TGF-β under hypoxic conditions, the breast cancer cell line MDA-MB-231 increases the expression of angiogenesis factor VEGF and homing receptor CXCR4 through hypoxia-inducible factor (HIF)-1α.[49] This effect may be via the cyclooxygenase-2 (COX-2) signaling pathway, as bone metastatic clone 1833 MDA-MB-231 cells enhance COX-2 expression under hypoxia and TGF-β treatment.[50] When the TGF-β pathway and HIF-1α are knocked down in MDA-MB-231 cells, tumor growth and osteolytic lesions in tumor-inoculated mice are diminished.[49] Moreover, when parental MDA-MB-231 cell-bearing mice are treated with HIF-1α inhibitor 2ME2 and/or TGF-β type I kinase inhibitor SD-208, which is also known to inhibit melanoma bone metastasis,[51] 2ME2 and SD-208 synergistically prevent bone metastasis and inhibit osteoclastogoenesis, all while enhancing osteoblastogenesis.[49] Furthermore, TGF-β-induced factor 2 (Tgif2) induces osteoclastogenesis owing to the down-regulation of microRNA miR-34a expression in osteoclasts.[52] Consequently, when mice were treated with miR-34a-carrying chitosan nanoparticles, the blockage of osteoclastgenesis prevented bone metastasis of human breast cancer cell line MDA231-BoM-1833 and B16/F10, whereas more metastases of these cell lines were observed in bones of miR-34a–knouckout (KO) mice.[52] These findings suggest that the bone

resorption mediated by the interaction between DTCs and osteoclasts is a key step for establishing bone metastasis.

Macrophages

Macrophages are hematopoietic cells that are well known to be involved in tumor progression and metastasis through the expression of inflammatory cytokines and proteases, especially in primary tumor sites.[53] These macrophages are referred to as tumor-associated macrophages (TAMs). Two types of macrophages are known to exist: M1 tumor-inhibiting macrophages and M2 tumor-initiating macrophages (known as TAMs). Macrophages are frequently found in the marrow, where they help establish a favorable tumor microenvironment. For example, the cysteine protease cathepsin K (CTSK) is one of the proteases that osteoclasts and macrophages secrete in the marrow. When PC3 cells are implanted directly into the bone marrow of CTSK-KO mice, less growth is observed compared with wild-type mice.[54] However, there are no significant differences in the growth of subcutaneously implanted tumors between CTSK-KO and wild-type mice.[54] Compared with wild type, CTSK-KO mice have fewer, less invasive macrophages and more osteoclasts, but functionally less bone resorption.[54] When normal macrophages directly interact with tumor cells, expression of inflammatory factors COX-2 and CCL2 is increased. However, macrophages from CTSK-KO mice decrease the expression of COX-2 (a 22-fold decrease) and CCL2 (a 17-fold decrease).[54] Therefore, it appears that marrow macrophages positively control tumor progression through the CTSK/COX-2/CCL2 pathway.

Marrow macrophages may promote metastatic growth by suppressing tumor-induced inflammation. When mouse bone marrow macrophages ($F4/80^+$) are cocultured with apoptotic mouse prostate cancer RM-1 cells, macrophages show more phagocytosis of apoptotic tumor cells (specifically termed efferocytosis) than nonapoptotic tumor cells, through the STAT3/SOCS3 pathway, by increasing the expression of a phagocytosis promoter, milk fat globule-EGF factor 8 (MFG-E8).[55] Consistent with this, high levels of MFG-E8 were found colocalized with macrophages in human prostate TMA samples.[55] In addition, these macrophages enhance the secretion of M2 macrophage-related proteins, IL-6, CCL2 and CCL1, and increase the expression of M2 macrophage-related genes, *IL-10*, *TGF-b1*, *Ym-1* and *arginase 1*, suggesting that MFG-E8-mediated efferocytosis promotes M2 polarization of macrophages.[55]

In contrast, myeloid-derived suppressor cells (MDSCs), which are progenitors of macrophages and osteoclasts, can induce tumor growth by differentiating into osteoclasts. MDSCs ($CD11b^+Gr\text{-}1^+$) obtained from the bone marrow of mice with murine breast cancer cell line 4T1 bone metastases ($MDSCs^{+bone\ mets}$) differentiate into TRAP-positive, bone resorptive osteoclasts *in vitro* and express CTSK, carbonic anhydrase-2, MMP-9 and NO.[56] However, MDSCs from the bone marrow of mice without bone metastases, regardless of other metastatic sites (lung, lymph node, spleen or blood), do not differentiate into osteoclasts, suggesting that the osteoclast differentiation of MDSCs is unique to the bone metastatic environment.[56] In addition, when $MDSCs^{+bone\ mets}$ are transplanted, osteoclast differentiation of $MDSCs^{+bone\ mets}$ and bone distraction are observed in recipient mice.[56] Interestingly, both *in vitro* and *in vivo* osteoclastogenesis mediated by $MDSCs^{+bone\ mets}$ are inhibited by blocking NO.[56] The high NO production in $MDSCs^{+bone\ mets}$ enhances HIF-1α expression through the PIK3 or ERK pathway.[56]

Lymphoid Cells

Bone marrow is also a lymphoid organ. There are many subclasses of T cells, some of which home to the marrow and support tumor progression. For example, an increased number of $CD4^+Foxp3^+$ regulatory T (Treg) cells can be found in the bone marrow of prostate cancer patients with bone metastases compared with prostate cancer patients with local disease or healthy controls.[57] Treg cells express high levels of homing receptor CXCR4, and treatment with an anti-CXCR4 antibody inhibits the migration of Treg cells to CXCL12-expressing bone marrow fluid obtained from prostate cancer patients with bone metastases, suggesting that Treg cells home to bone marrow through the CXCR4/CXCL12 axis.[57] These Treg cells can interfere with the immune response by preventing T-cell proliferation, decreasing the expression of interferon (IFN)-γ and IL-2 production and by suppressing osteoclastogenesis through activation by $RANK^+$ dendritic cells.[57] When Treg cells are co-inoculated with murine prostate cancer cells (RM1) into mice, less osteolytic metastases are observed owing to T-cell-mediated suppression of osteoclastogenesis.[57] In contrast, when Treg cells are depleted from these tumor-bearing animals, bone densities in the animals are reduced.[57] This suggests that Treg cells act within the metastatic niche in an immunosuppressive manner.

Similarly, when murine melanoma cell line B16 is injected into PLCγ2-KO mice, which have reduced myeloid cell function and numbers of osteoclasts, the bone tumor burden is significantly increased compared with wild-type mice.[58] When B16 cells are inoculated into wild-type mice transplanted with bone marrow cells from PLCγ2-KO mice, similar tumor growth is observed, further implicating myeloid cells with tumor growth in the bone.[58] In contrast, when the experiments are repeated using Lyn-KO mice in which the number of osteoclasts and myeloid cell function are enhanced, the growth of B16 cells in the bone is inhibited.[58] Interestingly, tumor growth in the marrow is impaired when the function of $CD8^+$ T cells is enhanced in tumor-bearing mice, whereas inoculated tumor grows in the marrow when $CD8^+$ T cells are diminished.[58] In addition, the inhibitive effects of zoledronic acid (ZA) on tumor growth are prevented in the $CD8^+$ T cell–deficient condition.[58] Importantly, when $CD8^+$ T cells are supplemented into PLCγ2-KO mice or when $CD8^+$ T cells are depleted from Lyn-KO mice, tumor growth in bone is normalized.[58] These findings suggest that $CD8^+$ T cells have important roles in tumor growth in the marrow independent of osteoclast condition.

When mice are inoculated with metastatic murine breast cancer cell line 4T1, more systemic bone loss is observed compared with mice inoculated with non-metastatic cell line 67NR.[59] Accordingly, more pro-osteoclastic cytokines (IL-1β, IL-6, IL-17F, RANKL, tumor necrosis factor (TNF)-α) but less osteoprotegerin (OPG), a decoy receptor for RANKL, are found in the serum obtained from 4T1-bearing animals.[59] Interestingly, production of these cytokines parallels what is seen during tumor dissemination. When $CD3^+$ T cells are isolated from 4T1- or 67NR-bearing mice and transplanted into nude mice, bone loss is observed only in recipients of T cells derived from 4T1-bearing donors, and this is reversed by inhibiting RANKL in

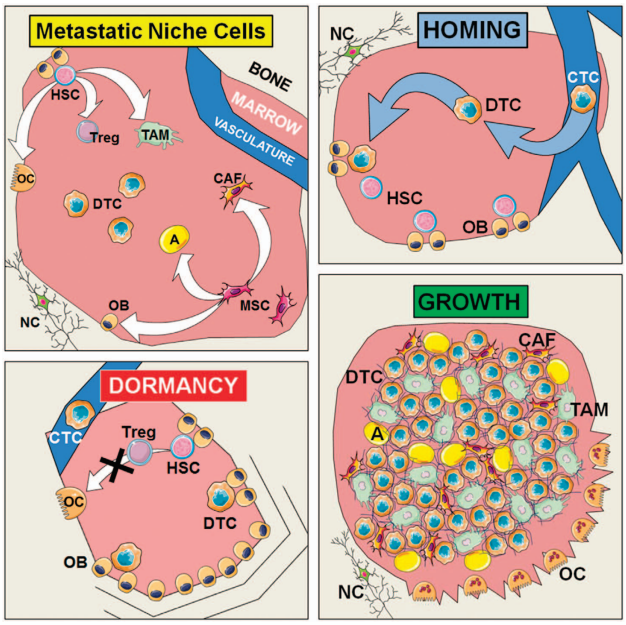

Figure 1 Development of the 'metastatic niche' by the interaction of disseminated tumor cells with the bone marrow microenvironment. Growing evidence supports the idea that tumor cell behavior is dependent on the surrounding microenvironment. This suggests that the microenvironment in distant tissues, such as bone, is essential for disseminated tumor cell (DTC) survival and metastatic growth. However, DTCs are not passive in the marrow—they also put pressure on their surroundings to create a more advantageous microenvironment (metastatic niche). Top left: bone marrow contains many cell types that directly influence one another and DTC fate. Hematopoietic stem cells (HSCs) can differentiate into macrophages, osteoclasts (OCs), T cells and other lymphocytes, whereas mesenchymal stem cells (MSCs) differentiate into adipocytes (A), osteoblasts (OB) and fibroblasts (white arrows). All of these cell types make up the deadly 'metastatic niche.' Top right: once in the marrow, DTCs home to where HSCs and OBs reside, or the 'HSC niche' (blue arrows). Bottom left: DTCs are kept dormant in the HSC niche through OB bone formation and regulatory T-cell (Treg) inhibition of osteoclastogenesis. In addition, endothelial cells that line the vasculature also help regulate circulating tumor cell (CTC) and DTC dormancy. Bottom right: DTCs can be allowed to grow with help from MSC-derived cancer associated fibroblasts (CAFs) and HSC-derived tumor-associated macrophages (TAMs), adipocytes and OC bone resorption. Nerve cells (NCs) also participate in the progression of DTCs.

the T cells before transplantation, but not with inhibition of IL-17F.[59] When 4T1 cells are implanted into control or RANKL-knockdown T-cell-transplanted mice, 95% of lymph node metastases and 100% of bone metastases are eliminated in the RANKL-knockdown T-cell-transplanted mice.[59] These findings suggest that bone metastatic cancer recruits T cells to the marrow to facilitate future bone metastasis by regulating osteoclastogenesis.

Endothelial Cells

During dissemination, cancer cells have constant contact with endothelial cells or pericytes, as DTCs must intravasate into and extravasate out of the blood stream to reach the secondary site. When the orthotopic injection of highly metastatic breast cancer cell line MDA-MB-231 cells or intracardiac injection of weakly metastatic line T4-2 cells into mice was performed, Ki67-negative dormant cells were observed near the thrombospondin-1 (TSP-1)-expressing perivascular niche in the lung and bone marrow.[4] Furthermore, a dormant population is maintained when cancer cells are cocultured with the mixture of MSCs and primary human umbilical vein endothelial cells (HUVECs), whereas coculture with MSCs alone does not.[4] The dormancy supportive effects of endothelial cells are canceled with an anti-TSP-1 antibody.[4] *In vivo* mouse and zebrafish models revealed that sprouting neovascular tips facilitate tumor growth, whereas dormant cancer cells are associated with the stable microvasculature, and *in vitro* culture studies demonstrated that this might be owing to the the high levels of TGF-β1 and periostin (POSTN) expressed by the sprouting endothelial tip cells.[4] These findings suggest that endothelial cells or pericytes serve as a potential metastatic niche that regulates tumor dormancy.

Nerve cells

It is accepted that the nervous system is also involved in tumor progression and metastasis. When PC3 cells are orthotopically implanted into immunocompromised mice, the development of nerves within the primary tumor is observed.[60] Chemical (6-hydroxydopamine, 6OHDA) or surgical denervation prevents development of the primary tumor and metastasis.[60] Moreover, when β_2- and β_3-adrenergic receptors are knocked down in mice, both primary tumor development and dissemination of PC3 and LNCaP cells are significantly impaired.[60] When sympathetic nerve ablation is initiated at a young age, tumor progression is inhibited in a spontaneous model of prostate cancer in which c-Myc is highly expressed in the prostate.[60] Interestingly, when cholinergic receptor muscarinic 1 (Chrm1) is chemically upregulated with carbamoylcholine chloride (carbachol), tumor dissemination to lymph node and bone is increased in both xenograft and spontaneous prostate cancer models, whereas if Chrm1 is blocked by a nonselective muscarinic antagonist, scopolamine, or is genetically ablated, tumor dissemination is inhibited, resulting in longer survival.[60] More importantly, the density of nerve fibers in the primary tumor is correlated with the clinical progression of human prostate cancer.[60]

Conclusions

Once cancer cells spread to distant organs such as bone, survival rates of cancer patients drastically decline. Each year, many patients who had been predicted to be cured of their cancer by surgery or radiation therapy present with incurable metastatic disease manifested as metastatic lesions in the bone, often years after primary treatment. DTCs derived from epithelial cancers, including prostate, breast, glioma and gastrointestinal cancer, have been detected in the bone marrow.[61–64] The presence of bone marrow DTCs has been correlated with a poor prognosis,[65] as DTCs frequently lead to lethal bone metastases.[66] This progression may also be environmentally influenced by pressures from the bone marrow microenvironment, or the 'metastatic niche'. Although the mechanisms are yet to be defined, it is generally believed that DTCs can become overt and clinically relevant metastases[63] that lead to disease recurrence even after treatment.[67] Therefore, new approaches to treat bone metastasis are urgently needed. For example, HSC mobilizing drug (for example, G-CSF and AMD3100) can be used to mobilize the niche-engaged dormant DTCs to re-enter the cell cycle.[68] Indeed, AMD3100 enhances the susceptibility to chemotherapy of acute myeloid leukemia[69] and multiple myeloma.[70] Recent clinical trials of adjuvant ZA have revealed that, when

DTCs only exist in the bone marrow of breast cancer patients, ZA improved disease-free survival and overall survival, suggesting that ZA interferes with the interaction of DTCs and the niche.[71,72] A recent study using xenograft breast cancer mouse models demonstrated that the hormonal status of the bone marrow microenvironment also influences tumor progression and ZA treatment effects on bone metastatic disease.[73] DTCs in mice given ovariectomies (OVX) grew better than those in sham-surgery-treated mice.[73] Moreover, ZA prevented OVX-induced tumor growth in the marrow, reflecting that antiresorptive therapy may be beneficial for postmenopausal breast cancer patients.[73] In contrast, ZA did not affect tumor growth in the marrow of sham-operated mice, suggesting that adjuvant ZA alone may not be a sufficient treatment in the premenopausal breast cancer setting.[73] Although further studies are clearly warranted, targeting the metastatic niche may be a promising treatment strategy for bone metastatic disease.

The concept that DTCs parasitize the harsh bone marrow microenvironment to grow and survive (**Figure 1**) is better understood, yet it remains an active area of investigation where some critical questions remain unanswered:

1. Do DTCs really parasitize the HSC niche?
2. Is the metastatic niche in the marrow the same as the HSC niche?
3. Can targeting the HSC niche serve as a potential therapy for bone metastatic disease?
4. Is it realistic to target a single cell type of the metastatic niche, especially in the marrow?
5. Do all cell types of the marrow interact to form the metastatic niche to support DTC survival? If so, how?
6. Does the metastatic niche control the chemoresistance of DTCs in the marrow?
7. How does the marrow metastatic niche influence tumor dormancy and recurrence?
8. Do the metabolic states of the metastatic niche affect the growth of DTCs?

To answer these questions, we must continue to place importance on the efforts to advance our understanding and technological capabilities, while developing a system or database to share new ideas and information with other experts in this field worldwide. Further multi-institutional research collaborations are absolutely paramount.

'Why does cancer recur even after a long disease-free interval?' This is a crucial question to answer if our goal is to cure cancer. DTCs shed from a primary tumor may lie dormant in distant tissues for long periods of time, all while retaining the potential to explode into metastatic growth with help from the bone marrow microenvironment. Therefore, it is vital to understand the interactions between DTCs and the bone marrow 'metastatic niche.' This review focuses on the fundamental mechanisms behind the provocative concept that the bone marrow microenvironment has a supportive role in bone metastasis. Observations discussed here are relevant to a more complete understanding of how this microenvironment functions in establishing DTCs, and what circumstances lead to dormancy and reactivation of DTCs in the marrow. Ultimately, it should be possible to develop targeted therapy for eradication of currently incurable bone metastatic disease by developing a deeper understanding of the cancer/niche interaction.

Conflict of Interest

The authors declare no conflict of interest.

Acknowledgements

This work is directly supported by the National Cancer Institute (CA093900 to R.S. Taichman, and CA163124 to Y. Shiozawa and R.S. Taichman), the Department of Defense (W81XWH-11-1-0636 to R.S. Taichman, and W81XWH-14-1-0403 to Y. Shiozawa and R.S. Taichman) and the Prostate Cancer Foundation (Y. Shiozawa and R.S. Taichman). Graphics adapted from Servier Medical Art (www.servier.com).

References

1. Ewing J. *A Treatise on Tumors*. 3rd edn (W.B. Saunders: Philadelphia and London, 1928.
2. Paget S. The distribution of secondary growth in cancer of the breast. *Lancet* 1889; **1**: 571–573.
3. Sosa MS, Bragado P, Aguirre-Ghiso JA. Mechanisms of disseminated cancer cell dormancy: an awakening field. *Nat Rev Cancer* 2014; **14**: 611–622.
4. Ghajar CM, Peinado H, Mori H, Matei IR, Evason KJ, Brazier H *et al.* The perivascular niche regulates breast tumour dormancy. *Nat Cell Biol* 2013; **15**: 807–817.
5. Sleeman JP. The metastatic niche and stromal progression. *Cancer Metastasis Rev* 2012; **31**: 429–440.
6. Calvi LM, Adams GB, Weibrecht KW, Weber JM, Olson DP, Knight MC *et al.* Osteoblastic cells regulate the haematopoietic stem cell niche. *Nature* 2003; **425**: 841–846.
7. Zhang J, Niu C, Ye L, Huang H, He X, Tong WG *et al.* Identification of the haematopoietic stem cell niche and control of the niche size. *Nature* 2003; **425**: 836–841.
8. Arai F, Hirao A, Ohmura M, Sato H, Matsuoka S, Takubo K *et al.* Tie2/angiopoietin-1 signaling regulates hematopoietic stem cell quiescence in the bone marrow niche. *Cell* 2004; **118**: 149–161.
9. Kiel MJ, Yilmaz OH, Iwashita T, Yilmaz OH, Terhorst C, Morrison SJ. SLAM family receptors distinguish hematopoietic stem and progenitor cells and reveal endothelial niches for stem cells. *Cell* 2005; **121**: 1109–1121.
10. Nombela-Arrieta C, Pivarnik G, Winkel B, Canty KJ, Harley B, Mahoney JE *et al.* Quantitative imaging of haematopoietic stem and progenitor cell localization and hypoxic status in the bone marrow microenvironment. *Nat Cell Biol* 2013; **15**: 533–543.
11. Katayama Y, Battista M, Kao WM, Hidalgo A, Peired AJ, Thomas SA *et al.* Signals from the sympathetic nervous system regulate hematopoietic stem cell egress from bone marrow. *Cell* 2006; **124**: 407–421.
12. Mendez-Ferrer S, Lucas D, Battista M, Frenette PS. Haematopoietic stem cell release is regulated by circadian oscillations. *Nature* 2008; **452**: 442–447.
13. Naveiras O, Nardi V, Wenzel PL, Hauschka PV, Fahey F, Daley GQ. Bone-marrow adipocytes as negative regulators of the haematopoietic microenvironment. *Nature* 2009; **460**: 259–263.
14. Sugiyama T, Kohara H, Noda M, Nagasawa T. Maintenance of the hematopoietic stem cell pool by CXCL12-CXCR4 chemokine signaling in bone marrow stromal cell niches. *Immunity* 2006; **25**: 977–988.
15. Mendez-Ferrer S, Michurina TV, Ferraro F, Mazloom AR, Macarthur BD, Lira SA *et al.* Mesenchymal and haematopoietic stem cells form a unique bone marrow niche. *Nature* 2010; **466**: 829–834.
16. Pinho S, Lacombe J, Hanoun M, Mizoguchi T, Bruns I, Kunisaki Y *et al.* PDGFRalpha and CD51 mark human nestin + sphere-forming mesenchymal stem cells capable of hematopoietic progenitor cell expansion. *J Exp Med* 2013; **210**: 1351–1367.
17. Shiozawa Y, Taichman RS. Getting blood from bone: an emerging understanding of the role that osteoblasts play in regulating hematopoietic stem cells within their niche. *Exp Hematol* 2012; **40**: 685–694.
18. Morrison SJ, Scadden DT. The bone marrow niche for haematopoietic stem cells. *Nature* 2014; **505**: 327–334.
19. Ugarte F, Forsberg EC. Haematopoietic stem cell niches: new insights inspire new questions. *EMBO J* 2013; **32**: 2535–2547.
20. Shiozawa Y, Havens AM, Pienta KJ, Taichman RS. The bone marrow niche: habitat to hematopoietic and mesenchymal stem cells, and unwitting host to molecular parasites. *Leukemia* 2008; **22**: 941–950.
21. Taichman RS, Cooper C, Keller ET, Pienta KJ, Taichman NS, McCauley LK. Use of the stromal cell-derived factor-1/CXCR4 pathway in prostate cancer metastasis to bone. *Cancer Res* 2002; **62**: 1832–1837.
22. Muller A, Homey B, Soto H, Ge N, Catron D, Buchanan ME *et al.* Involvement of chemokine receptors in breast cancer metastasis. *Nature* 2001; **410**: 50–56.
23. Schepers K, Pietras EM, Reynaud D, Flach J, Binnewies M, Garg T *et al.* Myeloproliferative neoplasia remodels the endosteal bone marrow niche into a self-reinforcing leukemic niche. *Cell Stem Cell* 2013; **13**: 285–299.
24. Knerr K, Ackermann K, Neidhart T, Pyerin W. Bone metastasis: Osteoblasts affect growth and adhesion regulons in prostate tumor cells and provoke osteomimicry. *Int J Cancer* 2004; **111**: 152–159.

25. Huang WC, Xie Z, Konaka H, Sodek J, Zhau HE, Chung LW. Human osteocalcin and bone sialoprotein mediating osteomimicry of prostate cancer cells: role of cAMP-dependent protein kinase A signaling pathway. *Cancer Res* 2005; **65**: 2303–2313.
26. Cox RF, Jenkinson A, Pohl K, O'Brien FJ, Morgan MP. Osteomimicry of mammary adenocarcinoma cells in vitro; increased expression of bone matrix proteins and proliferation within a 3D collagen environment. *PLoS ONE* 2012; **7**: e41679.
27. Zhau HE, He H, Wang CY, Zayzafoon M, Morrissey C, Vessella RL *et al.* Human prostate cancer harbors the stem cell properties of bone marrow mesenchymal stem cells. *Clin Cancer Res* 2011; **17**: 2159–2169.
28. Ono M, Kosaka N, Tominaga N, Yoshioka Y, Takeshita F, Takahashi RU *et al.* Exosomes from bone marrow mesenchymal stem cells contain a microRNA that promotes dormancy in metastatic breast cancer cells. *Sci Signaling* 2014; **7**: ra63.
29. Karnoub AE, Dash AB, Vo AP, Sullivan A, Brooks MW, Bell GW *et al.* Mesenchymal stem cells within tumour stroma promote breast cancer metastasis. *Nature* 2007; **449**: 557–563.
30. Jung Y, Kim JK, Shiozawa Y, Wang J, Mishra A, Joseph J *et al.* Recruitment of mesenchymal stem cells into prostate tumours promotes metastasis. *Nat Commun* 2013; **4**: 1795.
31. Zhang XH, Jin X, Malladi S, Zou Y, Wen YH, Brogi E *et al.* Selection of bone metastasis seeds by mesenchymal signals in the primary tumor stroma. *Cell* 2013; **154**: 1060–1073.
32. Nieman KM, Kenny HA, Penicka CV, Ladanyi A, Buell-Gutbrod R, Zillhardt MR *et al.* Adipocytes promote ovarian cancer metastasis and provide energy for rapid tumor growth. *Nat Med* 2011; **17**: 1498–1503.
33. Park J, Scherer PE. Adipocyte-derived endotrophin promotes malignant tumor progression. *J Clin Invest* 2012; **122**: 4243–4256.
34. Herroon MK, Rajagurubandara E, Hardaway AL, Powell K, Turchick A, Feldmann D *et al.* Bone marrow adipocytes promote tumor growth in bone via FABP4-dependent mechanisms. *Oncotarget* 2013; **4**: 2108–2123.
35. Brown MD, Hart C, Gazi E, Gardner P, Lockyer N, Clarke N. Influence of omega-6 PUFA arachidonic acid and bone marrow adipocytes on metastatic spread from prostate cancer. *Br J Cancer* 2010; **102**: 403–413.
36. Shiozawa Y, Pedersen EA, Havens AM, Jung Y, Mishra A, Joseph J *et al.* Human prostate cancer metastases target the hematopoietic stem cell niche to establish footholds in mouse bone marrow. *J Clin Invest* 2011; **121**: 1298–1312.
37. Shiozawa Y, Pedersen EA, Patel LR, Ziegler AM, Havens AM, Jung Y *et al.* GAS6/AXL axis regulates prostate cancer invasion, proliferation, and survival in the bone marrow niche. *Neoplasia* 2010; **12**: 116–127.
38. Jung Y, Shiozawa Y, Wang J, McGregor N, Dai J, Park SI *et al.* Prevalence of prostate cancer metastases after intravenous inoculation provides clues into the molecular basis of dormancy in the bone marrow microenvironment. *Neoplasia* 2012; **14**: 429–439.
39. Taichman RS, Patel LR, Bedenis R, Wang J, Weidner S, Schumann T *et al.* GAS6 receptor status is associated with dormancy and bone metastatic tumor formation. *PLoS ONE* 2013; **8**: e61873.
40. Jung Y, Song J, Shiozawa Y, Wang J, Wang Z, Williams B *et al.* Hematopoietic stem cells regulate mesenchymal stromal cell induction into osteoblasts thereby participating in the formation of the stem cell niche. *Stem Cell* 2008; **26**: 2042–2051.
41. Joseph J, Shiozawa Y, Jung Y, Kim JK, Pedersen E, Mishra A *et al.* Disseminated prostate cancer cells can instruct hematopoietic stem and progenitor cells to regulate bone phenotype. *Mol Cancer Res* 2012; **10**: 282–292.
42. Roodman GD. Biology of osteoclast activation in cancer. *J Clin Oncol* 2001; **19**: 3562–3571.
43. Michaelson MD, Smith MR. Bisphosphonates for treatment and prevention of bone metastases. *J Clin Oncol* 2005; **23**: 8219–8224.
44. Ford JA, Jones R, Elders A, Mulatero C, Royle P, Sharma P *et al.* Denosumab for treatment of bone metastases secondary to solid tumours: systematic review and network meta-analysis. *Eur J Cancer* 2013; **49**: 416–430.
45. Pivetta E, Scapolan M, Pecolo M, Wassermann B, Abu-Rumeileh I, Balestreri L *et al.* MMP-13 stimulates osteoclast differentiation and activation in tumour breast bone metastases. *Breast Cancer Res* 2011; **13**: R105.
46. Nannuru KC, Futakuchi M, Varney ML, Vincent TM, Marcusson EG, Singh RK. Matrix metalloproteinase (MMP)-13 regulates mammary tumor-induced osteolysis by activating MMP9 and transforming growth factor-beta signaling at the tumor-bone interface. *Cancer Res* 2010; **70**: 3494–3504.
47. Coenegrachts L, Maes C, Torrekens S, Van Looveren R, Mazzone M, Guise TA *et al.* Anti-placental growth factor reduces bone metastasis by blocking tumor cell engraftment and osteoclast differentiation. *Cancer Res* 2010; **70**: 6537–6547.
48. Krishnan B, Smith TL, Dubey P, Zapadka ME, Torti FM, Willingham MC *et al.* Angiotensin-(1-7) attenuates metastatic prostate cancer and reduces osteoclastogenesis. *Prostate* 2013; **73**: 71–82.
49. Dunn LK, Mohammad KS, Fournier PG, McKenna CR, Davis HW, Niewolna M *et al.* Hypoxia and TGF-beta drive breast cancer bone metastases through parallel signaling pathways in tumor cells and the bone microenvironment. *PLoS ONE* 2009; **4**: e6896.
50. Maroni P, Matteucci E, Luzzati A, Perrucchini G, Bendinelli P, Desiderio MA. Nuclear co-localization and functional interaction of COX-2 and HIF-1alpha characterize bone metastasis of human breast carcinoma. *Breast Cancer Res Treat* 2011; **129**: 433–450.
51. Mohammad KS, Javelaud D, Fournier PG, Niewolna M, McKenna CR, Peng XH *et al.* TGF-beta-RI kinase inhibitor SD-208 reduces the development and progression of melanoma bone metastases. *Cancer Res* 2011; **71**: 175–184.
52. Krzeszinski JY, Wei W, Huynh H, Jin Z, Wang X, Chang TC *et al.* miR-34a blocks osteoporosis and bone metastasis by inhibiting osteoclastogenesis and Tgif2. *Nature* 2014; **512**: 431–435.
53. Pollard JW. Tumour-educated macrophages promote tumour progression and metastasis. *Nat Rev Cancer* 2004; **4**: 71–78.
54. Herroon MK, Rajagurubandara E, Rudy DL, Chalasani A, Hardaway AL, Podgorski I. Macrophage cathepsin K promotes prostate tumor progression in bone. *Oncogene* 2013; **32**: 1580–1593.
55. Soki FN, Koh AJ, Jones JD, Kim YW, Dai J, Keller ET *et al.* Polarization of prostate cancer-associated macrophages is induced by milk fat globule-EGF factor 8 (MFG-E8)-mediated efferocytosis. *J Biol Chem* 2014; **289**: 24560–24572.
56. Sawant A, Deshane J, Jules J, Lee CM, Harris BA, Feng X *et al.* Myeloid-derived suppressor cells function as novel osteoclast progenitors enhancing bone loss in breast cancer. *Cancer Res* 2013; **73**: 672–682.
57. Zhao E, Wang L, Dai J, Kryczek I, Wei S, Vatan L *et al.* Regulatory T cells in the bone marrow microenvironment in patients with prostate cancer. *Oncoimmunology* 2012; **1**: 152–161.
58. Zhang K, Kim S, Cremasco V, Hirbe AC, Collins L, Piwnica-Worms D *et al.* CD8 + T cells regulate bone tumor burden independent of osteoclast resorption. *Cancer Res* 2011; **71**: 4799–4808.
59. Monteiro AC, Leal AC, Goncalves-Silva T, Mercadante AC, Kestelman F, Chaves SB *et al.* T cells induce pre-metastatic osteolytic disease and help bone metastases establishment in a mouse model of metastatic breast cancer. *PLoS ONE* 2013; **8**: e68171.
60. Magnon C, Hall SJ, Lin J, Xue X, Gerber L, Freedland SJ *et al.* Autonomic nerve development contributes to prostate cancer progression. *Science* 2013; **341**: 1236361.
61. Ellis WJ, Pfitzenmaier J, Colli J, Arfman E, Lange PH, Vessella RL. Detection and isolation of prostate cancer cells from peripheral blood and bone marrow. *Urology* 2003; **61**: 277–281.
62. Morgan TM, Lange PH, Vessella RL. Detection and characterization of circulating and disseminated prostate cancer cells. *Front Biosci* 2007; **12**: 3000–3009.
63. Schmidt-Kittler O, Ragg T, Daskalakis A, Granzow M, Ahr A, Blankenstein TJ *et al.* From latent disseminated cells to overt metastasis: genetic analysis of systemic breast cancer progression. *Proc Natl Acad Sci USA* 2003; **100**: 7737–7742.
64. Klein CA, Blankenstein TJ, Schmidt-Kittler O, Petronio M, Polzer B, Stoecklein NH *et al.* Genetic heterogeneity of single disseminated tumour cells in minimal residual cancer. *Lancet* 2002; **360**: 683–689.
65. Aguirre-Ghiso JA. Models, mechanisms and clinical evidence for cancer dormancy. *Nature Rev Cancer* 2007; **7**: 834–846.
66. Jemal A, Siegel R, Ward E, Hao Y, Xu J, Murray T *et al.* Cancer statistics, 2008. *Cancer J Clin* 2008; **58**: 71–96.
67. Morgan TM, Lange PH, Porter MP, Lin DW, Ellis WJ, Gallaher IS *et al.* Disseminated tumor cells in prostate cancer patients after radical prostatectomy and without evidence of disease predicts biochemical recurrence. *Clin Cancer Res* 2009; **15**: 677–683.
68. Shiozawa Y, Pienta KJ, Taichman RS. Hematopoietic stem cell niche is a potential therapeutic target for bone metastatic tumors. *Clin Cancer Res* 2011; **17**: 5553–5558.
69. Nervi B, Ramirez P, Rettig MP, Uy GL, Holt MS, Ritchey JK *et al.* Chemosensitization of acute myeloid leukemia (AML) following mobilization by the CXCR4 antagonist AMD3100. *Blood* 2009; **113**: 6206–6214.
70. Azab AK, Runnels JM, Pitsillides C, Moreau AS, Azab F, Leleu X *et al.* CXCR4 inhibitor AMD3100 disrupts the interaction of multiple myeloma cells with the bone marrow microenvironment and enhances their sensitivity to therapy. *Blood* 2009; **113**: 4341–4351.
71. Hartkopf AD, Taran FA, Wallwiener M, Hahn M, Becker S, Solomayer EF *et al.* Prognostic relevance of disseminated tumour cells from the bone marrow of early stage breast cancer patients - results from a large single-centre analysis. *Eur J Cancer* 2014; **50**: 2550–2559.
72. Banys M, Solomayer EF, Gebauer G, Janni W, Krawczyk N, Lueck HJ *et al.* Influence of zoledronic acid on disseminated tumor cells in bone marrow and survival: results of a prospective clinical trial. *BMC Cancer* 2013; **13**: 480.
73. Ottewell PD, Wang N, Brown HK, Reeves KJ, Fowles CA, Croucher PI *et al.* Zoledronic acid has differential antitumor activity in the pre- and postmenopausal bone microenvironment in vivo. *Clin Cancer Res* 2014; **20**: 2922–2932.

Citation: BoneKEy Reports **5**, Article number: 777 (2016) | doi:10.1038/bonekey.2016.4

www.nature.com/bonekey

LABORATORY METHODS

Mouse models for studying prostate cancer bone metastasis

Jinlu Dai[1,6], Janine Hensel[2,6], Ning Wang[3,6], Marianna Kruithof-de Julio[4,6] and Yusuke Shiozawa[5]

[1]Department of Urology, University of Michigan, Ann Arbor, MI, USA. [2]Department of Clinical Research, Urology Research Laboratory, University of Bern, Bern, Switzerland. [3]Department of Human Metabolism, The Mellanby Centre for Bone Research, The University of Sheffield, Sheffield, UK. [4]Department of Urology, Leiden University Medical Center, Leiden, The Netherlands. [5]Department of Cancer Biology and Comprehensive Cancer Center, Wake Forest University School of Medicine, Winston-Salem, NC, USA.

Once tumor cells metastasize to the bone, the prognosis for prostate cancer patients is generally very poor. The mechanisms involved in bone metastasis, however, remain elusive, because of lack of relevant animal models. In this manuscript, we describe step-by-step protocols for the xenograft mouse models that are currently used for studying prostate cancer bone metastasis. The different routes of tumor inoculation (intraosseous, intracardiac, intravenous and orthotopic) presented are useful for exploring the biology of bone metastasis.

BoneKEy Reports **5**, Article number: 777 (2016) | doi:10.1038/bonekey.2016.4

Introduction

Prostate cancer is the second leading cause of cancer death in men in the US. Because of the recent improvement of treatment strategies for localized disease, a 5-year overall survival rate of over 90% has been achieved in prostate cancer patients (http://www.cancer.org/cancer/prostatecancer/detailedguide/prostate-cancer-survival-rates). However, once cells spread to specific secondary organs such as bone, the 5-year survival rate of prostate cancer patients significantly decreases to 28% (http://www.cancer.org/cancer/prostatecancer/detailedguide/prostate-cancer-survival-rates). Aside from the poor prognosis, bone metastasis significantly impairs the quality of life of prostate cancer patients, as it is associated with myelophthisis, hypercalcemia, bone pain, fracture and/or nerve compression. Therefore, there is an urgent need to understand the biology of bone metastasis in order to fight against this complex disease and its painful consequences.

Prostate cancer is known as a heterogeneous tumor.[1] For instance, some prostate cancers, when they disseminate to the bone, present both osteolytic and osteoblastic bone lesions, although bone metastasis from prostate cancer is classically classified as osteoblastic. In addition to tumor heterogeneity, bone marrow also contains heterogeneous populations, including hematopoietic lineage cells and cells regulating bone remodeling. The interaction between these bone marrow cells and cancer cells is thought to be important for cancer progression.[2] This heterogeneous and complex organization makes revealing the mysterious bone metastatic properties of prostate cancer much more difficult.

Metastasis involves multiple steps. First, tumor cells induce neovascularization (angiogenesis), acquire an invasive phenotype (epithelial mesenchymal transition), invade surrounding tissues (invasion), move into the circulation through the basal membrane (intravasation), travel throughout the body (circulation), and then adhere to a specific endothelium and disseminate into a secondary organ (extravasation). Once there, these disseminated tumor cells adapt to this new environment (colonization), survive for a long time without growing (dormancy), and eventually regrow (metastatic growth or recurrence). As this extremely complicated metastatic process is impossible to recreate with an *in vitro* or *ex vivo* approach, and experiments with humans are not reasonable, we need to rely on a pre-clinical approach with animal models to study bone metastasis. However, to date, there has been no ideal animal model that allows us to follow all these steps simultaneously.

Recently, *in vivo* xenograft mouse models have been developed that involve intraosseous, intracardiac, intravenous

Correspondence: Dr Y Shiozawa, Department of Cancer Biology and Comprehensive Cancer Center, Wake Forest University School of Medicine, 1 Medical Center Blvd, Winston-Salem, NC 27157-1082, USA.
E-mail: yshiozaw@wakehealth.edu
[6]These authors contributed equally to this work.

Received 5 October 2015; accepted 19 December 2015; published online 17 February 2016

and orthotopic injections, which provide a means to better study prostate cancer bone metastasis. In this manuscript, we will provide details of the methods used in these animal models.

Xenograft mouse models for studying prostate cancer bone metastasis

Murine xenograft models are commonly used for experimental bone metastasis. Tumor growth in marrow is achieved through injection of human cancer cell lines via different routes.

Preparation before prostate cancer cell inoculation

Preparation of prostate cancer cell suspension

Materials

1. Prostate cancer cell lines.
2. Tissue culture flasks or dishes.
3. Appropriate antibiotics (for example, penicillin–streptomycin).
4. Culture medium supplemented with 10% fetal bovine serum (FBS) and antibiotics.
5. 0.05% trypsin-EDTA.
6. Sterile 1 × phosphate-buffered saline (PBS, pH = 7.2-7.4).
7. 70 μm cell strainer.
8. 15 ml and 50 ml sterile conical tubes.
9. 0.4% trypan blue.
10. Hemacytometer or automated cell counter.
11. Ca2 + -free and Mg2 + -free Hanks' Balanced Salt Solution with Phenol Red Indicator (HBSS).

Procedures

1. One day prior to inoculation, passage prostate cancer cells so they will be 70–80% confluent on the day of the experiment. This ensures that cells are in the exponential growth phase, as recommended for optimal tumor onset.

*NOTE: prepare approximately 2–3 times more cells than you anticipate needing.

*NOTE: slow growing cells (for example, LNCaP, LNCaP C4-2B, VCaP) may need to be passaged 3–4 days earlier.

2. Trypsinize the cells, quench the trypsin activity by adding a sufficient volume of media containing FBS and wash one or two times with 1 × PBS.
3. Filter cells through a 70 μm cell strainer to exclude large cell aggregates.
4. Count the total live and dead cell number and determine the viability of the cells with trypan blue by using hemacytometer or automated cell counter.

*NOTE: the viability of cells should be ⩾90% prior to injection.

5. Centrifuge the cells in a swinging bucket centrifuge at 100–400 *g* for 3 min.
6. Carefully remove the media without disturbing the cell pellet.
7. Re-suspend cells in an appropriate volume of HBSS.
8. Transport cells to surgical room on ice.
9. Draw the prepared cell suspensions into the syringe and push out any air bubbles that may exist.

*NOTE: the number of cells for injection depends on the metastatic ability of the cell line and the experimental model. Usually, osteolytic prostate cancer cells require fewer cells to grow within the marrow (for example, 2500–50 000 cells), whereas osteoinductive prostate cancer cells need more cells (for example, 500 000 cells). Recommended cell number and injection volume for different inoculation models are as follows:

- Intraosseous inoculation: 2500 cells—5×10^5 cells per 5–10 μl.
- Intracardiac inoculation: 1–5×10^5 cells per 100 μl.
- Intravenous inoculation: 1–5×10^6 cells per 100 μl.
- Orthotopic inoculation: 1–5×10^4 cells per 10 μl.

*NOTE: set up the experiment keeping time from harvest to injection at a minimum, to assure that the cells stay alive throughout the injection process. The viability of cells will decline with time. At the end of an injection experiment, the cell viability should be above 80%.

Preparation for surgery

Materials

1. Animals: depending on the prostate cancer cell line to be inoculated, immunodeficient mice (BALB/c nu/nu, CB17 SCID) are used. Animals should be between 4 and 8 weeks of age.
2. Isoflurane
3. Ketamine
4. Xylazine
5. Eye ointment (vitamin A)
6. Shaver or chemical hair remover
7. Warming pad

Procedures

1. Set up the laminar flow with all necessary equipment and materials (**Figures 1a and b**).

*NOTE: surgery should be conducted under aseptic conditions and use sterile instruments, supplies and wound closure materials within a designated surgical room, and following procedures approved by the facility department of animal care oversight.

2. Anesthetize animals if necessary.

- This anesthesia should be performed only if equipped with a proper ventilated area. Two percent isoflurane mixed with 98% oxygen in the induction chamber. Mice should be kept under anesthesia for the duration of the surgery by being placed on their back and their head (nose) inserted into the breathing tube.
- Alternatively, xylazine–ketamine cocktail (Ketamine (100 mg ml^{-1}): Xylazine (20 mg ml^{-1}): 1 × PBS = 3:2:5)

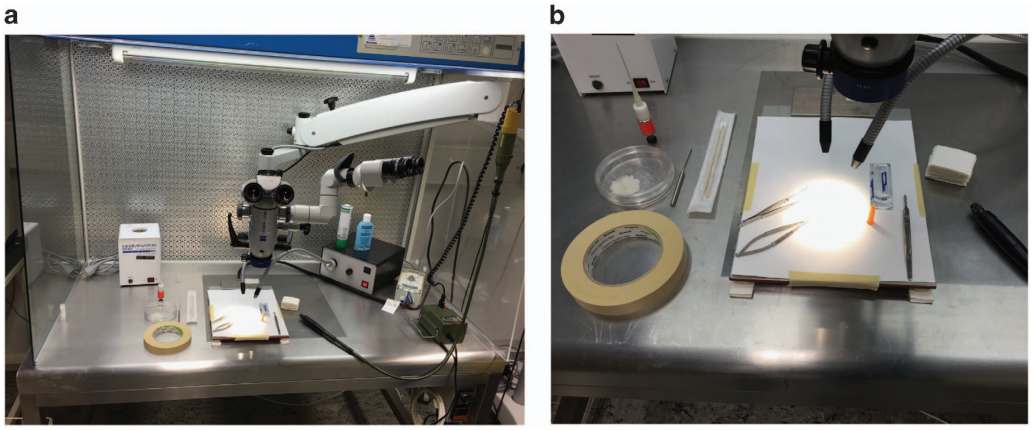

Figure 1 An example images for sterile surgical suite. (**a**, **b**) laminar flow with mounted microscope, heated operation table and necessary equipment.

can be administered 300 μl per 1 kg body weight intraperitoneally (i.p.)

3. Monitor animals until fully anesthetized (loss of reflexes) and place them on a warming pad.

*NOTE: prior to surgery, depth of anesthesia should be ensured by gently pinching the hind paw or tail tip. Mice should be unresponsive. If there is a response (movement) wait longer or (in the case of ketamine injection) administer another small dose. Please consult with your local authority, as the regulation may vary.

4. Apply ophthalmic ointment and remove the hair if necessary.
5. Place the animal in an appropriate position (for example, supine or prone) on a heated operation table within the laminar flow.
6. Disinfect the surgical area with 70% ethanol.

Prostate cancer cell inoculation routes

Intraosseous inoculation (Written by JH)

Materials

1. Sterile 1 × PBS.
2. Dental drill (power supply and drill, www.proxxon.com) and dental needles (Hedstroem files 28 mm size 30).
3. Surgical scissors, tweezers, scalpel and blade.
4. Cotton swabs.
5. 70% ethanol gauze.
6. 1 ml syringes with a 27G needle.
7. 0.5 or 1 ml insulin syringes (30G, ½ inch).
8. Surgical bone wax (Ethicon, Inc., Somerville, NJ, USA), capillary pistons (CP25, Gilson Microman, Gilson, Inc., Middleton, WI, USA) and spatula (**Figure 2a**).
9. Suturing thread.
10. Betadine, Purdue Pharma, Stamford, CT, USA.
11. Faxitron radiography system (MX-20, Faxitron, Tucson, AZ, USA).

Procedures

Intratibial injection (Method 1)

1. Place the animal in supine position on a heated operation table within the laminar flow (administer anesthesia as indicated above).
2. Disinfect the hind limb with 70% ethanol.
3. Flex the knee at about 90 angle.
4. Insert a 27G needle into the joint surface through the patellar tendon and tibial plateau in order to enter the intramedullary canal of the tibia.

*NOTE: the needle should be inserted with a drilling movement. Alternatively, an incision over the patellar tendon, followed by a longitudinal arthrotomy along the medial border of the patellar tendon, can be performed to expose the tibial plateau.

5. Inject the cancer cell suspension with a 30G needle via the proximal hole (10 μl maximal volume, but less volume would be ideal).
6. Inject an appropriate analgesic and monitor mice until they fully recover.

*NOTE: alternatively to this method, a needle can be used to drill a hole proximal to the tibial tuberosity. After penetration of the cortical bone, the cancer cell suspension can be injected.

*NOTE: bone marrow ablation creates space for the injection, and drilled holes can be sealed with bone wax preventing cancer cells to migrate out of the medullary cavity. (please see Method 2).

Intraosseous inoculation (Method 2)

1. Place the animal in supine position on a heated operation table within the laminar flow (administer anesthesia as indicated above).

*NOTE: tape the animal's hind limb to the operation table (if the leg is tape-fixed over a needle cap with a rotation to the inner side, drilling of the holes is facilitated) (**Figures 2b and c**).

2. Disinfect the hind limb with 70% ethanol.
3. Make a skin incision with a scalpel starting slightly below the knee joint to the end of the tibial bone marrow cavity (**Figure 2d**).

*NOTE: take care to not damage the tibial vein or artery.

4. Carefully resect the caput mediale of the gastrocnemius along the anterior tibial margin, and then continue to resect

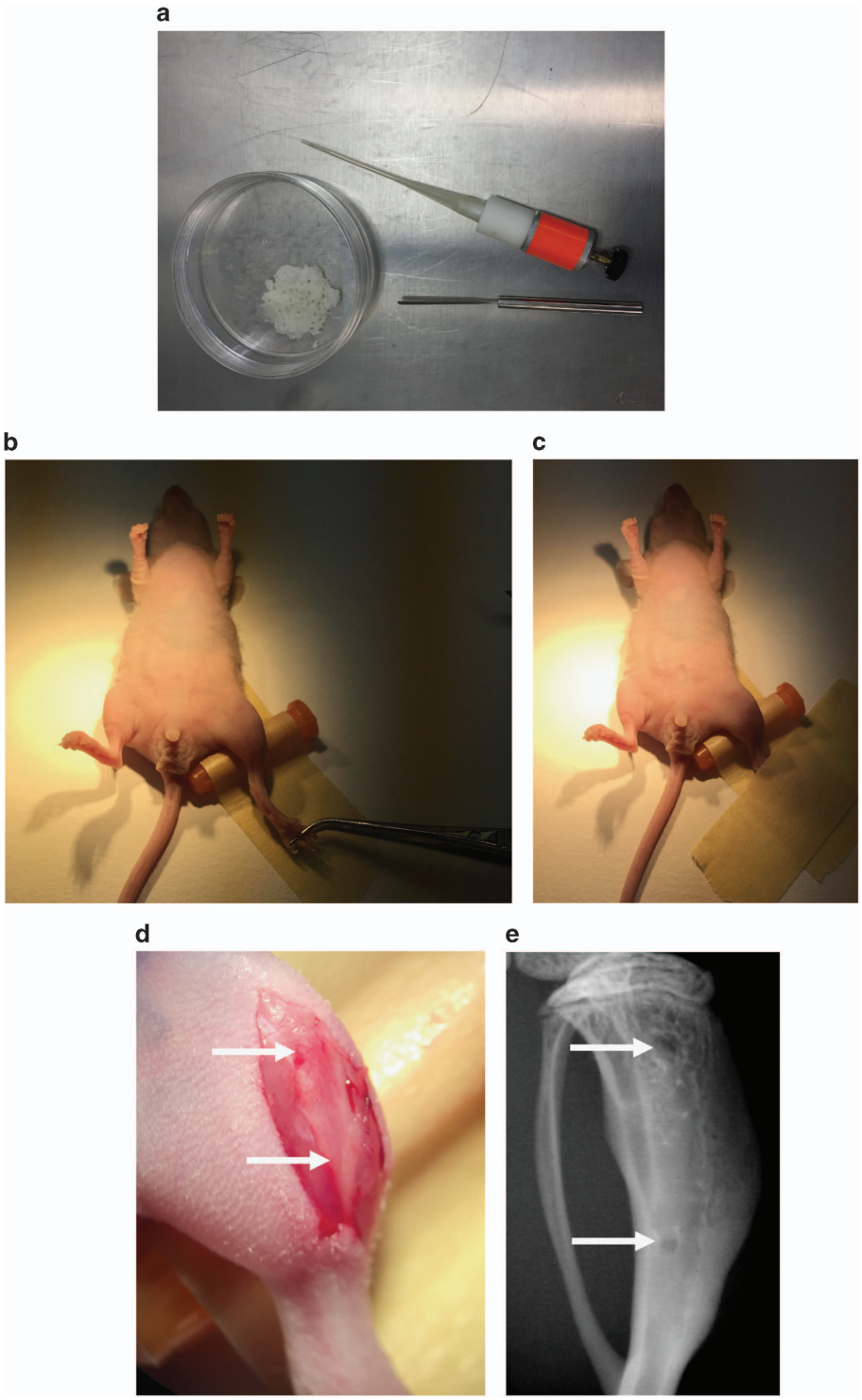

Figure 2 Intraosseous inoculation of prostate cancer cells. (**a**) Capillary piston, bone wax and spatula. (**b**, **c**) Fixation of hind limb. Gently grab the hind limb of the animal with a tweezer to avoid damaging to a mouse foot and tape it to the operation table. (**d**) Skin incision (white arrows point to the position of holes to be drilled). (**e**) Radiograph of tibia after intraosseous inoculation (white arrows point to the drilled holes).

its insertion on the medial surface of the tibia to uncover the underlying bone.

5. Constantly apply 1× PBS to prevent drying of the wound.
6. Drill two holes, one in close proximity to the metaphyseal growth plate and one at the distal end of the tibial bone marrow cavity (**Figure 2d**: arrows indicate the position of holes to be drilled; **Figure 2e**: arrows indicate position of drilled holes as seen on radiographs).

*NOTE: the dental drill bit should be held perpendicular to the tibia while drilling.

7. Flush the bone marrow with 0.5 ml 1 × PBS using a 30G needle.
8. Insert bone wax with a capillary piston into the distal hole and press with a spatula.
9. Inoculate the cancer cell suspension intramedullarily with a 30G needle via the proximal hole (10 μl maximal volume, but less volume would be ideal).
10. Seal the proximal hole with bone wax and suture the wound with 2–3 stitches.
11. Disinfect the wound with betadine.
12. Inject an appropriate analgesic and monitor mice until they fully recover.

*NOTE: both Method 1 and Method 2 are invasive. Either the injection channel using Method 1 or the drilled holes using Method 2 will be identified in histological sections. The injection volume has to be kept minimal for both methods because of the space limitation in the medullary cavity.

*NOTE: mice should be monitored regularly, according to an approved mouse protocol, and killed if clinical signs match the experimental end point. Signs include, but are not limited to, rapid weight loss and any condition interfering with daily activities (for example, eating or drinking, ambulation or elimination).

*NOTE: bone lesions can be monitored by radiography (Faxitron, 25 kV, 6 s) (**Figures 3a and b**: representative radiography pictures of osteolytic and osteoblastic bone metastases), and cancer cell growth can be monitored using bioluminescence imaging (only for luciferase-labeled cells).

Intracardiac inoculation (Written by NW)

Materials

1. 70% ethanol gauze
2. 0.5 or 1 ml Insulin syringes (30G, ½ inch)

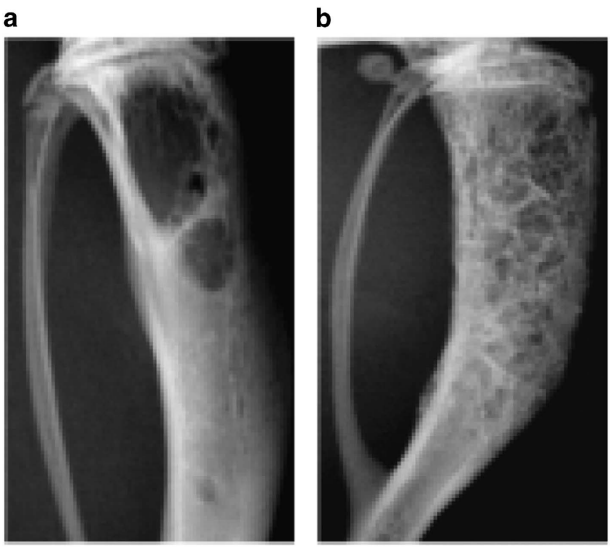

Figure 3 Representative radiographs after intraosseous inoculation. Representative images of radiographs after the intraosseous injection of (**a**) osteolytic prostate cancers cells (PC-3) into the bone marrow cavity of CB17 SCID mice (Day 32, 2 500 cells delivered) and (**b**) osteoinductive prostate cancer cells (VCaP) into the bone marrow cavity of CB17 SCID mice (day 91, 500 000 cells delivered).

Procedures

1. Hold the syringe with thumb, index finger and middle finger. Ring finger and little finger are used to withdraw and push the plunger, respectively (**Figure 4a**).
2. Use thumb and index finger of the other hand to slightly squeeze the rib cage of mouse from dorsal side upward to raise the position of the heart (**Figure 4b**) (administer anesthesia as indicated above).
3. Disinfect the chest area with 70% ethanol.
4. Insert needle horizontally into the injection point and slightly withdraw the plunger after the needle has been inserted 7–8 mm.

*NOTE: push and withdraw the plunger of syringe several time to reduce friction force before loading the syringe with 120 μl cell suspensions (20 μl in excess).

*NOTE: alternatively, needle can be inserted vertically.

*NOTE: injection point is 1–2 mm left of the midline and 1–2 mm beneath the edge of rib cage of the mouse (**Figure 4c**).

*NOTE: if the needle is properly inserted in the left ventricle, bright red blood will be pumped back into the cell suspension and pulsation should be visible from the air bubble remaining in the syringe (**Figure 4d**). If there is no blood pumping back or dark red blood observed, retract and re-insert the needle, but no more than three attempts should be carried out within 24 h.

5. Inject the cell suspension at a slow pace (~30 s for total 100 μl).

*NOTE: avoid positional change of injecting hand during injection.

*NOTE: correct injection can be verified during the process of injection by the color of blood pumped back to syringe. Should the needle be correctly injected into the left ventricle, bright red, oxygenated arterial blood will be seen, which is distinctive from the darker venous blood of the right ventricle (**Figure 5a**).

*NOTE: tumor cells in the systemic circulation can also be verified within 24 h after injection by bioluminescence imaging, if you are using luciferase-labeled cells. If tumor cells are correctly injected into the left heart ventricle, bioluminescence signals can be observed in the whole body (**Figure 5b**). Otherwise, signals will be concentrated in the chest area, and resemble the shape of lung, or will be completely absent (**Figure 5c**).

6. Slightly withdraw the plunger during the inoculation, and observe whether blood is still pumping back into the syringe to confirm that the needle is still placed in the left ventricle.
7. Complete the injection of 100 μl of cell suspension with the 20 μl excess remaining in the syringe. Wait for 5 s before the needle is taken out.
8. Monitor mice until they fully recover.

*NOTE: after the successful injection, the mouse is placed back into a clean cage on a heating pad, until fully recovered from the anesthesia. Closely monitor the mouse for the first 24 h after injection.

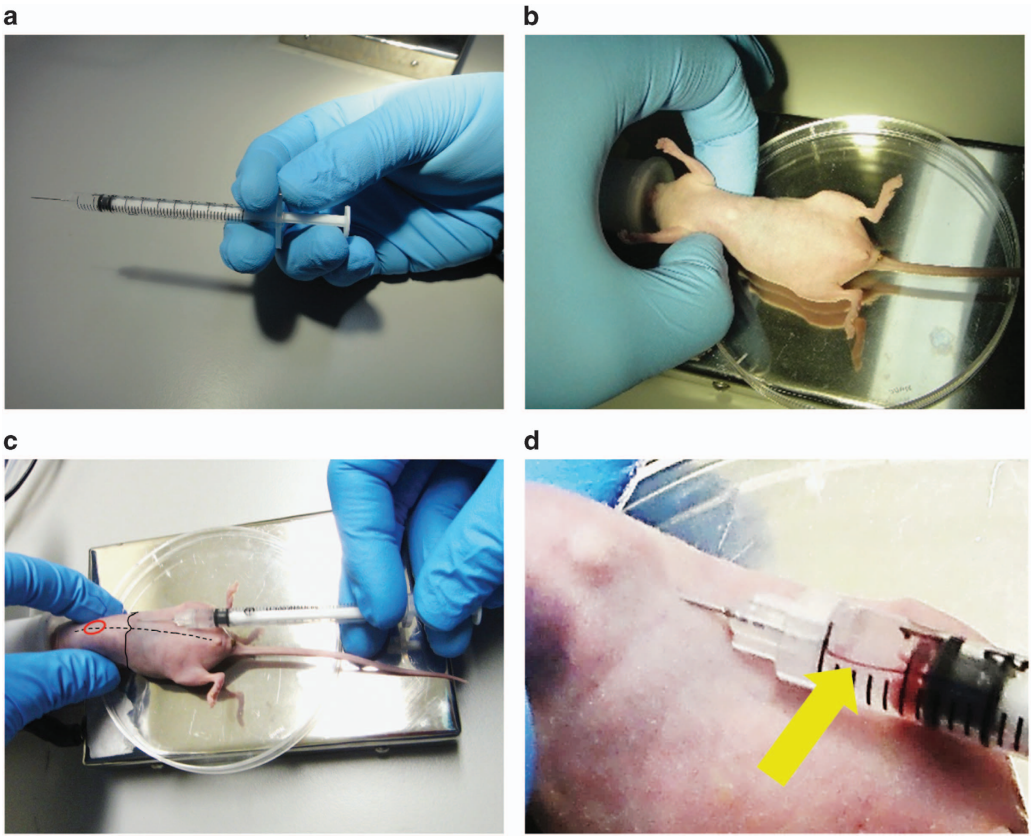

Figure 4 Intracardiac inoculation of prostate cancer cells. (**a**) Proper holding of the syringe. Thumb, index finger and middle finger are used to hold the syringe, whereas ring finger and little finger are responsible for withdrawing and pushing the plunger. (**b**) Mouse is placed in a supine position and the rib cage is squeezed up to raise the position of the heart. (**c**) Insert the needle horizontally into the injection point 1–2 mm left of the midline (the dotted line) and 1–2 mm beneath the edge of rib cage (the solid line). The approximate position of the heart is marked in red. (**d**) When the needle is successfully inserted into the left ventricle, slightly withdrawing the plunger will pump bright red blood back into the cell suspension in the syringe (yellow arrow).

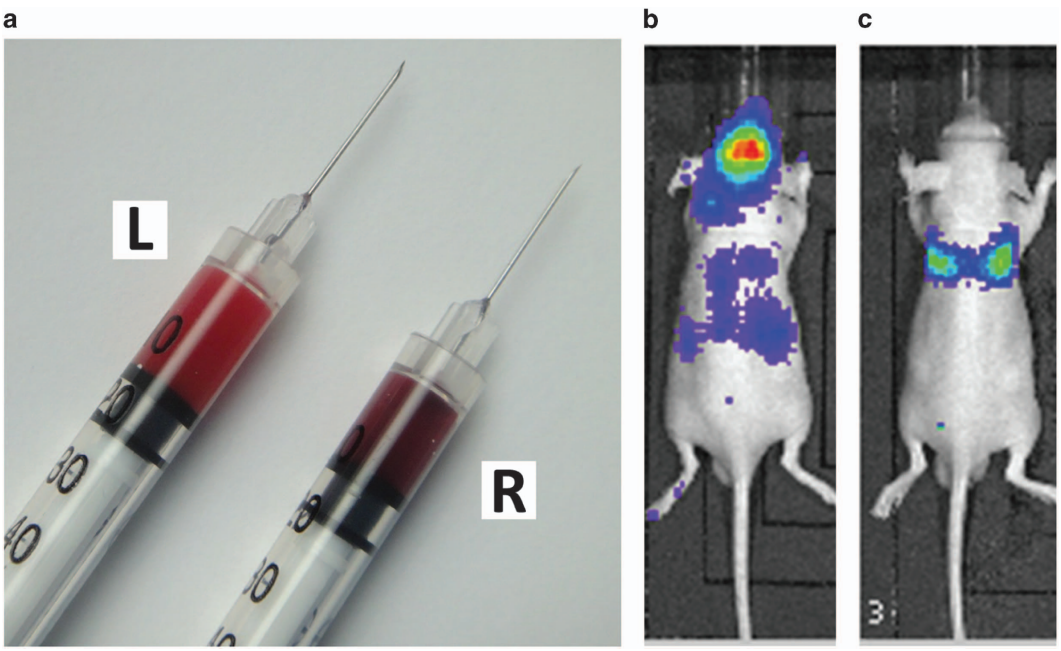

Figure 5 Verification after intracardiac inoculation. (**a**) Bright red, oxygenated arterial blood from correct injection into the left ventricle (L) and darker venous blood of the right ventricle from incorrect injection (R). Representative images of *in vivo* bioluminescence imaging within 24 h after injection (**b**) in the correctly injected mouse (whole body bioluminescence signals) and (**c**) in the incorrectly injected mouse (lung-shape signals over thorax).

Intravenous inoculation (Written by JD)

Materials

1. Mouse restrainers.
2. 70% ethanol gauze.
3. 1 ml syringes with 26–28G needle, ½ inch.

*NOTE: various mouse restrainers are available, but the mouse tail illuminator restrainer from Braintree Scientific, Inc. (Braintree, MA, USA) is recommended, because it efficiently illuminates and warms a mouse tail for easy injection.

Procedures

1. Gently grab the tail of a mouse and pull it into the commercial or custom mouse restrainer, with its back against the slit and its tail sticking out of the small opening in the back of the restrainer. Slowly close doors and keep mouse gently restrained.
2. Find the lateral tail vein (**Figure 6**) and promote vasodilation of the vein for easy injection by warming the mouse using a heat lamp or a warming device or by immersion of the tail in warm water for about 5 min.

*NOTE: the time will be dependent on the distance from the heat source, and the animals must be monitored carefully to prevent being burned or overheated by the heat source.

3. Disinfect the tail with 70% ethanol.
4. Pull the tail straight.
5. Hold the tip of tail with thumb, and support the point for injection with the index finger.
6. With the bevel facing up, insert a needle into one of the lateral tail veins in the proximal 1/3 of the tail, and gently inject 100 μl of the cell suspension.

*NOTE: a successful injection is based on lack of resistance while pushing the plunger.

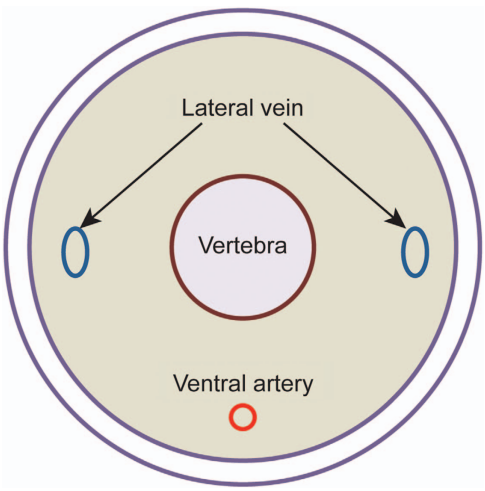

Figure 6 Anatomy of murine tail. Murine tail veins are found in both sides of murine tail (just under the skin). Intravenous injections should be performed via the lateral tail vein.

*NOTE: start from the distal end of the tail; thus, if the first trial fails, a more proximal region of the tail can be used if another attempt is needed.

*NOTE: the maximum volume that may be injected depends on numerous factors including the mouse's size, background strain and properties of the cells. Most users try to limit the injection to a maximum of 0.25 ml. Keep in mind that overconcentration of cells may lead to embolism in lung capillaries and death of the mice.

7. Withdraw the needle after injection and press a clean piece of paper towel or cotton swab on the injection site to facilitate clotting.
8. Release the mouse from the restrainer and return it to the cage.

*NOTE: most mice show only reduced activity levels. The mice should be observed for the first hour following injection. If no problems are observed other than reduced activity, the mice may be returned to standard housing.

Orthotopic inoculation (Written by MK-dJ)

Materials

1. Sterile 1 × PBS.
2. Surgical scissors and tweezers.
3. Cotton swabs.
4. 70% ethanol gauze.
5. 0.5 or 1 ml Insulin syringes (30G, ½ inch).
6. Suturing thread (wound clip is not ideal for imaging).
7. Betadine.

Procedure

1. Place a mouse in supine position, immobilization is not necessary (administer anesthesia as indicated above).
2. Disinfect the lower abdomen with 70% ethanol.
3. Make a small (1 cm) incision in the lower midline of the peritoneum.
4. Exteriorize and gently stabilize the prostate dorsal lobes with a wet (1 × PBS) cotton swab (**Figure 7**).

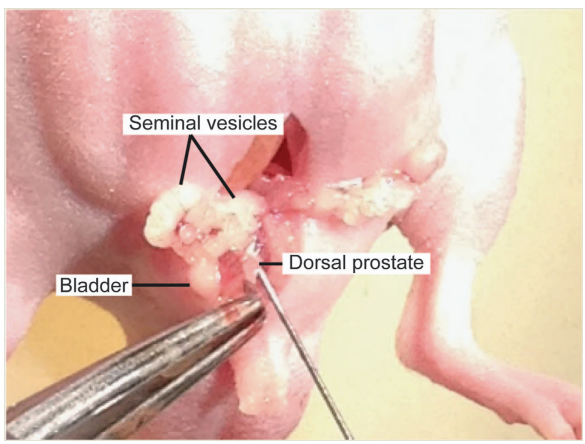

Figure 7 Orthotopic inoculation of prostate cancer cells. The prostate dorsal lobes are gently exteriorized, and prostate cancer cells will be inoculated.

5. Insert the needle into the right dorsal lobe of the prostate at a 45 angle.
6. Slowly inject 10 μl of the cell suspension.

*NOTE: a well-localized bleb indicates a successful injection.

7. Retract the needle gently and place a cotton swab over the injection site for about 1 min to prevent bleeding and spillage of material.
8. Return the prostate to the peritoneum and suture the abdominal wall first and the skin layer after with a 4–0 silk suture.
9. Disinfect the wound with betadine.
10. Inject an appropriate analgesic and monitor mice until they fully recover.

*NOTE: mice should be monitored regulary according to an approved mouse protocol and killed if clinical signs match experimental end point. Signs include, but are not limited to, rapid weight loss and any condition interfering with daily activities (for example, eating or drinking, ambulation or elimination).

In vivo bioluminescence imaging

Materials

1. Luciferase-labeled prostate cancer cell line (PCa-luc cells).

*NOTE: luciferase-labeled prostate cancer cells are greatly useful to follow metastasis *in vivo*. Lentiviral transfer of luciferase gene and subsequent selection and verification of stable clones should be performed in advance. Luciferase-labeled PC-3 cells can be purchased from Caliper Life Sciences or generated individually by transducing cells with lentiviral vectors and luciferase reporter vectors (pGL4 Luciferase Reporter Vectors from Promega, Madison, WI, USA). Verify luciferase activity in cells before injection.

2. Sterile 1 × PBS.
3. 1 ml syringes with a 25G needle.
4. D-Luciferin (from Regis Technologies, Morton Grove, IL, USA, or Caliper Life Sciences, Waltham, MA, USA or Promega).
5. Isoflurane.
6. Oxygen tank.
7. Isoflurane/oxygen-based anesthesia system fitted with an induction chamber and inhalation masks for mice.

*NOTE: xylazine–ketamine cocktail can be used if no Isoflurane/oxygen-based anesthesia system available.

8. *In vivo* imaging system (Xenogen IVIS, Perkin-Elmer, Waltham, MA, USA).

Procedure

1. Prepare a sterile stock solution of D-luciferin in 1 × PBS (40 mg ml^{-1}).
2. Inject 150 μg g^{-1} D-luciferin into the intraperitoneal cavity of mice, using a syringe with a 25G needle.
3. Initialize the 'Living Image software (Perkin-Elmer)' provided by the manufacturer on a computer attached to the IVIS machine.

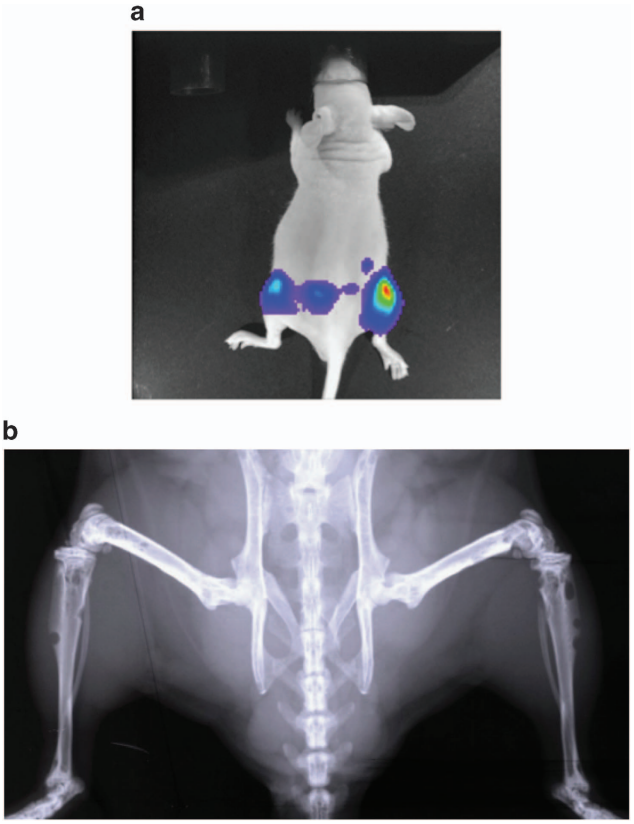

Figure 8 Representative images after intravenous injection. Representative images of (**a**) *in vivo* bioluminescence imaging and (**b**) radiograph after the intravenous injection of luciferase-labeled PC-3 cells into a nude mouse. Multiple bone metastatic lesions are detected at mouse hind limbs.

4. Set exposure time and imaging parameters.
5. Anesthetize the mice in 2% isoflurane mixed with 98% oxygen in induction chamber.
6. Place mice in the IVIS platform while keeping mice under anesthesia through a nose cone, and take the image 12 min after D-luciferin injection.

*NOTE: it is recommended to perform an initial kinetic experiment for each animal model taking images during different time points. This will allow you to determine the D-luciferin distribution for your experiment.

7. Analyze and quantify the photons emitted from luciferase-labeled cells within the animal according to the manufacturer's protocol.

*NOTE: for the intravenous inoculation model of prostate cancer, a highly metastatic cancer cell line (for example, PC-3 and DU145) typically gives rise to many metastases, especially at hind limb with bone metastatic lesions (**Figure 8a**), whereas very few metastases will be detected from a poorly metastatic cancer cell line (for example, LNCaP and LNCaP C4-2B).

*NOTE: bioluminescence is a well-established technique commonly utilized to track tumor growth and to locate and monitor the presence of metastases within living animals. *In vivo* bioluminescence imaging system is a highly sensitive imaging technology to quantify bioluminescence via a digital camera

Table 1 Prostate cancer cell line used in bone metastasis research

Cell line	*Origin*	*PSA*	*AR*	*Bone lesion*	*Model*	*References*
DU145	Central nerve system metastasis (Human)	Negative	Negative	Osteolytic	Intratibial injection, Intracardiac injection, Intravenous injection into human bone implanted animals	Conley-LaComb *et al.*,[3] Stone *et al.*,[4] Nemeth *et al.*,[5] Yin *et al.*[6]
PC-3	Vertebral bone metastasis (Human)	Negative	Negative	Osteolytic	Intratibial injection, Intrafemoral injection, intracardiac injection, Intravenous injection into human bone implanted animals	Kaighn *et al.*,[7] Nemeth *et al.*,[5] Chu *et al.*,[8] Wu *et al.*,[9] Zhang *et al.*[10]
LNCaP	Lymph node metastasis (Human)	Positive	Positive	Osteoblastic/ Osteolytic	Intrafemoral injection, Intravenous injection into human bone implanted animals	Nemeth *et al.*,[5] Horoszewicz *et al.*,[11] Wu *et al.*[9]
LNCaP C4-2	LNCaP subline C4 xenograft line	Positive	Positive	Osteoblastic	Intratibial injection, Intrafemoral injection, intracardiac injection	Thalmann *et al.*,[12] Wu *et al.*[9]
LNCaP C4-2B	LNCaP subline C4-2 xenograft line	Positive	Positive	Osteoblastic	Intrafemoral injection	Thalmann *et al.*,[12] Wu *et al.*[9]
MDA PCa 2b	Bone metastasis (Human)	Positive	Positive	Osteoblastic	Intrafemoral injection	Navone *et al.*,[13] Cheng *et al.*,[14] Yang *et al.*[15]
VCaP	Vertebral bone metastasis (Human)	Positive	Positive	Osteoblastic	Intratibial injection	Korenchuk *et al.*,[16] Kirschenbaum *et al.*[17]
22Rv1	CWR22R xenograft line	Positive	Positive	Osteoblastic/ Osteolytic	Intratibial injection	Sramkoski *et al.*,[18] Henry *et al.*[19]
LAPC-9	Femoral bone metastasis (Human)	Positive	Positive	Osteoblastic	Intratibial injection	Craft *et al.*,[20] Lee *et al.*,[21] Lee *et al.*[22]
ARCaP	Ascites of a patient with advanced metastatic disease (Human)	Positive	Positive	Osteoblastic/ Osteolytic	Intracardiac injection	Zhau *et al.*,[23] Odero-Marah *et al.*,[24] Xu *et al.*[25]
LuCaP23.1	Lymph node metastasis (Human)	Positive	Positive	Osteoblastic	Intratibial injection	Ellis *et al.*,[26] Morrissey *et al.*,[27] Brubaker *et al.*[28]

Abbreviations: AR, androgen receptor; PSA, prostate-specific antigen.

and advanced computer software. This system detects photons emitted from luciferase-expressing cells within the living animals.

*NOTE: in certain cases, it may be important to get both dorsal and ventral images.

*NOTE: many imaging techniques can also be used to detect the prostate cancer metastatic lesions in mice, such as molecular imaging techniques or small animal diagnostic imaging (microcomputed tomography or magnetic resonance imaging or Faxitron cabinet x-ray systems) (**Figure 8b**). If both bioluminescence and other imaging techniques are not available, histopathological examination of metastatic nodules subsequent to necropsy is the best approach.

Discussions/Conclusion

In this manuscript, we discussed the mouse xenograft models that are commonly used to study prostate cancer bone metastasis. Using these models with human prostate cancer cell lines (**Table 1**),[3–28] we have gained a greater understanding of the process of bone metastasis. However, there are limitations for using these xenograft models, as the immune systems of animals used for developing these models are weak or compromised to avoid an immune response to the human tissue. There are currently some transgenic spontaneous prostate cancer models that may overcome this limitation; however, the transgenic mice currently available rarely result in bone metastases, unlike those seen in human prostate cancer.[29] Although humanized animal models[30,31] or *ex vivo* tissue engineered models[32,33] have been recently proposed to potentially mimic bone metastasis, models that perfectly recapitulate the human prostate cancer bone metastatic process are still missing. To unveil the mystery of bone metastasis, further improvement of animal models currently available and/or development of new animal models to overcome the limitations that we are facing are clearly warranted.

Conflict of Interest

The authors declare no conflict of interest.

Acknowledgements

We thank Ms Janice E Berry for critical reading of this manuscript and Dr Antoinette Wetterwald for insightful scientific discussion. This work is directly supported by the National Cancer Institute (CA163124, YS; P01Ca093900, JD; and R01CA190554, JD), the Department of Defense (W81XWH-14-1-0403, YS), the Prostate Cancer Foundation (YS), Cancer Research UK (NW), Yorkshire Cancer Research (NW), and Wellcome Trust (NW). Supported by the IBMS-ECTS Young Investigators.

References

1. Boyd LK, Mao X, Lu YJ. The complexity of prostate cancer: genomic alterations and heterogeneity. *Nat Rev Urol* 2012; **9**: 652–664.
2. Shiozawa Y, Eber MR, Berry JE, Taichman RS. Bone marrow as a metastatic niche for disseminated tumor cells from solid tumors. *BoneKey Rep* 2015; **4**: 689.
3. Conley-LaComb MK, Saliganan A, Kandagatla P, Chen YQ, Cher ML, Chinni SR. PTEN loss mediated Akt activation promotes prostate tumor growth and metastasis via CXCL12/CXCR4 signaling. *Mol Cancer* 2013; **12**: 85.
4. Stone KR, Mickey DD, Wunderli H, Mickey GH, Paulson DF. Isolation of a human prostate carcinoma cell line (DU 145). *Int J Cancer* 1978; **21**: 274–281.
5. Nemeth JA, Harb JF, Barroso Jr U , He Z, Grignon DJ, Cher ML. Severe combined immunodeficient-hu model of human prostate cancer metastasis to human bone. *Cancer Res* 1999; **59**: 1987–1993.
6. Yin J, Pollock C, Tracy K, Chock M, Martin P, Oberst M *et al.* Activation of the RalGEF/Ral pathway promotes prostate cancer metastasis to bone. *Mol Cell Biol* 2007; **27**: 7538–7550.
7. Kaighn ME, Narayan KS, Ohnuki Y, Lechner JF, Jones LW. Establishment and characterization of a human prostatic carcinoma cell line (PC-3). *Invest Urol* 1979; **17**: 16–23.
8. Chu K, Cheng CJ, Ye X, Lee YC, Zurita AJ, Chen DT *et al.* Cadherin-11 promotes the metastasis of prostate cancer cells to bone. *Mol Cancer Res* 2008; **6**: 1259–1267.

9. Wu TT, Sikes RA, Cui Q, Thalmann GN, Kao C, Murphy CF *et al.* Establishing human prostate cancer cell xenografts in bone: induction of osteoblastic reaction by prostate-specific antigen-producing tumors in athymic and SCID/bg mice using LNCaP and lineage-derived metastatic sublines. *Int J Cancer* 1998; **77**: 887–894.
10. Zhang Z, Li K, Zhang X, Fang Z, Xiong W, Chen Q *et al.* Effect of Id1 knockdown on formation of osteolytic bone lesions by prostate cancer PC3 cells *in vivo*. *J Huazhong Univ Sci Technolog Med Sci* 2012; **32**: 364–369.
11. Horoszewicz JS, Leong SS, Chu TM, Wajsman ZL, Friedman M, Papsidero L *et al.* The LNCaP cell line–a new model for studies on human prostatic carcinoma. *Prog Clin Biol Res* 1980; **37**: 115–132.
12. Thalmann GN, Anezinis PE, Chang SM, Zhau HE, Kim EE, Hopwood VL *et al.* Androgen-independent cancer progression and bone metastasis in the LNCaP model of human prostate cancer. *Cancer Res* 1994; **54**: 2577–2581.
13. Navone NM, Olive M, Ozen M, Davis R, Troncoso P, Tu SM *et al.* Establishment of two human prostate cancer cell lines derived from a single bone metastasis. *Clin Cancer Res* 1997; **3** (12 Pt 1):2493–2500.
14. Cheng CJ, Ye XC, Vakar-Lopez F, Kim J, Tu SM, Chen DT *et al.* Bone microenvironment and androgen status modulate subcellular localization of ErbB3 in prostate cancer cells. *Mol Cancer Res* 2007; **5**: 675–684.
15. Yang J, Fizazi K, Peleg S, Sikes CR, Raymond AK, Jamal N *et al.* Prostate cancer cells induce osteoblast differentiation through a Cbfa1-dependent pathway. *Cancer Res* 2001; **61**: 5652–5659.
16. Korenchuk S, Lehr JE, L MC, Lee YG, Whitney S, Vessella R *et al.* VCaP, a cell-based model system of human prostate cancer. *In Vivo* 2001; **15**: 163–168.
17. Kirschenbaum A, Liu XH, Yao S, Leiter A, Levine AC. Prostatic acid phosphatase is expressed in human prostate cancer bone metastases and promotes osteoblast differentiation. *Ann NY Acad Sci* 2011; **1237**: 64–70.
18. Sramkoski RM, Pretlow 2nd TG , Giaconia JM, Pretlow TP, Schwartz S, Sy MS *et al.* A new human prostate carcinoma cell line, 22Rv1. *In Vitro Cell Dev Biol Anim* 1999; **35**: 403–409.
19. Henry MD, Silva MD, Wen S, Siebert E, Solin E, Chandra S *et al.* Spiculated periosteal response induced by intraosseous injection of 22Rv1 prostate cancer cells resembles subset of bone metastases in prostate cancer patients. *Prostate* 2005; **65**: 347–354.
20. Craft N, Chhor C, Tran C, Belldegrun A, DeKernion J, Witte ON *et al.* Evidence for clonal outgrowth of androgen-independent prostate cancer cells from androgen-dependent tumors through a two-step process. *Cancer Res* 1999; **59**: 5030–5036.
21. Lee Y, Schwarz E, Davies M, Jo M, Gates J, Wu J *et al.* Differences in the cytokine profiles associated with prostate cancer cell induced osteoblastic and osteolytic lesions in bone. *J Orthop Res* 2003; **21**: 62–72.
22. Lee YP, Schwarz EM, Davies M, Jo M, Gates J, Zhang X *et al.* Use of zoledronate to treat osteoblastic versus osteolytic lesions in a severe-combined-immunodeficient mouse model. *Cancer Res* 2002; **62**: 5564–5570.
23. Zhau HY, Chang SM, Chen BQ, Wang Y, Zhang H, Kao C *et al.* Androgen-repressed phenotype in human prostate cancer. *Proc Natl Acad Sci USA* 1996; **93**: 15152–15157.
24. Odero-Marah VA, Wang R, Chu G, Zayzafoon M, Xu J, Shi C *et al.* Receptor activator of NF-kappaB Ligand (RANKL) expression is associated with epithelial to mesenchymal transition in human prostate cancer cells. *Cell Res* 2008; **18**: 858–870.
25. Xu J, Wang R, Xie ZH, Odero-Marah V, Pathak S, Multani A *et al.* Prostate cancer metastasis: role of the host microenvironment in promoting epithelial to mesenchymal transition and increased bone and adrenal gland metastasis. *Prostate* 2006; **66**: 1664–1673.
26. Ellis WJ, Vessella RL, Buhler KR, Bladou F, True LD, Bigler SA *et al.* Characterization of a novel androgen-sensitive, prostate-specific antigen-producing prostatic carcinoma xenograft: LuCaP 23. *Clin Cancer Res* 1996; **2**: 1039–1048.
27. Morrissey C, Dowell A, Koreckij TD, Nguyen H, Lakely B, Fanslow WC *et al.* Inhibition of angiopoietin-2 in LuCaP 23.1 prostate cancer tumors decreases tumor growth and viability. *Prostate* 2010; **70**: 1799–1808.
28. Brubaker KD, Brown LG, Vessella RL, Corey E. Administration of zoledronic acid enhances the effects of docetaxel on growth of prostate cancer in the bone environment. *BMC Cancer* 2006; **6**: 15.
29. Winter SF, Cooper AB, Greenberg NM. Models of metastatic prostate cancer: a transgenic perspective. *Prostate Cancer Prostatic Dis* 2003; **6**: 204–211.
30. Hesami P, Holzapfel BM, Taubenberger A, Roudier M, Fazli L, Sieh S *et al.* A humanized tissue-engineered in vivo model to dissect interactions between human prostate cancer cells and human bone. *Clin Exp Metastasis* 2014; **31**: 435–446.
31. Holzapfel BM, Wagner F, Loessner D, Holzapfel NP, Thibaudeau L, Crawford R *et al.* Species-specific homing mechanisms of human prostate cancer metastasis in tissue engineered bone. *Biomaterials* 2014; **35**: 4108–4115.
32. Thibaudeau L, Taubenberger AV, Holzapfel BM, Quent VM, Fuehrmann T, Hesami P *et al.* A tissue-engineered humanized xenograft model of human breast cancer metastasis to bone. *Dis Model Mech* 2014; **7**: 299–309.
33. Curtin P, Youm H, Salih E. Three-dimensional cancer-bone metastasis model using *ex-vivo* co-cultures of live calvarial bones and cancer cells. *Biomaterials* 2012; **33**: 1065–1078.

INTERNATIONAL JOURNAL OF UROLOGY
International Journal of Urology (2016) doi: 10.1111/iju.13170

Review Article

Skeletal complications in cancer patients with bone metastases

Shunsuke Tsuzuki,[1] Sun Hee Park,[1] Matthew R Eber,[1] Christopher M Peters[2] and Yusuke Shiozawa[1]

[1]Department of Cancer Biology and Comprehensive Cancer Center, and [2]Department of Anesthesiology, Wake Forest School of Medicine, Winston-Salem, North Carolina, USA

Abbreviations & Acronyms
ADT = androgen deprivation therapy
Ang II = angiotensin II
APCC = AT3B rat prostate cancer cells
AT1R = angiotensin type I receptor
AT2R = angiotensin type II receptor
BP = bisphosphonate
CKI = cathepsin K inhibitor
COX-2 = cyclooxygenase-2
CRPC = castration-resistant prostate cancer
DRG = dorsal root ganglion
DTC = disseminated tumor cell
ET-1 = endothelin-1
ETAR = endothelin A receptor
ETBR = endothelin B receptor
HCM = hypercalcemia of malignancy
IL = interleukin
MAPK = mitogen-activated protein kinase
MESCC = metastatic epidural spinal cord compression
NGF = nerve growth factor
NSAIDs = non-steroidal anti-inflammatory drugs
OPG = osteoproteogerin
PTHrP = parathyroid hormone-related protein
QOL = quality of life
RANK = receptor activator of nuclear factor κB
RANKL = receptor activator of nuclear factor κB ligand
SRE = skeletal-related event
TrkA = tropomyosin receptor kinase A
TRPV1 = transient receptor potential vanilloid type 1 receptor
uNTX/Cr = ratio of N-telopeptide of type I collagen to creatinine
ZA = zoredronic acid

Correspondence: Yusuke Shiozawa M.D., Ph.D., Department of Cancer Biology, Wake Forest School of Medicine, 1 Medical Center Blvd, Winston-Salem, NC 27157-1082, USA. Email: yshiozaw@wakehealth.edu

Received 29 April 2016; accepted 7 June 2016.

Abstract: As a result of significant improvements in current therapies, the life expectancy of cancer patients with bone metastases has dramatically improved. Unfortunately, these patients often experience skeletal complications that significantly impair their quality of life. The major skeletal complications associated with bone metastases include: cancer-induced bone pain, hypercalcemia, pathological bone fractures, metastatic epidural spinal cord compression and cancer cachexia. Once cancer cells invade the bone, they perturb the normal physiology of the marrow microenvironment, resulting in bone destruction, which is believed to be a direct cause of skeletal complications. However, full understanding of the mechanisms responsible for these complications remains unknown. In the present review, we discuss the complications associated with bone metastases along with matched conventional therapeutic strategies. A better understanding of this topic is crucial, as targeting skeletal complications can improve both the morbidity and mortality of patients suffering from bone metastases.

Key words: bone metastasis, cancer-induced bone pain, hypercalcemia, metastatic epidural spinal cord compression, pathological bone fractures, skeletal complications.

Introduction

Although the survival of prostate cancer patients has improved over the past two decades, when the disease spreads to other organs, such as bone, the prognosis worsens drastically. Indeed, the 5-year relative survival rate of localized or regional prostate cancer is nearly 100%; but just 28.2% of patients with distant metastases survive past 5 years (http://seer.cancer.gov/statfacts/html/prost.html). In particular, the overall median survival of patients with bone metastases is just 19 months.[1] This is due to the fact that distant metastases are difficult to treat or even investigate, because the process of metastasis requires many steps: including detachment from the primary site, circulation throughout the body and dissemination to secondary organs.[2] Furthermore, growing evidence suggests that the interaction between metastatic cancer cells and their microenvironment is a complex, but essential, component of the metastatic process.[3,4]

Once in the marrow, bone metastatic cancer cells take advantage of the normal marrow physiology to survive away from the primary tumor.[5] Bone marrow is a unique environment in that it houses both the cells of hematopoietic lineage and the cells that are responsible for bone remodeling (e.g. osteoblasts and osteoclasts). Recent studies have shown that bone metastatic cancer cells home to the osteoblasts, or the hematopoietic stem cell niche,[6] which plays crucial roles in the early colonization of bone.[6,7] These DTCs also actively influence bone remodeling (e.g. osteoblastogenesis and osteoclastogenesis) to create a favorable environment for further recruitment and better survival of DTCs within the marrow.[8] Subsequently, DTCs become dormant, and eventually regrow. Currently, bone-targeting agents (BPs, denosumab) and/or external beam radiotherapy are the standards of care for prevention or delay of SREs.[9] However, these treatment strategies are not radical, but palliative or supportive. Therefore, there is a strong need to understand the mechanisms of bone metastasis to develop treatments that are more effective.

Generally, patients with advanced stage prostate cancer are treated with ADT, whereas patients with early stage, low- or intermediate-risk prostate cancer can be treated with prostatectomy or radiation. In most cases, ADT is only effective initially, when prostate cancer is

first cut off from its preferred growth factor, androgen. However, ADT alone is not sufficient to eliminate prostate cancer. Prostate cancer gradually acquires resistance to androgen deprivation, and eventually becomes CRPC, which often presents itself in the form of aggressive bone metastases. Once CRPC spreads to the bone, it is not only incurable, but also causes SREs that devastate one's QOL. As if the severe pain associated with bone metastases was not enough, many patients experience spinal cord compression so debilitating they become completely bedridden. It is therefore of the utmost importance to develop therapeutic agents that eradicate bone metastatic diseases, or in the very least improve the QOL of afflicted patients. In order to do this, we need to understand the mechanisms involved in skeletal complications associated with bone metastases.

In the present review, we compiled the known molecular mechanisms and current therapeutic strategies, as well as the shortcomings, associated with the four major skeletal complications caused by bone metastases.

Skeletal complications of bone metastasis

Cancer-induced bone pain

Pain is one of the most frequent complications in cancer patients. In fact, 68% of all cancer patients with advanced, metastatic or terminal disease experiences pain.[10] Specifically, 60–84% of cancer patients with bone metastasis develop bone pain.[11] The pain mediated by bone metastases is often described as "ongoing pain," which is dull and continuous. However, as cancer grows, this pain might become more severe. Bone cancer pain can also produce episodes of intense pain often triggered by movement that breakthrough a standard opioid-based regimen (breakthrough pain). Recent studies suggest the following mechanisms of cancer-induced bone pain: (i) cancer cells directly or indirectly interact with nociceptors in the marrow by secreting chemical mediators, such as prostaglandins, nerve growth factor, endothelins and bradykinin;[12] (ii) cancer cells also interact with surrounding inflammatory cells, such as macrophages and mast cells, within the metastatic lesion, which also secrete chemical mediators that lead to bone pain;[12] and (iii) once cancer cells reach the bone, they interfere with homeostatic bone remodeling. Cancer cells stimulate osteoclastogenesis by secreting factors, such as PTHrP.[13] The resulting osteoclasts can demineralize and destroy regions of bone rich with peripheral nerve innervation, causing bone pain.[14] In addition, the bone destruction process leads to an acidic environment, further stimulating pain through pH sensing channels.[15,16] Therefore, blocking the interactions between chemical mediators and their receptors on peripheral nociceptors, or preventing osteoclastogenesis altogether are both analgesic strategies used for cancer-induced bone pain.[12,17]

Currently, pain associated with cancer is treated by following the three-step analgesic ladder approach developed by the World Health Organization.[18,19] The first step of this approach is to use non-opioids, such as NSAIDs or acetaminophen, for mild pain. As pain progresses, the patient is next prescribed weak opioids (mild-moderate pain), and finally, a patient with moderate to severe pain is prescribed strong opioids. Although opioids are extremely effective analgesics and, as such, are the current mainstay for severe cancer pain management, opioid abuse and addiction are a serious and growing concern.[20] Therefore, alternative strategies to reduce opioid use are urgently required. One such strategy is a combination regimen of non-opioids and opioids, allowing an overall reduction of opioid intake. This combination strategy has been shown to actually improve treatment efficacy in patients with moderate to severe cancer pain.[21] Radiotherapy has also been used for the management of pain caused by bone metastases.[22] It has been shown that 60–80% of patients with bone metastases experience pain relief after radiotherapy.[23] Additionally, agents that target bone remodeling, such as BPs and denosumab, a monoclonal antibody against RANKL, have been reported to relieve pain in patients suffering from bone metastasis.[24]

As stated above, NSAIDs are widely used analgesics for cancer-induced bone pain, but can have serious side-effects including ulcers and bleeding.[24] However, it was recently shown that patients who took a new type of NSAID (a selective COX-2 inhibitor) had fewer gastrointestinal side-effects than those who took non-selective traditional NSAIDs.[25] Although the mechanisms whereby the COX-2 inhibitor relieves pain are still unknown, it has been suggested that COX-2 is responsible for the synthesis of prostaglandins, resulting in inflammation and pain.[26] Indeed, selective COX-2 inhibitors attenuated both ongoing and movement-evoked bone cancer pain behaviors in mice inoculated with murine osteolytic NCTC 2472 sarcoma cells in the intramedullary space of the femur.[27] Additionally, inhibition of COX-2 prevented bone resorption and reduced tumor growth mediated by COX-2 expressing-NCTC 2472 osteosarcoma cells.[27]

NGF, known to promote prenatal nerve growth,[28,29] is involved in the adult regulation of both nociceptive and neuropathic pain through one of its receptors, TrkA.[30,31] Along with this notion, NGF causes hyperalgesia in adult rats,[29] and muscle pain and skin hyperalgesia in humans.[32,33] Accumulating evidence suggest a role for NGF in cancer-induced bone pain. In *in vivo* bone metastatic models of prostate cancer (ACE-1 cells) and breast cancer (MDA-MB-231-BO cells), treatments with antibodies against NGF significantly attenuated cancer-induced bone pain.[34,35] More interestingly, growth and metastasis of MDA-MB-231 breast cancer cells *in vivo* were inhibited by either an NGF blocking antibody or small interfering RNAs specific to NGF, demonstrating in two ways that NGF is involved in both bone metastatic progression and cancer-induced bone pain.[36] In several chronic musculoskeletal pain conditions, tanezumab, a humanized monoclonal antibody against NGF with high selectivity and specificity, showed significant pain relief.[37–40] However, tanezumab failed to improve the analgesic efficacy in cancer patients with bone metastases.[41] As NGF is an attractive and promising target for the treatment of cancer-induced bone pain, further studies in this area are clearly warranted.

Likewise, ET-1 is thought to be involved in both pain and tumor outgrowth within the marrow. ET-1 has two distinct receptors: ETAR and ETBR. ET-1 appears to promote both tumor progression[42,43] and pain behavior[44,45] through ETAR. Ongoing and movement-evoked cancer bone pain mediated by ET-1 expressing 2472 osteosarcoma cells were attenuated by the ETAR selective antagonist, ABT-627, but not by the ETBR selective antagonist, A-192621.[44] In addition, local injection of ET-1 enhanced spontaneous pain behaviors of mice with bone cancer, and this tumor-induced nociception was blocked by the ETAR antagonist BQ-123, suggesting that local levels of ET-1 are involved in the development of cancer-induced bone pain.[46] A human breast cancer cell line, ZR-75-1, is well known to develop osteoblastic bone lesions *in vivo*. It has been shown that ZR-75-1 cells express high levels of ET-1; and ETAR antagonist treatments in mice inoculated with ZR-75-1 cells, when compared with vehicle treatments, cause a significant reduction in the number of osteoblastic lesions and overall tumor burden in the marrow.[47] In contrast, this strategy did not attenuate the bone metastatic progression of animals inoculated with osteolytic breast and prostate cancer cells.[47] These findings suggest that the ET-1–ETAR interaction plays a crucial role in the progression of osteoblastic bone metastases. However, although in a recent analysis of nine clincal studies examining ETAR antagonists in patients with CRPC, atrasentan-treated patients had a reduced incidence of bone pain;[48] two different small molecule inhibitors of ETAR, atrasentan and zibotentan, both failed to improve the survival of CRPC patients with bone metastases.[49,50]

Ang II, a peptide involved in the control of blood pressure, is also known to have nociceptive capabilities.[51] There are two receptors for Ang II: AT1R and AT2R. It has been shown that Ang II mediates pain through the AT2R expressed on sensory neurons.[52,53] In a rat model of neuropathic pain, augmented Ang II levels in the DRG contributes to hyperexcitability and abnormal sprouting of DRG sensory neurons.[52] Consistent with these observations, Ang II increases capsaicin-induced neuronal excitability and neurite outgrowth in both cultured rat and human DRG neurons.[53] Most importantly, with regard to cancer, increased levels of Ang II were observed in the lumbar DRGs of rats inoculated with APCCs directly into the tibia, and these APCC-bearing animals expressed hypersensitivity compared with sham-operated animals.[54] Intriguingly, treatments of a small molecule inhibitor for AT2R decreased the levels of Ang II in DRGs, and reduced hypersensitivity in APCC-bearing animals.[54] In addition to its effectiveness in reducing cancer-induced bone pain, the AT2R inhibitor showed analgesic effects in a rat model of chronic neuropathic pain,[55] whereas AT1R inhibitor did not.[53] The mechanisms behind the analgesic effects of AT2R inhibitor treatments were speculated to involve the reduction of p38 MAPK and p44/p42 MAPK activation in sensory neurons within lumbar DRGs.[54,55]

An acidic environment within the bone marrow can also cause cancer-induced bone pain.[15] Osteoclasts secrete HCl by expressing high levels of the vacuolar electrogenic H^+-ATPase.[56] The resulting acidic environment after osteoclastic bone resorption is thought to cause pain behaviors through TRPV1,[15] which is a well-known acid-sensing ion channel,[26,57,58] and also activated by capsaicin, an ingredient in hot peppers. Therefore, TRPV1 can also be a potential therapeutic target for cancer-induced bone pain. Indeed, in the 2472 osteosarcoma-inoculated bone cancer models, a TRPV1 antagonist or genetic deletion of TRPV1 significantly reduced ongoing and movement-evoked nocifencive behaviors.[16]

As we discussed earlier, tissue damage, or bone resorption, mediated by osteoclasts is one of the mechanisms of bone pain.[59] Therefore, therapeutic strategies that directly target osteoclastic activities have also been used as analgesics for cancer-induced bone pain. BP is an analog of pyrophosphate and an effective inhibitor of bone resorption mediated by osteoclasts. BP inhibits farnesyl diphosphate synthase, and subsequently decreases the level of geranylgenyl disphosphate, which is required for prenylation of GTP-binding proteins in osteoclasts.[60] Therefore, BP inactivates osteoclasts and induces their apoptosis. A randomized, placebo-controlled, phase III trial in men with hormone-refractory prostate cancer showed that patients who received ZA (a third-generation nitrogen containing BP) experience fewer SREs, compared with those who received a placebo (33.2 *vs* 44.2%).[61] In addition, placebo-treated patients experienced more pain than ZA-treated patients.[61] In contrast, a double-blind, placebo-controlled trial with first-generation BPs, etidronate and clodronate, failed to show significant pain relief effects in cancer patients with bone metastases.[62–64] This suggests that only the newer generation of BPs should be used as analgesics for cancer-induced bone pain.

Osteoclasts express RANK, which binds to RANKL expressed by osteoblasts, resulting in osteoclast differentiation.[59] Therefore, blocking the RANK–RANKL axis is a promising strategy for relieving cancer-induced bone pain. Osteoblasts also produce a decoy receptor for RANKL, OPG, which inhibits osteoclast formation and activity by binding to RANKL.[59] OPG treatments attenuated both ongoing and movement-evoked pain, and osteoclastogenesis in the femurs of mice inoculated with 2472 osteosarcoma cells.[65] A fully human immunoglobulin G2 monoclonal antibody against RANKL, denosumab, has also been widely used for the prevention of SREs associated with bone metastasis.[66] The effects of denosumab on SREs were compared with those of ZA in a randomized, double-blind, phase III study of men with castration-resistant bone metastatic prostate cancer.[67] In that study, denosumab delayed the occurrence of SREs (20.7 months) compared with ZA (17.1 months). Likewise, a randomized, double-blind, double-dummy phase III study of breast cancer patients with bone metastases showed that denosumab delays the occurrence of SREs better than ZA,[68] and consequently, denosumab reduces the severity of pain when compared with ZA.[69]

A liposomal cystein proteinase secreted by osteoclasts, cathepsin K, might also be a potential molecular target for inhibiting osteoclast activities.[59] Cathepsin K degrades the demineralized collagenous matrix. It has been reported that mice with osteoclasts without cathepsin K show an osteopetrotic phenotype associated with impaired osteoclastic activities.[70] CKI reduced 59% of osteolytic lesions in the tibiae of mice inoculated with cathepsin K-expressing human BT474

breast cancer cells, similar to the 66% reduction observed with ZA treatments.[71] Interestingly, CKI shrunk the tumor burden within the marrow, whereas ZA did not influence tumor size.[71] Additionally, CKI failed to decrease the size of subcutaneously implanted tumors, suggesting that CKI specifically targets the bone marrow microenvironment.[71] A randomized, double-blind, phase II trial comparing the CKI odanacatib with ZA was carried out in breast cancer patients with bone metastases.[72] In that study, a urine detectable bone resorption marker (uNTX/Cr: the ratio of N-telopeptide of type I collagen to creatinine) was measured after treatment with either odanacatib or ZA. After 4 weeks of treatments, odanacatib suppressed uNTX/Cr similar to ZA (77 *vs* 73%). Furthermore, odanacatib showed robust efficacy and a favorable benefit/risk profile in a randomized fracture trial in osteoporosis patients.[73] As CKI also inhibits osteoclastic lesions associated with bone metastases, these findings suggest that CKI can be used as an analgesic for patients who suffer from cancer-induced bone pain. Further studies are clearly required.

Hypercalcemia

Hypercalcemia is a common paraneoplastic syndrome, and is frequently seen in breast cancer, lung cancer and multiple myeloma.[74] In general, 80% of cancer-induced hypercalcemia is mediated by PTHrP produced by tumor cells.[74] PTHrP derived from tumor cells increases serum calcium levels by enhancing calcium reabsorption in the loop of Henle ascending limb and distal convoluted tubule, and inhibiting phosphate reabsorption in the proximal convoluted tubule.[75–77] In contrast, bone resorption caused by bone metastases is responsible for the remaining 20%.[74] Bone metastatic cancer cells also secrete several factors that stimulate osteoclastogenesis, including PTHrP, IL-6, IL-11 and vascular endothelial growth factor.[8] These factors are known to enhance osteoclast activity by increasing RANKL and inhibiting OPG secretion from osteoblasts. Interestingly, PTHrP secreted from bone metastatic cancer cells contributes to the release of skeletal calcium and phosphate by activating oseteoclastic bone resorption through the PTH/PTHrP receptor expressed on osteoclasts.[78] The most common symptoms of hypercalcemia are nausea, vomiting, anorexia and abdominal pain. Hypercalcemia can also impair cognition (fatigue to coma) and normal cardiac functions (e.g. short QT syndrome, cardiac arrhythmia).[79] Surprisingly, it has been reported that approximately half of all patients die within the first month of developing hypercalcemia.[80] Thus, prompt and proper treatments are required.

The principal goals of treatment are to promote renal calciuresis and inhibit pathological bone resorption. Hydration is essential to increase the glomerular filtration rate, and inhibit calcium reabsorption in the proximal nephron.[81] Thereafter, loop diuretics can be used for promoting the renal excretion of calcium.[74] Currently, the Food and Drug Administration approves the use of BPs[74] and denosumab[82] for the treatment of HCM due to their anti-osteoclastic effects. Denosumab is used for the treatment of patients with BP refractory HCM, based on the results from a single-arm multicenter, international phase II study.[83] In that study, 64% of patients with BP refractory HCM reached complete response (serum calcium levels corrected for albumin ≤10.8 mg/dL). Furthermore, pooled analysis of two randomized, double-blinded, phase III trials between denosumab and ZA showed that denosumab significantly delayed the occurrence of HCM and decreased the recurrence risk of HCM compared with ZA. Therefore, denosumab can be used as a first-line therapy for patients with HCM. Calcitonin can also be used, as it is known to interfere with osteoclast functions, stimulate osteoblast activities, increase renal calcium excretion and inhibit calcium reabsorption by the intestines.[84] However, the use of calcitonin is limited, as: (i) the duration of efficacy is relatively short; (ii) the reduction of calcium levels is not robust; and (iii) calcitonin itself downregulates calcitonin receptors on osteoclasts.[85]

Pathological bone fractures

It has been reported that 9–29% of patients who suffer from bone metastases develop pathological fractures.[86,87] In general, pathological fractures are common in the long bones,[88] although the spine is the most common site of skeletal metastases.[89] Importantly, the 3-year survival rate of patients with bone metastases and pathological fractures is significantly lower than those without pathological fractures (19 *vs* 35%).[87] Furthermore, pathological fractures are painful, resulting in further reduced QOL. Therefore, a deep understanding of the pathological fracture risk in bone metastatic disease is an unmet need for the prevention, detection and treatment of pathological fracture. The following are currently considered to be the risk factors for pathological fracture in patients with bone metastases: (i) increasing pain; (ii) radiographic osteolytic appearance; (iii) lesion size (>25 mm); (iv) axial cortical involvement (>30 mm); and (v) circumferential cortical involvement (>50%).[90–94]

Patients with pathological fractures are mainly treated with surgery to stabilize the fractured bones with the goal of pain relief, function and mobility restoration, and general QOL improvement.[89] Intriguingly, a population-based study of patients with femoral metastases showed that patients who receive prophylactic stabilizations of bone metastatic disease have better survival outcomes than those who receive surgical interventions post-fracture.[95] Adjuvant radiotherapy is often given to target residual microscopic disease so that disease and fracture recurrence can be prevented.[96] Although the appearance of osteolytic bone lesions is a risk factor for malignant fractures, the implementation of adjuvant treatments with osteoclast inhibitors for the prevention of malignant fractures remains controversial.[97]

Metastatic epidural spinal cord compression

MESCC is another oncological emergency related to bone metastasis, as it leads to reduced life expectancy and QOL if accurate diagnosis and treatments are not immediate.[98] MESCC occurs in 15–20% of patients with bone metastatic cancer, such as prostate, breast and lung cancer.[99] The overall median survival of MESCC patients is 3–6 months, and the improvement of mobility is thought to be a crucial factor to

Table 1 Treatment strategies for skeletal complications of bone metastases

Skeletal complications of bone metastases	Treatment route	Treatments	Predicted effects	Food and Drug Administration status
Cancer-induced bone pain	Systemic	Opioids	Analgesic effects	Approved
		NSAIDs, acetaminophen	Analgesic effects, tumor shrinkage effects	Approved
		Bisphosphonate	Inhibition of osteoclast activities, analgesic effects, tumor shrinkage effects	Approved
		Anti-RANKL antibody	Inhibition of osteoclast activities, analgesic effects, tumor shrinkage effects	Approved
		NGF/TrkA inhibitor	Analgesic effects, tumor shrinkage effects	Not yet approved
		ETAR antagonist	Analgesic effects, tumor shrinkage effects	Not yet approved
		AT2R antagonist	Analgesic effects	Not yet approved
		TRPV1 antagonist	Analgesic effects	Not yet approved
		Cathepsin K inhibitor	Inhibition of osteoclast activities, analgesic effects, tumor shrinkage effects	Not yet approved
	Local	Radiation therapy	Analgesic effects, tumor shrinkage effects	
Hypercalcemia	Systemic	Hydration	Increase of glomerular filtration rate	Approved
		Loop diuretics	Increase of renal calcium excretion	Approved
		Bisphosphonate	Inhibition of osteoclast activities	Approved
		Anti-RANKL antibody	Inhibition of osteoclast activities	Approved
		Calcitonin	Inhibition of osteoclast activities, increase of osteoblast activities, increase of renal calcium excretion	Approved
Pathological bone fractures	Systemic	Opioids	Analgesic effects	Approved
		NSAIDs, acetaminophen	Analgesic effects	Approved
		Bisphosphonate	Inhibition of osteoclast activities, analgesic effects	Approved
		Anti-RANKL antibody	Inhibition of osteoclast activities, analgesic effects	Approved
	Local	Surgery	Stabilization of fracutures	
		Radiotherapy	Analgesic effects	
Metastatic epidural spinal cord compression	Systemic	Corticosteroids	Stabilization of vascular membranes, reduction of edema, reduction of inflammation	Approved
		Opioids	Analgesic effects	Approved
		NSAIDs, acetaminophen	Analgesic effects	Approved
	Local	Surgery	Direct decompression of spianl cord	
		Radiotherapy	Analgesic effects, tumor shrinkage effects	

prolonging survival.[99] MESCC causes severe pain, motor weakness, sensory deficits and gait disturbance, and, in some cases the functions of the bladder, bowels or sexual organs are disturbed.[98,99] The preferential location of compression in the spine depends on the size and blood flow of the vertebrae: 15% of MESCC occurs in the cervical spine; 60% in the thoracic spine; and 25% in the lumbosacral spine.[99] MESCC is thought to occur in two ways:[99] (i) direct compression of the spinal cord mediated by perivertebral tumors; and (ii) indirect compression derived from bone tissues in which DTCs grow. The spinal cord is damaged by these compressions or by vascular compromise caused by growing tumors.[99] Once arterial flow to the spinal cord is disturbed, MESCC becomes irreversible.[100–102]

In most cases, immediate treatment is essential for patients with MESCC. Corticosteroids are the first-line treatment for MESCC, as they are known to stabilize vascular membranes and reduce edema, reduce inflammation, and delay the onset of neurological manifestations (motor power and skills, reflexes and sensory or any other neurological symptoms).[103] In addition, the therapeutic effects of radiation on MESCC are promising, although appropriate dose and duration are not yet agreed on. When MESCC patients were treated with high-dose dexamethasone followed by radiation, significantly greater numbers of patients were able to walk at 3 months and 6 months, compared with those who received radiation alone.[104] Surgery is another powerful mode of relief for spinal compression. A randomized trial showed that patients with MESCC who received direct decompressive surgery were able to walk and maintain their momentum longer (median 122 days) than those who received radiotherapy (median 13 days).[105] More importantly, the patients in the surgery group obtained longer survival benefits (126 *vs* 100 days). Although further studies are clearly warranted, these findings suggest that surgical intervention with adjuvant radiotherapy improves the QOL of patients with MESCC.

Conclusion

In the present article, we discussed the major skeletal complications of bone metastatic disease including cancer-induced bone pain, hypercalcemia, pathological fractures and spinal

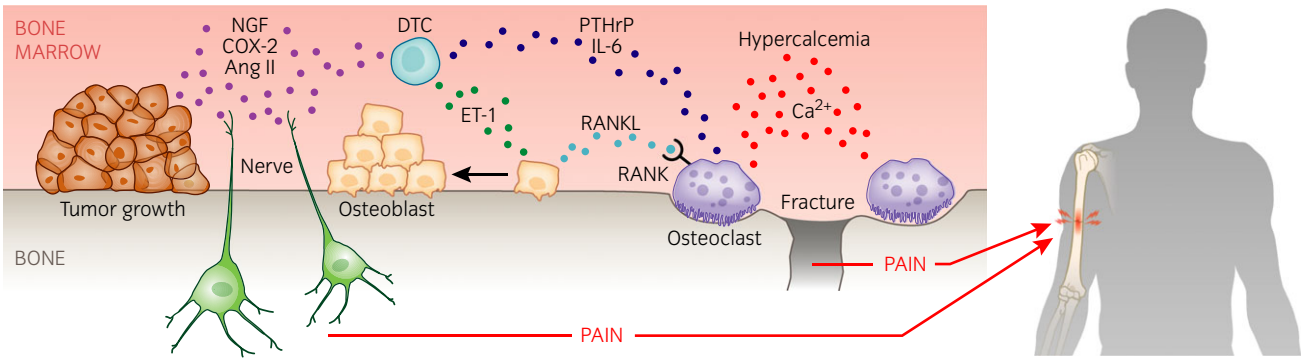

Fig. 1 The mechanisms whereby DTCs are directly involved in the development of skeletal complications associated with bone metastasis. Growing evidence suggests that once in the marrow, DTCs create a favorable microenvironment for their own metastatic progression by interfering with the normal functions of bone marrow. Indeed, DTCs disturb bone remodeling by altering the balance between osteoclastogenesis and osteoblastogenesis. Osteolytic tumor cells stimulate osteoclastic activities by expressing PTHrP or IL-6, and/or by inducing RANKL secretion by osteoblasts. Osteoclastogenesis mediated by DTCs plays a crucial role in the development of serious complications involved with bone metastasis, including bone pain, hypercalcemia and malignant fracture. In addition, ET-1 expressed by DTCs develops osteoblastic metastatic lesions in the bone and is related to cancer-induced bone pain. At the same time, DTCs engage with sensory neurons in the marrow directly through NGF, COX-2 and Ang II signaling pathways, resulting in cancer-induced bone pain. These pain transmitters might also affect metastatic growth. Therefore, targeting bone remodeling and blocking the cancer/nerve interactions might be a successful therapeutic strategy for eradicating bone metastatic disease and improving patient QOL.

cord compression, and current therapeutic strategies (Table 1). As mentioned earlier, cancer patients with bone metastases often experience severe skeletal complications that significantly impair their QOL. Additionally, recent studies suggest that bone metastasis is associated with the development of cancer cachexia. Cachexia is the term used to describe the fatal culmination of symptoms including extreme weight loss, anorexia, muscle wasting and fatigue.[106] Several factors that are enriched in the bone matrix, including transforming growth factor-β, activin A, myostatin and GDF-11, are believed to cause cachexia.[107–109] Therefore, osteolytic activities associated with bone metastasis surely play important roles in the development of cachexia.[110] These findings further suggest that a better understanding of the mechanisms of skeletal complications caused by bone metastasis will aid in developing new therapeutic targets for both treating bone metastatic disease and improving patient QOL.

Once cancer cells invade the bone marrow, they interfere with the normal physiology of the marrow microenvironment. Although genetic mutations in tumor cells contribute largely to the metastatic process and are therefore used as logical therapeutic targets for bone metastasis, understanding of the unique crosstalk between tumor cells and their microenvironment is perhaps less intuitive, but crucial in any efforts to eradicate bone metastatic disease. Although bone destruction initiated by DTCs is widely believed to be a direct cause of skeletal complications (Fig. 1), the mechanisms by which DTCs interact with the surrounding bone marrow microenvironment and ultimately cause skeletal complications remain unanswered questions in cancer biology. More importantly, we still do not confidently know if the skeletal complications of bone metastatic disease even influence overall patient survival. Clearly, a better understanding of bone metastasis is necessary if we truly hope to improve patient survival, and showing the mechanisms of its complications will be equally vital to the improvement of patient well-being.

Acknowledgments

This work was directly supported by the National Cancer Institute (CA163124; Y Shiozawa), the Department of Defense (W81XWH-14-1-0403; Y Shiozawa), the Prostate Cancer Foundation (Y Shiozawa), and the National Institutes of Health (GM099863; CM Peters). Y Shiozawa is supported as the Translational Research Academy which is supported by the National Center for Advancing Translational Sciences (NCATS), National Institutes of Health, through Grant Award Number UL1TR001420.

Conflict of interest

None declared.

References

1 Pond GR, Sonpavde G, de Wit R, Eisenberger MA, Tannock IF, Armstrong AJ. The prognostic importance of metastatic site in men with metastatic castration-resistant prostate cancer. *Eur. Urol.* 2014; **65**: 3–6.
2 Christofori G. New signals from the invasive front. *Nature* 2006; **441**: 444–50.
3 Sleeman JP. The metastatic niche and stromal progression. *Cancer Metastasis Rev.* 2012; **31**: 429–40.
4 Murgai M, Giles A, Kaplan R. Physiological, tumor, and metastatic niches: opportunities and challenges for targeting the tumor microenvironment. *Crit. Rev. Oncog.* 2015; **20**: 301–14.
5 Olechnowicz SW, Edwards CM. Contributions of the host microenvironment to cancer-induced bone disease. *Cancer Res.* 2014; **74**: 1625–31.
6 Shiozawa Y, Pedersen EA, Havens AM *et al.* Human prostate cancer metastases target the hematopoietic stem cell niche to establish footholds in mouse bone marrow. *J. Clin. Invest.* 2011; **121**: 1298–312.
7 Wang H, Yu C, Gao X *et al.* The osteogenic niche promotes early-stage bone colonization of disseminated breast cancer cells. *Cancer Cell* 2015; **27**: 193–210.
8 Clines GA, Guise TA. Hypercalcaemia of malignancy and basic research on mechanisms responsible for osteolytic and osteoblastic metastasis to bone. *Endocr. Relat. Cancer* 2005; **12**: 549–83.
9 Coleman R, Body JJ, Aapro M, Hadji P, Herrstedt J. Bone health in cancer patients: ESMO Clinical Practice Guidelines. *Ann. Oncol.* 2014; **25** (Suppl 3): iii124–37.

10 van den Beuken-van Everdingen MH, de Rijke JM, Kessels AG, Schouten HC, van Kleef M, Patijn J. Prevalence of pain in patients with cancer: a systematic review of the past 40 years. *Ann. Oncol.* 2007; **18**: 1437–49.
11 Coleman RE. Skeletal complications of malignancy. *Cancer* 1997; **80**: 1588–94.
12 Jimenez-Andrade JM, Mantyh WG, Bloom AP, Ferng AS, Geffre CP, Mantyh PW. Bone cancer pain. *Ann. N. Y. Acad. Sci.* 2010; **1198**: 173–81.
13 Liao J, McCauley LK. Skeletal metastasis: established and emerging roles of parathyroid hormone related protein (PTHrP). *Cancer Metastasis Rev.* 2006; **25**: 559–71.
14 Peters CM, Ghilardi JR, Keyser CP *et al.* Tumor-induced injury of primary afferent sensory nerve fibers in bone cancer pain. *Exp. Neurol.* 2005; **193**: 85–100.
15 Yoneda T, Hiasa M, Nagata Y, Okui T, White F. Contribution of acidic extracellular microenvironment of cancer-colonized bone to bone pain. *Biochim. Biophys. Acta.* 2015; **1848**: 2677–84.
16 Ghilardi JR, Rohrich H, Lindsay TH *et al.* Selective blockade of the capsaicin receptor TRPV1 attenuates bone cancer pain. *J. Neurosci.* 2005; **25**: 3126–31.
17 Mantyh PW. Bone cancer pain: from mechanism to therapy. *Curr. Opin. Support. Palliat. Care* 2014; **8**: 83–90.
18 McGrath PA. Development of the World Health Organization guidelines on cancer Pain relief and palliative care in children. *J. Pain Symptom Manage.* 1996; **12**: 87–92.
19 Burton AW, Cleeland CS. Cancer pain: progress since the WHO guidelines. *Pain Pract.* 2001; **1**: 236–42.
20 Pergolizzi JV, Zampogna G, Taylor R, Gonima E, Posada J, Raffa RB. A guide for pain management in low and middle income communities. Managing the risk of opioid abuse in patients with cancer pain. *Front Pharmacol.* 2016; **7**: 42.
21 Nabal M, Librada S, Redondo MJ, Pigni A, Brunelli C, Caraceni A. The role of paracetamol and nonsteroidal anti-inflammatory drugs in addition to WHO Step III opioids in the control of pain in advanced cancer. A systematic review of the literature. *Palliat. Med.* 2012; **26**: 305–12.
22 Chow E, Harris K, Fan G, Tsao M, Sze WM. Palliative radiotherapy trials for bone metastases: a systematic review. *J. Clin. Oncol.* 2007; **25**: 1423–36.
23 Lutz S, Berk L, Chang E *et al.* Palliative radiotherapy for bone metastases: an ASTRO evidence-based guideline. *Int. J. Radiat. Oncol. Biol. Phys.* 2011; **79**: 965–76.
24 Ripamonti CI, Santini D, Maranzano E, Berti M, Roila F. Management of cancer pain: ESMO Clinical Practice Guidelines. *Ann. Oncol.* 2012; **23** (Suppl 7): vii139–54.
25 van der Linden MW, Gaugris S, Kuipers EJ *et al.* COX-2 inhibitors: complex association with lower risk of hospitalization for gastrointestinal events compared to traditional NSAIDs plus proton pump inhibitors. *Pharmacoepidemiol. Drug Saf.* 2009; **18**: 880–90.
26 Julius D, Basbaum AI. Molecular mechanisms of nociception. *Nature* 2001; **413**: 203–10.
27 Sabino MA, Ghilardi JR, Jongen JL *et al.* Simultaneous reduction in cancer pain, bone destruction, and tumor growth by selective inhibition of cyclooxygenase-2. *Cancer Res.* 2002; **62**: 7343–9.
28 Hirose M, Kuroda Y, Murata E. NGF/TrkA Signaling as a therapeutic target for pain. *Pain Pract.* 2016; **16**: 175–82.
29 Lewin GR, Ritter AM, Mendell LM. Nerve growth factor-induced hyperalgesia in the neonatal and adult rat. *J. Neurosci.* 1993; **13**: 2136–48.
30 Thacker MA, Clark AK, Marchand F, McMahon SB. Pathophysiology of peripheral neuropathic pain: immune cells and molecules. *Anesth. Analg.* 2007; **105**: 838–47.
31 Basbaum AI, Bautista DM, Scherrer G, Julius D. Cellular and molecular mechanisms of pain. *Cell* 2009; **139**: 267–84.
32 Petty BG, Cornblath DR, Adornato BT *et al.* The effect of systemically administered recombinant human nerve growth factor in healthy human subjects. *Ann. Neurol.* 1994; **36**: 244–6.
33 Dyck PJ, Peroutka S, Rask C *et al.* Intradermal recombinant human nerve growth factor induces pressure allodynia and lowered heat-pain threshold in humans. *Neurology* 1997; **48**: 501–5.
34 Halvorson KG, Kubota K, Sevcik MA *et al.* A blocking antibody to nerve growth factor attenuates skeletal pain induced by prostate tumor cells growing in bone. *Cancer Res.* 2005; **65**: 9426–35.
35 Bloom AP, Jimenez-Andrade JM, Taylor RN *et al.* Breast cancer-induced bone remodeling, skeletal pain, and sprouting of sensory nerve fibers. *J Pain.* 2011; **12**: 698–711.
36 Adriaenssens E, Vanhecke E, Saule P *et al.* Nerve growth factor is a potential therapeutic target in breast cancer. *Cancer Res.* 2008; **68**: 346–51.
37 Lane NE, Schnitzer TJ, Birbara CA *et al.* Tanezumab for the treatment of pain from osteoarthritis of the knee. *N. Engl. J. Med.* 2010; **363**: 1521–31.
38 Brown MT, Murphy FT, Radin DM, Davignon I, Smith MD, West CR. Tanezumab reduces osteoarthritic knee pain: results of a randomized, double-blind, placebo-controlled phase III trial. *J. Pain.* 2012; **13**: 790–8.
39 Brown MT, Murphy FT, Radin DM, Davignon I, Smith MD, West CR. Tanezumab reduces osteoarthritic hip pain: results of a randomized, double-blind, placebo-controlled phase III trial. *Arthritis Rheum.* 2013; **65**: 1795–803.
40 Katz N, Borenstein DG, Birbara C *et al.* Efficacy and safety of tanezumab in the treatment of chronic low back pain. *Pain* 2011; **152**: 2248–58.
41 Sopata M, Katz N, Carey W *et al.* Efficacy and safety of tanezumab in the treatment of pain from bone metastases. *Pain* 2015; **156**: 1703–13.
42 Pinto A, Merino M, Zamora P, Redondo A, Castelo B, Espinosa E. Targeting the endothelin axis in prostate carcinoma. *Tumour Biol.* 2012; **33**: 421–6.
43 Nelson JB, Carducci MA. The role of endothelin-1 and endothelin receptor antagonists in prostate cancer. *BJU Int.* 2000; **85** (Suppl 2): 45–8.
44 Peters CM, Lindsay TH, Pomonis JD *et al.* Endothelin and the tumorigenic component of bone cancer pain. *Neuroscience* 2004; **126**: 1043–52.
45 Pomonis JD, Rogers SD, Peters CM, Ghilardi JR, Mantyh PW. Expression and localization of endothelin receptors: implications for the involvement of peripheral glia in nociception. *J. Neurosci.* 2001; **21**: 999–1006.
46 Wacnik PW, Eikmeier LJ, Ruggles TR *et al.* Functional interactions between tumor and peripheral nerve: morphology, algogen identification, and behavioral characterization of a new murine model of cancer pain. *J. Neurosci.* 2001; **21**: 9355–66.
47 Yin JJ, Mohammad KS, Kakonen SM *et al.* A causal role for endothelin-1 in the pathogenesis of osteoblastic bone metastases. *Proc. Natl. Acad. Sci. USA* 2003; **100**: 10954–9.
48 Qiao L, Liang Y, Li N *et al.* Endothelin-A receptor antagonists in prostate cancer treatment-a meta-analysis. *Int. J. Clin. Exp. Med.* 2015; **8**: 3465–73.
49 Nelson JB, Fizazi K, Miller K *et al.* Phase 3, randomized, placebo-controlled study of zibotentan (ZD4054) in patients with castration-resistant prostate cancer metastatic to bone. *Cancer* 2012; **118**: 5709–18.
50 Carducci MA, Saad F, Abrahamsson PA *et al.* A phase 3 randomized controlled trial of the efficacy and safety of atrasentan in men with metastatic hormone-refractory prostate cancer. *Cancer* 2007; **110**: 1959–66.
51 Patil J, Schwab A, Nussberger J, Schaffner T, Saavedra JM, Imboden H. Intraneuronal angiotensinergic system in rat and human dorsal root ganglia. *Regul. Pept.* 2010; **162**: 90–8.
52 Smith MT, Woodruff TM, Wyse BD, Muralidharan A, Walther T. A small molecule angiotensin II type 2 receptor (AT(2)R) antagonist produces analgesia in a rat model of neuropathic pain by inhibition of p38 mitogen-activated protein kinase (MAPK) and p44/p42 MAPK activation in the dorsal root ganglia. *Pain Med.* 2013; **14**: 1557–68.
53 Anand U, Facer P, Yiangou Y *et al.* Angiotensin II type 2 receptor (AT2 R) localization and antagonist-mediated inhibition of capsaicin responses and neurite outgrowth in human and rat sensory neurons. *Eur. J. Pain* 2013; **17**: 1012–26.
54 Muralidharan A, Wyse BD, Smith MT. Analgesic efficacy and mode of action of a selective small molecule angiotensin II type 2 receptor antagonist in a rat model of prostate cancer-induced bone pain. *Pain Med.* 2014; **15**: 93–110.
55 Smith MT, Wyse BD, Edwards SR. Small molecule angiotensin II type 2 receptor (AT(2)R) antagonists as novel analgesics for neuropathic pain: comparative pharmacokinetics, radioligand binding, and efficacy in rats. *Pain Med.* 2013; **14**: 692–705.
56 Blair HC. How the osteoclast degrades bone. *Bioessays* 1998; **20**: 837–46.
57 Reeh PW, Kress M. Molecular physiology of proton transduction in nociceptors. *Curr. Opin. Pharmacol.* 2001; **1**: 45–51.
58 Nagae M, Hiraga T, Yoneda T. Acidic microenvironment created by osteoclasts causes bone pain associated with tumor colonization. *J. Bone Miner. Metab.* 2007; **25**: 99–104.
59 Rodan GA, Martin TJ. Therapeutic approaches to bone diseases. *Science* 2000; **289**: 1508–14.
60 Coxon FP, Helfrich MH, Van't Hof R *et al.* Protein geranylgeranylation is required for osteoclast formation, function, and survival: inhibition by bisphosphonates and GGTI-298. *J. Bone Miner. Res.* 2000; **15**: 1467–76.

61 Saad F, Gleason DM, Murray R *et al.* A randomized, placebo-controlled trial of zoledronic acid in patients with hormone-refractory metastatic prostate carcinoma. *J. Natl Cancer Inst.* 2002; **94**: 1458–68.

62 Smith JA Jr. Palliation of painful bone metastases from prostate cancer using sodium etidronate: results of a randomized, prospective, double-blind, placebo-controlled study. *J. Urol.* 1989; **141**: 85–7.

63 Strang P, Nilsson S, Brandstedt S *et al.* The analgesic efficacy of clodronate compared with placebo in patients with painful bone metastases from prostatic cancer. *Anticancer Res.* 1997; **17**: 4717–21.

64 Kylmala T, Taube T, Tammela TL, Risteli L, Risteli J, Elomaa I. Concomitant i.v. and oral clodronate in the relief of bone pain–a double-blind placebo-controlled study in patients with prostate cancer. *Br. J. Cancer* 1997; **76**: 939–42.

65 Luger NM, Honore P, Sabino MA *et al.* Osteoprotegerin diminishes advanced bone cancer pain. *Cancer Res.* 2001; **61**: 4038–47.

66 Dougall WC. Molecular pathways: osteoclast-dependent and osteoclast-independent roles of the RANKL/RANK/OPG pathway in tumorigenesis and metastasis. *Clin. Cancer Res.* 2012; **18**: 326–35.

67 Fizazi K, Carducci M, Smith M *et al.* Denosumab versus zoledronic acid for treatment of bone metastases in men with castration-resistant prostate cancer: a randomised, double-blind study. *Lancet* 2011; **377**: 813–22.

68 Stopeck AT, Lipton A, Body JJ *et al.* Denosumab compared with zoledronic acid for the treatment of bone metastases in patients with advanced breast cancer: a randomized, double-blind study. *J. Clin. Oncol.* 2010; **28**: 5132–9.

69 Cleeland CS, Body JJ, Stopeck A *et al.* Pain outcomes in patients with advanced breast cancer and bone metastases: results from a randomized, double-blind study of denosumab and zoledronic acid. *Cancer* 2013; **119**: 832–8.

70 Saftig P, Hunziker E, Wehmeyer O *et al.* Impaired osteoclastic bone resorption leads to osteopetrosis in cathepsin-K-deficient mice. *Proc. Natl. Acad. Sci. USA* 1998; **95**: 13453–8.

71 Le Gall C, Bellahcene A, Bonnelye E *et al.* A cathepsin K inhibitor reduces breast cancer induced osteolysis and skeletal tumor burden. *Cancer Res.* 2007; **67**: 9894–902.

72 Jensen AB, Wynne C, Ramirez G *et al.* The cathepsin K inhibitor odanacatib suppresses bone resorption in women with breast cancer and established bone metastases: results of a 4-week, double-blind, randomized, controlled trial. *Clin. Breast Cancer* 2010; **10**: 452–8.

73 Bone HG, Dempster DW, Eisman JA *et al.* Odanacatib for the treatment of postmenopausal osteoporosis: development history and design and participant characteristics of LOFT, the Long-Term Odanacatib Fracture Trial. *Osteoporos. Int.* 2015; **26**: 699–712.

74 Stewart AF. Clinical practice. Hypercalcemia associated with cancer. *N. Engl. J. Med.* 2005; **352**: 373–9.

75 Gesek FA, Friedman PA. On the mechanism of parathyroid hormone stimulation of calcium uptake by mouse distal convoluted tubule cells. *J. Clin. Invest.* 1992; **90**: 749–58.

76 Pfister MF, Lederer E, Forgo J *et al.* Parathyroid hormone-dependent degradation of type II Na+/Pi cotransporters. *J. Biol. Chem.* 1997; **272**: 20125–30.

77 Horiuchi N, Caulfield MP, Fisher JE *et al.* Similarity of synthetic peptide from human tumor to parathyroid hormone in vivo and in vitro. *Science* 1987; **238**: 1566–8.

78 Abou-Samra AB, Juppner H, Force T *et al.* Expression cloning of a common receptor for parathyroid hormone and parathyroid hormone-related peptide from rat osteoblast-like cells: a single receptor stimulates intracellular accumulation of both cAMP and inositol trisphosphates and increases intracellular free calcium. *Proc. Natl. Acad. Sci. USA* 1992; **89**: 2732–6.

79 Clines GA. Mechanisms and treatment of hypercalcemia of malignancy. *Curr. Opin. Endocrinol. Diabetes Obes.* 2011; **18**: 339–46.

80 Ralston SH, Gallacher SJ, Patel U, Campbell J, Boyle IT. Cancer-associated hypercalcemia: morbidity and mortality. Clinical experience in 126 treated patients. *Ann. Intern. Med.* 1990; **112**: 499–504.

81 Hosking DJ, Cowley A, Bucknall CA. Rehydration in the treatment of severe hypercalcaemia. *Q J Med.* 1981; **50**: 473–81.

82 Thosani S, Hu MI. Denosumab: a new agent in the management of hypercalcemia of malignancy. *Future Oncol.* 2015; **11**: 2865–71.

83 Hu MI, Glezerman IG, Leboulleux S *et al.* Denosumab for treatment of hypercalcemia of malignancy. *J. Clin. Endocrinol. Metab.* 2014; **99**: 3144–52.

84 Sternlicht H, Glezerman IG. Hypercalcemia of malignancy and new treatment options. *Ther. Clin. Risk Manag.* 2015; **11**: 1779–88.

85 Purdue BW, Tilakaratne N, Sexton PM. Molecular pharmacology of the calcitonin receptor. *Receptors Channels* 2002; **8**: 243–55.

86 Aaron AD. Treatment of metastatic adenocarcinoma of the pelvis and the extremities. *J. Bone Joint Surg. Am.* 1997; **79**: 917–32.

87 Bohm P, Huber J. The surgical treatment of bony metastases of the spine and limbs. *J. Bone Joint Surg. Br.* 2002; **84**: 521–9.

88 Sarahrudi K, Hora K, Heinz T, Millington S, Vecsei V. Treatment results of pathological fractures of the long bones: a retrospective analysis of 88 patients. *Int. Orthop.* 2006; **30**: 519–24.

89 Bryson DJ, Wicks L, Ashford RU. The investigation and management of suspected malignant pathological fractures: a review for the general orthopaedic surgeon. *Injury.* 2015; **46**: 1891–9.

90 Parrish FF, Murray JA. Surgical treatment for secondary neoplastic fractures. A retrospective study of ninety-six patients. *J. Bone Joint Surg. Am.* 1970; **52**: 665–86.

91 Snell W, Beals RK. Femoral metastases and fractures from breast cancer. *Surg. Gynecol. Obstet.* 1964; **119**: 22–4.

92 Yazawa Y, Frassica FJ, Chao EY, Pritchard DJ, Sim FH, Shives TC. Metastatic bone disease. A study of the surgical treatment of 166 pathologic humeral and femoral fractures. *Clin. Orthop. Relat. Res.* 1990; **251**: 213–9.

93 Menck H, Schulze S, Larsen E. Metastasis size in pathologic femoral fractures. *Acta Orthop. Scand.* 1988; **59**: 151–4.

94 Van der Linden YM, Dijkstra PD, Kroon HM *et al.* Comparative analysis of risk factors for pathological fracture with femoral metastases. *J. Bone Joint Surg. Br.* 2004; **86**: 566–73.

95 Ristevski B, Jenkinson RJ, Stephen DJ *et al.* Mortality and complications following stabilization of femoral metastatic lesions: a population-based study of regional variation and outcome. *Can. J. Surg.* 2009; **52**: 302–8.

96 Frassica DA. General principles of external beam radiation therapy for skeletal metastases. *Clin. Orthop. Relat. Res.* 2003; **451** Suppl: S158–64.

97 Wolanczyk MJ, Fakhrian K, Adamietz IA. Radiotherapy, Bisphosphonates and Surgical Stabilization of Complete or Impending Pathologic Fractures in Patients with Metastatic Bone Disease. *J. Cancer.* 2016; **7**: 121–4.

98 Prasad D, Schiff D. Malignant spinal-cord compression. *Lancet Oncol.* 2005; **6**: 15–24.

99 Cole JS, Patchell RA. Metastatic epidural spinal cord compression. *Lancet Neurol.* 2008; **7**: 459–66.

100 Ushio Y, Posner R, Posner JB, Shapiro WR. Experimental spinal cord compression by epidural neoplasm. *Neurology* 1977; **27**: 422–9.

101 Ramsey R, Doppman JL. The effects of epidural masses on spinal cord blood flow. An experimental study in monkeys. *Radiology* 1973; **107**: 99–103.

102 Kato A, Ushio Y, Hayakawa T, Yamada K, Ikeda H, Mogami H. Circulatory disturbance of the spinal cord with epidural neoplasm in rats. *J. Neurosurg.* 1985; **63**: 260–5.

103 Fawzy M, El-Beltagy M, Shafei ME *et al.* Intraspinal neuroblastoma: treatment options and neurological outcome of spinal cord compression. *Oncol. Lett.* 2015; **9**: 907–11.

104 Sorensen S, Helweg-Larsen S, Mouridsen H, Hansen HH. Effect of high-dose dexamethasone in carcinomatous metastatic spinal cord compression treated with radiotherapy: a randomised trial. *Eur. J. Cancer* 1994; **30A**: 22–7.

105 Patchell RA, Tibbs PA, Regine WF *et al.* Direct decompressive surgical resection in the treatment of spinal cord compression caused by metastatic cancer: a randomised trial. *Lancet* 2005; **366**: 643–8.

106 Andreyev HJ, Norman AR, Oates J, Cunningham D. Why do patients with weight loss have a worse outcome when undergoing chemotherapy for gastrointestinal malignancies? *Eur. J. Cancer* 1998; **34**: 503–9.

107 Sakai R, Eto Y. Involvement of activin in the regulation of bone metabolism. *Mol. Cell. Endocrinol.* 2001; **180**: 183–8.

108 Wildemann B, Kadow-Romacker A, Haas NP, Schmidmaier G. Quantification of various growth factors in different demineralized bone matrix preparations. *J. Biomed. Mater. Res. A* 2007; **81**: 437–42.

109 Lee SJ, Reed LA, Davies MV *et al.* Regulation of muscle growth by multiple ligands signaling through activin type II receptors. *Proc. Natl. Acad. Sci. USA* 2005; **102**: 18117–22.

110 Waning DL, Mohammad KS, Reiken S *et al.* Excess TGF-beta mediates muscle weakness associated with bone metastases in mice. *Nat. Med.* 2015; **21**: 1262–71.